Rational Chemical Design of Solar-Powered Nano Photocatalysts for Environmental Applications

Being a Thesis submitted for the Degree of Doctor of Philosophy degree (PhD)

in the University of Hull

By

Khadijah Mohammedsaleh M Katubi

(January 2015)

Declaration

I, Khadijah Mohammedsaleh M Katubi of Student Number: 200892573, hereby declare that this project, Rational Chemical Design of Solar-Powered Nano Photocatalysts for Environmental Applications being the requirement of the Hull University PhD Faculty of Science of Engineering (FOSE), Chemistry department, Academic Year 2015, is entirely of my own effort and work with the exception of excerpts cited from other works of which the sources were duly noted and acknowledged in the bibliography.

Copyright © 2015 by Khadijah Mohammedsaleh M Katubi. All rights reserved. No part of this publication may be reproduced without the written permission of the copyright holder

E-mail: Katubi707@gmail.com and drkhadijahkatubi@gmail.com

Acknowledgements

Firstly, I would like to express my deepest gratitude to Almighty Allah for the assistance. Allah has given me patience, continued support and guidance without which this work would not be accomplished. Secondly, I owe sincere thanks to my supervisor Dr M. Grazia Francesconi for her continued backing, sincere affection and the assistance given to me throughout my PhD. I would also like to thank Dr Nigel A. Young for his assistance in FT-IR and UV-Vis spectroscopy. Lots of thanks go to Dr M. Grazia Francesconi, Dr Timothy J. Prior, Dr Vincent Rocher and PhD Simon Fellows for the assistance and sharing knowledge in XRD analysis. Many thanks go to Zabeada Aslamb at Leeds University for their help in TEM, SAED and EELS. Many thanks go to Monika Kusc and Vera Meynenc for trying do some Photocatalytic tests on our samples. I owe thanks to the technical support staff; Julia Malle (glass blower), Mr Ian Dobson, Mrs Carol Kennedy (technician), Mr Paul Green storekeeper, Mr Mike Horne storekeeper, Mr Mark Richardson (porter), Mr Ian Rossiter (porter) and Mrs Maxine Tyler (Publicity Manager). I would like to thank my colleagues at Hull University. I owe thanks to my Royal Embassy of Saudi Arabia Cultural Bureau for their funding on the research. Finally I would like to say a big thank you to my parents and my husband for all their support and encouragement during my studies.

Presentations

Presentations containing work described within this thesis:

Oral presentations

- K. M. M. Katubi "Preparation of New Potential of $TiO_{2-x}(C_2N_3)_{2x}$ and $(S)_z(CS)_{4y}Ti_{1-2y-z}O_{2-x}(S)_x$ Nanoparticles" (oral presentation), PhD Experience Conference (PhDEC), Hull University, United Kingdom, 7th and 8th April 2015
- K. M. M. Katubi "Preparation of New Potential Nano-photocatalysts: N-modified and S-modified TiO_2" (oral presentation), 8th Saudi Students Scientific Conference-UK, Imperial College London, United Kingdom, 31st of January 2015 and 1st of February 2015
- K. M. M. Katubi "Preparation of New Potential Nano-photocatalysts: N-modified and S-modified TiO_2" (oral presentation), Postgraduate Research Colloquium 2014, Hull University, Hull, United Kingdom, 18th and 19th June 2014
- K. M. M. Katubi "Determination of the chemical formula of a new potential photocatalyst: N-modified titanium dioxide" (oral presentation), 7th Saudi Students Scientific Conference-UK, Edinburgh University, United Kingdom, 1st and 2nd of February 2014

Poster presentations

- K. M. M. Katubi "Preparation of New Potential of $TiO_{2-x}(CN_2)_x$ and $(CS)_{4y}Ti_{1-2y}O_{2-x}(SO_4)_x$ Nanoparticles" (poster presentation), PhD Experience Conference (PhDEC), Hull University, United Kingdom, 7th and 8th April 2015
- K. M. M. Katubi "The Estimation of Forming $TiO_{2-x}(CN_2)_x$ Formula" (poster presentation), Huddersfield University, Huddersfield, United Kingdom , 17th June 2014

- K. M. M. Katubi "A Pure Anatase TiO_2 Nanopowder Prepared From $Ti(OCH(CH_3)_2)_{4-x}(OH)_x$ At lower temperature" (poster presentation), RSC Inorganic Reaction Mechanisms Group Dalton 2014 Conference, Warwick University, Coventry, United Kingdom, 15-17 April 2014
- K. M. M. Katubi "The Estimation of Forming $TiO_{2-x}(CN_2)_x$ Formula" (poster presentation), RSC Inorganic Reaction Mechanisms Group Dalton 2014 Conference, Warwick University, Coventry, United Kingdom, 15-17 April 2014
- K. M. M. Katubi "Reactions of TiO_2 with Urea towards Anion Doping" (poster presentation), 7th Saudi Students Scientific Conference-UK, Edinburgh University, United Kingdom, 1st and 2nd of February 2014
- K. M. M. Katubi "Reactions of TiO_2 with Urea towards Anion Doping" (poster presentation), Research Colloquium 2013, University of Hull, Hull, United Kingdom, 8th and 9th of July 2013
- K. M. M. Katubi "Reactions of TiO_2 with Urea towards Anion Doping" (poster presentation), RSC North of England Region Dalton Meeting, University of York, York, United Kingdom, 24th June 2013
- K. M. M. Katubi "RATIONAL CHEMICAL DESIGN OF SOLAR-POWERED NANO PHOTOCATALYSTS FOR ENVIRONMENTAL APPLICATIONS" (poster presentation), 6th Saudi Scientific International Conference, Brunel University, London, United Kingdom, 11-14 of October 2012

Abbreviations

COSHH	Control of Substances Hazardous to Health
FT-IR	Fourier Transform – Infrared
UV-Vis	Ultraviolet – Visible
XRD	X-Ray Diffraction
PXRD	Powder X-Ray Diffraction
C_B	Conduction Band
V_B	Valence Band
E_g	Band gap energy
TMZ	Temozolomide
SSEC	supercritical seed crystallization
CDS	Chemical Database Service
Avg.	Average
JCPDS	Joint Committee on Powder Diffraction Standards
FWHM	Full Width at Half Maximum
DFT	Density Functional Theory
EPR	Electron paramagnetic resonance
U	Urea
CM	Cyanamide

ANA	Anatase
AM	Amorphous
TU	Thiourea
DT	Dodecanethiol
CS	Carbon disulfide
CYA	Cyanuric acid
E. coli	Escherichia coli
VOC	Volatile organic compounds
RhB	Rhodamine B
MO	Methyl orange
APCVD	Atmospheric pressure chemical vapour deposition
TEM	Transmission Electron Microscopy
EDX	Electron Microscope Energy-dispersive X-ray spectroscopy
EA	Elemental Analysis
EELS	Electron energy loss spectroscopy
XPS	X-ray photoelectron spectroscopy
SAED	Selected area electron diffraction
V	Volume
Å	Angstrom

eV	Electron volt
nm	Nanometre
cm^{-1}	centimetre power minus one
MSDS	Material safety data sheets
PVP	Polyvinylpyrrolidone

COSHH

Safety assessments were carried out approved prior to beginning any practical work. The completed COSHH form (reference; KMKMGF) is included in Appendix 12.

Abstract

Photo-catalysis, which relies on semiconducting materials as catalysts, has become an important approach in the search for ways to utilise solar energy. Because titanium dioxide has excellent properties, shows oxidative power and has a high efficiency for the photocatalytic degradation of harmful pollutants, it is considered to be the best semiconductor photo-catalyst. However, it absorbs in the ultraviolet region, due to its large band gap. To narrow this band gap accompanied with visible light absorption, N- and S-modifying were used in this project.

First, there are successfully synthesised pure anatase TiO_2 nanoparticles with a crystallite size ranging between 6 nm and 20 nm. The preparation involved only titanium (IV) isopropoxide, a small amount of water and a *tube furnace*, instead of alcohols, acidic chemicals or an autoclave pressure vessel as in other studies. The Fourier Transform Infrared (FT-IR) data proved the formation of the Ti—O—Ti bonds. The UV-Vis data showed the absorption at a wavelength of 384 nm with a band gap at 3.22 eV, in good agreement with the TiO_2 in the anatase phase. The Selected Area (Electron) Diffraction (SAED) also proved that the defined (*hkl*) planes formed TiO_2 anatase. Additionally, the Electron Energy Loss Spectroscopy (EELS) clearly showed that the Ti $L_{2,3}$ edge was present for the Ti^{4+} compounds, in particular for the formula TiO_2.

Second, the N-modified TiO_2 chapter showed the forming of new potential titanium-oxy-carbodiimide in the general formula $TiO_{2-x}(CN_2)_x$ by reacting the urea with amorphous titanium isopropoxide hydroxide /anatase TiO_2. The FT-IR spectra showed the band at about 2055 cm^{-1} for the carbodiimide group and a decrease of the band gap less than 3.22 eV. $TiO_{2-x}(C_2N_3)_{2x}$ and $TiO_{2-x}(CN_2H)_{2x}$ are two other possible new formulas that were produced

by reacting amorphous $Ti(OCH(CH_3)_2)_{4-x}(OH)_x$ with cyanamide at 400 °C. This reaction also showed a new decomposition of cyanamide, which is N-(iminomethylene)-cyanamide.

Third, the S-modified TiO_2 chapter showed a cationic-anionic co-modifying TiO_2 accompanied with the producing an estimation of the possible coordinations: SO_4—TiO_2 and CS—TiO_2. This was done by reacting the carbon disulfide gaseous with anatase TiO_2. On the other hand, reacted thiourea with amorphous $Ti(OCH(CH_3)_2)_{4-x}(OH)_x$ at 500 °C for 4 hours produced cationic-cationic-anionic co-modifying accompanied with the producing an estimation of a possible coordinations: Ti—O—S, CS—TiO_2, and Ti—S. Additionally, this product showed one absorption edge in the UV-Vis spectra.

Organization of the Dissertation

An overview of the dissertation provides on the following Chapters:

Chapter 1

This chapter introduces the subject of the study and aims of the study. It provides an overview of the dissertation, which presents information on the following topics: semiconductor photocatalysis, nanoparticles, band gap energy, absorption spectroscopy, and a literature review of previous studies focusing on titanium dioxide, N-modified TiO_2 and S-modified TiO_2.

Chapter 2

This chapter discusses the synthetic technique, analysis methods and materials that were used in this study.

Chapter 3

This chapter discusses the synthesis of pure single crystal anatase TiO_2 from titanium isopropoxide hydroxide using a different method than has been used in other studies.

Chapter 4

This chapter discussed the N-modification of TiO_2 and decreasing its band gap by using urea and cyanamide. It also presents information about the preparation of new potential nanoparticles with the general formula $TiO_{2-x}(CN_2)_x$ in the case of urea reactions with anatase TiO_2/amorphous titanium isopropoxide hydroxide and with the general formulas ($TiO_{2-x}(C_2N_3)_{2x}$ and $TiO_{2-x}(CN_2H)_{2x}$) in the case of cyanamide reactions with amorphous titanium isopropoxide hydroxide. This chapter also provides information about the new decomposition of cyanamide.

Chapter 5

This chapter discusses the S-modification of TiO_2 using three sources of sulfur: dodecanethiol, carbon disulfide and thiourea. The band gap of TiO_2 was decreased by using carbon disulfide and thiourea reactions. This chapter also provides information about anionic-doping by the presence of TiS_2 in the CS_2 (gaseous) reactions. The CS_2 (gaseous) reactions also demonstrate cationic-anionic co-doping and the formation of new potential nanoparticles. This chapter also provides on the formation of cationic-cationic-anionic co-doping via the thiourea reactions and the formation of new potential nanoparticles.

Final three parts of the dissertation

This dissertation ended by overall conclusions section, which includes summaries of the overall work, accompanied by highlights of the principle conclusion based on the work that was done. Finally, the References and the Appendixes sections were completed and they are included in this report.

Table of Contents

List of Figures

Chapter 1

Chapter 2

Chapter 3

Chapter 4

Chapter 5

List of Tables

Chapter 1

Chapter 4

Chapter 5

Chapter 1 – Introduction

1.1. Semiconductor Photocatalysis

In chemistry, the term 'photocatalysis' refers to the quickening of the process of photoreaction when a catalyst is present.[1] Alternately, it can be defined as a chemical reaction brought about when the solid materials are subject to photoabsorption.[1] When light is present, a photocatalyst can boost reactions without being used up in the total reaction.[2] A good photocatalyst is chemically and biologically inert, photoactive, non-toxic, inexpensive and able to use visible and/or near UV light.[2]

The general mechanism of photocatalysis is photoabsorption followed by electron-hole generation via band-to-band excitation, which involves the following: valence band, forbidden band (also known as the band gap), and conduction band.[1] Through the use of irradiated semiconductors, the role of photocatalysis is to begin or quicken particular redox (oxidation) and reduction reactions. The electronic structure of titanium dioxide (TiO_2) and other semiconductors allows them to act as sensitizers for light-induced redox processes.[3] This electronic structure is made up of an empty conduction band (CB) and an electron-filled valence band (VB). When the semiconductor materials soak up the photons with energies higher than the band gap energy (E_g), electrons (e_{CB}^-) move up from the VB into the CB, leaving behind holes (h_{VB}^+).[2, 3] When electrons and holes are in their generated excited state they can: a) react with the electron acceptors and the donors absorbed on the semiconductor's surface; or b) become stuck in metastable surface states; or c) recombine and emit the input energy as heat.[3]

Many research studies have designed and developed photocatalysts that can absorb under visible light radiation. It is also important to mention that photocatalytic activity is greatly affected by particle size. A smaller particle size leads to a larger surface area, which increases the adsorption ability of the catalytic surface and also produces enhanced photo-excitement of the electron-hole pairs in the active sites.[4, 5]

Figure 1-11 shows a wide spectrum of solar radiation from about 250 nm to 1000 nm, which combines short-wavelength (high-energy ultraviolet photons), long-wavelength (low-energy infrared photons), and all the visible light photons in between.[6, 7]

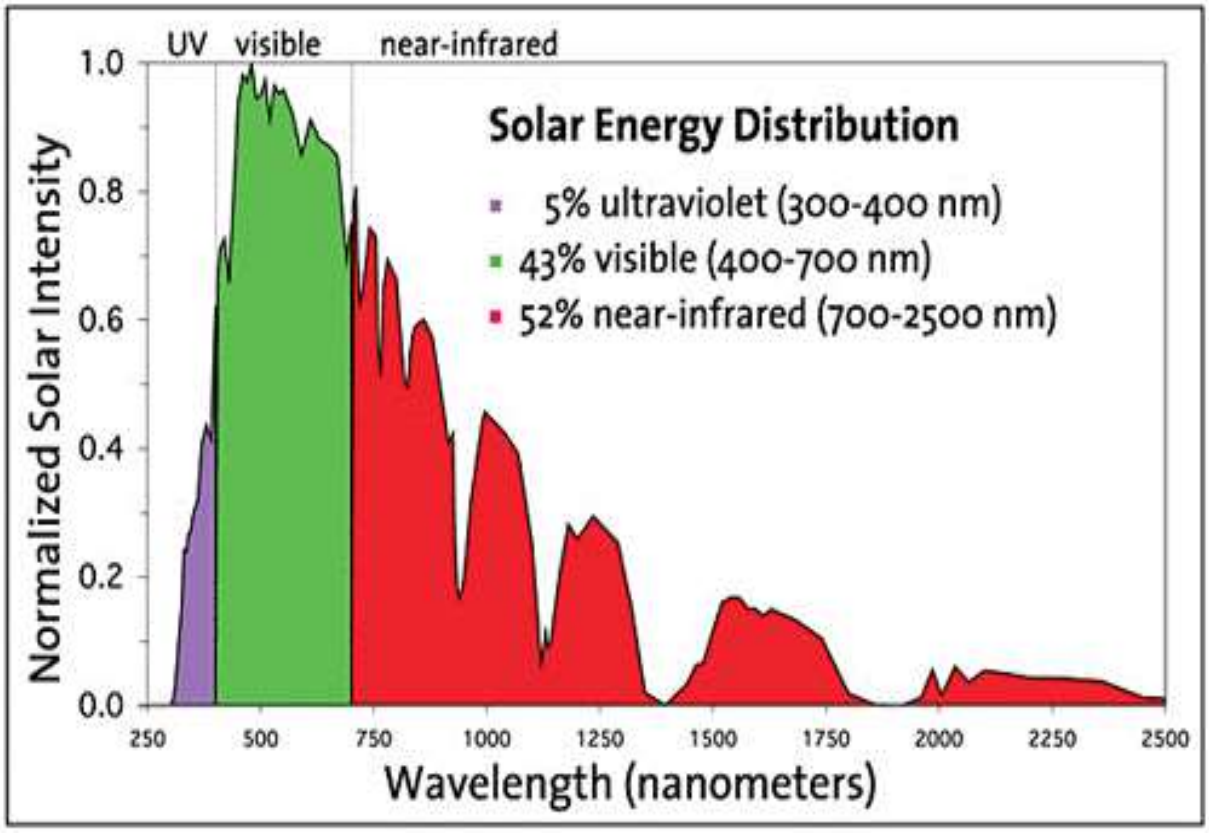

Figure 1- 1: A spectrum of solar radiation.[7]

1.2. Nanoparticles (Quantum Dot–Sizes)

Nanotechnology involves small objects that act as whole units in terms of their characteristics and transport mechanisms.[8] Nanopowders are agglomerates of ultrafine particles, nanoparticles, or nanoclusters.[8, 9] Nanoparticles are particles with a diameter of less than 100 nm; nanoclusters have at least one dimension between 1 nm and 10 nm.[8-10]

Nanotechnology has produced a great deal of interest because nano-sized materials have many new and unusual properties,[8] including new phase transition behaviours, electronic and magnetic characteristics, mechanical properties, surface activity, catalysis, and unusual optical properties.[8] Another interesting property is quantum confinement (quantum indicates reflection of the atomic realm of particles; confinement is when the motion of a randomly moving electron is restricted to specific energy levels), which dominates the movement of electrons and holes in semiconductor materials.[8]

A semiconductor is characterised by a band gap between its VB and its CB, and the band gap depends on the size of the materials (Figure 1-1).[11] As shown in Figure 1-1-a, a valence band consists of a continuum of many energy levels and contains the bonding electrons. Each energy level can accommodate two electrons. In general, the state diagrams of orbital density show that the top and bottom of the band presents a lower density of states. However, the middle of the band contains a higher density of states (indicated by shading).[11] A conduction band lies at higher energies above the valence band, and these bands are separated by a band gap that can differ in size.[11] A solid will show conductivity if electrons are promoted from the valance band to the empty conduction band.[11] These electrons need enough energy to jump the band gap; this energy is often provided by light or heat.[11]

The crystal of the semiconductor converts fewer atomic orbitals, which are available to contribute, into the bands (Figure 1-1-b). In this case, two things happen; first, each band stops to become an orbitals continuum, and then the individual orbitals are revealed. Second, the orbitals are removed from each of the band edges, which leads to an increase in the band gap. At this point, the crystals become quantum dots. Quantum dots are no longer a continuum of orbitals but instead are individual quantised orbital energy levels where the crystal is very small. As a result, as the size of the nanoparticles of most semiconductors decreases, the band gap increases. For example, the band gap of CdSe crystals is around 1.8 eV for crystals 11.5 nm in diameter; however, for crystals with a diameter of 1.2 nm, the band gap is about 3 eV.[11]

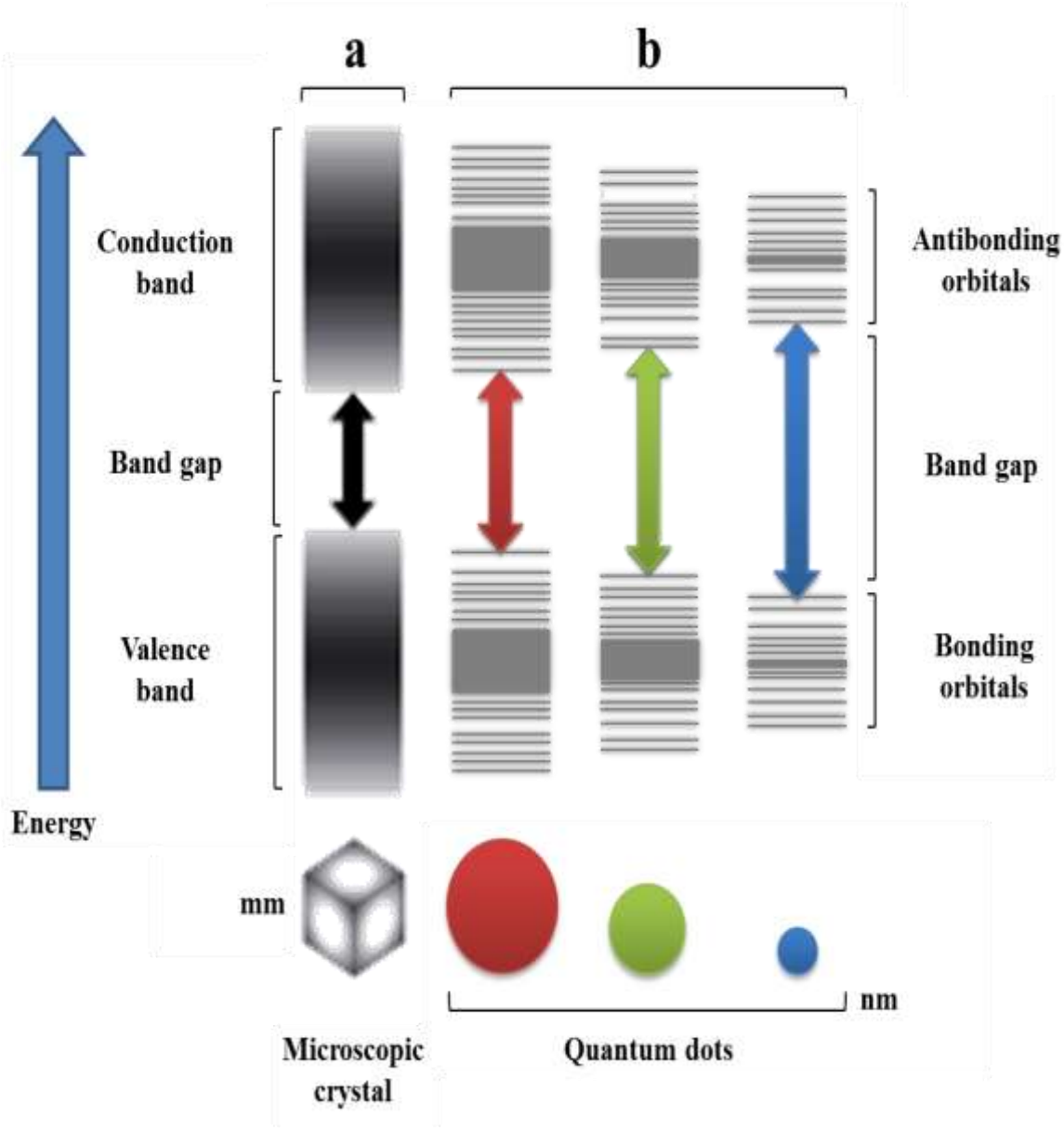

Figure 1- 2: The semiconductor band gap depends on the size of the nanoparticle (redrawn from Smart et al., 2005)[11]

1.3. Band Gap Energy

Bonding and antibonding combinations are generated in a diatomic molecule by combining the atomic orbital of one atom with an atomic orbital of another atom (Figure 1-2).[12]

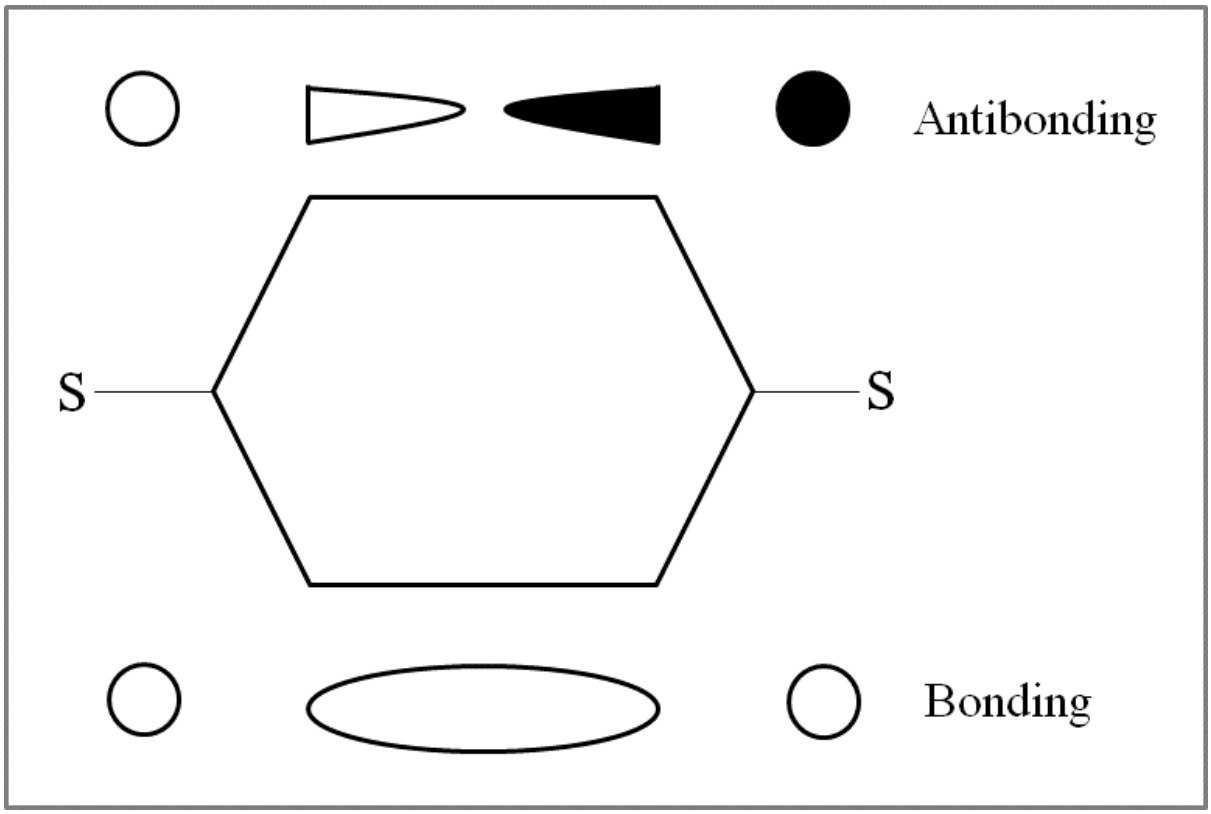

Figure 1-3: Bonding and antibonding combinations of two s-orbitals (redrawn from Dann et al., 2000) [12]

Each atomic orbital generates one molecular orbital, and the extension of this *n* atomic orbital creates *n* molecular orbitals (*n* = 1, 2, 3, …..∞).[12] Bonding (the levels lower energies) and antibonding (the levels higher energies) combinations will be then generated by every pair of orbitals, and these combination levels are separated by non-bonding lines.[12] The separation between bonding and antibonding combinations becomes smaller as the number of atoms is increased (Figure 1-3).

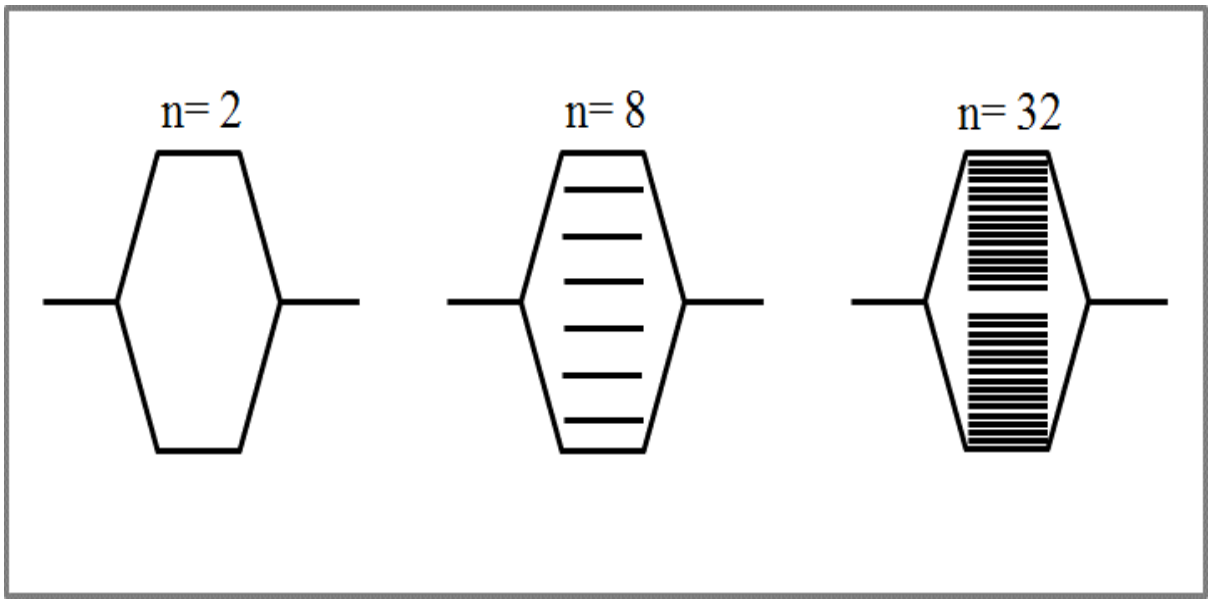

Figure 1- 4: Formation of *n* molecular orbitals from *n* atomic orbitals and the relation between *n* atomic orbitals and nonbonding lines(redrawn from Dann et al.,2000).[12]

For an infinite number of atoms ($n = \infty$), the difference between the molecular orbital energies becomes unnoticeable, so the levels are most suitably drawn as a block to illustrate the continuous band.[12] These bands are separated by gaps where there are no molecular orbitals (known as band gaps; Figure 1-4).[12] Each set of orbitals will create a band by overlapping with the orbitals on neighbouring atoms in the lattice, if the atomic orbitals are large enough.[12, 13] These can result from both unfilled and filled levels. A valence band is the highest energy band that contains electrons, while a conduction band is the lowest energy band above the valence band that remains empty.[12, 13]

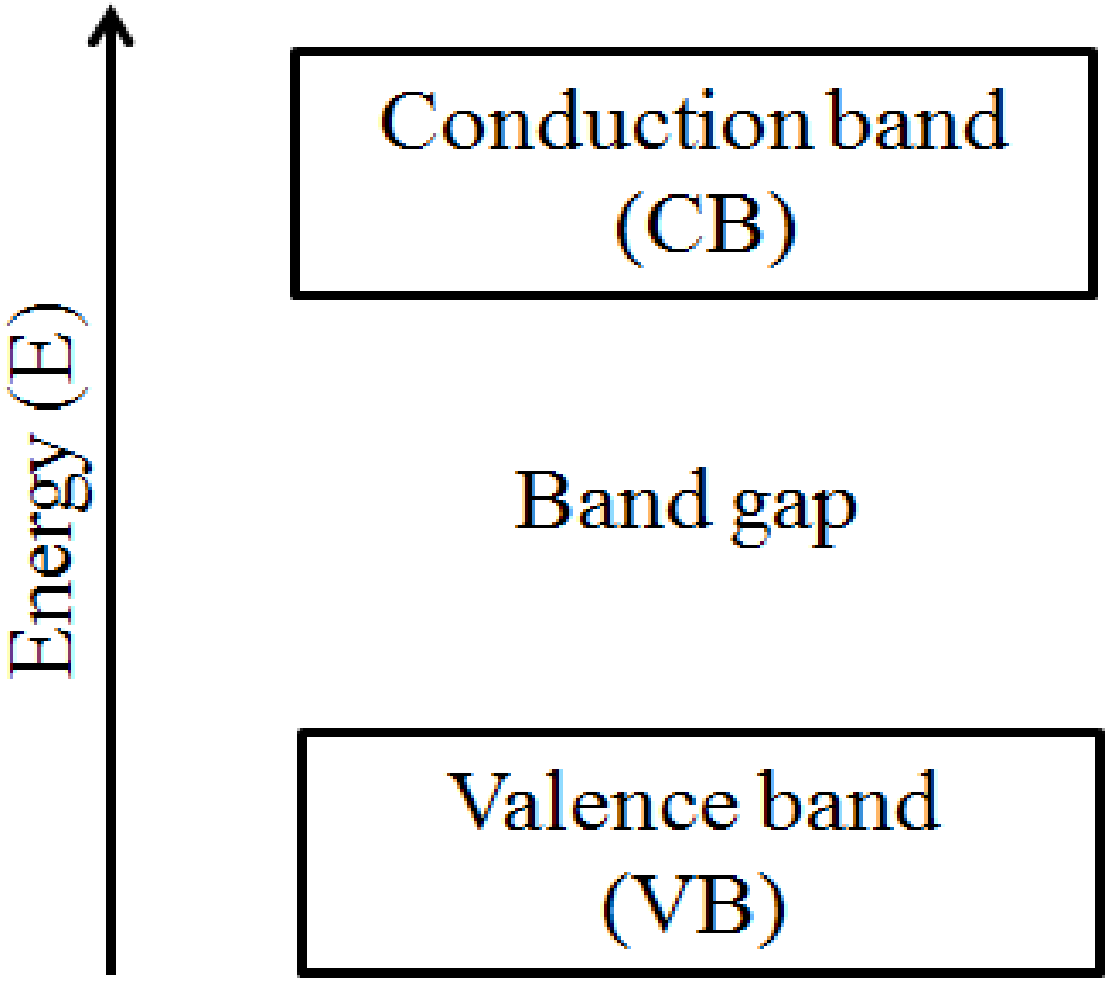

Figure 1- 5: formation of a band gap between the valence band (VB) the conduction band (CB) and for infinite atomic numbers (n = ∞) (redrawn from Dann et al., 2000).[12]

Intrinsic semiconductors are materials that naturally have a small band gap, such as silicon and germanium.[13] The band gap, E_g, in an intrinsic semiconductor is defined as the energy levels between the VB (the highest occupied band) and the CB (the lowest unoccupied band) that are also empty.

The bonding that occurs in metal oxide (MO) semiconductors is different from the bonding that takes place in semiconductors, such as silicon and germanium, whose bonds are

covalent.[14] In silicon, the neighbouring sp^3 orbitals, which are formed by the combination of *3s* and *3p* orbitals, interact to produce a combination of bonding and antibonding orbitals, leading to the formation of VBs and CBs.[14] However, the bonding in MO semiconductors, such as TiO_2, is different because the VBs are either full or partially full of electrons.[14] These electrons are transferred from the oxygen to the metal ion; the electro-negativity of the oxygen is higher than that of the metal.[14] In the case of titanium dioxide, the VB is mainly formed by oxygen-*2p* orbitals, whereas the CB is principally composed of titanium-*3d* orbitals.

There are two electronic transitions from VB to CB: direct transition and indirect transition. Direct transition occurs when the highest energy in the VB and the lowest energy of the CB are found at the same value of the electron wavevector (k). When this condition is met, a photon will have enough energy $E_{bg} = h\upsilon$ to bring an electron across the gap. On the other hand, indirect transition will take place when the maximum energy of the valence band and the minimum energy of the conduction band occur at different values of electron wavevector (k).[14] Therefore, in addition to the energy E_{bg}, there is a requirement for a change in the electron momentum.[14] This change is provided by a phonon, which is a vibration in the lattice. In other words, direct transitions do not need the assistance of a phonon to achieve the transition of electrons from VB to CB. However, indirect transitions do require phonon assistance. Optical transitions in semiconductors with both direct and indirect transitions are illustrated in Figure 1-5.

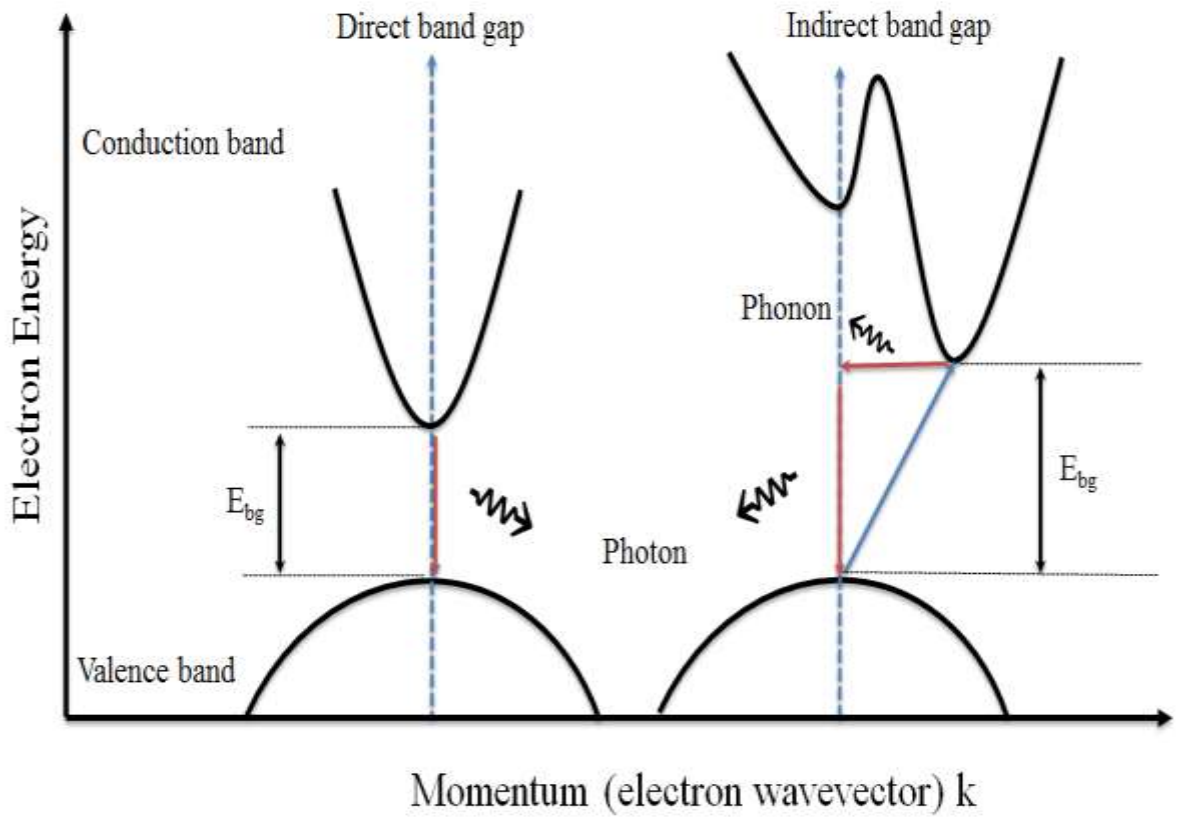

Figure 1- 6: Direct and indirect transitions in semiconductor materials (redrawn from Van De Krol et al., 2012)[14]

A measurement of the absorption coefficient versus the wavelength can determine the band gap of a material. The absorption coefficient in m^{-1}, which is measured when the conduction band bottom and the valence band top have a parabolic shape, is expressed in Equation (1.1):

$$\alpha = \frac{A(E-E_g)^m}{E} \qquad \textbf{(1. 1)}$$

Where α: the absorption coefficient; A: a constant that depends on the properties of the material; E: the photon energy; E_g: the band gap; m: a factor dependent on the nature of the optical transition; $m = 1/2$ for a direct band gap and $m = 2$ for an indirect band gap. An indirect band

gap is calculated by plotting $(\alpha hv)^{0.5}$ vs. hv; however, a direct band gap is determined by plotting $(\alpha hv)^2$ vs. hv. This plot is called a Tauc Plot and is used in both photo-electrochemistry and photocatalysis.

1.4. Absorption Spectroscopy and Compound Colours

In general, colours result from only a portion of the visible spectrum being absorbed and then transmitted or reflected such that those frequencies are not absorbed through our eyes to produce the sensation called colour.[15] Therefore, compounds appear to be coloured because they absorb some wavelength of visible light and transmit or reflect others.[15]

A coordination compound, ML_6, appears orange in colour, while a coordination compound, ML'_n, looks purple M = M, L ≠ L′, and n = or ≠ 6 (M = metals, L = Ligands, and n = number of ligands).[15] Figure 1-6 shows that the ML_6 compound reflects or transmits orange to our eyes; thus, it absorbs the higher frequencies. On the other hand, the ML'_n compound reflects or transmits a purple colour to our eyes; thus, it would appear to absorb lower-frequency visible light (Figure 1-7).[15]

According to the equation of energy absorbed $E = hv$, which was first proposed by Max Plank,[15] a higher frequency (v) leads to a higher energy (E). Consequently, the ML_6 compound showed a greater difference between the energy levels than that of the ML'_n compound.[15] These energy levels are allocated to the various degenerates of d orbitals sets, which lead to coordination compounds and the key of the colours of these compounds.[15] The energy levels are responsible for visible light absorption, and then the colour is presented.[15] In other words, the presence of a ligand field leads to the difference in the energies of various sets of d orbitals, and then the light of frequencies is absorbed.[15]

The difference in the colours of the ML_6 and ML'_n compounds might be due to a change in the geometry of the crystal field from octahedral field to a tetrahedral field.[15] The energy difference between sets of *d* orbitals is normally smaller for a tetrahedral field than it is for an octahedral field.[15]

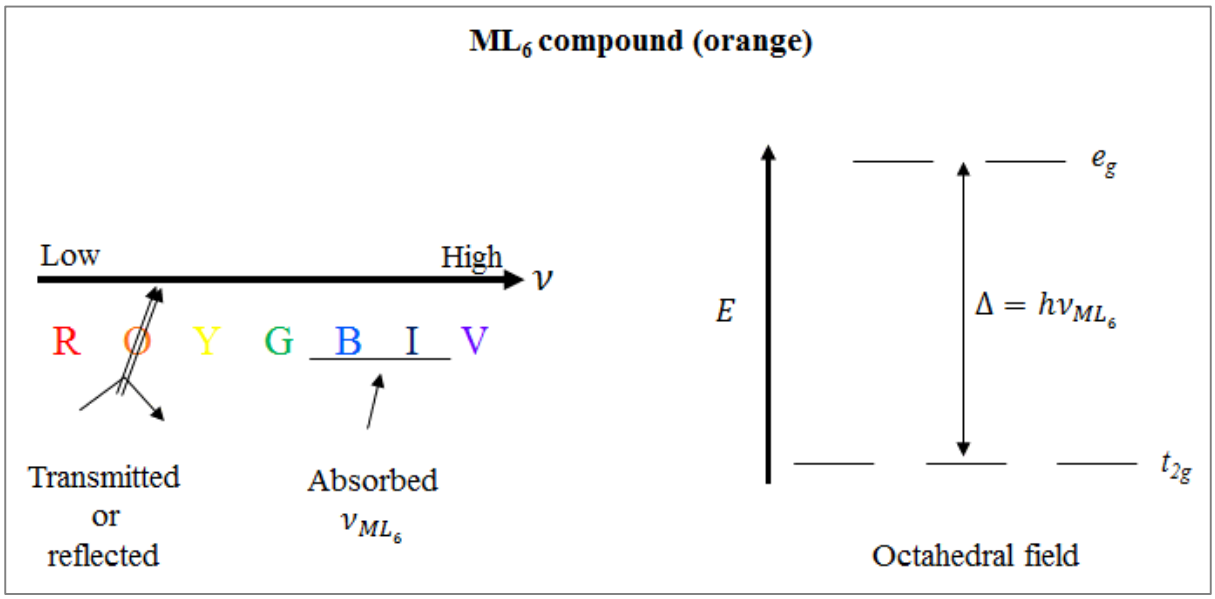

Figure 1- 7: Hypothetical coloured coordination compound of ML_6. It absorbs higher frequencies and transmitters or reflects lower frequencies of visible light and appears orange in colour. The absorbed frequencies could be due to the large difference between the degenerate sets of *d* orbitals in the octahedral field. The letters "ROYGBIV" are related to the colours of visible light from lowest to highest frequencies (Redrawn from Rodgers, 1994). [15]

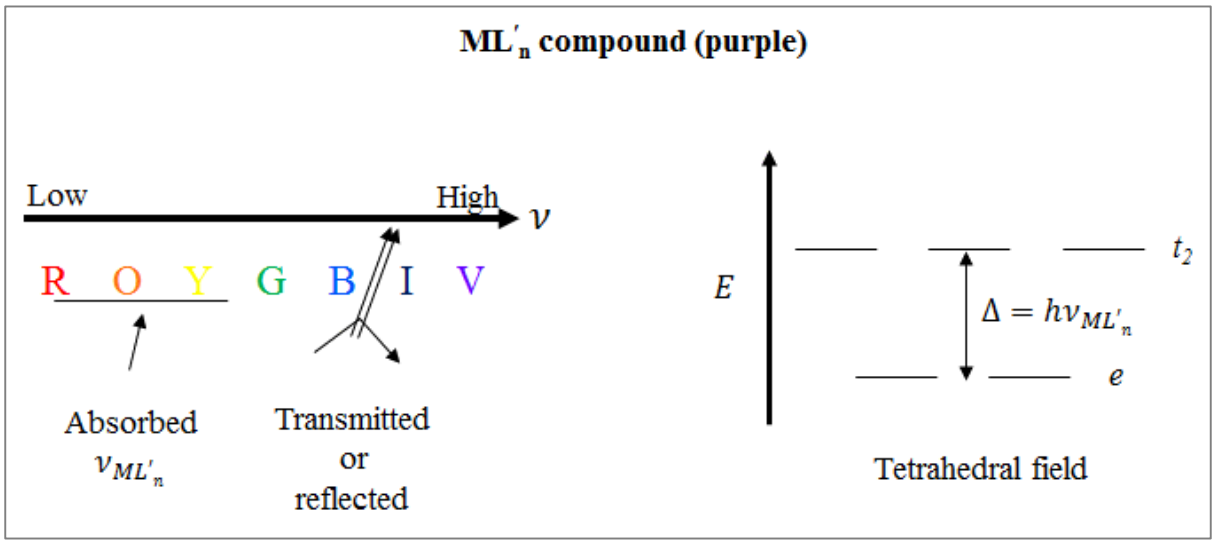

Figure 1- 8: Hypothetical coloured coordination compound of ML′n. It absorbs lower frequencies and transmitters or reflects higher frequencies and appears purple in colour. The absorption of lower frequencies could be due to the small difference between the degenerate sets of *d* orbitals in the tetrahedral field. The letters "ROYGBIV" are related to the colours of visible light from the lowest to the highest frequencies (Redrawn from Rodgers, 1994).[15]

1.5. Titanium Dioxide, Titanium (IV) Oxide, or Pigment White

This section will present information about titanium dioxide gathered from the current literature, including synthetic methods, a description of its structure and polymorphs, and its importance and applications, with a focus on photocatalysis.

In the hunt for methods that harness solar energy, photocatalysis (which is dependent upon semiconductors as catalysts) has become increasingly significant.[16, 17] Titanium dioxide has a molecular weight of 79.88 g/mol and the chemical formula TiO_2; it is an ideal semiconductor photocatalyst that was first produced commercially in 1923.[18, 19] The titanium dioxide is sometimes called titanium white,[20] and is extensively used in technology applications as a pigment.[21-23] In the formula TiO_2, the outer *d* configuration of the titanium is $d^0$and the

oxidation state is *+4*. The TiO_2 has many outstanding properties.[3, 24] It is inexpensive and non-toxic, it displays high efficiency and oxidative power in terms of the photocatalytic degradation of damaging pollutants and it is stable in both water and air. Thus, it is seen as the optimal semiconductor photocatalyst.[3, 24]

There are different polymorphs for TiO_2; however, the most commonly used are anatase, rutile, and brookite. The coordination number is *CN = 6* for titanium and *CN = 3* for oxygen in TiO_2. Each titanium atom in TiO_2 is coordinated by six oxygen atoms to form TiO_6 in an octahedral configuration, and the stacking of this octahedral configuration in all phases of TiO_2 produces three-fold, coordinated oxygen atoms. However, the structural unit of TiO_6 also occurs with different arrangements. Rutile shows the smallest unit cell. Its structure is simple (primitive) with a tetragonal space group $P4_2/mnm$ and lattice parameters $a = b \neq c$.[25-28] The TiO_6 octahedra are connected in the rutile phase by contributing an edge along the *c-axis* to produce chains, which are then interlinked by sharing the corners of oxygen atoms to form a three-dimensional (3D) framework.[8, 28] Brookite shows a primitive structure with an orthorhombic space group, *Pbca*, and lattice parameters $a \neq b \neq c$. The brookite polymorph is rare compared to the rutile and anatase ones.[25-27] Additionally, its cell volume is larger than both rutile and anatase, and both the corners and the edges are shared by octahedra TiO_6.[8] The anatase crystallizes in a body-centred tetragonal unit cell, *I*, and its phase TiO_6 octahedral formations share four edges that produce zigzag chains.[8] In summary, the anatase structure consists only of edges sharing TiO_6, whereas the rutile and brookite phases share both edges and corners.

Some data for the unit cell of the three polymorphs are included in Table 1-1, and their structures are shown in Figure 1-8.

Table 1- 1: Unit cell parameters, space groups, and JCPDS reference code for rutile, anatase, and brookite.

TiO_2	Rutile	Anatase	Brookite
a (Å)	4.5933	3.7852	5.4558
b (Å)	4.5933	3.7852	9.1819
c (Å)	2.9592	9.5139	5.1429
Space Group	$P4_2/mnm$	$I4_1/amd$	Pcab
JCPDS*	00-021-1276	00-021-01272	00-029-1360

*Joint Committee on Powder Diffraction Standards

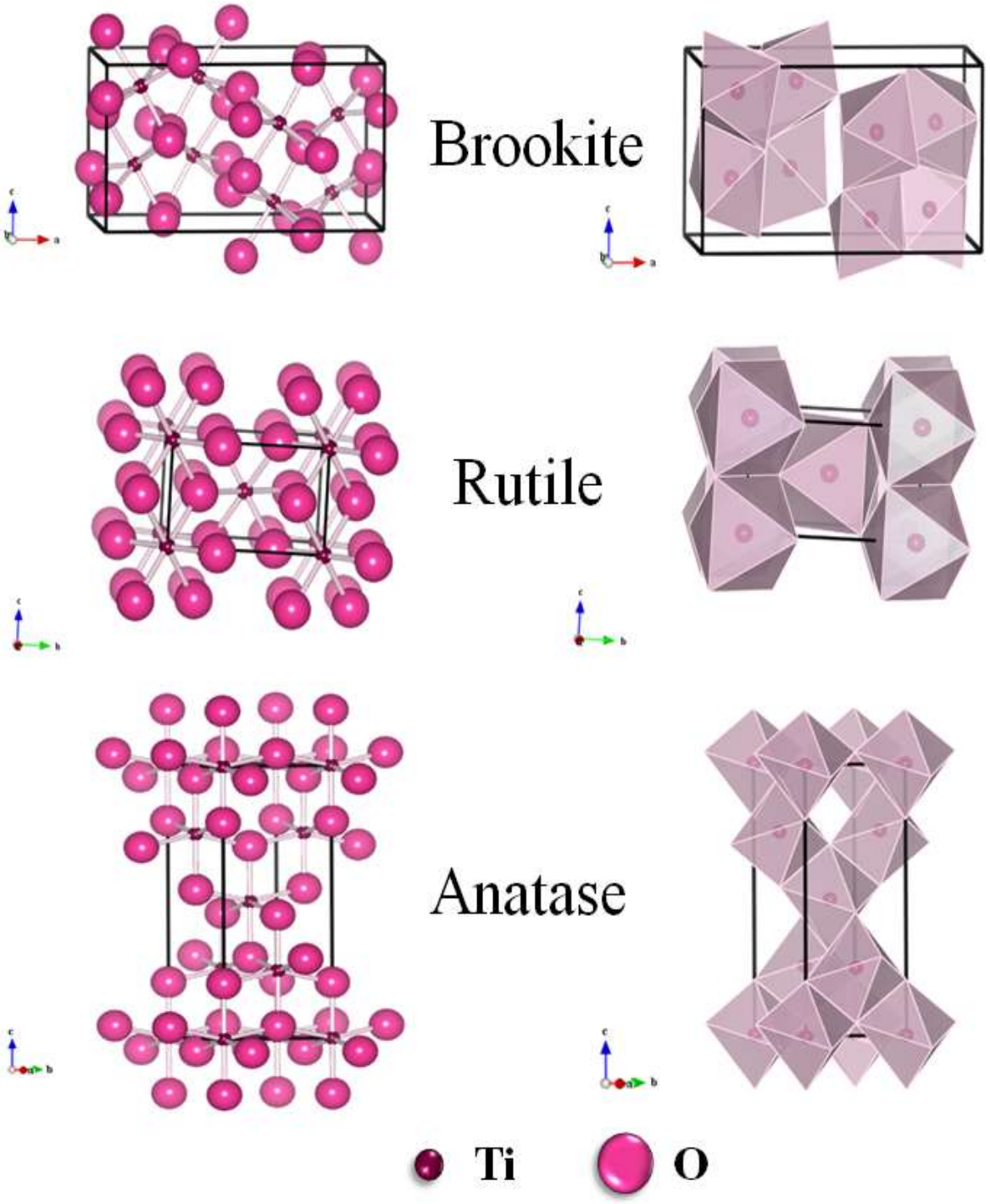

Figure 1- 9: **Crystal structures of rutile, anatase and brookite. Image was created using VESTA software.**

For photocatalysis applications, the anatase and rutile phases have more desirable properties than brookite.[8] The rutile polymorph is also more thermally stable at high temperatures,[29] although the anatase polymorph, which is produced at lower temperatures,[18] exhibits the highest photocatalytic activity.[27] Both the anatase and rutile phases are poor absorbers of solar light due to their band gaps of 3.2 and 3.0 eV, respectively.[30-33] Anatase can be transformed into rutile when heated at $T > 600\ ^{\circ}C$.[24, 34] The transformation from anatase to rutile involves an overall reduction of the oxygen structure and a movement of ions so that a cooperative rearrangement of the Ti^{4+} and O^{2-} ions occurs.[30] Additionally, Zang and Banfield (2000), reported that decreasing the particle size (<11 nm) renders the anatase phase the most thermodynamically stable. Increasing the particle size to 35 nm allows the brookite phase to be more thermodynamic stable, while increasing the size to > 35 nm makes the rutile phase most stable thermodynamically.[35]

1.5.1. Anatase as a Photocatalyst

1.5.1.1. Ultraviolet Active Anatase

A general explanation of ultraviolet (UV) active titanium dioxide is included in this section. Anatase TiO_2 is a semiconductor with a band gap of 3.2 eV. Upon excitation by light of a wavelength less than or equal to 385 nm (greater than or equal to 3.2 eV), the photon energy that is absorbed by TiO_2 creates electron–hole pairs.[32] The light absorption results in electrons being promoted from the valence to the conductance band, generating a hole ($h_{VB}{}^{+}$) in the VB and an electron ($e_{CB}{}^{-}$) in the CB.[36-39] The reaction between the hole and water (H_2O) or hydroxide ions (OH^-) adsorbed on the surface of the VB can produce hydroxyl radicals ($OH^{\bullet}$),[32, 40] which can easily oxidise any organic groups to carbon dioxide (CO_2) and H_2O. The

CB quickly lowers the oxygen levels to create the superoxide anion (O_2^-) as it has no hole allowing it to recombine with the electron.[41] The hydroxyl radical can then be reformed when this superoxide anion reacts with water.[41]

The creation of a hole–electron pair in TiO_2 is characteristically initiated by the absorption of UV light (Figure 1-9), and only a small fraction of solar light can be absorbed because of the large band gap of 3.2 eV in the anatase. Therefore, there are many challenges in producing anatase titanium dioxide with smaller band gaps because it is difficult to shift its absorption from the UV-region to the visible region.[42]

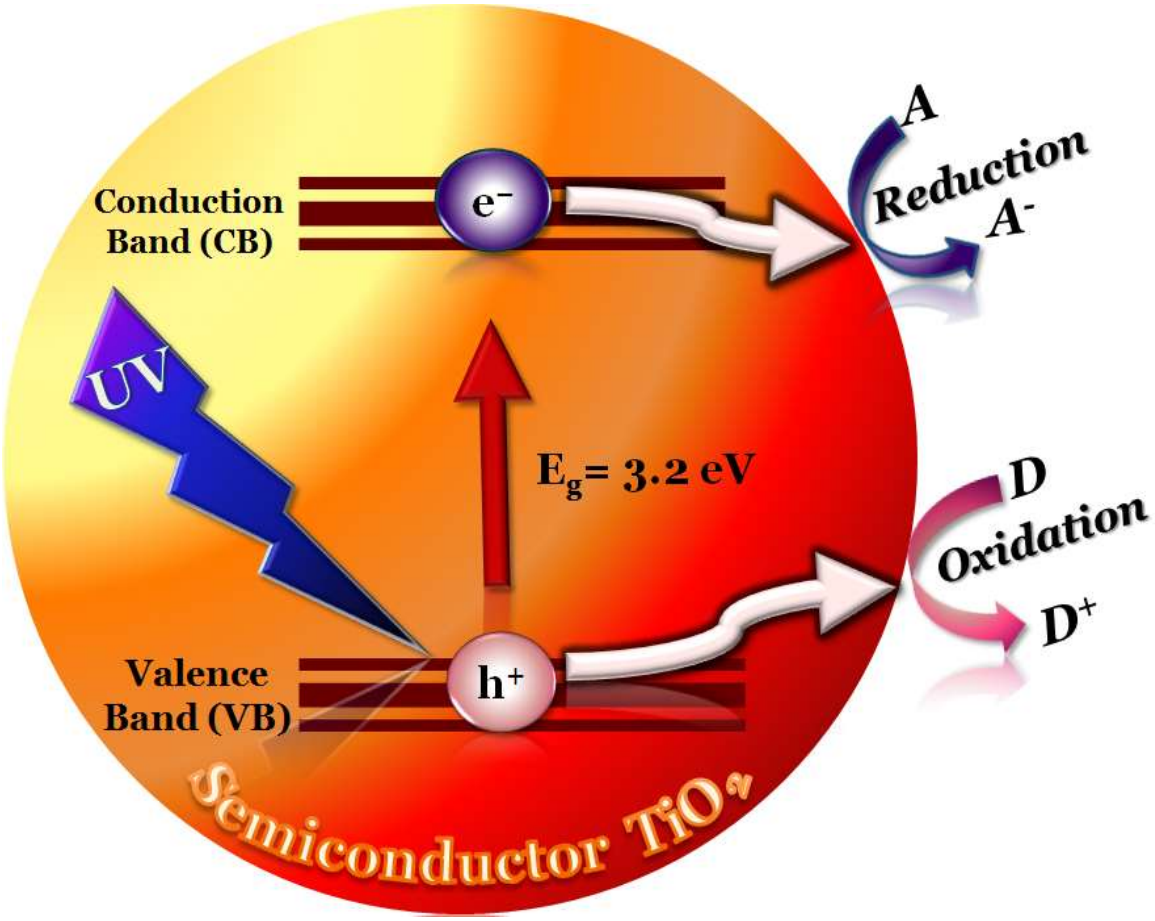

Figure 1- 10: Schematic of TiO_2 anatase in a photocatalysis reaction that absorbs under UV-light

1.5.1.2. Visible Light-activated Anatase

The main strategies presented in the literature to create visible light-activated anatase include the replacement of titanium with the metals Ni, Fe, and Cr or the formation of Ti^{3+} by the creation of oxygen vacancies.[43] Because these two strategies produce a reduction in chemical stability and reproducibility, they were not extensively recommended.[43] Anion-doping of TiO_2 is considered a good method to produce TiO_2 that is sensitive to visible light. The high photoreactivity of anatase makes it a popular choice for photocatalysis. Rutile, with its effective light scattering, is primarily used for pigments.[43] It is also known that anatase titanium dioxide becomes thermodynamically more stable than rutile in small crystallites at particle sizes less than 14 nm; [44, 45] doping titanium dioxide aims to produce a stable structure with a narrower band gap and a higher absorption of visible light. The introduction of non-metal anions N,[46, 47] C,[48, 49] S,[46, 50] F,[51, 52] B,[53] P,[54, 55] and I[56] in titanium dioxide was found to be an efficient method to increase photocatalytic activity under visible light irradiation.[30, 57-59] This project focused on anionic-doping using nitrogen and sulfur. The reason why anionic doping is less commonly found in studies can be explained by the fact that it seems to be far more complicated to replace the O^{2-} anions than to substitute the Ti^{4+} atoms with other cations.[60] Bigger differences in the charge states of different anions and in ionic radii are believed to be the cause of this.[60] Anion doped semiconductors may also be less common due to their synthetic challenge.[60]

Anion doping is believed to narrow the band gap of TiO_2 by combining the anion orbitals of the substituting anion with the oxygen *2p* orbital.[43] This mixing with the valence band of oxygen occurs with the introduction *2p* orbitals of N and a narrowing band gap in the case of N/O substitution. A S/O substituting anion can narrow its band gap by mixing the *3p* orbitals of sulfur with the *2p* orbitals of oxygen. A summary of N-doped and S-doped titanium dioxide is illustrated in Figure 1-10.

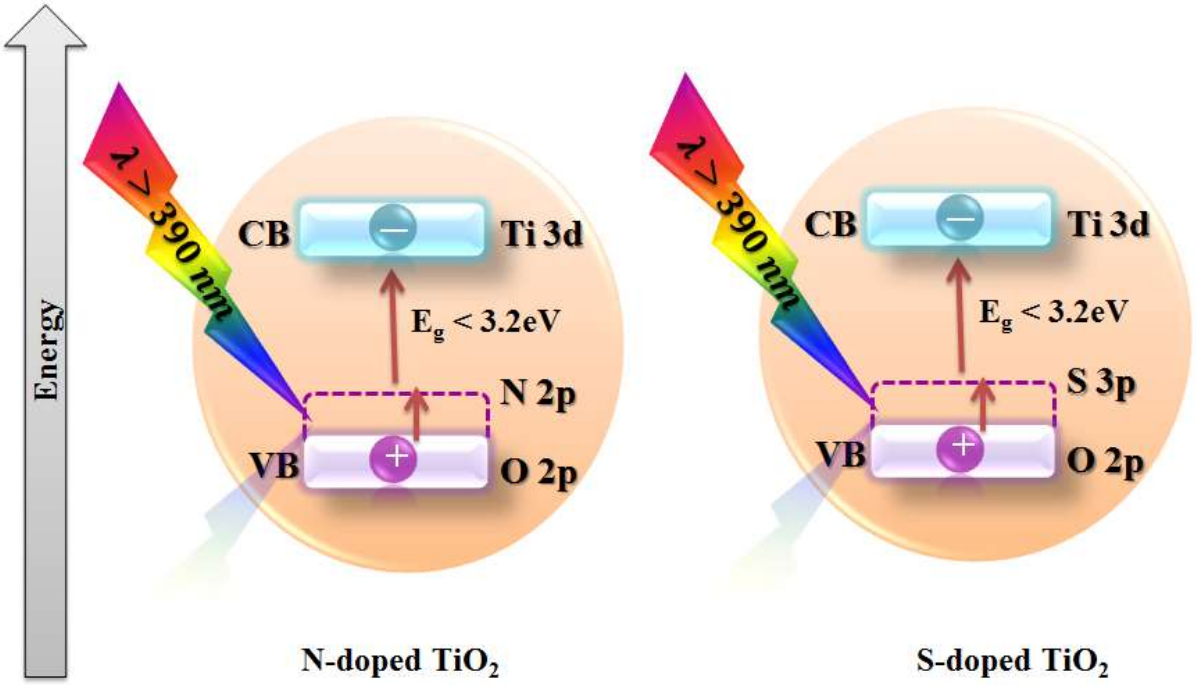

Figure 1- 11: Schematic of TiO_2 photocatalyst absorption under visible-light.

In general, the activity of the visible light responsive to photocatalysis absorption is affected by factors such as crystal size and surface area. Thus, using high temperature synthetic methods will produce an increase in crystal size with a decrease in surface area followed by a reduction of the anion-doping quantity, which subsequently leads to a reduction of the absorption of visible light.[61]

1.5.1.3. Oxygen Vacancies

Oxygen vacancies (OV) are created by the direct loss of oxygen to maintain charge neutrality when titanium dioxide is calcined in a reducing atmosphere and/or a low partial oxygen pressure environment, such as hydrogen gas or ammonia.[62] The oxygen vacancy is classified as the greatest defect of titanium dioxide, as well as many other metal oxides, and its formation may induce donor levels in the electronic structure.[63] The reason OV is classified as an important defect in TiO_2 is because oxygen vacancies affect the physical and chemical properties of metal oxides.[63] Moreover, the defect influences the photocatalytic properties of TiO_2, such as surface properties, electronic structure, and charge transfer.[63] A Ti^{3+} is created by the formation of oxygen vacancies in the TiO_2.[63] It is believed that oxygen vacancies (OVs) cause changes in the chemical rates that are reliant on the charge transfer from either the holes or the electrons; thus, they have an effect on the electron-hole recombination process in photocatalysts.[63] The surface absorption and absorbent reactivity (e.g. oxygen, water) on TiO_2 are affected by the excess electrons found in the OV states.[63] The electrons found in the oxygen vacancy states form a donor level with energy ranging from 0.75 eV to 1.18 eV below the CB and, because of this, they have a direct effect on the electronic structure of TiO_2.[63] The formation of OVs in the TiO_2 lattice typically occurs alongside the doping of the metal or non-metal ions.[63]

Doping with metals at lower valence cations (eg. M^{3+}) can occupy Ti^{4+} positions and present oxygen vacancies, preventing the formation of Ti^{3+}.[63] On the other hand, doping with higher valence cations (e.g., M^{5+}) that occupy Ti^{4+} positions produces Ti^{3+}, preventing the formation of oxygen vacancies.[63] Chauke et al. (2010) investigated the structure of Ti-doped zirconia surfaces by applying density functional theory calculations, and they found that oxygen vacancies were formed.[64] Their analysis of the electronic structure of the doped and reduced

surfaces revealed that the oxidation state of Ti will be reduced from Ti^{4+} to Ti^{2+} if an oxygen vacancy is formed around an isolated titanium dopant.[64] On the other hand, the oxidation state of Ti will be reduced from Ti^{4+} to Ti^{3+} if the oxygen vacancy is produced in the neighbourhood of a pair of dopants (each of the titanium atoms adopts a Ti^{3+} oxidation state).[64]

Doping with non-metals, such as nitrogen, will create oxygen vacancies on the titanium dioxide lattice.[63, 65] The occurrence of oxygen vacancies or N-doping was the result of removing or replacing one O atom in the TiO_2, resulting in TiO_{2-x} or $TiO_{2-3x}N_{2x}$.[66-68] Heating pure titanium dioxide at temperatures greater than 400 ˚C in an oxygen-poor environment, for example, with argon (Ar), nitrogen (N_2), or helium (He) gases, or in vacuum conditions can help to create oxygen vacancies.[63] Electronic structure and valence states in mono-doped titanium dioxide were studied by Xi et al. (2014).[69] They found that both anion mono-doped TiO_2 (the substitution of oxygen with e.g., C^{4-} or N^{3-} or S^{2-}, etc.) and cation mono-doped TiO_2 (the substitution of titanium with e.g., C^{4+} or N^{3+} or S^{6+}, etc.) produced vacancies.[69] In theory, the substitution of an element with a different charge (i.e., oxidation state) causes an imbalance of charge, which then forms a crystallographic point defect, such as a titanium or oxygen vacancy.[69] Xi et al. (2014) checked the condition of (S) cation-doping TiO_2, and they suggested that the S dopant exists as an S^{6+} ion and limits the formation of OVs.[69]

In general, oxygen vacancies are believed to be more likely to affect conversion from the anatase to the rutile phase.[62] Increasing the temperature to more than 550 ˚C was favourable for raising the OV concentration, which decreased the thermal stability of TiO_2.[62] The dopant had as beneficial effect on raising the photocatalyst's lifetime by adding oxygen vacancies, changing the titanium dioxide structure, and modifying the electronic properties.[70]

1.5.1.4. Applications of Titanium Dioxide

The nano-material titanium dioxide has a wide variety of possible applications, such as in a dye-sensitized solar cell.[8] It can be used for hydrogen production, as in the photocatalytic splitting of water, or it can be employed for sensing humidity, ammonia, and oxygen.[8] TiO_2 has been used in lithium ion batteries and poly-aniline/titanium dioxide composite in rechargeable batteries,[8] for controlled drug release, in photocatalytic cancer cell treatment, and to treat reservoirs with temozolomide (TMZ).[8] Further application includes electro-catalysis, such as the electro-catalysis of methanol and electrochemical wastewater treatment,[8] and it is also used for self-cleaning and antibacterial or fogging activity in residential areas, road construction, vehicles, hospital air cleaning, and glass self-cleaning.[8,27]

Nowadays, this semiconductor has been studied extensively as a possible photocatalyst for environmental contamination, water- and air- decontamination, and wastewater and hazardous waste control[27] due to its efficiency in removing organic pollutants, low cost,[71] photo-stability, non-toxicity and widespread availability.[72]

1.5.1.5. Previous Works of TiO_2 Preparations

The preparation of anatase TiO_2 holds great attention for many researchers, and there are several different ways to prepare anatase titanium dioxide. The majority of these methods, some of which are complex, use alcohols, acidic chemicals, or autoclave pressure vessels in their reactions. However, the method used in this study was simple and inexpensive and involved only a small amount of water and titanium (IV) isopropoxide. Additionally, this study used the tube furnace for heating. Titanium isopropoxide was used in this work because it is

commonly used as a precursor for the TiO_2 preparation and also it has low cost. Previous work on synthetic titanium dioxide is summarised in the following paragraphs.

Different studies have synthesised TiO_2 using titanium (IV) isopropoxide. Beusen et al. (2007) reported the possibility of synthesizing anatase titanium dioxide in one step using a pressure vessel.[73] They mixed titanium isopropoxide with a large amount of distilled water in a pressure vessel at 100 °C and 200 °C for 2 hours and 24 hours, respectively.[73] In 2003, Chae et al. calcined the precipitate from the reaction of titanium isopropoxide in an acidic water/ethanol solution at 240 °C for 4 hours.[74] Qourzal et al. (2004) prepared anatase titanium dioxide through a calcinated mixture of titanium isopropoxide, distilled water, and HNO_3 at 400 °C.[75] A sol-gel technique, which involved a reaction of $Ti(OR)_4$ with water and alcohol,[76] a process that was subsequently modified by a supercritical seed crystallization (SSEC) process, was also previously reported.[77] Anatase nanopowder titanium dioxide was prepared in supercritical CO_2 with seeding material added at 100 °C and with reaction times from two to eight hours.[77] Anatase titanium dioxide nanopowder was prepared by Mahshid et al. (2007);[78] their method was by hydrolysis of two solutions a solution of titanium isopropoxide and isopropanol mixed with a solution of distilled water and HNO_3 or NH_4OH, which was then heated from 200 °C to 800 °C for 2 hours and dried at 100 °C for 3 hours in a vacuum system.[78] They found that a pure anatase powder was obtained from a solution at pH 2 at temperatures between 100 °C and 400 °C; on the other hand, the rutile phase was formed by increasing the temperature from 600 °C to 800 °C.[78] Ismagilove et al. (2009) reported that the nanocrystalline anatase phase was prepared by dissolving titanium isopropoxide in an organic solvent, mixing it with acetylacetone and heating it to 450 °C.[79] Anatase TiO_2 powder was produced by calcining titanium isopropoxide, water, and isopropanol at 60 °C for 2 hours (Ang et al, 2010).[5] Collazzo et al. (2011) also observed that a pure anatase TiO_2 nanopowder with a high surface area was produced using the hydrothermal method.[80] They heated a mixture of titanium isopropoxide,

water, and glacial acetic acid at 150 ˚C and 200 ˚C with reaction times from 6 to 36 hours,[80] and found that increasing the temperatures and the reaction times led to an increase in the size of the crystallite and a decrease in the surface area of anatase TiO_2.[80]

Other studies have synthesised TiO_2 without titanium (IV) isopropoxide. Anatase titanium dioxide was prepared by heating a mixture of $TiCl_4$, H_2SO_4, water, and NaOH at 500 ˚C for 6 hours.[33] Nanocrystalline anatase TiO_2 was prepared by heating a yellow solution of $TiCl_4$, ethanol, and anhydrous benzyl alcohol at 80 ˚C for 9 hours, as reported by Wang et al.; (2007).[81] Ranade (2002) produced anatase titanium dioxide by heating a mixture of $(NH_4)_2Ti(OH)_2(C_3H_5O_3)_2$, cetyltrimethylammonium chloride (CTAC), and water at 350 ˚C for 2 hours.[29] Yin et al. (2002) synthesised a pure anatase TiO_2 nanocrystallites with a size rang of 2-10 nm.[82] They heated a mixture of $TiCl_4$, citric acid, and water in a Teflon-lined autoclave for 4 hours at temperature 220 ˚C.[82] A mixture of tetra isopropyl titanate, water, and ethanol was heated at 90 ˚C for 3 hours to produce anatase titanium dioxide by Guo et al.; (2003).[27]

1.6. N-modified TiO_2

Currently, the challenge technique for the use of solar energy is semiconductor photocatalysis. Titanium dioxide has chemical stability and high activity under ultraviolet light, so it has been widely investigated as a photocatalyst.

Anatase is the most commonly used polymorph of TiO_2 in photocatalysis. It has a large band gap around 3.2 eV. This band gap allows titanium dioxide to use just 3% of solar radiation for photochemical reactions.[64] Moreover, TiO_2 absorbs a smaller part of the solar spectrum around < 390 nm,[83] which is in the UV-region. Shifting the activity of the TiO_2 from the UV-region to the visible-region, which composes the largest part of solar radiation, is the main research focus

on semiconductor photocatalysis. A strategy used to meet this objective is doping TiO_2 with a non-metal, such as nitrogen (N). The advantages of N are that it is a non-toxic dopant,[83] has similar properties to oxygen, and can increase visible light activity by encouraging the formation of crystal lattice imperfections.[64] Mitroraj and Kisch (2010) reported that due to not knowing whether the species of the nitrogen was a dopant in titanium dioxide or just a modification on the surface of titanium dioxide, the nomenclature should change from "N-doped" to the general term "N-modified".[64] The band gap of titanium dioxide is narrowed by mixing the 2*p* states of the N with the *2p* states of oxygen, leading to an increase in the valence band (VB) level.[8] This project will use urea and cyanamide as sources of nitrogen.

1.6.1. The Location of Nitrogen Ions within the TiO_2 Lattice

The preparation technique of N-doped titanium dioxide is essential in determining the properties of the final products.[84] Different doping methods form systems with different activities and different sites of N-dopant in the titanium dioxide lattice.[83] Viswanathan and Krishanmurthy (2012) investigated the states and positions of nitrogen in the lattice of titanium dioxide[85] and found that the exact chemical state of the nitrogen dopant and its positions in the titanium dioxide lattice are still unclear.[85] Fittipaldi et al. (2013) suggested that density functional theory (DFT) revealed that there were two ways to introduce nitrogen into TiO_2.[84] The first was the N_i interstitial configuration of nitrogen in which the bond formed between an N atom and an oxygen atom. The other was N_s oxygen substitution, where the bond formed between a nitrogen atom and three atoms of Ti^{4+}.[84] They compared these theoretical calculations with electron paramagnetic resonance (EPR) results and found that both configurations of the N_i and N_s were possible with an agreement slightly better for the N_i

interstitial configuration.[84] However, both of them formed energy states above the VB level[84] (Figure 1-12).

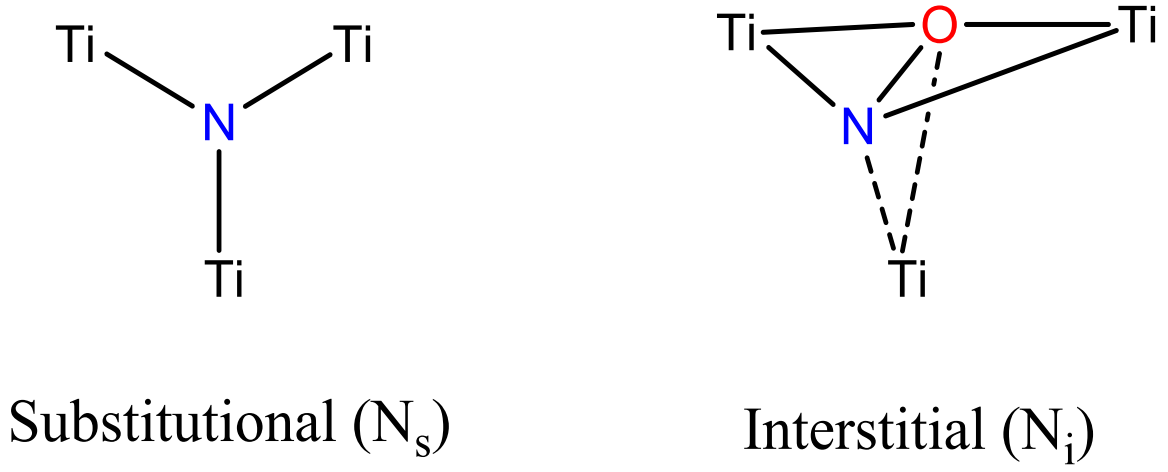

Figure 1-12: Substitutional and interstitial model structures of N-dopant titanium dioxide (anatase phase) (adapted from Fittipaldi et al., 2013).[84]

1.6.2. Decomposition of Urea

In this study, urea was used as a source of nitrogen to prepare N-modified TiO_2, and titanium dioxide was reacted with urea at various temperatures. Ammonia is one of the products of the thermal decomposition of urea.

A study of the thermal decomposition of urea in air at various temperatures by Schaber et al. in 2004 found a series of reactions took place at different temperatures.[86] For example, at a temperature below 190 ˚C, the decomposition and vaporization of urea began to form ammonia and cyanic acid, and the cyanic acid then reacted with urea to produce biuret.[86] Cyanic acid then reacted with biuret to create cyanuric acid (CYA), ammonia, water, and ammelide components.[86] After increasing the temperature to 250 ˚C, decomposition and melting of biuret

yielded urea, cyanic acid, ammonia, CYA, water and ammelide.[86] The production of ammeline, cyanamide, and melamine products started at temperatures < 250 °C. Cyanamide products were produced in this case either by the decomposition of urea or the reaction between ammonia and cyanic acid. Increasing the temperature up to 450 °C induced the CYA, ammelide and ammeline to begin to decompose.[86] A summary of urea decomposition can be seen in Figure 1-13.

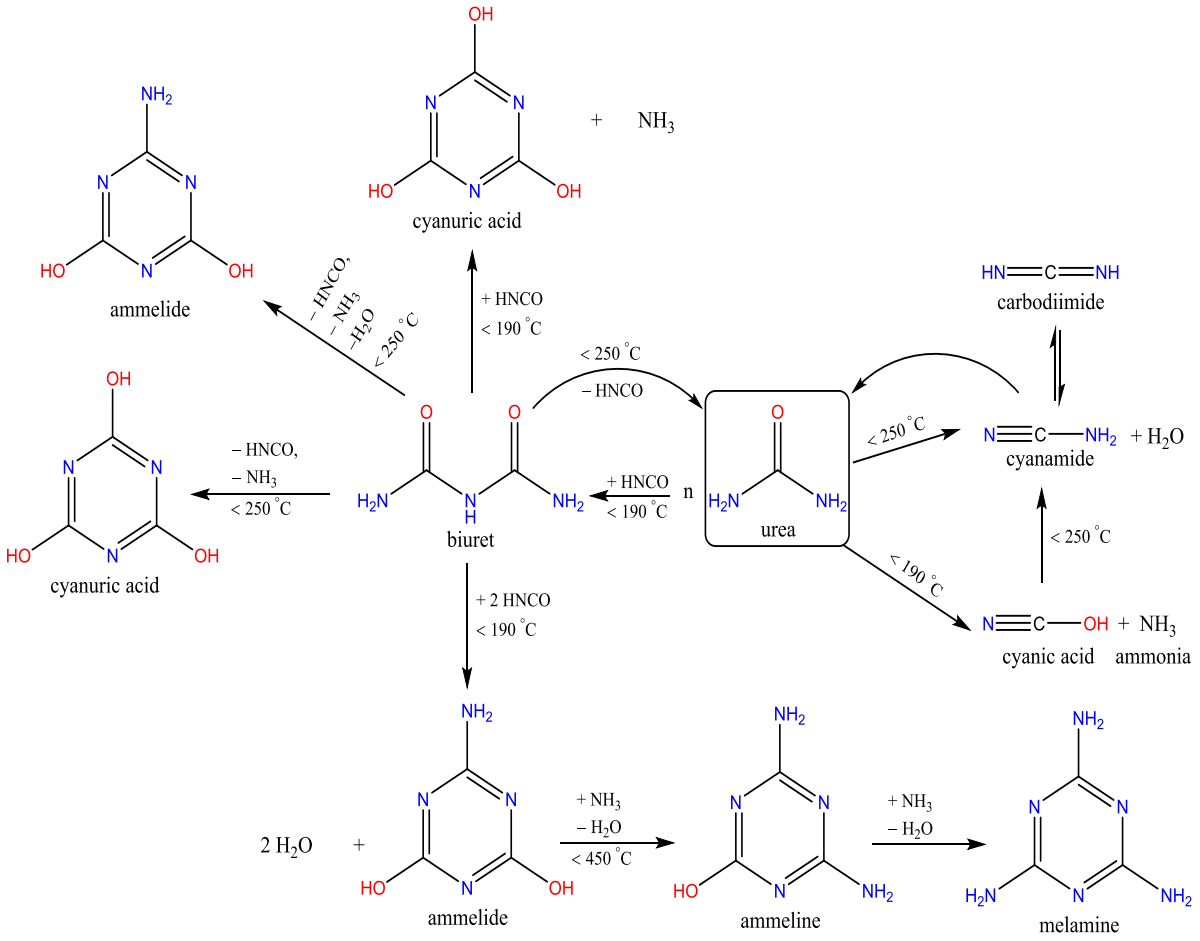

Figure 1- 13: A summary of urea decomposition

Figure 1-14 shows the mechanism of decomposition for urea in two paths as reported by Gao et al. (2012),[87] who found that the decomposition of urea to ammonia and cyanic acid can be induced in one of two ways depending on the hydrogen atom re-binding technique.[87] Through this process, the N–H bond in the amino group is broken, and the hydrogen then bonds with a different nitrogen in another amino group, which at the same time splits with the carbon atom in the carbonyl group.[87] Therefore, this process requires the hydrogen atom to split from one amino group via two possible paths. The first path, or path A, is an indirect transfer process,[87] which is applied by the oxygen atom in the carbonyl group for the transfer of the hydrogen atom H_A from N1 to N2. If, due to the long distance between H_A and N2, a direct transfer is unworkable, then an indirect process takes place. This path has three transition structures—two intermediates and a product complex are components of this reaction procedure.[87] When the bond between H_A and N1 in the amino group splits, H_A bonds with the oxygen atom in the carbonyl group to form the first intermediate product.[87] The H_A approaches the oxygen atom in the carbonyl group and is ready to bond with it. At this point, the electron density is pulled from the C═O bond to the end of the oxygen, changing the double bonds to a single bond between the oxygen and carbon in the carbonyl group and forming a double bond between N1 and C.[87] Because the N atom with a lone pair of electrons is more electronegative than the oxygen in the carbonyl group, the H_A–N1 bond requires more energy to break and to re-bond to oxygen as H_A–O.[87] The process changes from a first intermediate component to a second intermediate component by an endothermic process (7.7 kcal/mol) with a small energy barrier (9.9 kcal/mol) and increases the length of the N2–C bond.[87] The bond between H_A and the oxygen in the carbonyl group breaks, and this hydrogen then bonds with the N2 in another amino group to form a new bond, H_A–N2. This transfer of H_A from oxygen to nitrogen atoms is easier than that from N to O atoms due to the nitrogen atom being more electronegative than the oxygen atom.[87] In this step, the carbon atom re-bonds with the oxygen atom to form C═O

double bonds.[87] The intermediate component will change to its final state, which is a complex component. In this final state, the production of ammonia and cyanic acid is achieved by breaking the bond between C and N2; this last step is exothermic by 14.6 kcal/mol.[87]

The second path, or path B, is a direct hydrogen re-bonding process and is formed when the bond between H_B and N1 breaks and H_B directly bonds with N2.[87] In this path, no intermediate products are created due to the formation of new bonds between C═N1 and between N2–H_B and also because of the splitting of the old bonds between N2–C and N1–H_B, which all occur in one step.[87] Figure 1-14 shows the transition structure and the product complex. In the case of the transition structure, the bond between the H_B and N1 breaks and then H_B rebinds with N2 to form a new bond of H_B–N2. After that, the bond between the nitrogen and carbon atoms completely breaks (N2–C). At this point the hydrogen-bonded product complex is formed and consists of NH_3 and HNCO products.[87] This path is expected to be endothermic by 18.9 kcal/mol, with an energy barrier of 41.8 kcal/mol.[87]

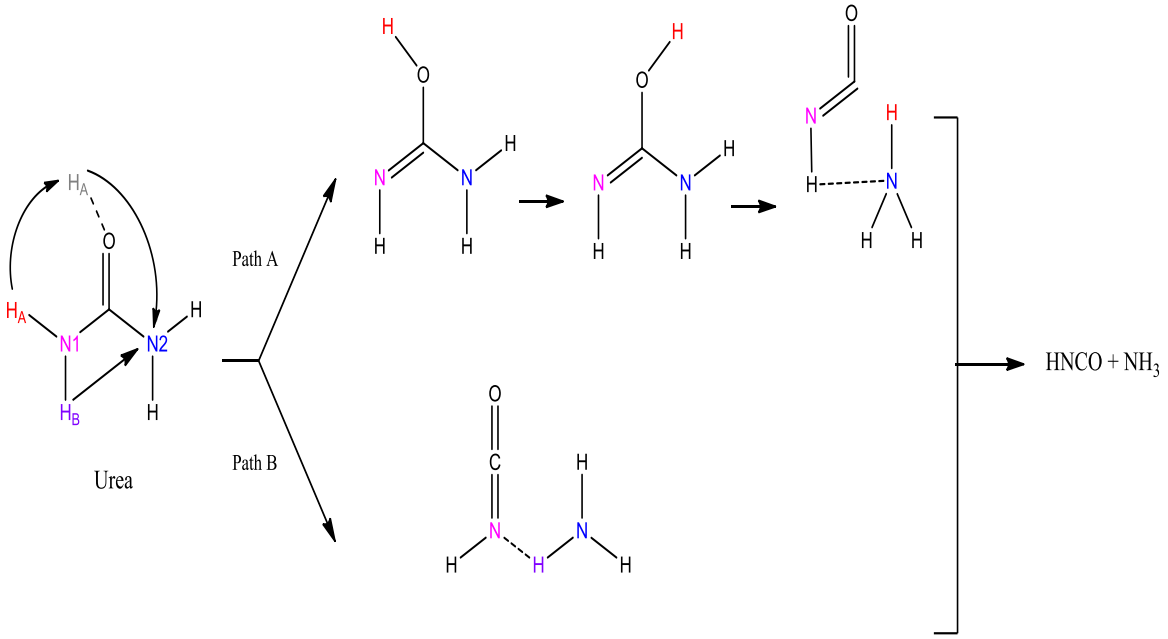

Figure 1- 14: Mechanism of urea decomposition in two paths (redrawn from Gao et al., 2012).[87]

1.6.3. Decomposition of Cyanamide

In this study, cyanamide was used as a source of nitrogen to prepare N-modified TiO_2 under various temperatures. Cyanamide was first prepared in 1838 by mixing ammonia with cyanogen chloride.[88] Cyanamide is now commercially available and cheap.[88] As was reported in 2009 by Wehrstedt et al., cyanamide can dimerize to produce dicyandiamide at temperatures lower than 150 $^{\circ}$C.[88] It can also polymerize to produce trimer melamine by the reaction of cyanamide with dicyandiamide at temperatures higher than 180 $^{\circ}$C.[88] Increasing the temperature to more than 300 $^{\circ}$C produces 1,3,5-triazines melam, melem, and melon from melamine.[88] The decomposition of cyanamide is illustrated in Figure 1-15.

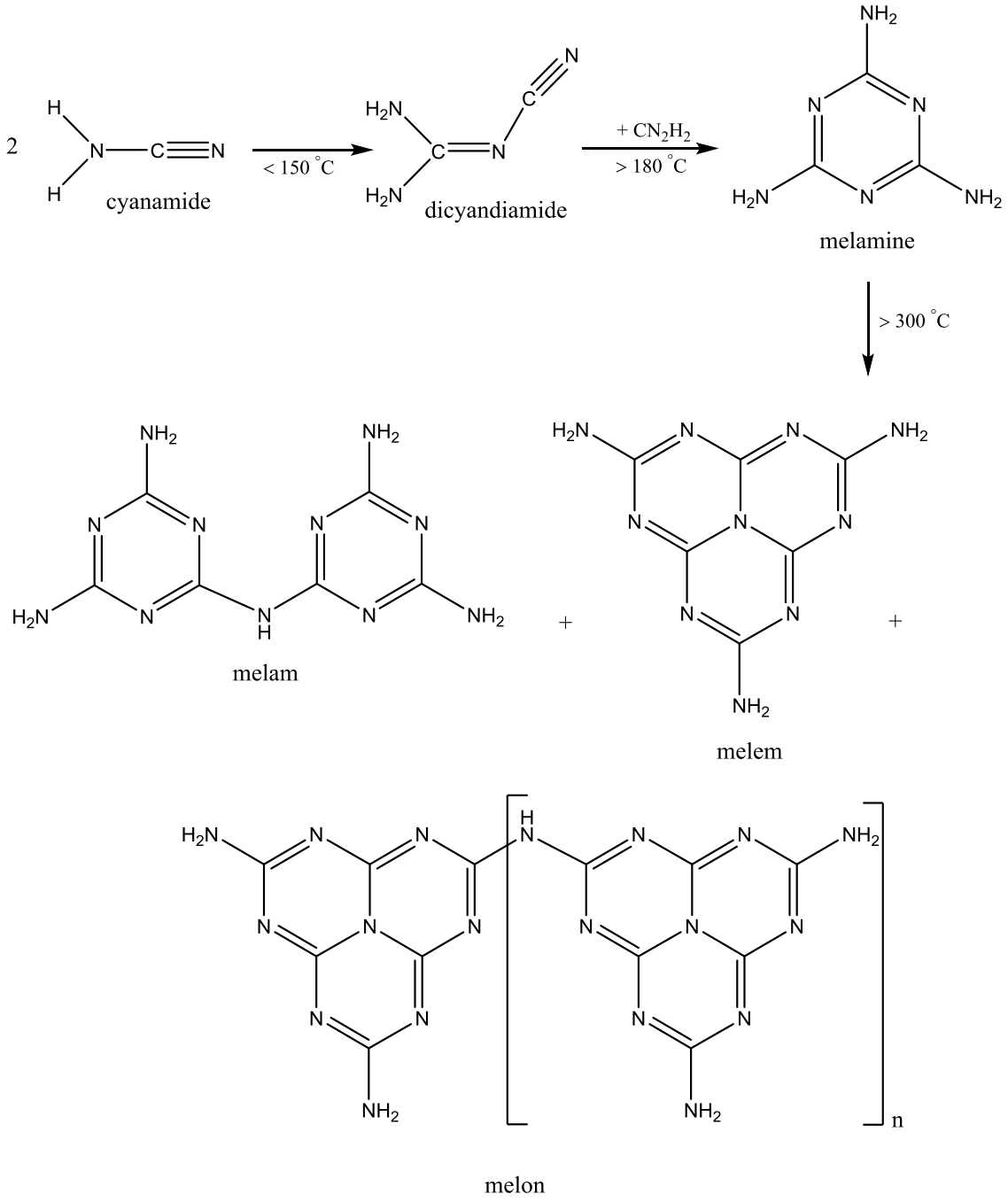

Figure 1- 15: Dimerization and polymerization of cyanamide.

Cyanamide can be converted into its isomer carbodiimide through a favoured tautomerization reaction.[89] Carbodiimide is the most stable isomer of cyanamide.[90] Duvernay et al. (2005) reported that carbodiimide can be formed by condensed cyanamide at temperatures lower than 250 °C (Figure 1-16). [90]

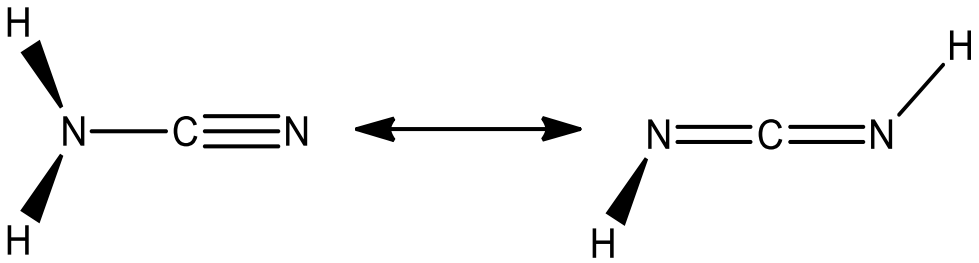

Figure 1- 16: Isomerisation reaction of Cyanamide-Carbodiimide (redrawn from Duvernay et al., 2005).[90]

1.6.4. Applications for N-modified Titanium Dioxide

According to Liu et al. (2007), nitrogen-doped titanium dioxide can be used as an antibacterial agent against *Escherichia coli* (*E. coli*) and bio-film heterotrophic bacteria under visible light.[91] Rtimi et al. (2012) presented the first report of TiN-surfaces as an effective bactericide photocatalyst when exposed to low-intensity visible light; they found that a three minutes TiN sputtered sample had the ability to disable 99.9% of *E. coli* bacteria in 30 minutes.[92] Typical photocatalytic studies that were reported on nitrogen substituted titanium dioxide (N-TiO_2) are photo generation of phenol nitrogen-TiO_2 anatase, degradation of methylene blue, photo-degradation of methyl orange, photodecomposition of isopropyl alcohol, photo-electrochemical decomposition of water, degradation of ethylene glycol, decomposition of 2-chlorophenol, decomposition of volatile organic compounds (VOC), decomposition of

Rhodamine B, and decomposition of acetaldehyde.[85] Viswanathan and Krishanmurthy (2012) reported that previous studies on the decomposition of water in the visible range by N-doped titanium dioxide did not show considerable enhancement, and they found that making nitrogen-doped TiO_2 stable under radiation during photo-electrolysis of water is a challenge that needs to be addressed.[85] Irie et al. (2003) observed the decomposition of gaseous 2-propanol and the generation of carbon dioxide by ($x < 0.02$) in $TiO_{2-x}N_x$ powder under visible light.[93]

1.6.5. Previous Preparations of N-modified Titanium Dioxide

This section presents studies that used different sources of nitrogen, including cyanamide and urea, for the preparation of N-modified TiO_2 and also presents some studies of CN_2 fragments formed through a novel formula.

Different studies have synthesised N-modified TiO_2 using different sources of nitrogen and different techniques. Asahi et al. (2001) synthesised powder and film of $TiO_{1.9925}N_{0.0075}$ within the general formula $TiO_{2-x}N_x$; a mixture of the anatase and rutile phases of $TiO_{2-x}N_x$ film was formed by sputtering titanium dioxide in a mixture of N_2/Ar gas and then heating it to 550 °C for 4 hours in nitrogen.[94] They also prepared $TiO_{2-x}N_x$ powder by calcinating TiO_2 anatase in NH_3/Ar gas to 600 °C for 3 hours.[94] Both the powder and film of $TiO_{2-x}N_x$ showed a shift in the absorption edge to more than 400 nm, which meant that these samples could absorb visible light.[94]

Irie et al. (2003) reported the preparation of $TiO_{1.995}N_{0.005}$, $TiO_{1.989}N_{0.011}$, and $TiO_{1.981}N_{0.019}$ powders within the general formula $TiO_{2-x}N_x$ by calcinating anatase titanium dioxide powder under ammonia (NH_3) conditions at 550 °C, 575 °C, and 600 °C for 3 hours.[93] Temperatures of 550 °C and 575 °C produced samples yellow in colour, but the colour changed to dark green at

600 °C.[93] Their results showed two edges in the UV-vis spectra, and there was a narrowing in the band gap, which was not only related to the nitrogen atom substituted for the oxygen atom but also corresponded to the oxygen vacancies and Ti^{3+}.[93] These oxygen vacancies showed a band gap from 0.75 eV to 1.18 eV.[93] Kim and Kumta (2003) prepared a TiN nanostructure by using a hydrazide sol-gel technique.[95] This process was carried out by reacting titanium isopropoxide with anhydrous hydrazine and anhydrous acetonitrile in an ultra-high purity atmosphere of N_2, Ar and NH_3 at a temperature of 800 °C.[95]

Aita et al. (2004) and Yin et al. (2005) produced three single phases of anatase, rutile and brookite powder of nitrogen-doped titanium dioxide within the general formula $TiO_{2-x}N_y$ using a homogenous precipitation-solvothermal technique.[61, 96] These yellow or beige powders were created by heating the mixture of $TiCl_3$, hexamethylenetetramine ($C_6H_{12}N_4$), and water or pure alcohol to 190 °C for 2 hours in a stainless steel autoclave.[61] These powders showed good photocatalytic activity and excellent absorption in the visible light region.[61] These samples presented two adsorption edges in the UV-Vis spectra; the first step was related to undoped titanium dioxide. The other one, which showed a wavelength at 535 nm, was due to the formation the band of N*2p* that was located above the valence band of O*2p*.[57]

Cong et al., (2006) used a microemulsion hydrothermal technique (wet method) to prepare a powder of N-doped TiO_2.[97] This method required two phases—an oil phase as cyclohexane and an aqueous phase as tetrabutyltitanate mixed with either nitric acid or hydrochloric acid; these phases were heated with triethylamine to 120 °C for 13 hours in an autoclave.[97] It was reported that the anatase phase formed when tetrabutyltitanate dissolved in nitric acid, and the rutile phase was obtained when it dissolved in hydrochloric acid; the estimate of the particles' size was between 8 and 10 nm.[97]

Martinez-Ferrero et al. (2007) prepared a titanium oxynitride porous thin film in two steps: first, anatase TiO_2 was synthesised by heating a mixture of $TiCl_4$, EtOH, H_2O, and F127, which is $HO(CH_2CH_2O)_{106}(CH_2CH(CH_3)O)_{70}(CH_2\ CH_2O)_{106}H$, to 550 ˚C.[98] Next, the sample was heated from 400 ˚C to 900 ˚C under a flow of ammonia gas to produce TiN and $TiN_{1-x}O_x$.[98] They found that at 500 ˚C, the nitrogen starts introducing into a structure of TiO_2 anatase that was by the substitution with oxygen and then bonded to titanium. This then resulted the formation of TiN($TiN_{1-x}O_x$), which is occurred when the temperature reached 700 ˚C.[98]

Graciani et al. (2009) conducted a theoretical analysis of the $TiN_{1-x}O_x$ structure by using the first-principles periodic density functional theory (DFT) calculation.[99] They found that the $TiN_{1-x}O_x$ structure changed from NaCl (cubic) type to the α-TiO (monoclinic) arrangement, depending on the *x* values.[99] Ma et al. (2009) prepared nanocrystalline titanium nitride by heating titanium dioxide, ammonium chloride, and metallic magnesium for 10 hours at a temperature of 650 ˚C.[100]

Viswanathan and Krishanmurthy (2012) gave a summary of the many techniques used to prepare N-doped TiO_2, and they studied the relationship between the techniques employed for nitrogen doping and the position of nitrogen in the lattice of titanium dioxide and its chemical character.[85] These techniques included reacting titanium dioxide powder with either ammonia or nitrogen containing organic components, such as guanidine carbonate, urea, or guanidine hydrochloride at temperatures ranging from 500 ˚C to 700 ˚C.[85] Other techniques were also investigated, such as the sol-gel method, the plasma method at 400 ˚C, the oxidation method of TiN_x film, electrochemical anodization of titanium foils with a source of nitrogen to control the incorporation system and the low-ion implantation technique for adding nitrogen to a single crystal phase of titanium dioxide.[85] Viswanathan and Krishanmurthy also reported that the pattern in powder x-ray diffraction (PXRD) of N-doped titanium dioxide had a similar pattern

as undoped TiO_2.[85] Legrand et al. (2012) formed the anatase structure $TiO_{2-x}N_y \equiv Ti(O/N)_2$ and the rock-salt structure $Ti_zO_xN_y \equiv Ti(O/N)$ from amorphous $Ti(OH)_4$.[101] They synthesised amorphous $Ti(OH)_4$ by using the hydrolysis precipitation of titanium chloride, which was then treated with NH_3 at temperatures ranging from 25 °C to 700 °C. The anatase structure of $Ti(O/N)_2$ formed at a temperature of 570 °C for 12 hours, and this structure then changed to a rock-salt structure of Ti(O/N) at 700 °C for 7 hours.[101] This formula of a $Ti_zO_xN_y$ rock-salt structure changed completely to titanium nitride (TiN) at a temperature of 700 °C after one week.[101]

In 2013, Seo et al. synthesised hollow rock-salt $TiO_{1-x}N_x$ nanoparticles using a simple process.[102] They heated titanium dioxide (P25) nanoparticles under a flow of NH_3, which is a source of nitrogen, for 9 hours at a temperature of 800 °C, and then added $Ti_{0.7}(O_{0.67}N_{0.33})$.[102] They found that by increasing the temperature to 1250 °C, the product phase changed from TiO rock-salt (cubic) to a TiO monoclinic phase.[102]

Other studies focused on the preparation of N-doped TiO_2 using cyanamide or urea as the source of nitrogen. Kobayakawa et al. (2005) produced a powder of N-doped titanium dioxide by first converting titanium hydroxide $Ti(OH)_4$ to TiO_2, then heating it with urea at 400 °C for 60 minutes; their results revealed that the product adsorbed in the visible light region about 550 nm and had two edges in the UV-vis spectra.[103] Buha et al. (2007) prepared TiN by reacting an anatase TiO_2 nanopowder with cyanamaide and urea, respectively, at 800 °C under the flow of nitrogen gas.[104] Factorovich et al. (2011) obtained anatase powder of N-doped titanium dioxide using temperatures up to 500 °C.[83] They dried a mixture of three solutions in air—titanium isopropoxide, urea, and water in ethanol.[83] They found urea decomposed to biuret, cyanuric acid, ammelide, ammeline, melamine, cyanate, and cyanide at temperatures < 375 °C.[83] All of these components except cyanate and cyanide decreased when the temperature was increased to 500 °C.[83] Preparation of nitrogen-modified TiO_2 was also reported by Livraghi et al. (2013),

who used a pyrolysis method: they heated a mixture of titanium isopropoxide, hydrocholoric acid (HCl), urea, and ethanol at 500 ˚C for one hour in air.[105] Amadelli et al. (2003) prepared N-doped TiO_2 with a pure anatase phase and produced a form of Ti–N–O.[106] They applied the sol-gel method in two similar ways: first by hydrolysis of the solution of titanium isopropoxide and urea in alcohol (ethanol) and second by mixing a solution of $TiOSO_4$, water, and ammonium hydroxide. Both of these sol-gel routes were calcinated for 2 hours at 450 ˚C.[106]

Some studies found CN_2 fragments in their products. Hashimoto et al. (1995) prepared a new compound, lanthanaum dioxymonocyanamide ($La_2O_2CN_2$).[107] The first magnetic transition metal carbodiimide phase, $MnCN_2$, was synthesised and studied by Liu et al. in 2003.[108] Xin et al. (2013) prepared N-doped titanium dioxide by heating a mixture of titanic acid and graphitic carbon nitride (g-C_3N_4) at temperatures higher than 500 ˚C.[109]

The techniques to prepare N-modified titanium dioxide used in this work are based on the use of low-cost equipment and materials, and they consisted of applying heat to a mixture of urea or cyanamide with amorphous $Ti(OCH(CH_3)_2)_{4-x}(OH)_x$ and TiO_2 anatase at temperatures lower than 500 ˚C. The reasons for preferring urea as a source of nitrogen-doped titanium dioxide were that it is non-toxic, inexpensive, and commonly used, and it yielded ammonia and isocyanic acid when heated to approximately 400 ˚C.[17, 110] Cyanamide also has the advantages of being inexpensive, commercially available, and less toxic than hydrogen cyanide (HCN).

1.7. S-modified TiO_2

One of the aims of this project was anion doping of titanium dioxide such as nitrogen doping and sulfur doping. N-doping was presented in the previous section, so this section of the project will focus on sulfur doping.

1.7.1. Introduction of S-modified TiO_2

The advantages of using sulfur are that doping titanium dioxide with sulfur can extend the absorption of light to visible light, is non-poisonous to the environment, and can considerably increase photocatalytic activity.[111] As reported in 2010, nitrogen is theoretically classified as the best dopant for the purpose of narrowing the band gap of TiO_2 by doping.[5] This distinction is due to the similarity of the ionic sizes of N and O, which makes it easy to incorporate N into the TiO_2 lattice.[5] However, sulfur-doping by the S^{2-} anion was studied and found less favourable for this purpose; the partial substitution of O^{2-} anion with S^{2-} anion is thought to narrow the band gap of anatase by mixing the S *3p* orbitals with O *2p* orbitals.[30, 58] Due to S^{2-} (1.7 Å) having a larger ionic radius compared to that of O^{2-} (1.22 Å), the anionic sulfur doping appears difficult to carry out.[5, 112] However, the photoabsorptivity of S-doping in the visible light region is better than that of N-doping.[5] The substitution of the Ti^{4+} ion by S^{4+} or S^{6+} ions (sulfur-cationic doping) is chemically more favourable than the substitution of the O^{2-} with the S^{2-} (sulfur-anionic doping).[104] Some studies in the literature have reported that using sulfur for cationic doping as S^{6+} or S^{4+} absorbed visible light more strongly than sulfur anion doping as S^{2-} and also showed photocatalytic activity under visible light.[57, 113]

1.7.2. Thermal Decomposition of Thiourea

Thiourea is one of the most used sulfurating agents to prepare S-doped TiO_2. Studying the decomposition of thiourea is very useful for understanding how it works during the chemical reaction with titanium dioxide and also for determining which residues can be formed. Wang et al. (2005) studied the thermal decomposition reactions of thiourea at different temperatures.[114] Figure 1-17 shows a summary of thiourea decomposition from 149 °C to 251 °C; it produces ammonia, carbon disulfide, and cyanamide at a temperature of 218 °C. However, at temperatures lower than 187 °C, only ammonium thiocyanate was produced.[114] Heating the ammonium thiocyanate residue above 189 °C resulted in the production of isothiocyanic acid; when the temperature was increased to 246 °C, the isothiocyanic acid produced trithiocyanuric acid. This product was also formed by first heating isothiocyanic acid with thiourea at 220 °C, at which point the residue reacted again with isothiocyanic acid. Wang et al. found that the decomposition of thiourea formed three major products: carbon disulfide, ammonia, and isothiocyanic acid.[114] Theoretical study on the decomposition of thiourea was done in 2013 by Wang et al.[115] They reported that the thiourea can decompose to carbodiimide/cyanamide accompanied with hydrogen sulfide; it also can decompose to thiocyanic acid/isothiocyanic acid accompanied with ammonia.[115]

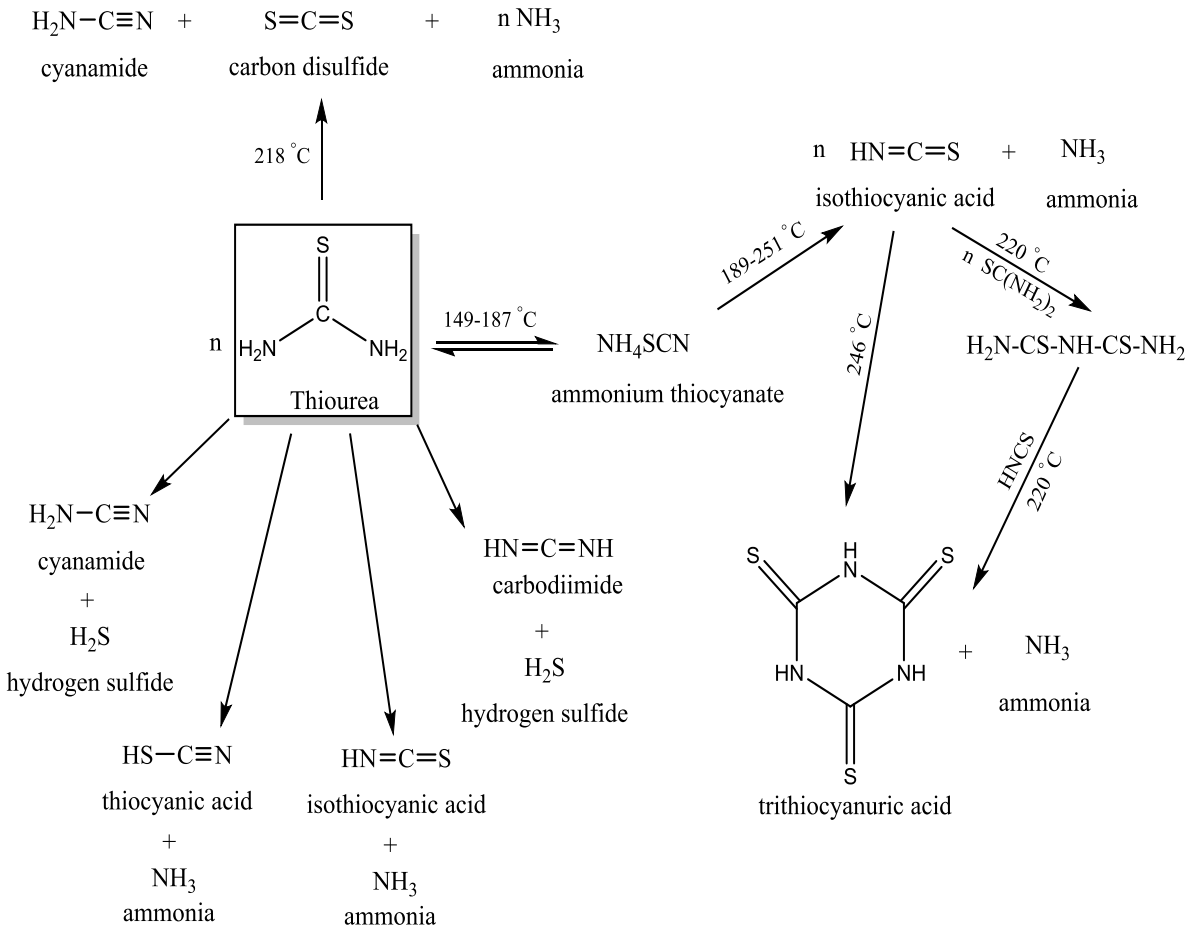

Figure 1- 17: Thermal decomposition of thiourea.[114, 115]

1.7.3. Applications of S-modified Titanium Dioxide

New possibilities for the production of solar-induced photocatalytic materials have been revealed by sulfur-doped TiO_2.[58] Under visible light irradiation, sulphur-doped TiO_2 photocatalysts were observed to have anti-bactericidal effects on *Micrococcus lylae* in water.[58] S-doped TiO_2 was also revealed to be an effective photocatalyst and was tested for antibacterial

applications; it was able to kill 99.5 % of *Escherichia coli* after 24 hours of light irradiation in the United Kingdom (UK) hospitals.[116] S-doped TiO_2 was also used for the photocatalytic degradation of phenol and the conversion of $CO_2 + H_2O$ into alcohol, which is a tool to counteract the international problem of rising CO_2 in the atmosphere.[4, 33] S-modified TiO_2 was tested as a highly active photocatalyst for methylene blue degradation.[4, 117, 118] It was also used to decompose the organic pollutant azo dye Rhodamine B (RhB) and to degrade methyl orange (MO).[4, 119] S-modified titanium dioxide has also been studied for its potential in photo-electrochemical hydrogen generation.[120]

1.7.4. Preparation Methods for S-modified TiO_2

This section presents previous works on the preparation of S-doped TiO_2 using various sources of sulfur, including thiourea and carbon disulphide. The method used in this project is also presented in this section.

Using thiourea as a source of sulfur is documented by several studies in the literature. Ma et al. (2014) reported that cationic-doping by substituting Ti^{4+} with S^{6+} to produce S-doped titanium dioxide was achieved by heating a mixture of thiourea, tetra-isopropoxide, polyvinylpyrrolidone, ethanol and acetic acid at 500 $^{\circ}$C.[121] Yang et al. (2012) prepared anatase $TiO_{2-x}S_x$, by a hydrothermal technique based on heated on a mixture of titanium butoxide, ethanol, acetic acid and thiourea at 450 $^{\circ}$C for 3 hours.[4] Szatmary et al. (2011) reported that heating a mixture of titanium butoxide, thiourea, and methanol at 400 $^{\circ}$C for 3 hours produced S^{6+} that substituted for Ti^{4+}.[122] Ang et al. (2010) reported a mechanochemical method to prepare S-doped titanium dioxide as a mixture of anatase and brookite.[5] They mixed anatase titanium dioxide powder and thiourea in a planetary mill and subsequently heated the mixture for 5 hours at 400 $^{\circ}$C.[5] Bidaye et al. (2010) produced anatase S-doped TiO_2, which has high

photocatalytic activity, by heating a mixture of $TiCl_3$, HNO_3, oxalic acid and thiourea at 450 ˚C for 4 hours.[118] Hamadanian et al. (2009) produced S-doped titanium dioxide nanostructure in the anatase phase by using a modified sol-gel method with a crystal size between 8 nm and 11 nm.[57] They mixed titanium isopropoxide, acetic acid, water, and thiourea, then heated the mixture at 500 ˚C for 2 hours.[57] Kim et al. (2008) reported that S-doping formed SO_4^{2-} and Ti−S in the titanium dioxide lattice.[123] They used a sol-gel method to prepare anatase S-doped titanium dioxide nanoparticles at 11.3 nm by heating the mixture of tetrabutyl-orthotitanate Ti $(O\text{-}Bu)_4$, thiourea, water, ethanol, and HCl between 450 ˚C and 600 ˚C for 5 hours.[123] Ohno et al. (2004) prepared S-doped titanium dioxide in which S^{4+} was substituted for Ti^{4+} in the TiO_2 lattice by heating with titanium isopropoxide, ethanol, and thiourea at 500 ˚C.[113] Tian et al. (2009) formed S-doped titanium dioxide (used hydrothermal synthesis) by heating an autoclave device with a mixture of $CS(NH_2)_2$, $TiCl_4$, water, and alcohol at 180 ˚C for 20 hours.[124]

Other procedures used carbon disulfide as a source of sulfur. In 2007, Li et al., reported that the S−Ti−O bond was formed by using supercritical treatment.[117] In this method, nitric acid, ethanol, water, and titanium isopropoxide were heated under high pressure using a 500 mL autoclave containing a CS_2/EtOH solution.[117] Dunnill et al. (2009) reported that S-doped titanium dioxide was prepared using atmospheric pressure chemical vapour deposition (APCVD) of $TiCl_4$, CS_2, and ethyl acetate (EtAc) at 500 ˚C.[116] Ma et al. (2014) observed that forming the S−Ti−O bond resulted from the substitution of S^{2-} with O^{2-}, and the preparation applied by heating a mixture of carbon disulfide, tetra-isopropoxide, polyvinylpyrrolidone, ethanol, and acetic acid at 500 ˚C.[121]

Other sources of sulfur were also used. For example, He et al. (2010) prepared S-doping and formed TiS_2 by heating the mixture of titanium sulfate ($Ti(SO_4)_2$), sodium sulphide (Na_2S), sodium thiosulfate ($Na_2S_2O_{3.5}H_2O$) and n-heptane at 200 ˚C for 4 hours.[111] Liu et al. (2009) formed S-doped titanium dioxide by using Na_2SO_4 as a source of sulfur, and heated it with

titanium tetra chloride ($TiCl_4$) and water at 60 °C for 12 hours.[125] Takeshita et al. (2006) prepared S-doped TiO_2 powder by oxidation annealing of TiS_2 at 300- 600 °C and then the dispersed the powder in water and spread the mixture on a CaF_2 plate.[126] Oxidation of TiS_2 was also reported by Umebayashiet et al. (2002), who found that heating TiS_2 at 300 °C for 5 hours in air produced $TiO_{2-x}S_x$.[50]

The method used in this project for producing S-modified TiO_2 included dodecanethiol, carbon disulfide, and thiourea as sources of sulfur. The CS_2 was used as a source of sulfur because it is more reactive toward nucleophiles and easy to reduce. The thiourea easily releases ammonia and is commonly used as a source of sulfide (S^{2-}). The dodecanethiol was used because it easily produces sulfide by decomposing the long organic chain. To date, no studies have investigated the use of dodecanethiol as a sulfurating agent. Therefore, it was thought that the method used in this project was different from the aforementioned previous studies. Some of these studies that used thiourea as a source of sulfur carried out the reaction in a planetary mill, while others involved chemicals in their preparation, including ethanol, acetic acid, water, HCl, or titanium butoxide. Secondly, few studies used CS_2 as a source of sulfur, and some of them used an autoclave in their reactions; however, the majority used additional materials such as ethyl acetate or nitric acid in the CS_2 reactions. In contrast, the reaction used in this project to prepare S-doped TiO_2 was based on the reaction of TiO_2 with three different sources of sulfur thiourea, CS_2, and dodecanethiol, respectively. The mixture were then heated using a tubular furnace at temperatures between 400 °C and 500 °C.

1.8. Project Objectives

This project focused on synthesising and characterising pure anatase titanium dioxide nanoparticles using a simple route. Moreover, it focused on modifying TiO_2 (in pure phase and

in nanoparticle scale) to narrow its band gap which shifts its absorption from the UV-region to the vis-region. Anionic-modification such as N- and S- modification were used in this study. Emphasis was also placed on the characterization of the chemical formulas and the selected physical properties. All the synthetic and characterisation methods used in this project relied on simple and inexpensive equipment, which helped decrease the cost of synthesising large amounts of the products.

Chapter 2 - Experimental Techniques

This chapter will describe the synthetic technique, the characterizations technique and the materials. Examples of characterization used in this project are: diffraction techniques, such as PXRD and SAED; spectroscopic techniques, such as FT-IR, UV-Vis, EDX and EELS; and microscopic and microanalytical techniques, such as TEM and EA.

2.1. Synthetic Technique

This project used a high temperature ceramic method, which is classified as the method that is most commonly used for the preparation of solids.[11] In the ceramic method, the reactant solids are simply ground up and then they are heated until they react. The basic equipment for the ceramic method includes pestles and mortars, which are used to ensure a uniform small particle size; the type of crucible and furnace that are to be used must also be selected.[11]

Because solid state reactions require temperatures up to 2000 $^{\circ}$C, conventional glassware is often not suitable.[12] Many types of vessels are used for solid state synthesis, such as borosilicate glass (Pyrex), gold tubing, silica (quartz), platinum, alumina (Al_2O_3), zirconia (ZrO_2) and magnesia (MgO).[12] The selection of the container depends upon the type of reactant that is being used and the temperature of the furnace. In some cases, the containers are coated with graphite before they are used.[12] This is done in order to avoid reaction with the material under study. At such high temperatures, even the containers can become reactive.[12] This project used an alumina (Al_2O_3) crucible and that crucible was coated with graphite (note graphite coated crucible only for sulfides).

2.1.1. Furnaces

Two different furnaces were used in this project: a box furnace (also known as a muffle furnace or a chamber furnace) and a tubular furnace.

The box furnace − This type of furnace heats a large volume to a fixed temperature.[12] The box furnace used in this project was a Carbolite CWF 1200, as shown in Figure 2-1. The temperature controller for the furnace is built into the unit and it operates in the temperature range of 0-1200 ˚C.

Figure 2- 1: The interior and exterior of the box furnace used in this project.

The tubular furnace – This type of furnace has a smaller heated area at the centre of the tube and the temperature falls off rapidly toward the end of the tube.[12] It can be used to heat samples under different gases by placing the samples inside the tube connected to a gas cylinder.[12] The furnace used in this work is the Linn Elektro Therm tube furnace with a control temperature range of 0−1200 ˚C.

This furnace was used in this project either to carry out reactions under an inert atmosphere (nitrogen gas) or to perform solid-gas reactions using CS_2 for sulfuration reactions (see Figure 2-2 and Figure 2-3, respectively).

Reactions that were carried out under nitrogen atmosphere were conducted using the tubular furnace shown in Figure 2-2. The reactions were first loaded into an alumina crucible and then placed into a silica (quartz) tube. A set of taps is found at each end of the silica tube. The silica tube was then placed in the centre of the furnace and the furnace was closed. Rubber tubing was attached to each of the taps at the ends on the silica tube. At one end of the silica tube, the rubber tubing is connected to the gas flow monitor of the nitrogen cylinder and the other end is connected to paraffin oil contained in a Dreschel bottle. The silica tube was flushed with nitrogen gas for at least 15 minutes prior to the thermal treatments.

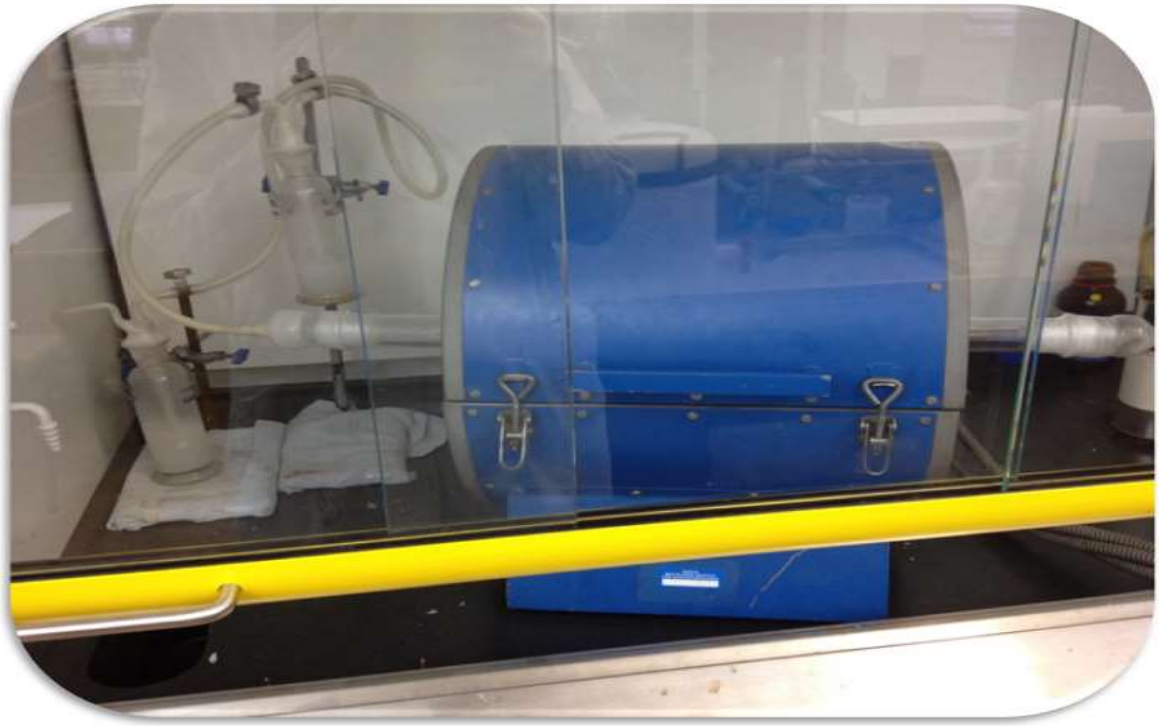

Figure 2- 2: Tubular furnace for reactions under flowing N_2 (g) (sealed tube) or in air (released tube).

The reactions that were carried out under nitrogen atmosphere and carbon disulfide were conducted using the furnace shown in Figure 2-3. Carbon disulfide is a liquid with low vapour pressure. In other words when nitrogen gas is bubbled through the CS_2 liquid; the gas acts as a carrier allowing a vapour of CS_2 with N_2 to follow through the tubular furnace. In this experiment, the nitrogen cylinder was connected to the Dreschel bottle containing CS_2 liquid by means of plastic pipes. This pipe then leads from the Dreschel bottle to the silica tube. A bypass system was made using a pair of two-way taps. One tap is situated before the CS_2 Dreschel bottle and one tap is situated after the bottle. This was necessary in order to allow the N_2 gas to flush the system of air before the reaction was started and to remove CS_2 once the reaction was completed. The other side of the silica tube was connected to a Dreschel bottle containing paraffin oil. This paraffin oil is used to seal the system from air and it acts as a post-reaction scrubber, reducing the release of any residual CS_2. The protocol in this work applied

by grinding the materials, which was to be reacted with CS_2, and then it was placed on the boat of alumina that was coated with graphite (carbon boat), which was then placed into the centre of silica tube. The system was then sealed. The nitrogen gas was allowed to flow through the system with the isolated CS_2 for about 15 minutes. This was done to remove any air from the system. Once the system was flushed, the programme for the reaction was run. When the temperature of the furnace reached the reaction temperature, the taps were adjusted to enable the flow of the CS_2 vapour carried by the continuous flowing of the nitrogen gas. The CS_2 vapour was allowed to flow until the reaction temperature started to cool down. Once the system starts to cool down, the CS_2 becomes isolated, accompanied with enables the nitrogen gas flow to continue until the system reaches room temperature.

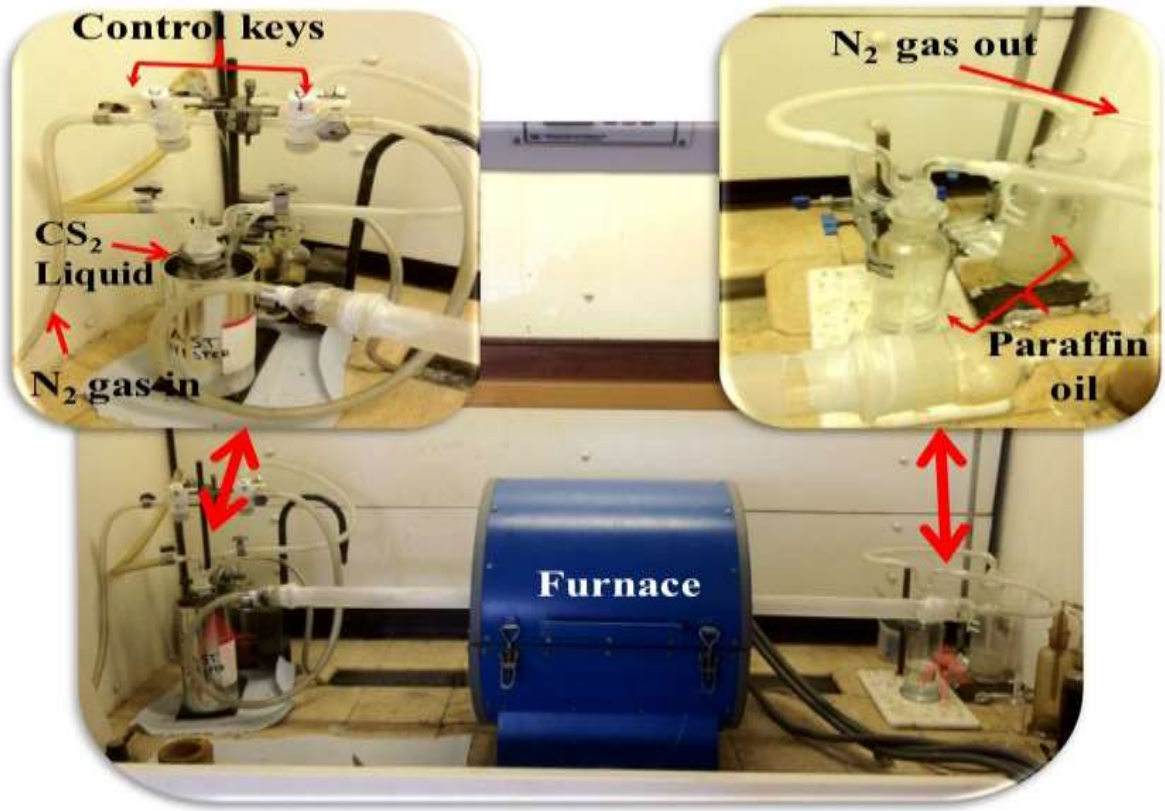

Figure 2- 3: Tubular furnace that used CS_2 (g) and N_2 (g) for the sulfurating reactions

2.2. Characterizations

2.2.1. Powder X-ray Diffraction (PXRD)

A crystal is an arrangement of the ions or molecules in well-defined positions.[127] Examination of a crystal structure shows that the ions contained within the crystal form planes in three dimensions.[127] When a mono-chromatic X-ray beam falls on a crystal, the beam is then reflected by each plane of the crystal.[127] This result in a diffraction pattern of strengthened beams, which happens when

$$n\lambda = 2d \sin\theta \qquad \text{2- 1}$$

where the wavelength of the X-ray beam is (λ), the integral number of wavelengths (n), the angle of incidence of the X-ray beam is (θ) and the distance between the crystal planes is (d).[127]

Phase composition (for a particular compound) was determined from the patterns obtained using powder X-ray diffraction (PXRD). The PXRD was carried out through using a Siemens D5000 X-ray Diffractometer and a PANalytical Empyrean Powder Diffractometer (PEPD). The devices operated at a current of 30 mA and a voltage of 40 kV. They used copper K-alpha (Cu Kα) radiation. The D5000 X-ray Diffractometer has a weighted average wavelength of 1.5418 Å (Cu $K\alpha_1$ = 1.5406 Å, Cu $K\alpha_2$ 1.5444 Å); but the Empyrean has a primary monochromator by using pure $K\alpha_1$ instead of the $K\alpha_{1,2}$ doublet ($K\alpha_1$ = 1.5406 Å). A Ni foil is used to filter Cu Kβ radiation. The devices were run for a maximum of 12 hours and the measurements were focused within a 10° to 120° range of 2θ. Software programmes were utilised to analyse the X-ray findings. The EVA programme (for the D5000 Diffractometer) and the HighScore Plus programme (for the PANalytical Diffractometer) were used to interpret the PXRD patterns, such as phase identification. Data Viewer software was used for the pattern comparisons.

Additionally, Chekcell software was used to calculate the unit cell parameters. Moreover, the crystallite size was estimated through the use of the Scherrer Equation

$$\mathbf{D = \frac{k\lambda}{\beta \cos \theta}} \qquad \textbf{2- 2}$$

where *D (*nm*)* is the average crystallite size of the phase under investigation, β is the full width of the diffraction peak at half of the maximum intensity (FWHM) in radians, *k* is Scherrer's constant (0.9), θ is the Bragg angle (radians), and λ (nm) is the X-ray wavelength used (CuK_α, 1.5418 Å).[11, 12, 128] The Scherrer Equation relates the crystallite thickness to the width of its diffraction peaks and it is extensively used for particle size determination.[8] An evaluation of peak width with reducing particle size is shown in Figure 2-4.

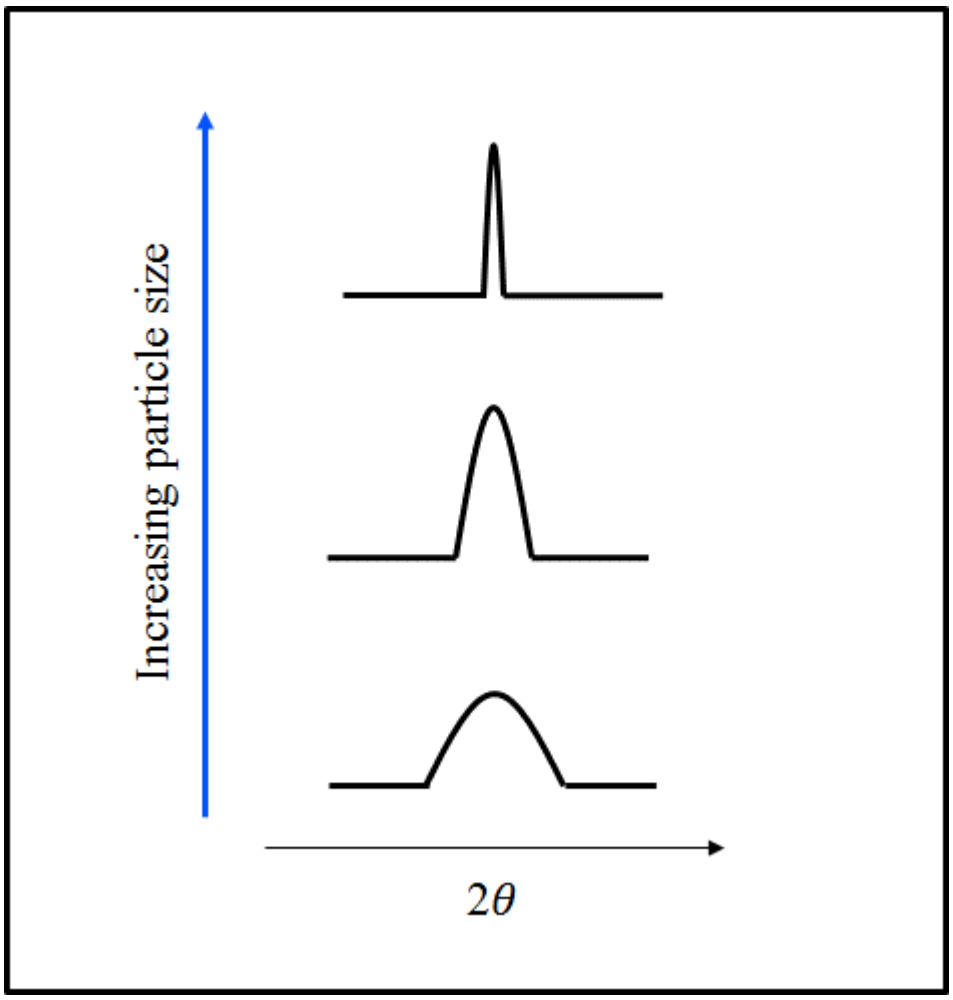

Figure 2- 4: The effect of increasing the size particle on the width of the reflections (image is redrawn from Rodgers, 1994). [8]

2.2.2. Selected Area Electron Diffraction (SAED)

Crystallographic information from select regions of the sample (ranging from 1 micron to around 100 nm) is illustrated by the selected area electron diffraction (SAED) patterns. The unit cell parameters and symmetry can be inferred from the spot positions. It was also possible to obtain the SAED patterns on all of the TEMs centres and record them digitally on the JEOL 2100. The SAED patterns were collected and interpreted by Dr Zabeada Aslam (Faculty of Engineering, University of Leeds, UK).

2.2.3. Fourier Transform Infrared Spectroscopy (FT-IR)

Infrared radiation has a higher photon energy than radio waves but a lower photon energy than visible radiation.[127] Its wavelength ranges from 0.78 μm to 40 μm.[127] The infrared radiation frequency range could be known from the infrared radiation wavelength range by the following equation:

$$\boldsymbol{\nu = \frac{c}{\lambda}} \qquad \textbf{(2- 3)}$$

where the frequency is (ν), the speed of the light is (c) and the wavelength is (λ). Hence, when the wavelength (λ) is short, the frequency (ν) is high.[127] The term wavenumber (the number of radiation waves per centimetre), is commonly used instead of the term wavelength.[127] In this case, the frequency radiation is described as ($\bar{\nu}$).[127] The wavenumber ranges from13,000 cm^{-1} to 250 cm^{-1}.[127]

The functional groups in the molecules were identified using Fourier-transform infrared (FT-IR) spectroscopy, which also enabled the molecular structure to be identified. This process is founded on the absorption of IR radiation over different frequencies of the sample.[129] Vibrations, including stretching and bending, resulted from the absorption. A Perkin Elmer Paragon 1000 Spectrometer or a Bruker IFS 66 was used to conduct the FT-IR spectroscopy. The sample was ground into a homogenous, fine powder using potassium bromide (KBr). The sample was then made into transparent pellets by pressing it under high pressure. Potassium bromide was chosen as the material that was used to contain the sample because it is transparent to IR radiation a cross a wavelength range of 400-4000 cm^{-1} that needs to be examined in this work. Each sample was scanned four times; the resolution was set to 4.0 cm^{-1} and the interval was set to 2.0 cm^{-1}. The FT-IR data was then interpreted using OPUS software.

2.2.4. Ultraviolet-Visible Absorption Spectroscopy (UV-Vis)

A Varian Cary 5E UV-Vis-NIR Spectrophotometer equipped with a Harrick Praying Mantis™ diffuse reflectance device was used to obtain the diffuse reflectance UV-visible spectra. The reference material used was $BaSO_4$, which was also used as a diluent (ca. 2:1 $BaSO_4$: sample). Data were recorded over the range of 800 nm to 200 nm and a plot of the square root of the Kubelka-Munk function against the electron volts was used to estimate the band gap energies:[130]

$$\mathbf{F(R) = \frac{(1-R)^2}{2R}} \qquad \textbf{(2- 4)}$$

where R is reflectance and plotting $[F(R) \times h\nu]^{\frac{1}{n}}$ against $h\nu$, or the Tauc plot, is used to estimate the energy band gap, F(R) is the Kubelka-Munk function and n= the number connected with the character of the transition between energy bands $h\nu$ with units eV; n=2 for TiO_2 anatase.[120, 121] This is because TiO_2 anatase has an indirect transition band gap.[130, 131] The band gap (E_g) is estimated using a plot of $[F(R) \times eV]^{\frac{1}{2}}$ against eV and it is determined by extrapolating the edge of absorption so that it intercepts the *x axis* at a particular eV.

2.2.5. Electron Energy Loss Spectroscopy (EELS)

Complementary data to energy-dispersive X-ray spectroscopy was obtained using the electron energy loss spectroscopy (EELS) microanalysis technique. The amount of energy lost by electrons when they pass through the sample can be investigated using EELS.[13] As the typical peaks for energy loss are comparable to the peaks found using EDX spectroscopy, it is possible to determine what elements are present. Data on bonding and valence states can be gleaned

from the fine structure of the energy loss peaks. The collection and interpretation of the data were conducted by Dr Aslam of the Leeds University Faculty of Engineering.

2.2.6. Energy-Dispersive X-ray Spectroscopy (EDX)

The arrangement of the sample was established using energy-dispersive X-ray (EDX) spectroscopy, a microanalysis technique. In this process X-rays with distinctive energies for each element are produced when the electron beam strikes the sample. The X-rays can be used in the quantitative and qualitative analysis of the elements.[11] In this work, a Zeiss EVO60 scanning electron microscope was used with an electron beam energy of 20 KV, a resolution of 2 nm (with LaB6 emitter), magnification ranging from ×5 to ×1,000,000 and a variable pressure chamber up to 3000 Pa (air) or 2000 Pa (water vapour). In this experiment, only 40 Pa, cold stage down to −30 °C and an Oxford Instruments INCA Energy 350 X-ray spectrometer (EDX) were used.[132]

2.2.7. Transmission Electron Microscopy (TEM)

Transmission Electron Microscopy (TEM) involves a high energy, high intensity beam of electrons passing through a thin sample that is no more than 200 nm. The formation of a two-dimensional projection of the sample was done by detecting the electrons that passed through the sample.[11] TEM used elastic and/or inelastic scattering of the electrons to form an image, which can be interpreted either on a photographic plate or on screen.[8, 11]

2.2.8. Elemental Analysis (EA)

Elemental analysis (EA) is a microanalysis technique that can be used to determine the types and amounts of the elements that are present in a sample. EA usually uses CHN analysis, which measures the mass fractions of the carbon, hydrogen and nitrogen contained in the sample. The data were used to identify the unknown compound's structure. The findings were analysed by identifying the ratio of the elements present in the sample and using those findings to then identify the corresponding chemical formula. This study used a Fisons CHN Elemental Analyser (Thermo Scientific), type EA-1108.

2.3. Materials

The following materials were used in this study: titanium (IV) isopropoxide (Sigma-Aldrich, > 97%), distilled water, urea (Sigma-Aldrich), cyanamide (Sigma-Aldrich), thiourea (Sigma-Aldrich, ≥ 99 %), dodecanethiol (Sigma-Aldrich, ≥ 99 %), CS_2 (Fisher Scientific, 99 %), Parafilm, alumina (Al_2O_3) crucible, carbon boat, nitrogen cylinder, paraffin oil, potassium bromide (KBr) (Fisher Scientific) for IR spectroscopy, barium sulfate ($BaSO_4$) (Sigma-Aldrich, 99%) for UV-Vis spectroscopy, and high vacuum grease (50 g, Dow Corning).

Chapter 3 – Amorphous and Anatase TiO_2

There are many methods used to synthesise TiO_2 nanoparticles mentioned in section *1.5.1.5.* of *Previous Works of TiO_2 Preparations*. Of those methods, the one closest to that which will be implemented in this work in the one reported in 2007 by Beusen et al.[73] However, while this method includes the use of large amount of water in the reaction and the heating of the water and titanium isopropoxide mixture using a pressurised vessel, this work will use a small amount of water and the reaction mixture will be heated using a furnace i.e. no pressure will be involved.

3.1. Experimental

3.1.1. Preparation of Anatase TiO_2 Nanoparticles

Titanium dioxide was formed from amorphous titanium isopropoxide hydroxide, $Ti(OCH(CH_3)_2)_{4-x}(OH)_x$, in two steps as follows:

In the first step, 6.980 g of white $Ti(OCH(CH_3)_2)_{4-x}(OH)_x$ powder was prepared by adding 5 mL distilled water by drops to 20 mL of titanium (IV) isopropoxide (Sigma-Aldrich, > 97%) while continuously stirring the mixture using a glass rod. The mixture was then left in an oven for 24 hours at a temperature of 100 $^{\circ}C$. The resulting samples, obtained after this drying process, were then labelled AM (amorphous).

In the second step, anatase titanium dioxide, TiO_2, was prepared by loading 1 g of the white $Ti(OCH(CH_3)_2)_{4-x}(OH)_x$ powder in a tube furnace and heating for 5 hours at a temperature of 400 $^{\circ}C$ in air. The samples obtained after the heating were labelled ANA (anatase). The samples were then characterised by the FT-IR spectrum, UV-Vis, TEM, SAED, EELS, and PXRD.

3.2. Results and Discussion

The formation of anatase TiO_2 nanoparticles from amorphous $Ti(OCH(CH_3)_2)_{4-x}(OH)_x$ was analysed as discussed in the following subsections.

3.2.1. Phase Identification of the AM and ANA Samples via PXRD

The PXRD pattern of the white solid that was produced after the drying process (100 °C, 24 hours) shows the absence of diffraction peaks, thereby indicating $Ti(OCH(CH_3)_2)_{4-x}(OH)_x$ in the amorphous phase (AM) (see Appendix 1). This amorphous phase was converted to the crystalline phase after the heating process (400 °C, 5 hours) and it produced an ANA sample. Figure 3-1 shows the diffraction pattern of the ANA sample (black pattern) and its match, the pattern (purple solid lines) of anatase from the Joint Committee on Powder Diffraction Standards (JCPDS, No. 00-021-01272) database. The solid orange lines on the top of the PXRD pattern (Figure 3-1) represent the number of experimental diffraction peaks matching those of the anatase reference pattern (purple solid line), and this confirms that a pure anatase phase was prepared. No diffraction peaks corresponding to the other TiO_2 polymorphs are present. The crystallographic parameters of the experimental ANA sample are ($a = b$ = 3.785(10) Å, c = 9.514(8) Å, V = 136.3(8) Å^3), which are in agreement with the parameters of the anatase published data ($a = b$ = 3.7852 Å, c = 9.5139 Å, V = 136.31 Å^3 ($\alpha = \beta = \gamma = 90^\circ$, $I4_1/amd$ (141)). It can be said that the conversion from the amorphous phase to the anatase phase depends on the experimental conditions and the materials. For example, Sugimoto et al. (2003) formed anatase TiO_2 nanopowder by drying the $Ti(OH)_4$ gel at 140 °C for 72 hours, which was their second aging[133]. However, in this project, a pure anatase was formed by heating $Ti(OCH(CH_3)_2)_{4-x}(OH)_x$ to 400 °C for 5 hours. A schematic diagram of the reactions involved in this process is shown in Figure 3-2. The crystallite size calculation *(D)* of anatase TiO_2 gave

a value of ≈11 nm, which was calculated from the most intense X-ray diffraction peak (101) at angle 2θ = 25.25° using the Scherrer Equation.

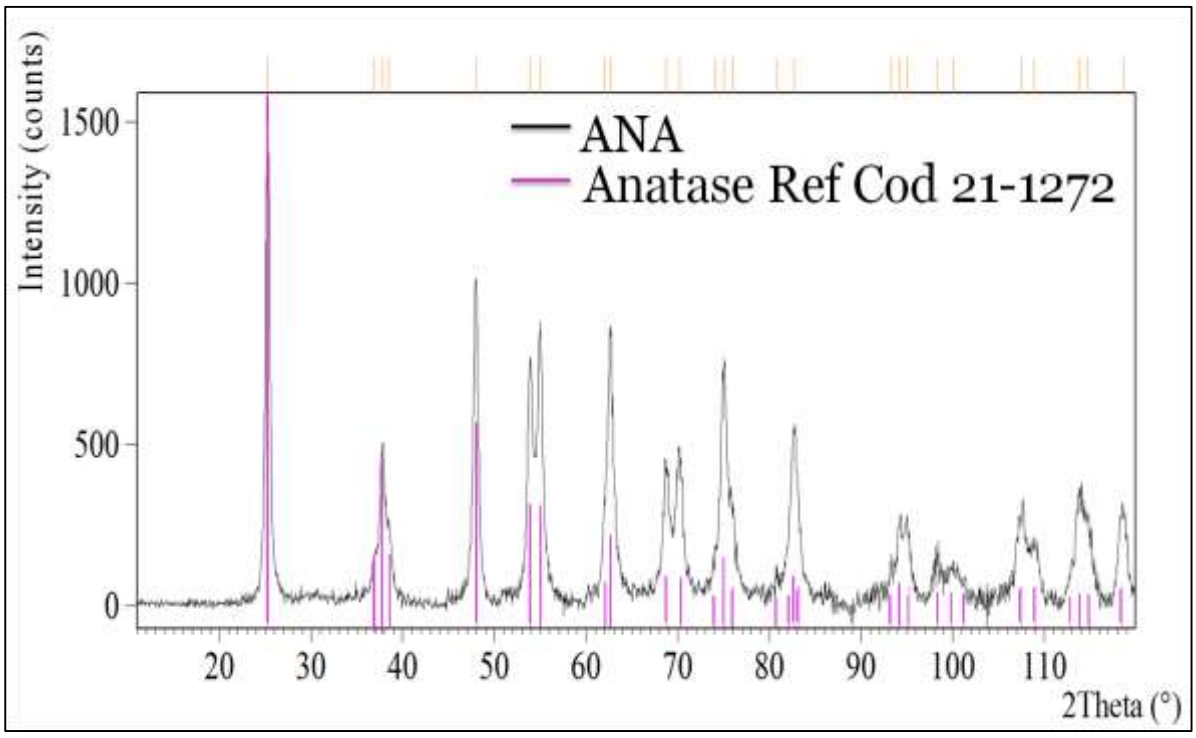

Figure 3- 1: PXRD patterns of anatase TiO_2 (ANA) compared with anatase in the Joint Committee on Powder Diffraction Standards (JCPDS, No. 00-021-01272) database, using Highscore Plus software.

$$Ti(OCH(CH_3)_2)_4 + H_2O \xrightarrow[100\ ^{\circ}C,\ 24\ hrs]{Air} \underset{(amorphous,\ AM)}{Ti(OCH(CH_3)_2)_{4-x}(OH)_x} + HOCH(CH_3)_2$$

$$\underset{(amorphous,\ AM)}{Ti(OCH(CH_3)_2)_{4-x}(OH)_x} \xrightarrow[400\ ^{\circ}C,\ 5\ hrs]{Air} \underset{(anatase,\ ANA)}{TiO_2}$$

Figure 3- 2: Synthesis of TiO_2 anatase nano-powder.

3.2.2. Fourier-Transform Infrared Spectroscopy

Figure 3-3 and Figure 3-4 show the Fourier Transform Infrared (FT-IR) spectra of the AM and ANA samples. There are three regions that show the presence of moisture and carbon dioxide. The first region is a broad band ranging from 3400 cm^{-1} to 3250 cm^{-1} this is related to the hydroxide groups (O—H).[83] The second region is a strong sharp peak at 1636 cm^{-1} and it is attributed to H—O—H bonds.[80, 134] The final region is a weak multi-peak area ranging between 2980 cm^{-1} and 2347 cm^{-1}, which corresponds to O=C=O bonds.[27, 76]

As seen in Figure 3-3, the FT-IR spectrum of the AM sample shows absorption bands for saturate aliphatic –C—H chains at 2972 cm^{-1},[135] a symmetrical deformation of the bands at 1465 cm^{-1} attributed to the bending vibrations of –CH, and bands at 1385 cm^{-1} and 1377 cm^{-1} attributed to the $–CH_3$ groups.[27, 76, 135] The peaks in the 1166 cm^{-1}, 1130 cm^{-1}, and 1032 cm^{-1} ranges suggest the presence of –C—O– stretching bonds.[27, 76] A broad peak ranging from 800 cm^{-1} to 400 cm^{-1} is divided into three positions. The first position shows a broad peak at 786 cm^{-1} related to Ti—OH in the Ti(OH) fragment[136]; the second position shows a weak sharp peak at 668 cm^{-1} and it corresponds to –O—$CH(CH)_3$ in the isopropoxide fragment[136]; the last position shows a broad band associated with the typical vibrational mode of the Ti–OC bond at 630 cm^{-1}.[136] Hence, by combining these fragments and considering the reaction formula, the AM scheme is assumed to be $Ti\,(OCH\,(CH_3)_2)_{4-x}\,(OH)_x$, i.e. the residue of Ti isopropoxide hydrolysis that was produced after drying at 100 ˚C. Heating the solid powder (AM) to 400 ˚C removed the Ti isopropoxide residue, and this was indicated by the FT-IR spectrum (Figure 3-4) that shows no peaks, thereby suggesting that the spectrum is from $Ti(OCH(CH_3)_2)_{4-x}(OH)_x$. The ANA sample spectra revealed the existence of a broad band in the range between 700 cm^{-1} and 400 cm^{-1}. This band is linked to the characteristic vibrational mode of the Ti—O—Ti

bonding complex.[80, 134, 135] Consequently, from the IR spectroscopy data it can be said that pure anatase TiO_2 was formed.

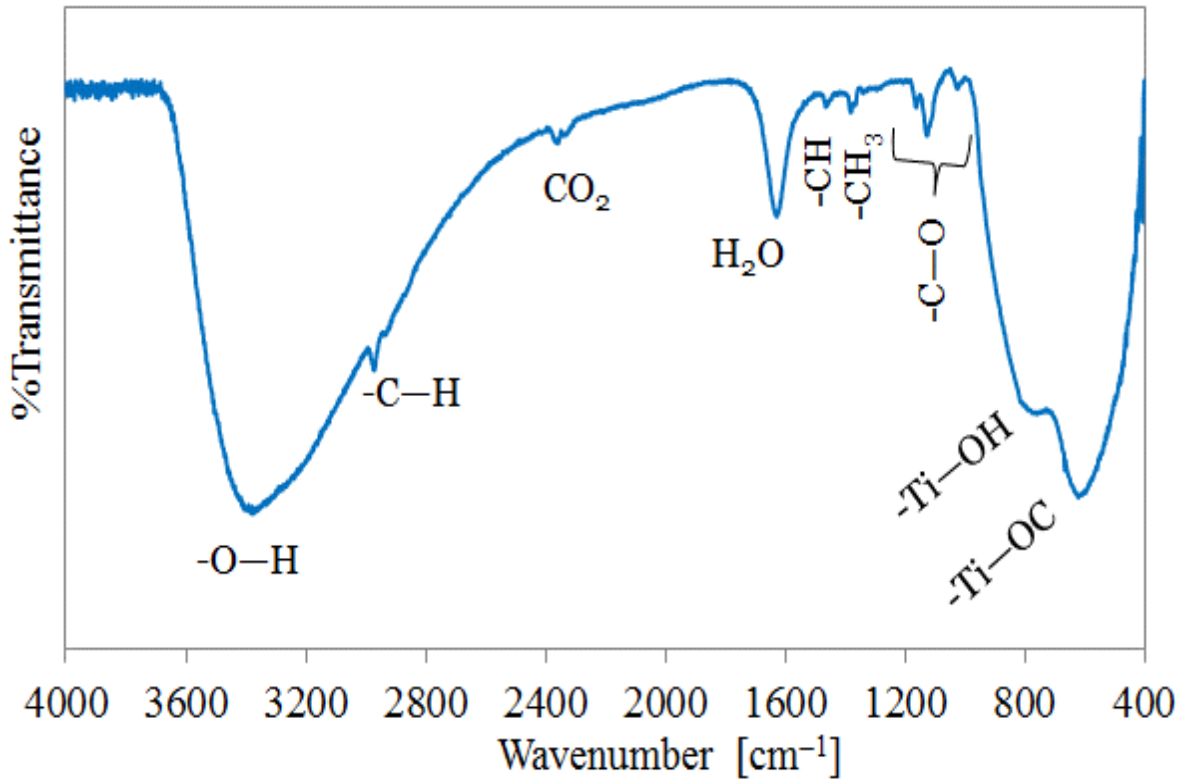

Figure 3- 3: FT-IR spectrum of AM (amorphous) sample, after the drying process (100 ˚C, 24 hours in air).

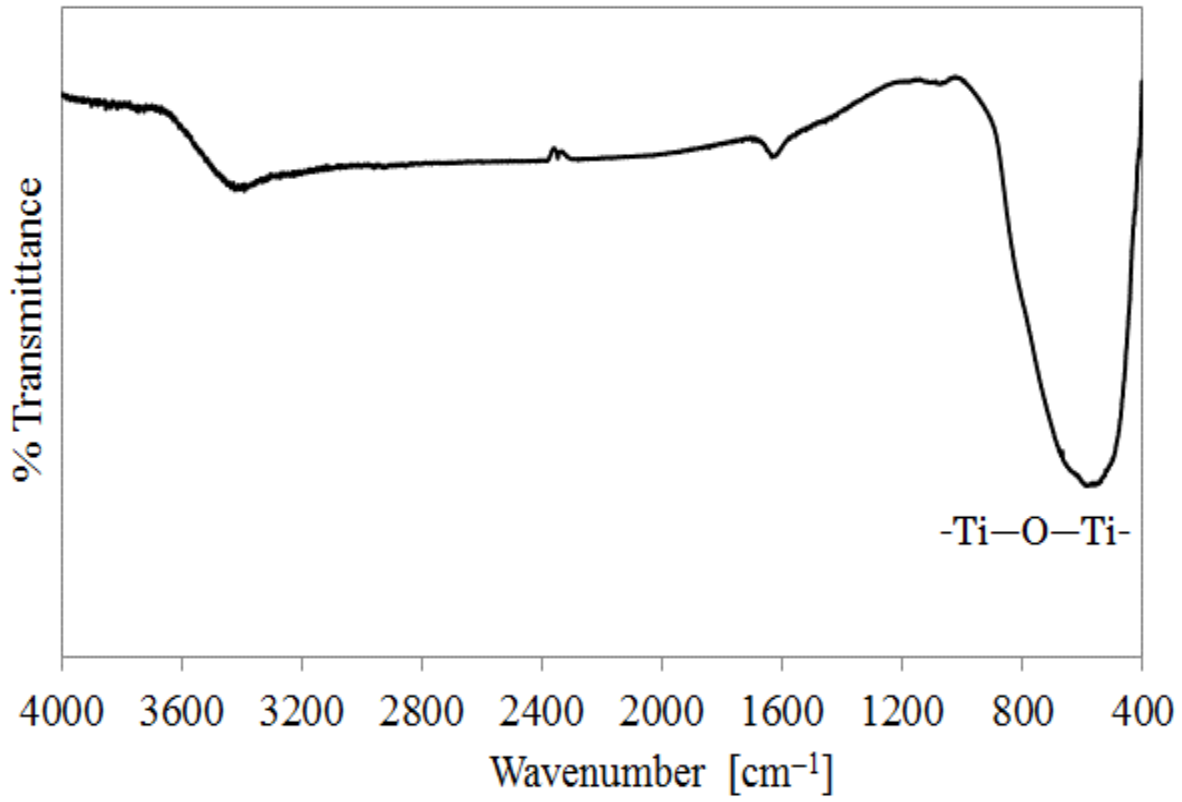

Figure 3- 4: FT-IR spectrum of the ANA (anatase TiO_2) sample, after the heating process (400 °C, 5 hours in air).

3.2.3. Ultraviolet-Visible Spectroscopy

The ultraviolet-visible (UV-vis) spectrum and the band gap calculation diagram for the TiO_2 anatase (ANA) are shown in Figure 3-5. The ANA sample shows absorption at a wavelength of 384 nm in the ultraviolet region. The band gap of titanium dioxide was calculated to be 3.22 eV by using the Kubelka-Munk function.[17, 57, 137] This calculation of the band gap for anatase TiO_2, is in agreement with the data reported in the literature by Yuan et al.,(2006).[138] The band gap for rutile TiO_2 was calculated to be 3 eV, as reported by Pelaez et al., (2012).[139] Considering the PXRD pattern, the IR data and the UV-vis spectra it can be concluded that the AM-sample converted to a single anatase sample (ANA-sample).

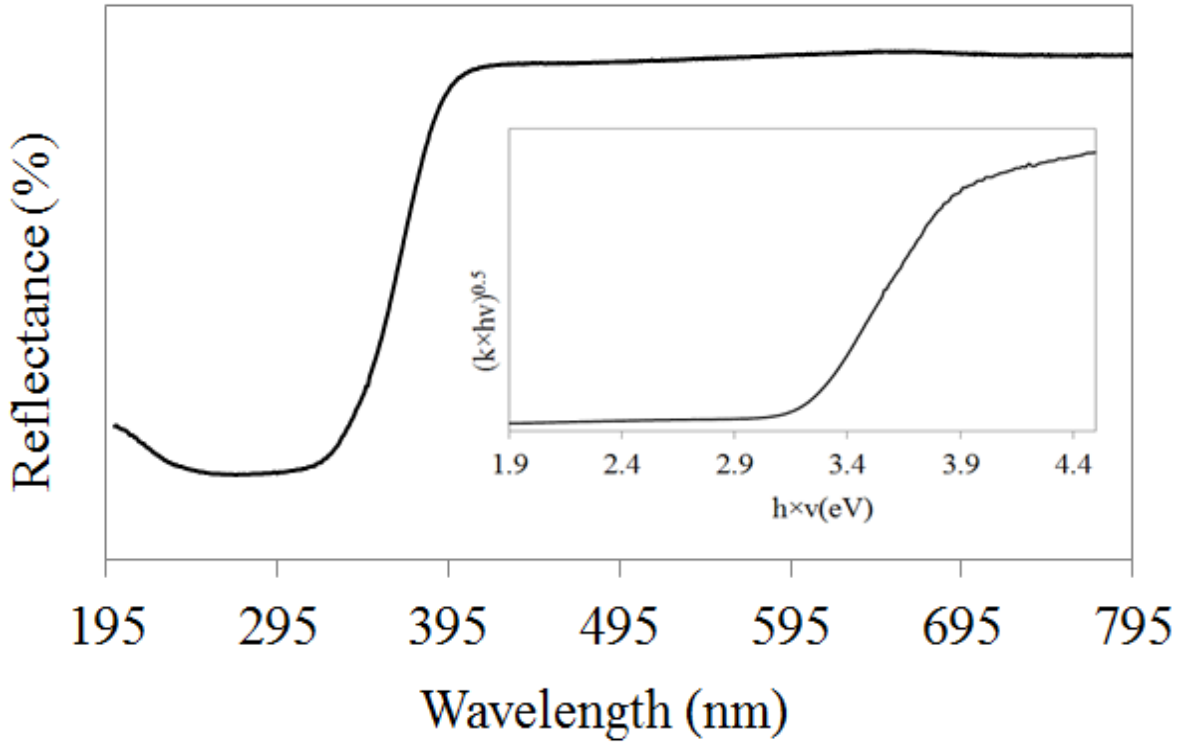

Figure 3- 5: UV-vis spectrum of anataseTiO_2 (ANA) and the band gap calculation spectrum using the Kubelka–Munk function.

3.2.4. EELS, SAED, and TEM Characterizations

Electron Energy Loss Spectroscopy (EELS), Transmission Electron Microscopy (TEM), and Selected Area Electron Diffraction (SAED) were used to analysed the TiO_2 sample. Interpretation of the data was performed by Dr Zabeada Aslam, Faculty of Engineering, University of Leeds, UK.

The particles have slightly irregular shapes with sizes ranging between 6 nm and 20 nm, as shown in Figure 3-6. The selected area electron diffraction pattern (SAED) is shown in Figure 3-6d from the area identified in Figure 3-6a. The nanoparticles are at different orientations relative to the incident beam and this gives rise to diffraction rings rather than just diffraction spots. The clearly defined (*hkl*) planes are identifiable and correspond to TiO_2 anatase.

The EEL spectrum of the area identified in Figure 3-6a is shown in Figure 3-7. It clearly shows the Ti $L_{2,3}$ edge present for the Ti^{4+} compounds, in particular TiO_2, with 56.8±7 % at Ti and 43.2±5.3 % at O. The spectrum splitting the peaks of the Ti L-edge and the O K-edge in Ti^{4+} (TiO_2) compares well with the spectrum that is reported by Huang et al. (2010).[140] The EEL spectra of Ti^{4+} and Ti^{3+} are shown in Appendix 3.

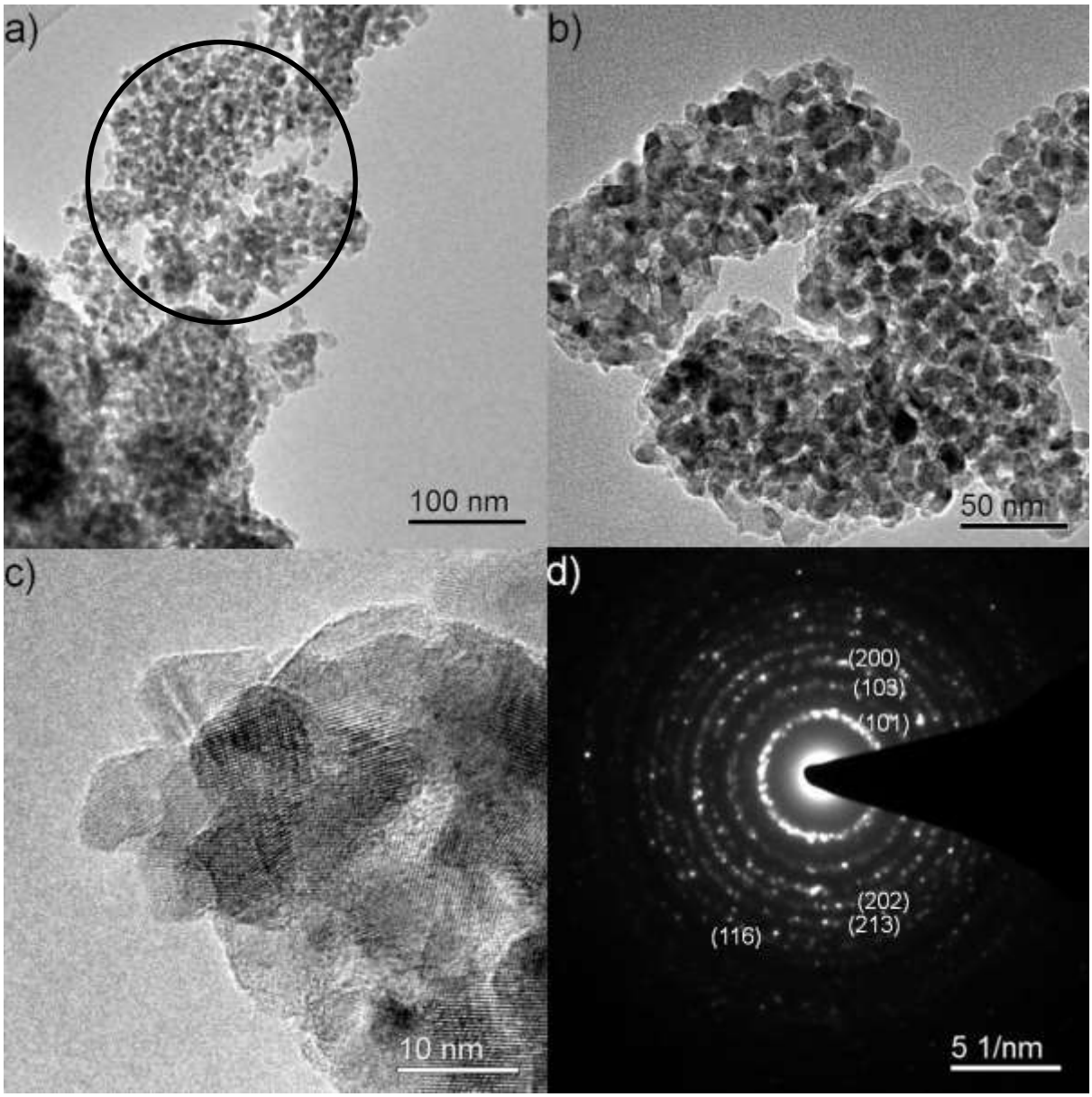

Figure 3- 6: The TEM images show agglomerates of (ANA) TiO_2 nanoparticles at different magnifications (a-c). The SAED of the region marked in a) of anatase TiO_2 is shown in (d). The clearly defined (*hkl*) planes are identified and correspond to TiO_2 anatase.

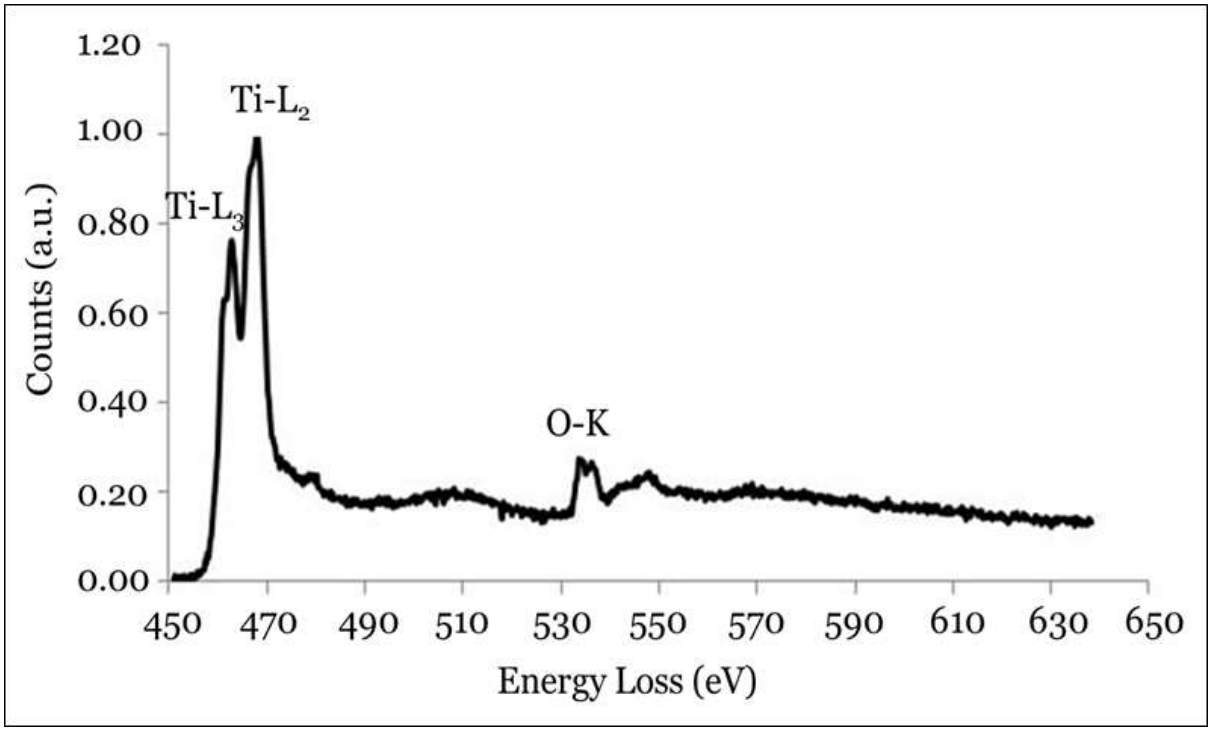

Figure 3- 7: The electron energy loss spectrum (EELS) shows the Ti-L_3 and Ti-L_2 edges and the oxygen K-edge for (ANA) TiO_2 of the area identified in Figure 3-6a.

3.3. Conclusions

The preparation of anatase TiO_2 holds great interest for many researchers. Many different methods can be used to prepare anatase titanium dioxide. The majority of these methods have used either autoclave pressure vessels or alcohols and acidic chemicals in their reactions, and some of the methods are very complex. The method presented here is simple and inexpensive; it also only required a small amount of water and titanium (IV) isopropoxide and a short heating process. Two steps were used to produce a pure TiO_2 anatase nanopowder with a crystallite ranging between 6 nm and 20 nm. In the first step, a reaction between titanium isopropoxide and water followed by a drying process (100 $^{\circ}$C, 24 hours) formed amorphous titanium isopropoxide hydroxide $Ti(OCH(CH_3)_2)_{4-x}(OH)_x$. In the second step, the heating process (400

°C, 5 hours) formed anatase TiO_2 nanoparticles. The PXRD patterns showed amorphous to anatase transformation. The FT-IR data showed the presence of Ti—O—Ti bonds with bands in the regions ranging from 700-400 cm^{-1} and the removal of all Ti isopropoxide residues at 400 °C. The UV-vis spectrum data showed absorption at a wavelength of 384 nm with a band gap at 3.22 eV, which were in good agreement with the data reported for TiO_2 in the anatase phase. SAED also proved that anatase TiO_2 was formed by the defined (*hkl*) planes. Additionally, EELS clearly showed the splitting of the Ti L-edge that was present for the Ti^{4+} compounds, in particular TiO_2 and allowed the atomic percentages of the elemets to be calculated (56.8±7 % for Ti and 43.2±5.3 % for O), which were found to be agreement with the values presented in the literature.

Chapter 4 – N-modified TiO_2

One of the aims of this project was to decrease the band gap of anatase TiO_2 to less than 3.2 eV for shifting the absorption activity of titanium dioxide from the UV-region to the Vis-region. N-modified TiO_2 is one of the suggestions for decreasing this band gap. This chapter will be divided into two sections: N-modification using urea and N-modification using cyanamide.

4.1. Experimental

4.1.1. N-modification Using Urea

A number of previous studies have used urea as a source of nitrogen (Section 1.6.5.Previous Preparations of N-modified Titanium Dioxide). Some of these methods prepared N-doped TiO_2 by first converting titanium hydroxide $Ti(OH)_4$ to TiO_2, then heating it with urea at 400 $^{\circ}C$ for 60 minutes.[103] However, the reaction in this work is by reacted urea with titanium isopropoxide hydroxide ($Ti(OCH(CH_3)_2)_{4-x}(OH)_x$) and titanium dioxide ($TiO_2$) respectively (Note: TiO_2 was prepared from $Ti(OCH(CH_3)_2)_{4-x}(OH)_x$). Other methods produced TiN by reacting TiO_2 with urea at 800 $^{\circ}C$ under the flow of nitrogen gas.[104] On the other hand, this study produced $TiO_{2-x}(CN_2)_x$ series by reacting TiO_2 with urea at a temperature of 450 $^{\circ}C$ under N_2 gas.

The discussion of N-modifying using urea will be divided into two subsections: Reactions of Urea with $Ti(OCH(CH_3)_2)_{4-x}(OH)_x$ and Reactions of Urea with Anatase TiO_2

4.1.1.1. Reactions of Urea with $Ti(OCH(CH_3)_2)_{4-x}(OH)_x$

This section discusses N-doping by the reaction between urea and amorphous isopropoxide hydroxide heated to more than 400 °C (400 °C ≤ T ≥ 600 °C) for 5 hours in both air and nitrogen gas.

Preparation of N-doped titanium dioxide used urea as a nitrogen source. Amorphous $Ti(OCH(CH_3)_2)_{4-x}(OH)_x$ (See *section 3.1.1.* of *Preparation of Anatase TiO_2 Nanoparticles*, for synthesis) was mixed and ground with urea (Sigma-Aldrich) in various molar ratios: 1:5, 1:10, and 1:15 (amorphous, AM : urea, U), and then heated at various temperatures from 400 °C to 600 °C for 5 hours in air or N_2. After that, the samples were analysed using powder X-ray diffraction (PXRD) and elemental analysis (EA).

Samples were labelled as follows: ANA (anatase TiO_2, blank), 1:5_AM_U_400_Air, 1:10_AM_U_400_Air, 1:15_AM_U_400_Air, 1:5_AM_U_500_Air, 1:10_AM_U_500_Air, 1:15_AM_U_500_Air, 1:5_AM_U_600_Air, 1:10_AM_U_600_Air and 1:15_AM_U_600_Air. These labels indicated the ratios of amorphous to urea and temperatures of 400 °C, 500 °C or 600 °C in air. Similar labels were used for the same reactions carried out under flowing nitrogen gas, but for these samples the labels 'Air' were replaced with 'N'.

4.1.1.2. Reactions of Urea with Anatase TiO_2

This section discusses N-doping by the reaction between urea and anatase TiO_2 (ANA) at temperatures of more than 400 °C for 5 hours in both air and nitrogen gas.

Anatase titanium dioxide (See *section 3.1.1.* of *Preparation of Anatase TiO_2 Nanoparticles*, for synthesis) was mixed and ground with urea (Sigma-Aldrich) in various molar ratios of 1:5, 1:10 and 1:15 (anatase : urea) and was then heated at various temperatures from 400–500 °C

for 5 hours in air and N_2. Samples were analysed using powder X-ray diffraction (PXRD) and Fourier transform infrared spectroscopy (FT-IR).

Samples were labelled as follows: ANA (anatase TiO_2, blank), 1:5_ANA_U_400_N, 1:10_ANA_U_400_N, 1:15_ANA_U_400_N, 1:5_ANA_U_450_N, 1:10_ANA_U_450_N, 1:15_ANA_U_450_N, 1:5_ANA_U_500_N, 1:10_ANA_U_500_N and 1:15_ANA_U_500_N, indicating the ratios of anatase to urea heated at 400 °C, 450 °C and 500 °C for 5 hours under flowing nitrogen gas. Similar labels were used for the same reactions carried out under flowing nitrogen gas, but for these samples the labels 'N' were replaced with 'Air.'

4.1.2. N-modification Using Cyanamide

The previous section, which discussed N-modifying titanium dioxide using urea (U), showed the presence of carbodiimide anion in general formula $TiO_{2-x}(CN_2)_x$; which is quite novel up to date. Carbodiimide is one of the decomposition products of urea; however, cyanamide (CM) can be converted to carbodiimide by resonance since carbodiimide is more stable than cyanamide.[90] The decision was made to use CM as a source of nitrogen instead of U. A direct reaction of TiO_2 with carbodiimide would have provided a cleaner synthetic route for $TiO_{2-x}(CN_2)_x$ samples. However, no direct carbodiimide samples are commercially available, so cyanamide was used.

This section discusses two subsections: Reaction of Cyanamide with Anatase TiO_2 and Reaction of Cyanamide with Amorphous $Ti(OCH(CH_3)_2)_{4-x}(OH)_x$,.

4.1.2.1. Reactions of Cyanamide with Anatase TiO_2

Anatase TiO_2 (*See section 3.1.1.*) was reacted with cyanamide (Sigma-Aldrich) in molar ratios 1:1 and 1:2 (anatase : cyanamide). The mixtures, creamy light yellow in colour, were then heated via a tube furnace at temperatures from 400 °C to 600 °C for 5 hours under flowing nitrogen gas.

The samples were labelled as follows: 1:1_ANA_CM_400, 1:2_ANA_CM_400, 1:1_ANA_CM_450, 1:2_ANA_CM_450, 1:1_ANA_CM_500, 1:2_ANA_CM_500, 1:1_ANA_CM_600 and 1:2_ANA_CM_600. These labels indicate the ratios of anatase to cyanamide at various temperatures. The samples were then analysed using powder x-ray diffraction (PXRD) and Fourier transform infrared spectroscopy (FT-IR).

4.1.2.2. Reactions of Cyanamide with Amorphous $Ti(OCH(CH_3)_2)_{4-x}(OH)_x$

Light yellow creamy powder was prepared by grinding amorphous titanium alkoxide-hydroxide (*section 3.1.1.*) with cyanamide (Sigma-Aldrich) in molar ratios 1:1 and 1:2 (amorphous : cyanamide). The mixture was then heated in a tube furnace at temperatures ranging from 400 °C to 600 °C for 5 hours under flowing nitrogen gas.

Samples were labelled as follows: AM (amorphous), ANA (anatase TiO_2) for the blanks, 1:0.25_AM_CM_400, 1:0.5_AM_CM_400, 1:0.75_AM_CM_400, 1:1_AM_CM_400, 1:2_AM_CM_400, 1:1_AM_CM_450, 1:2_AM_CM_450, 1:1_AM_CM_500, 1:2_AM_CM_500, 1:2_AM_CM_550, 1:1_AM_CM_600, and 1:2_AM_CM_600, indicating the ratios of amorphous to cyanamide and the various temperatures at which reaction occurred. Samples were analysed by using Powder X-ray Diffraction (PXRD), Fourier Transform Infrared spectroscopy (FT-IR), and Elemental Analysis (EA).

4.2. Results and discussion

4.2.1. Reactions of Urea with $Ti(OCH(CH_3)_2)_{4-x}(OH)_x$

Samples of AM_U heated in N_2 at various temperatures showed amorphous phases in their PXRD patterns. For example, Figure 4-1 shows the pattern of 1:10_AM_U samples. Because of the amorphous phases, no further tests were carried out on these samples. However, the experiments were repeated by performing the heating process in air instead of nitrogen gas. This yielded better crystallised products, the PXRD patterns of which are shown in Figure 4-2.

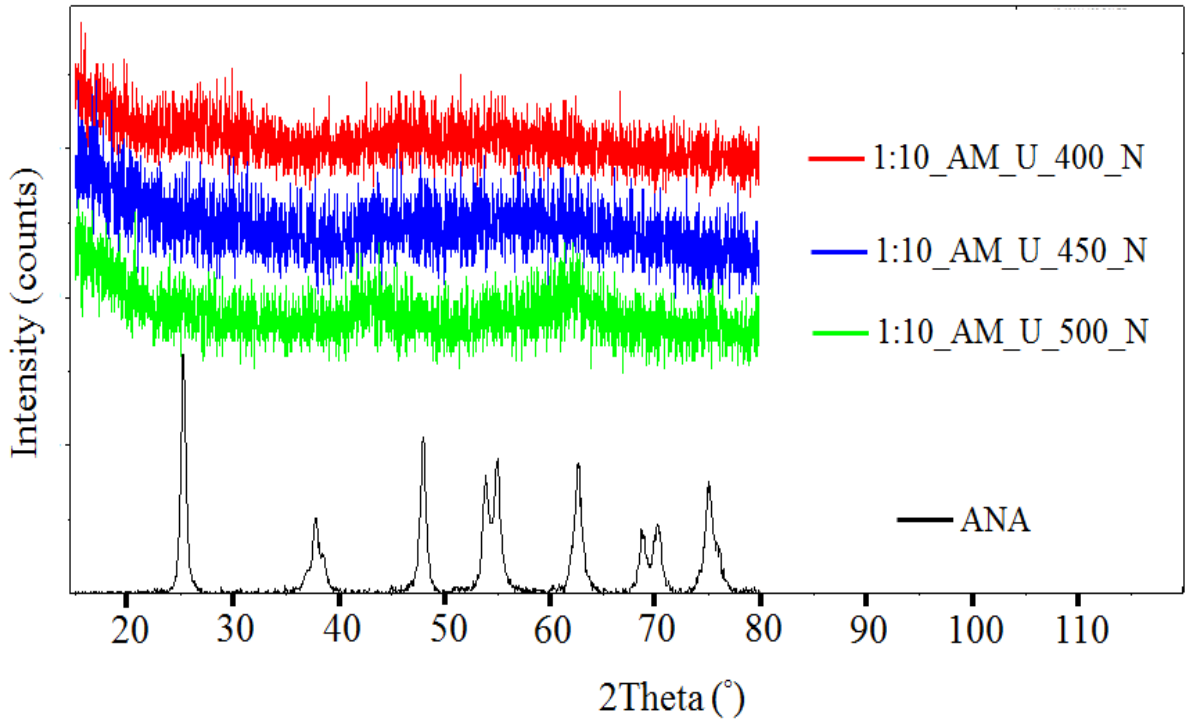

Figure 4- 1: PXRD patterns of 1:10_AM_U samples (amorphous : urea) heated in N_2 for 5 hours at 400 °C , 450 °C and 500 °C.

Figure 4-2 and Table 4-1 show the results of heating the amorphous titanium isopropoxide hydroxide with urea in air for 5 hours at various temperatures. The colour of all samples changed from white to yellow powder. The patterns of samples 1:5_AM_U_400 and 1:10_AM_U_400 formed a single anatase phase. However, the 1:15_AM_U_400 sample seemed to begin forming a rutile phase. When the temperature was increased from 500 ˚C to 600 ˚C, the 1:5, 1:10, and 1:15 AM_U samples began to show the presence of a rutile phase. EA was performed on 1:5 and 1:10 AM_U samples heated at 400 ˚C in air for 5 hours. Samples of 1:5 AM_U showed 0% nitrogen. Samples of 1:10 AM_U showed 0.24% nitrogen. Further analysis of the 1:10_AM_U_400 sample will be discussed later.

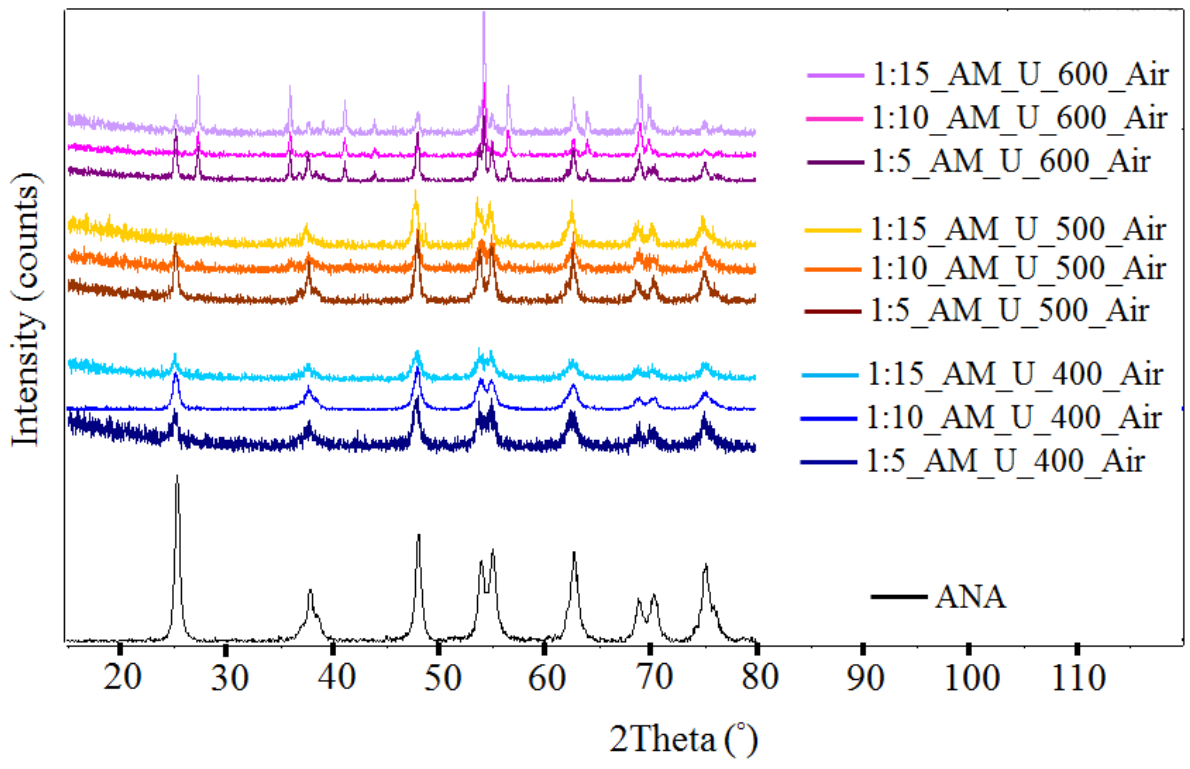

Figure 4- 2: PXRD patterns of ANA (anataseTiO₂) and AM_U for amorphous reaction with urea at the ratios 1:5, 1:10 and 1:15. Samples were heated to 400 ˚C, 500 ˚C and 600 ˚C for 5 hours in air.

Table 4- 1: Summary of PXRD results and product colours for the amorphous titanium isopropoxide hydroxide heated with urea in air at T= 400 ˚C, 500 ˚C and 600 ˚C. EA results of 1:5 AM_U and 1:10 AM_U

Sample	Product Colour	PXRD	EA percentages (%)		
ANA (blank)	White	Anatase	**N**	**C**	**H**
1:5_AM_U_400_Air	Yellow	Anatase	0	0.13	0
1:10_AM_U_400_Air		Anatase	0.24	0.14	0
1:15_AM_U_400_Air		Anatase + rutile			
1:5_AM_U_500_Air		Anatase + rutile			
1:10_AM_U_500_Air		Anatase + rutile			
1:15_AM_U_500_Air		Anatase + rutile			
1:5_AM_U_600_Air		Anatase + rutile			
1:10_AM_U_600_Air		Anatase + rutile			
1:15_AM_U_600_Air		Anatase + rutile			

4.2.2. Reactions of Urea with Anatase TiO_2

Samples of ANA_U heated in air at various temperatures showed no change in colour, remaining white powder. Therefore, no further heating was carried out on these samples. However, heating the ANA_U samples under flowing nitrogen gas created changes in colour, with the majority of samples producing yellow powders. This colour change was interpreted as a sign that some reaction had occurred.

Figure 4-3 and Table 4-2 show the resulting PXRD patterns and observations in the samples from heating the anatase TiO_2 with urea in N_2 for 5 hours at temperatures of $400 \leq T/^{\circ}C \leq 500$ $^{\circ}C$. All samples seemed to present a single phase, the anatase phase. They showed good agreement with the reference pattern (JCPDS 21-1272) for the anatase phase. In addition, it can be seen that no further peaks are present. In particular, diffraction peaks of the rutile phase (JCPDS 21-1276) are not present.

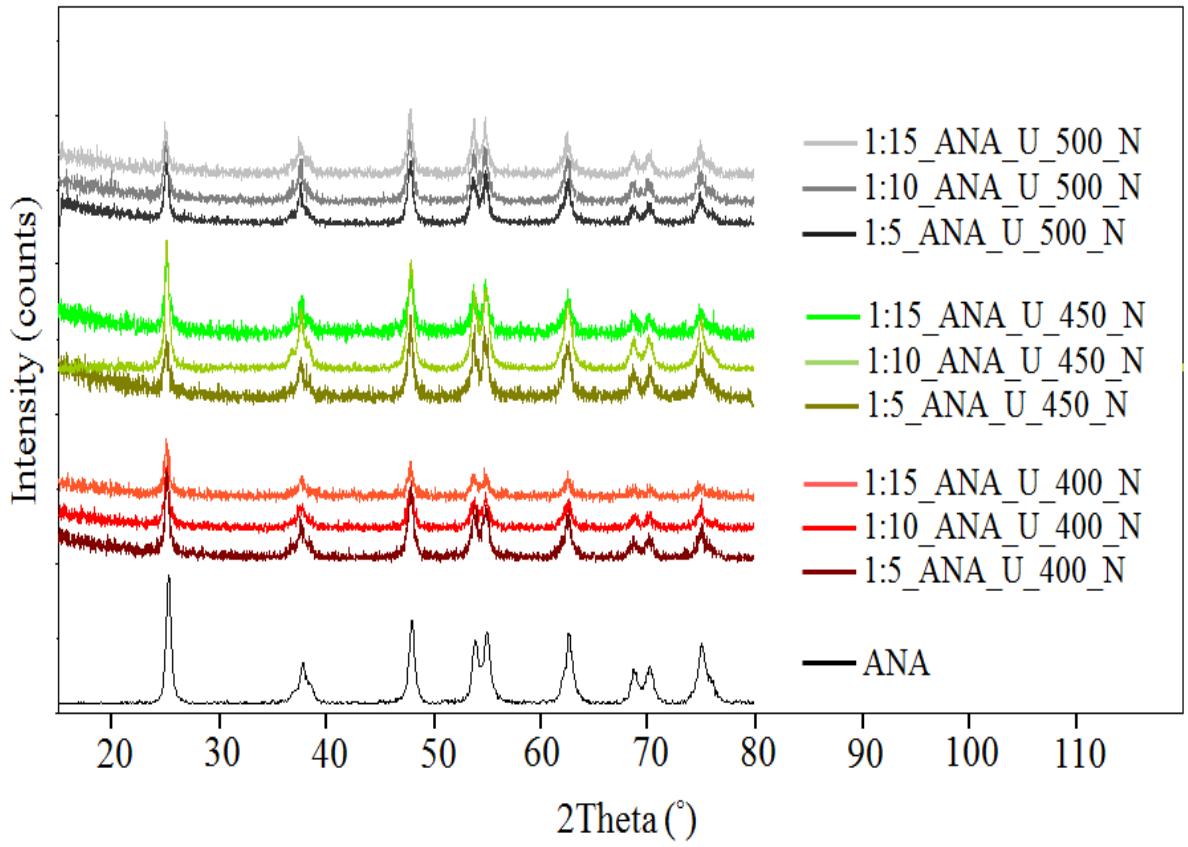

Figure 4- 3: PXRD patterns of ANA (anataseTiO_2) and ANA_U (anatase TiO_2 reacted with urea) in ratios of 1:5, 1:10 and 1:15. Samples were heated to 400 $^{\circ}C$, 450 $^{\circ}C$ and 500 $^{\circ}C$ for 5 hours under flowing nitrogen gas.

Figure 4-4 and Table 4-2 illustrate the FT-IR spectra of anatase TiO_2 (blank) and the 1:10_ANA_U series samples on KBr in the spectra range of 4000−400 cm^{-1}. There were three reasons for choosing and illustrating only the ratio (1:10) of ANA:U samples here. First, the

spectrum of the 1:15_ANA_U_400_N sample presented the same results as 1:10_ANA_U_400_N (see Appendix 7). Second, the 1:5 and 1:15 ANA_U samples heated at 500 °C showed the same spectra as 1:10_ANA_U_500_N (see Appendix 8). Finally, the 1:10_ANA_U sample is easy to compare with the 1:10_AM_U_400 sample, which was classified as the best sample (See *the previous section 4.1.1.Reactions of Urea with* $Ti(OCH(CH_3)_2)_{4-x}(OH)_x$).

All three spectra in Figure 4-4 show a broad peak in the region ranging from 700 cm^{-1} to 400 cm^{-1}, associated with the typical vibrational mode of the Ti—O bonds.[80, 134] The spectrum of the 1:10_ANA_U_400_N sample showed three more regions: a split, broad peak at about 2056 cm^{-1}; multi-peaks in the region of 1578–1254 cm^{-1}; and a sharp, weak peak at about 814 cm^{-1}. The splitting, broad stretching band at about 2056 cm^{-1} corresponded to the carbodiimide group (−N═C═N−).[141] The multi-peaks in the region from 1578 cm^{-1} to 1254 cm^{-1} and the sharp, weak peak at about 814 cm^{-1} could be related to urea residues produced by decomposition of urea (section 1.6.2.Decomposition of Urea). However, none of these regions were present when the temperature was increased to 500 °C (see the spectrum of the 1:10_ANA_U_500_N sample). Thus, it was decided to heat the 1:10_ANA_U sample to a temperature between 400 °C and 500 °C. The sample was heated to 450 °C and showed a spectrum with a single, broad band at about 2055 cm^{-1} and no peaks due to urea residues (i.e. released all urea residues). The 1:10_ANA_U_450_N sample is classified as the best sample, so it will be discussed more in the section *Preparation of New Potential* $TiO_{2-x}(CN_2)_x$ *Nanoparticles*. The samples of1:10_ANA_U_400 and 1:10_ANA_U_400 are not recommended as the best samples because the FT-IR data showed the presence of urea residues with carbodiimide fragments in the 1:10_ANA_U_400 sample and released carbodiimide from the 1:10_ANA_U_500 sample.

All spectra showed bands attributed to moisture adsorbed from the air. A broad band from 3600–3250 cm^{-1} is related to the hydroxide groups (O—H) [83]. A strong, sharp peak at 1636

cm^{-1} is attributed to H—O—H bonds[80, 134] and weak multi-peaks in the region from 2380 cm^{-1} to 2247 cm^{-1} are due to O=C=O bonds.[142] A peak due to impure KBr was found at 1384 cm^{-1}.

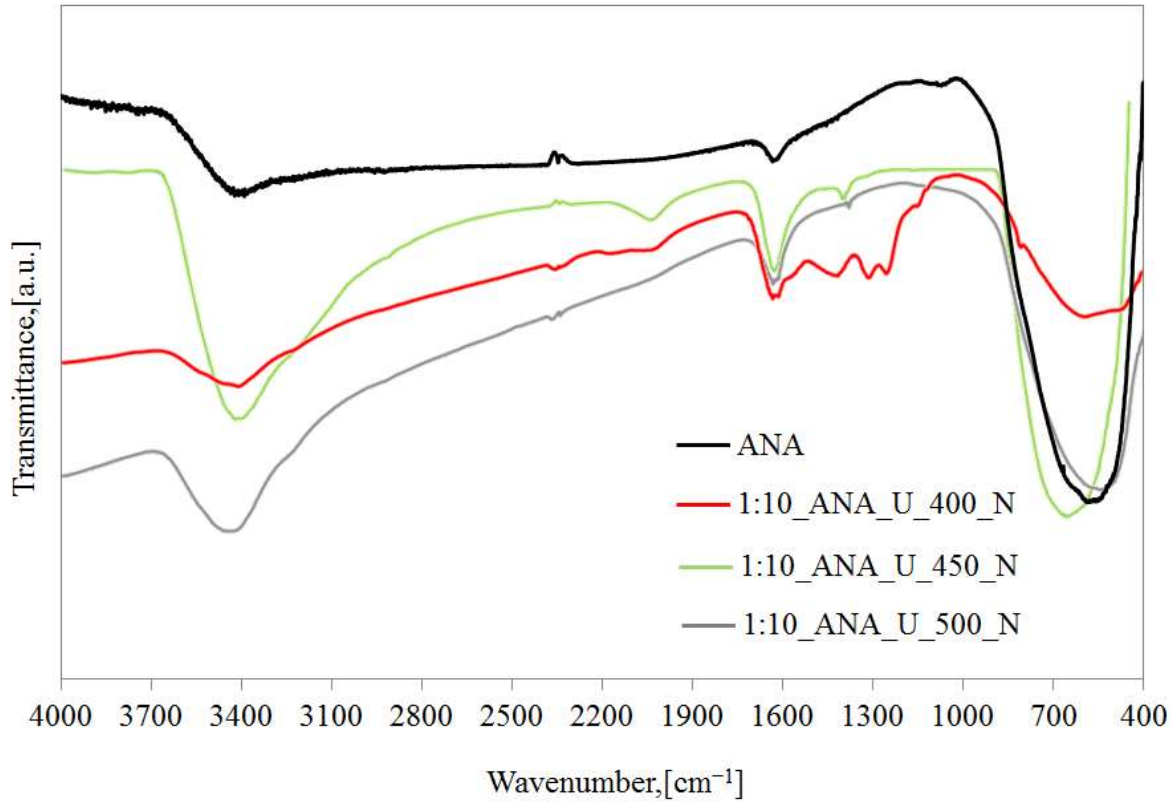

Figure 4- 4: FT-IR spectra of ANA (anatase, TiO_2) and ANA_U (anatase TiO_2 reacted with urea) in the ratio of 1:10. These samples were heated to 400 ˚C, 450 ˚C and 500 ˚C for 5 hours under flowing nitrogen gas.

Table 4- 2: Summary of FT-IR results and product colours of anatase titanium dioxide heated with urea in N_2.

Sample	Product colour	PXRD	FT-IR
ANA (blank)	White	Anatase	Ti-O bond
1:5_ANA_U_400_N	Yellow	Anatase	-
1:10_ANA_U_400_N			Urea residues + carbodiimide
1:15_ANA_U_400_N			
1:5_ANA_U_450_N			-
1:10_ANA_U_450_N			Carbodiimide
1:15_ANA_U_450_N			-
1:5_ANA_U_500_N	Light yellow		No urea residues + no carbodiimide
1:10_ANA_U_500_N	Yellow/brown		
1:15_ANA_U_500_N	Brown		

4.2.3. Preparation of New Potential $TiO_{2-x}(CN_2)_x$ Nanoparticles

This section further discusses the samples 1:10_AM_U_400_Air and 1:10_ANA_U_450_N, which were classified as the best results in the sections, 4.1.1.1. Reactions of Urea with $Ti(OCH(CH_3)_2)_{4-x}(OH)_x$ and 4.1.1.2. Reactions of Urea with Anatase TiO_2. These samples were characterised by FT-IR, UV-Vis, EA, and PXRD.

Amorphous Ti isopropoxide-hydroxide was used in two different reaction pathways (see Figure 4-5). First, it was heated in air for 5 hours at 400 ˚C to form a white anatase titanium dioxide (ANA), which was used as a blank sample. This anatase TiO_2 was then heated with urea to produce a yellow powder of 1:10_ANA_U_450_N. Second, AM

$Ti(OCH(CH_3)_2)_{4-x}(OH)_x$ was heated directly with urea, producing a yellow powder of 1:10_AM_U_400_Air (see Table 4-3). According to Rodgers in 1994, composites are coloured due to absorbing some wavelengths of visible light but reflecting or transmitting others.[15] The white colour of the AM and ANA powder samples is a result of absorption as well as reflection or transmission of the whole visible light spectrum, and they will still absorb ultraviolet light.[11, 15] The product colour changes that were obtained indicated that, within the visible light spectrum, the products were absorbing light; consequently, this raised the potential for band gap energy reduction through the use of the N-modification of the structure of TiO_2.

Figure 4- 5: Synthesis of ANA (TiO_2) and of amorphous/anatase reacted with urea.

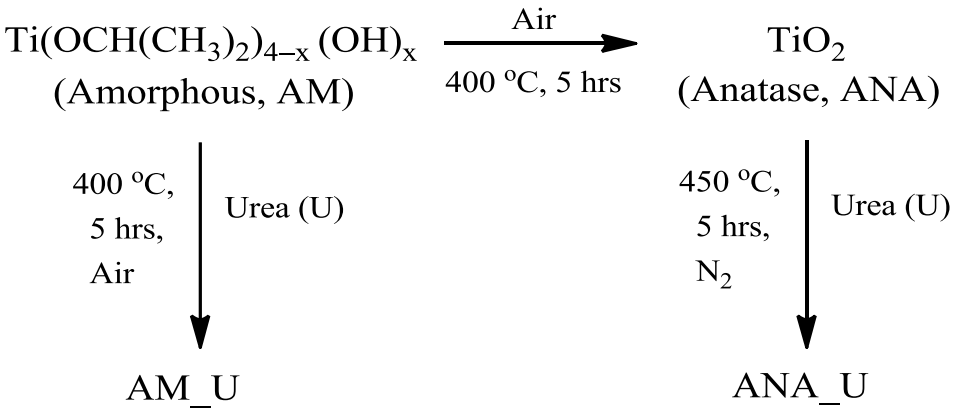

The PXRD patterns in Figure 4-6 illustrate the Ti isopropoxide-hydroxide (AM) converted crystallite structure before and after being reacted with urea. Additionally, ANA_U samples showed a single anatase phase after the reaction of TiO_2 (ANA) with urea. There was formation of an anatase phase in AM/ANA_U samples and no clear-cut changes in the structure. According to Viswanathan and Krishanmurthy (2012), formation of an anatase phase could be

due to small amount of nitrogen incorporated into the structure, hence the patterns of doped samples in PXRD being similar to that of pure TiO_2.[85] This means that in general, if the sample before and after doping with nitrogen did not show any change in PXRD patterns, this is consistent with a small amount of doping. PXRD is insensitive to small local changes in structure and may not indicate the presence in small amounts of nitrogen or other species (e.g. carbodiimide). Therefore further analysis such as FTIR analysis and elemental analysis is required.

Notably, the diffraction peaks in the PXRD patterns of both the 1:10_AM_U_400_Air and the 1:10_ANA_U_450_N samples were slightly shifted to lower angles when compared to the pattern of TiO_2 (blank). These shifts were perhaps due to changes in unit cell parameters. This could occur because of partial substitution, or doping, of the TiO_2 lattice with an external particle source that has a larger ionic radius than oxygen.[143] This leads to increased unit cell parameters compared to those in pure TiO_2, which leads to decreased 2θ angles for diffraction peaks.[143]

Table 4-3 shows the calculation of unit cell parameters using the *CHECKCELL* program and shows the crystallite size calculated using the Scherrer Equation.[11, 12, 128] All patterns were indexed using a tetragonal-body-centred ($\alpha=\beta=\gamma=90°, I4_1/amd$ *(141)*) unit cell. The blank anatase (ANA) had a = b = 3.785(10) *Å* and *c* = 9.514(8) Å, and the AM_U and ANA_U samples showed no changing in the axes and in unit cell volumes compared to TiO_2.

Crystallite size was calculated from the highest diffraction peak (101) using the Scherrer Equation.[11, 12, 128] The results of these calculations showed that the 1:10_ANA_U samples decreased in size to 8 nm, compared to the particle size of pure TiO_2. The reason for this decrease in particle size of the 1:10_ANA_U sample compared to pure ANA TiO_2 is still unclear.

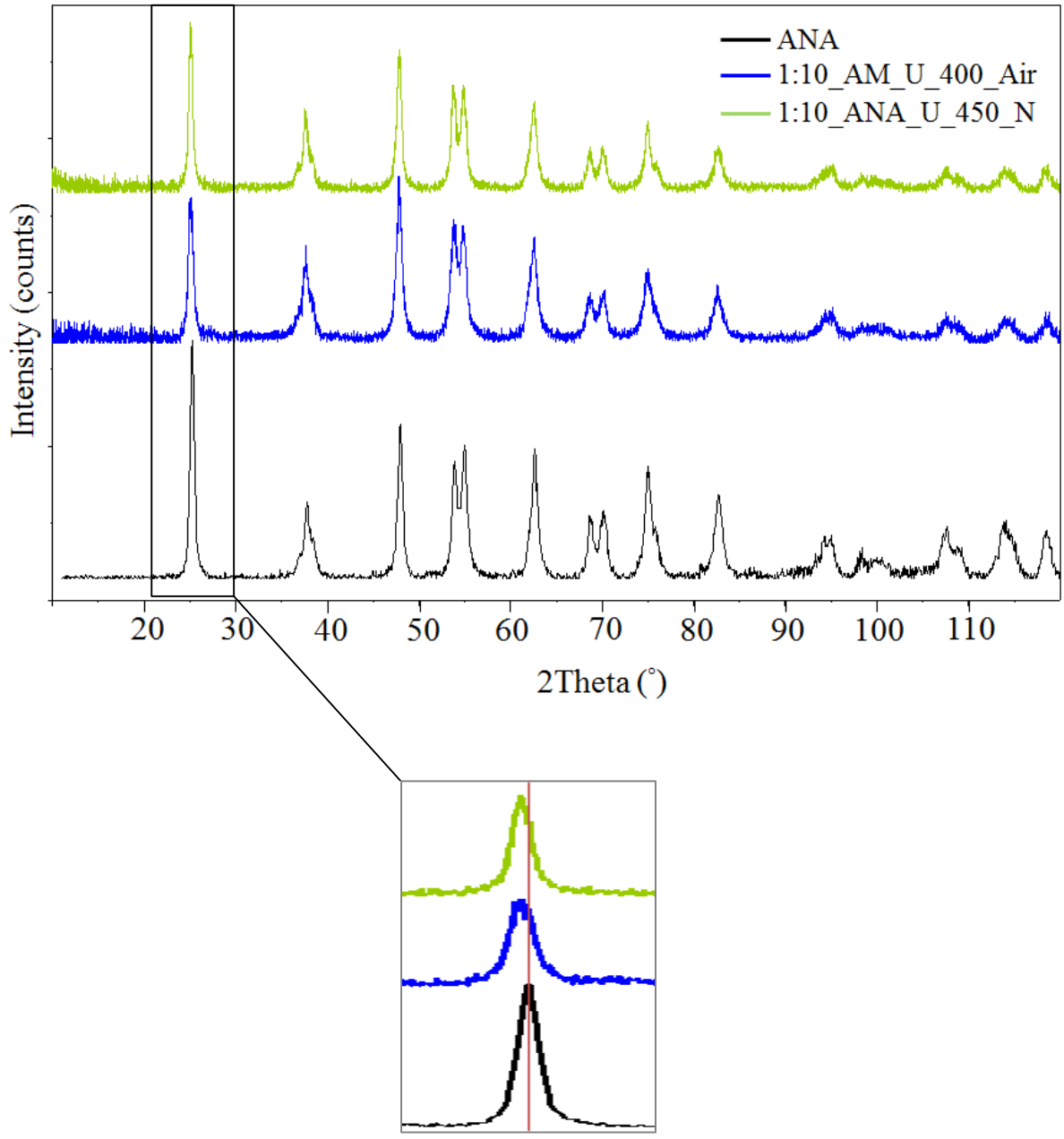

Figure 4- 6: PXRD patterns of ANA (anataseTiO_2, blank) and AM_U (amorphous heated with urea) at 400 °C in air and ANA_U (anatase heated with urea) at 450 °C under flowing nitrogen. Both samples had a ratio of 1:10 and a reaction time of 5 hours.

Table 4- 3: Unit cell parameter and crystallite size calculations of ANA (anatase), AM_U (amorphous to urea) at 400 ˚C and ANA_U (anatase to urea) at 450˚C.

Sample	Sample colour	Unit cell parameter (Å)			Volume (Å)^3	Crystallite size (nm)
		a	b	c		
ANA	White	3.785(10)	3.785(10)	9.514(8)	136.3(8)	11
1:10_AM_U	Yellow	3.792(2)	3.792(2)	9.506(3)	136.65(18)	11
1:10_ANA_		3.789(9)	3.789(9)	9.507(5)	136.5(7)	8

Figure 4-7 illustrates the FT-IR spectra of the anatase TiO_2 (blank), AM_U and ANA_U samples in KBr in the spectral range of 4000−400 cm^{-1}. Moisture adsorbed from the air presents a broad band from 3600 cm^{-1} to 3250 cm^{-1}, which is related to the hydroxide groups (O—H) [83]; a strong, sharp peak at 1636 cm^{-1}, which is attributed to H—O—H bonds[80, 134]; and weak multi-peaks in the region of 2380−2247 cm^{-1}, which are attributed to O═C═O bonds.[142] In all spectra, the only impurity peak was found at 1384 cm^{-1}, due to of impurity found in the KBr.

The spectra of both the 1:10_AM_U_400_Air and the 1:10_ANA_U_450_N samples show a broad peak in the region from 700 cm^{-1} to 400 cm^{-1}, associated with the typical vibrational mode of the Ti—O bonds.[80, 134] Moreover, they showed an interesting, broad weak peak at about 2055 cm^{-1}, corresponding to the carbodiimide group (−N═C═N−).[141] The story of carbodiimide formation is as follows: at temperatures of less than 250 ˚C, urea decomposes to cyanamide by two methods, either by forming cyanic acid and then cyanamide, or by forming from urea directly. This cyanamide will convert to the more stable carbodiimide, by resonance (see *Section 1.6.2. Decomposition of Urea*).[141, 86] The cyanamide spectrum showed a band of (−N−C≡N) at about 2260 cm^{-1}, which was not present in the spectra of 1:10_AM_U_400_Air

and 1:10_ANA_U_450_N.[144, 145] These samples also did not contain a band in the range of 3500–3300 cm^{-1}, which can be assigned to the (N−H) bond.[141, 142] Finally, no extra peaks of undecomposed urea residues are present in the spectra of ANA_U or AM_U. The FT-IR spectra support the formation of titanium oxide-carbodiimide with the formula $TiO_{2-x}(CN_2)_x$ by reacted urea with anatase at a temperature of 450 ˚C, and with amorphous titanium isopropoxide-hydroxide at a temperature of 400 ˚C. In the $TiO_{2-x}(CN_2)_x$ small amount of O^{2-} anion substituted with $(CN_2)^{2-}$ anion as shown in Table 4-4; therefore the anatase structure is maintained. Although the most comment formulas for the introduction of nitrogen into the TiO_2 lattice are TiN, $TiO_{2-x}N_y$, and $TiN_{1-x}O_x$, as reported in other studies (*see Section 1.6.5. Previous Preparations of N-modified Titanium Dioxide*),[61, 96, 100, 104, 106] this study showed different formula $TiO_{2-x}(CN_2)_x$. The innovation in this study was not in its finding of the presence of the $(CN_2)^{2-}$ anion in the product because some previous studies have also shown this; rather, the value in this study was the presence of the $(CN_2)^{2-}$ anion in TiO_2. Some examples of these studies; the preparation of lanthanum dioxymonocyanamide ($La_2O_2CN_2$) and the magnetic transition metal carbodiimide phase, $MnCN_2$, were reported by Hashimoto et al. (1995) and Liu et al. (2003).[107, 108] Moreover, the synthesis and structure of crystalline copper carbodiimide (CuNCN) was reported by Jacobs et al. (2013).[146, 147] These examples show the presence of metals other than Ti, which is addressed in this current work; therefore, to date, the preparation of $TiO_{2-x}(CN_2)_x$ has not been reported.

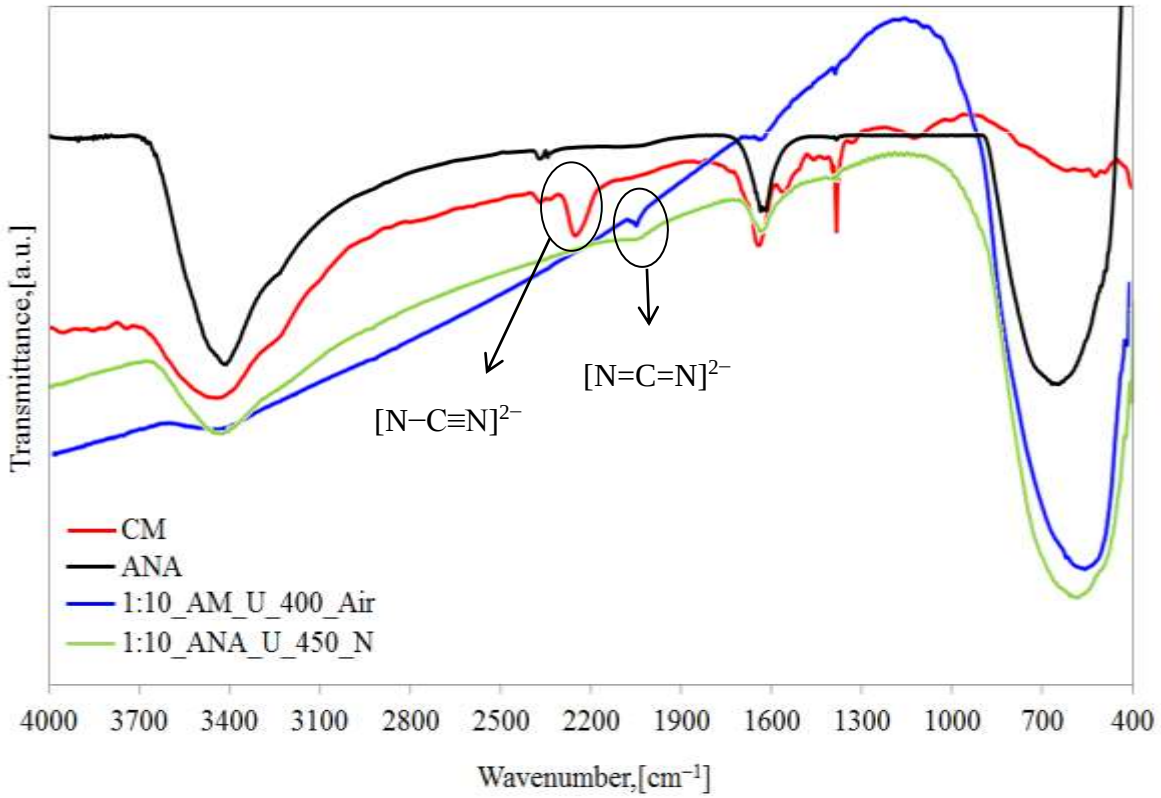

Figure 4- 7: FT-IR spectra of ANA (blank anatase), KBr, AM_U (amorphous heated with urea) at 400 ˚C in air and ANA_U (anatase heated with urea) at 450 ˚C under flowing nitrogen. Both samples had a ratio of 1:10 and a reaction time of 5 hours.

Table 4-4 illustrates elemental analysis (EA) results on N and C content and the formula calculation. The AM_U and the ANA_U samples both showed negligible amounts of hydrogen. This is in good agreement with the FT_IR spectra, which show no N−H band in both samples. These samples showed approximately a 2:1 ratio of N:C, which supports the presence of the $(CN_2)^{2-}$ anion (carbodiimide chemical). The estimation of the chemical formula then is $TiO_{2-x}(CN_2)_x$. The average value of x from cal. data is x = 0.01 for AM_U sample and x = 0.04 for ANA_U sample. This of course assumes homogeneity of substitution, which is probably not the case, as indicated by the UV-Vis spectra (Figure 4-8).

Table 4- 4: EA results and calculation of the formula $TiO_{2-x}(CN_2)_x$.

Sample labelled	EA percentages (%)			Calculation (%)		Formula
	N	C	H	N	C	
1:10_AM_U_400_Air	0.24	0.14	0	0.35	0.15	$TiO_{1.99}(CN_2)_{0.01}$
1:10_ANA_U_450_N	1.33	0.62	0	1.39	0.59	$TiO_{1.96}(CN_2)_{0.04}$

Figure 4-8 shows UV-Vis spectra of the pure anatase TiO_2 (ANA), AM_U and ANA_U samples. Figure 4-9 and Table 4-5 present the results of band-gap calculation. The ANA sample showed one edge that absorbed at the UV-region at a wavelength of 384 nm and band gap of 3.22 eV. However, the AM_U and ANA_U samples both produced two edges, one absorbed in the Vis region and the other in the UV region. These samples showed decrease band gap at less than 3.22 eV of pure TiO_2 at 2.37 eV and 2.30 eV, followed by absorbing in the visible region at 523 and 539 nm in the AM_U and ANA_U samples, respectively. In addition, they showed absorbed ultraviolet in the region of 380 nm and of 372 nm with a band gap at 3.26 eV and 3.33 eV for the AM_U and ANA_U samples, respectively. The edge showing absorption in the UV-region corresponds to the edge present in the pure ANA sample. The presence of two edges of absorption indicate that the AM_U and ANA_U samples produced a mixture of $TiO_{2-x}(CN_2)_x$ and TiO_2. Yin et al. (2005) report that N-doped TiO_2 showed good photocatalytic activity and excellent absorption in the visible light region with presented two adsorption edges in the UV-Vis spectra.[61] Cong et al., 2007, report that N-TiO_2 products produced with anatase phase, their UV-Vis spectra showed two adsorptions band, and showed the highest

photocatalytic activity for rhodamine B decomposition in the visible region.[148] This means that there is a possibility of $TiO_{2-x}(CN_2)_x$ product to show high visible light activity.

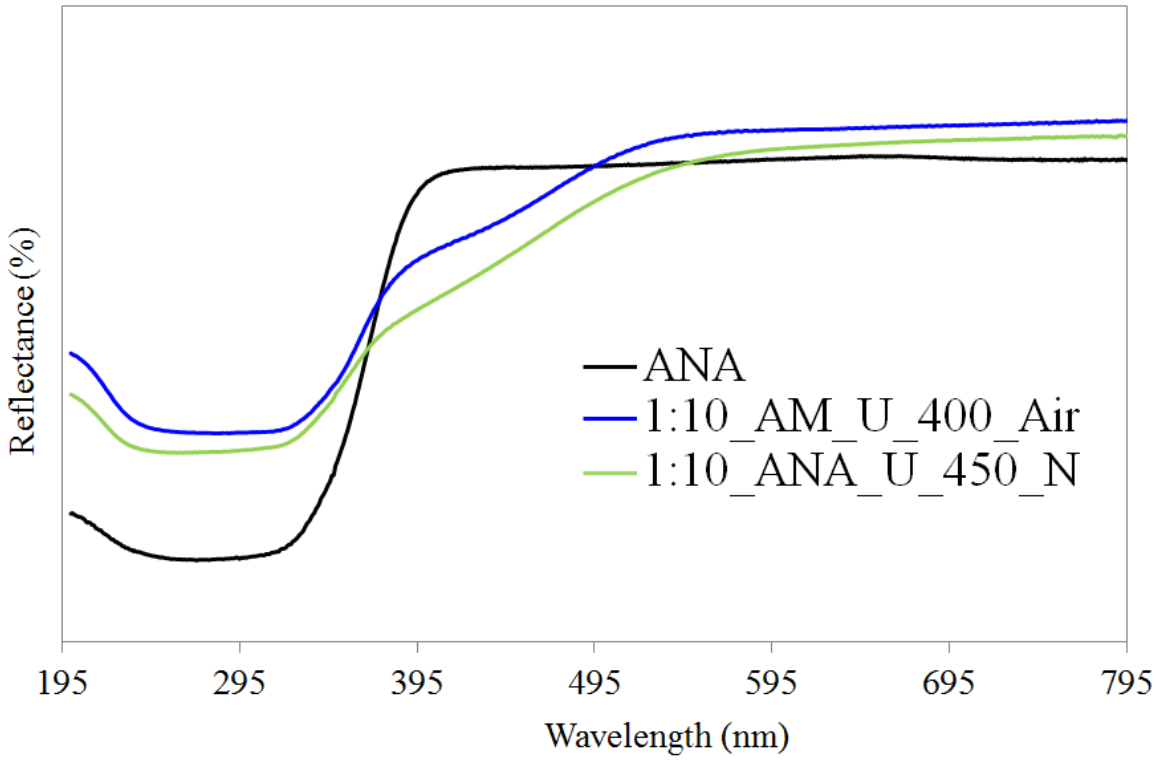

Figure 4- 8: UV-Vis spectra of ANA (blank anatase), AM_U (amorphous heated with urea) at 400 ˚C in air and ANA_U (anatase heated with urea) at 450 ˚C under flowing nitrogen. Both samples had a ratio of 1:10 and a reaction time of 5 hours.

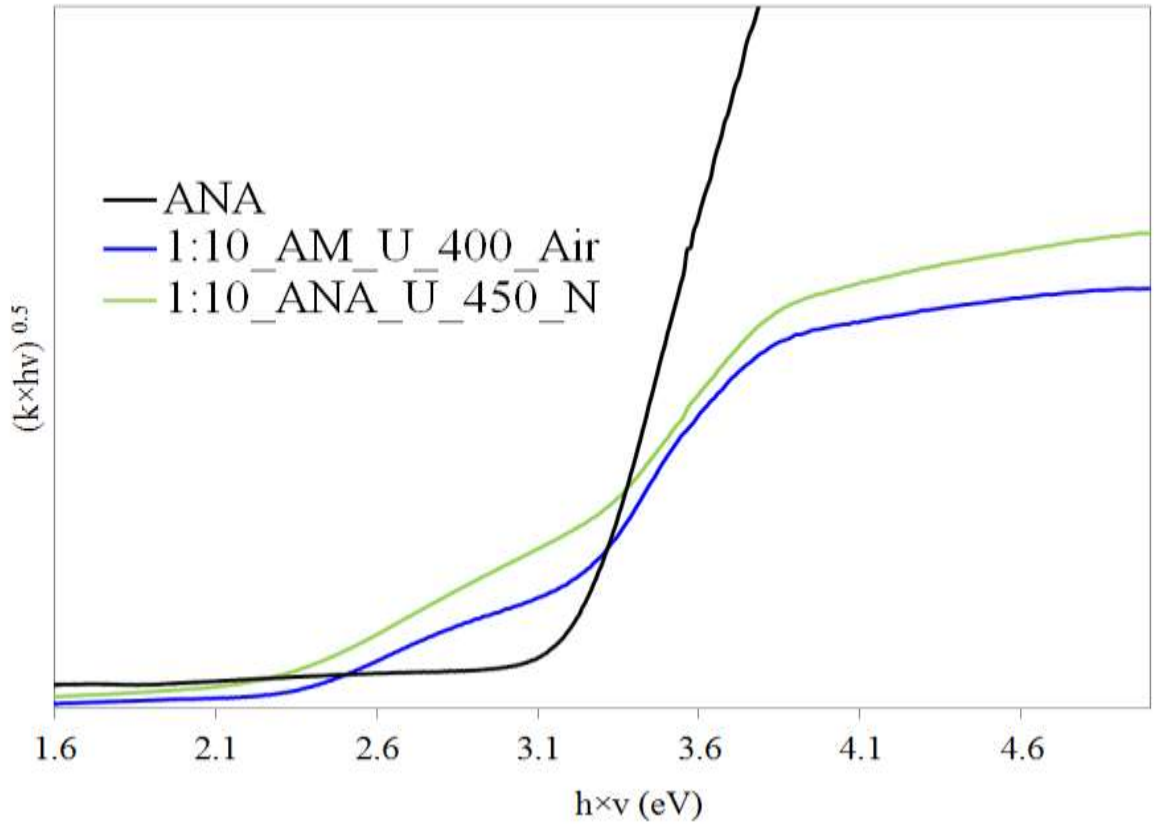

Figure 4- 9: Band-gap calculation using the Kubelka–Munk function for ANA (blank anatase), AM_U (amorphous heated with urea) at 400 ˚C in air and ANA_U (anatase heated with urea) at 450 ˚C under flowing nitrogen. Both samples had a ratio of 1:10 and a reaction time of 5 hours.

Table 4- 5: Band-gap energies (E_{bg}) and wavelengths (λ) using the Kubelka–Munk function calculation

Sample	E_{bg} (eV)	λ (nm)
TiO_2	3.22	384
1:10_AM_U_400_Air	2.37 3.26	523 380
1:10_ANA_U_450_N	2.30 3.33	539 372

4.2.4. Reactions of Cyanamide with Anatase TiO_2

Figure 4-10 illustrates the PXRD patterns of the products resulting from the reactions between anatase TiO_2 and cyanamide at temperatures of 400˚C, 450 ˚C, 500 ˚C, and 600 ˚C for 5 hours under flowing nitrogen gas. All samples showed changes in colour compared to the original mixtures, including orange, yellow, grey, green and blue (Table 4-6).

All samples showed mixed phases of anatase and rutile except the three ratios (1:1, 1:2 and 1:3) of the ANA_CM_400 samples and the ratio (1:1) of the ANA_CM_450 sample. These samples showed single anatase phase. Therefore, these four samples were of interest, thus FT-IR analysis was conducted.

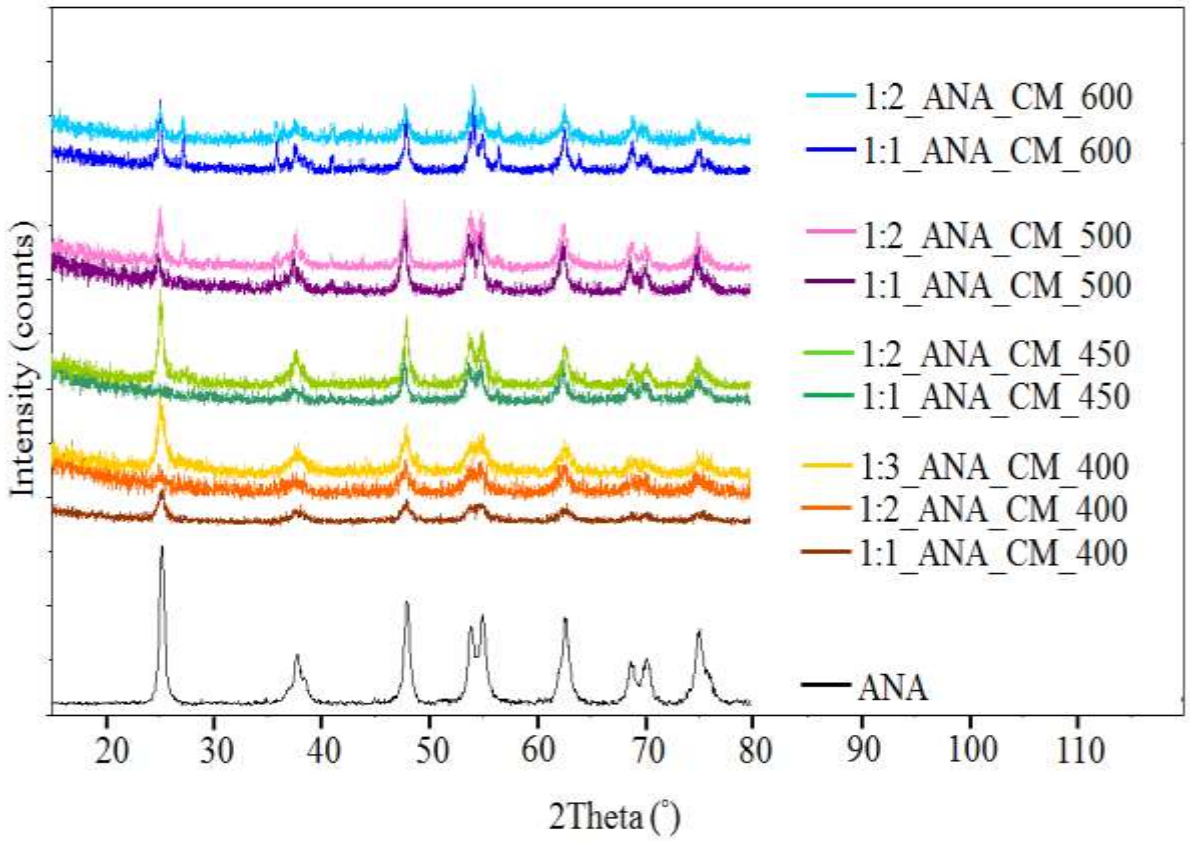

Figure 4- 10: PXRD patterns of ANA (anataseTiO_2, blank) and ANA_CM (anatase TiO_2 reacted with cyanamide) at various ratios and various temperatures in N_2.

Table 4- 6: Summary of product colours and phase assignation to PXRD patterns for products of reactions between TiO_2 and cyanamide in N_2.

Sample	Product Colour	PXRD
ANA	White	Anatase
1:1_ANA_CM_400	Orange	
1:2_ANA_CM_400		
1:3_ANA_CM_400		
1:1_ANA_CM_450	Yellow	
1:2_ ANA_CM_450	Dark yellow	Anatase + rutile
1:1_ ANA_CM_500	Grey	
1:2_ ANA_CM_500	Light Green	
1:1_ ANA_CM_600	Dark blue	
1:2_ ANA_CM_600		

Figure 4-11 shows the FT-IR spectra of 1:1_ANA_CM_400, 1:2_ANA_CM_400, 1:3_ANA_CM_400, and 1:1_ANA_CM_450. Note that all spectra show moisture absorbed from air in the regions 3600–3250 cm^{-1}, 1636 cm^{-1}, and 2380–2247 cm^{-1}, which correspond to hydroxide groups (O—H)[83], H—O—H bonds[80, 134] and O═C═O bonds[142], respectively. Impurity peaks were found at 1384 cm^{-1} and in the region ranging 2900–2800 cm^{-1} because of impurities in KBr (see Appendix 4). All samples presented a broad beak in the region 700–400 cm^{-1}, which is associated with the typical vibrational mode of Ti—O bonds.[80, 134]

The spectra of 1:1, 1:2, and 1:3 ANA_CM at 400 °C presented four regions, located at: 2923-2850 cm^{-1}, 2051 cm^{-1}, 1592–1168 cm^{-1}, and 814 cm^{-1}. The band at 2051 cm^{-1} revealed that it had split into two bands and was assigned in relation to carbodiimide fragments (−N═C═N−).[142] Multi-peaks were present in the regions from 1592 cm^{-1} to 1168 cm^{-1}, double peaks at 2923-2850 and a sharp peak was present at 814 cm^{-1}. These could be related to melamine, which is one of the decomposition products of cyanamide (spectrum of melamine in Appendix 9) (*section 1.6.3. Decomposition of Cyanamide*). Similarly, at the increased temperature of 450 °C, the 1:1_ANA_CM sample also showed the residues of cyanamide (could be melamine) accompanied with the appearance of carbodiimide at 2051 cm^{-1}. However, no splitting band could be seen at this carbodiimide peak; this need further study in the future. Because these samples showed cyanamide residues, no further analyses were conducted.

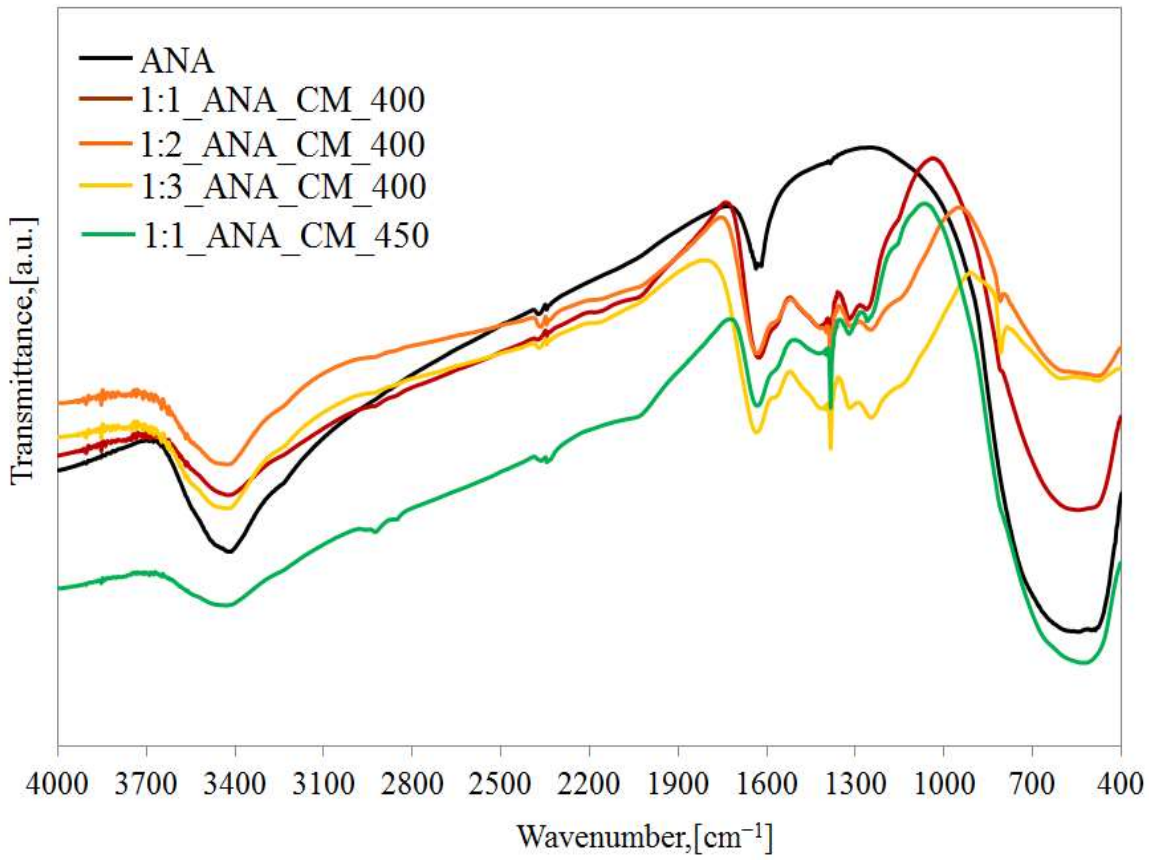

Figure 4- 11: FT-IR spectra of ANA (blank anatase) and ANA_CM (anatase reacted with cyanamide) at 400 ˚C and 450 ˚C in N_2.

4.2.5. Reactions of Cyanamide with Amorphous $Ti(OCH(CH_3)_2)_{4-x}(OH)_x$

Figures 4-12 to 4-14 and Table 4-7 show the PXRD patterns and a summary of AM_CM reactions at various temperatures of reactions and ratios. All samples showed changes in colour, including green, orange, yellow, and a mix of black and yellow (Table 4-7). The PXRD patterns of the samples showed various results, which were divided into three types: patterns that showed single anatase phase as in the samples of 1:0.25_AM_CM_400, 1:0.5_AM_CM_400, 1:0.75_AM_CM_400, and 1:1_AM_CM_400 (Figure 4-12); patterns that showed a single phase of the NaCl type/rock-salt structures (samples 1:2_AM_CM_450, 1:2_AM_CM_500, and 1:2_AM_CM_550) (Figure 4-13); and finally, PXRD patterns that showing mixed phases (Figure 4-14). The mixed phases were either a mix of two phases of anatase and rock-salt

structures as in the samples of 1:1_AM_CM_450 and 1:1_AM_CM_500, or a mix of three phases: anatase, rutile and rock-salt structures (samples 1:1_AM_CM_600 and 1:2_AM_CM_600).

Further analyses focused on single-phase patterns; so in accordance with previous PXRD patterns, any samples that showed single phases were classified as candidates for further analysis. Therefore, this study will be focused on the samples are presented in the Figures 4-12 and 4-13. The samples that showed single anatase phases (Figures 4-12) will be studied in the next section *(4.2.6. Preparation of New Potential Nanoparticles via the Use of Cyanamide*). However, those samples that formed rock-salt structures (Figures 4-13) were discussed as follows.

Figure 4-13 illustrates the PXRD patterns of the three samples that showed rock-salt structures and produced mixtures of black and yellow powders. This visual absorption leads to the conclusion that at least two phases are present in these samples. However, the broadness of the peaks only allows the identification of a NaCl-type structure. The patterns of the samples at the ratio 1:2_AM_CM at temperatures of 450 ˚C, 500 ˚C, and 550 ˚C showed positive correlation with some modules that have cubic crystal systems, which is rock-salt structure, see Appendix 13. These module references of Joint Committee on Powder Diffraction Standards are: 00-031-1403 database for titanium nitride, and/or 00-049-1325 database for titanium nitride oxide.

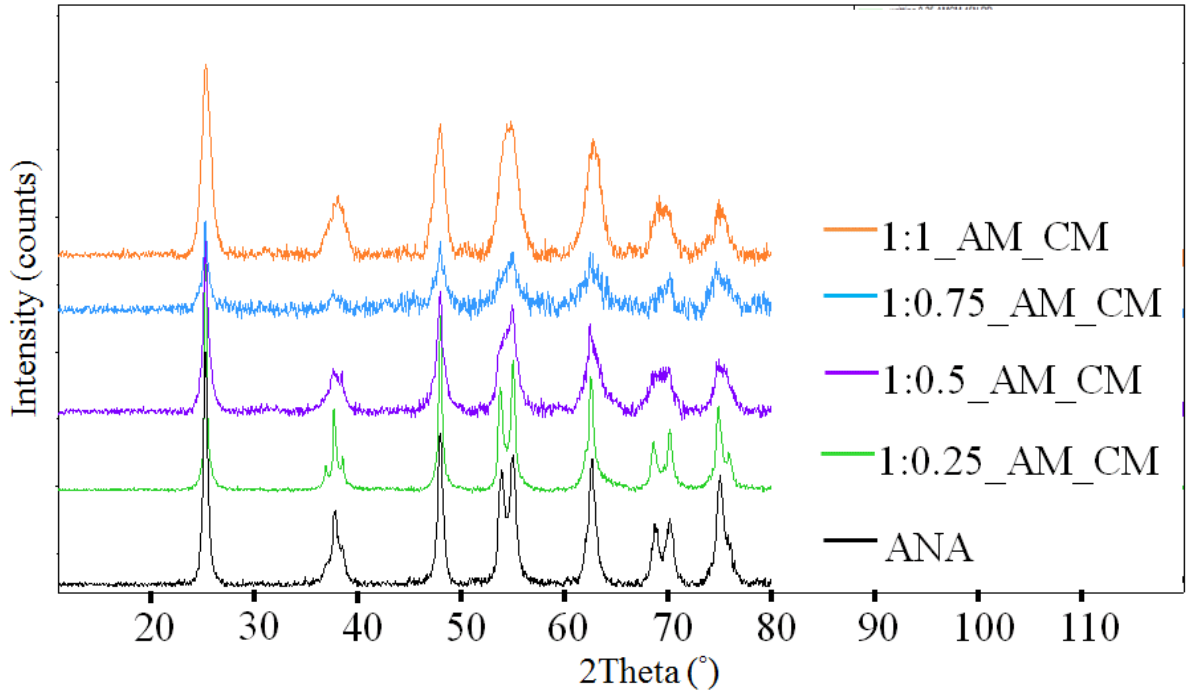

Figure 4- 12: PXRD patterns show single anatase phase of the samples 1:0.25, 1:0.75, 1:0.5, and 1:1 (AM:CM) at T= 400˚C, which are compared to the ANA sample (blank). CM=cyanamide; ANA=anatase; AM=amorphous

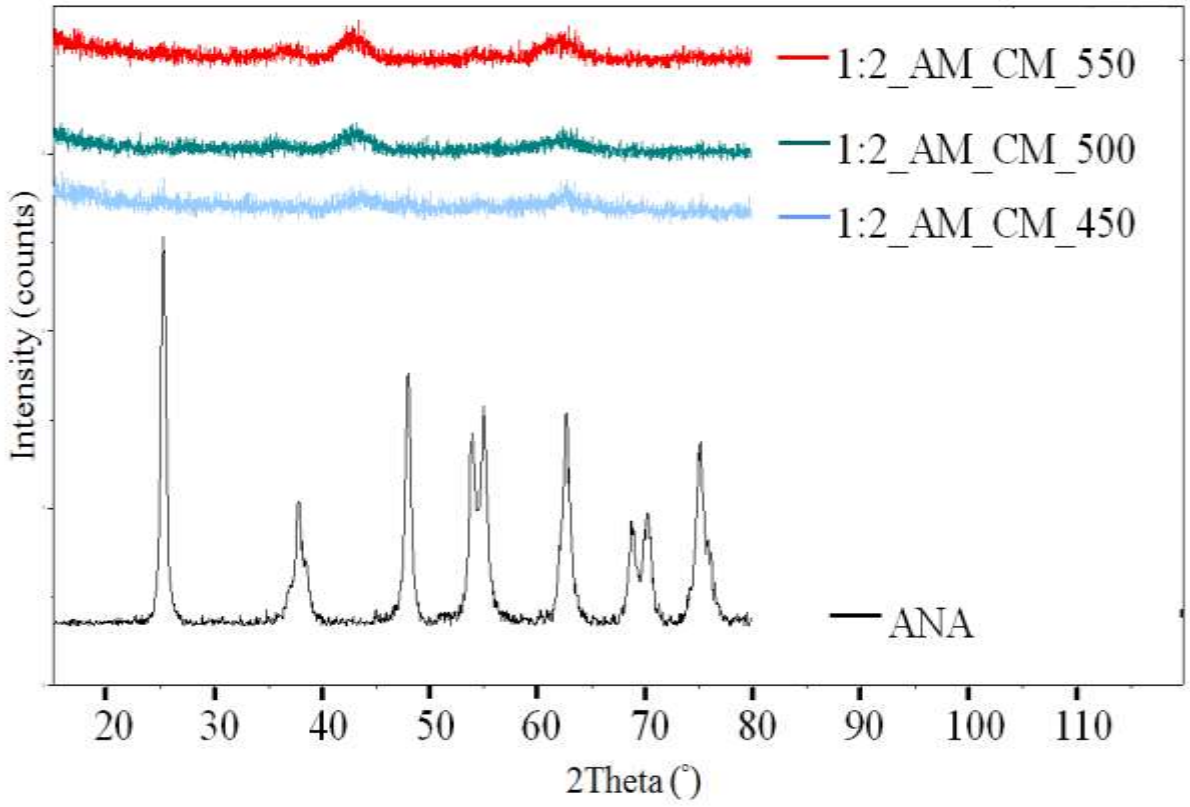

Figure 4- 13: PXRD patterns show single NaCl-type (rock-salt structure) phase of the ratio 1:2_AM_CM at T= 450 ˚C, 500 ˚C, and 550 ˚C, which are compared to the ANA sample (blank). CM=cyanamide; ANA=anatase; AM=amorphous

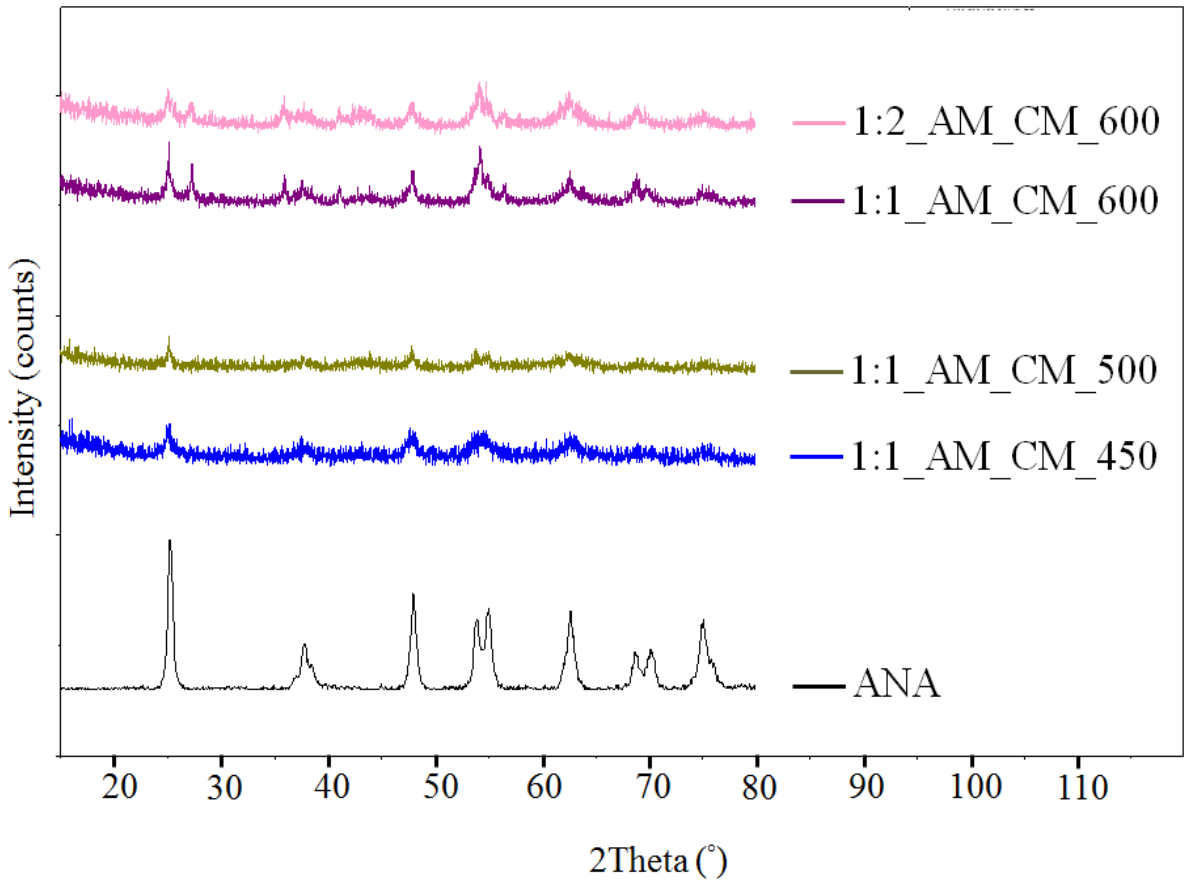

Figure 4- 14: PXRD patterns show mixed phases of 1:1_AM_CM_450, 1:1_AM_CM_500, 1:1_AM_CM_600, and 1:2_AM_CM_600 samples, which are compared to the ANA sample (blank). CM=cyanamide; ANA=anatase; AM=amorphous

Table 4- 7: Summary of product colours and phase evaluation of AM_CM (amorphous to cyanamide) at various ratios and temperatures.

Sample	Product Colour	PXRD
ANA	White	Anatase
1:0.25_AM_CM_400	Light green	
1:0.5_AM_CM_400	Green	
1:0.75_AM_CM_400	Yellow	
1:1_AM_CM_400	Dark yellow/orange	
1:2_AM_CM_400	Orange	Amorphous (Appendix 15)
1:1_AM_CM_450	Green	Anatase + rock-salt structure
1:2_AM_CM_450	Mix of black and yellow	Rock-salt structure
1:1_AM_CM_500		Anatase + rock-salt structure
1:2_AM_CM_500		Rock-salt structure
1:2_AM_CM_550		
1:1_AM_CM_600	Dark Green	Anatase + rutile + rock-salt structure
1:2_AM_CM_600	Mix of black and yellow	

Figure 4-15 shows the FT-IR spectra, which usually absorb moisture from the air and contain impurity peaks due to the use of various KBr, as mentioned in the previous section. The spectra of the 1:2_AM_CM_450 sample showed a broad peak at band 2052 cm^{-1}, which corresponds to carbodiimide.[142] This peak decreases with increased temperatures of 500 ˚C and 550 ˚C. As Table 4-8 shows for these samples, EA showed that the weight percentages of nitrogen (N) were greater than the percentages of carbon (C). EA also showed that increasing temperatures led to decreased hydrogen percentages (H). Given these results, it was very difficult to decide which compound would be formed: titanium nitride oxide, and/or titanium nitride (as PXRD showed), and/or new compounds could be formed, such as titanium carbodiimide or titanium oxide carbodiimide (as FT-IR showed).

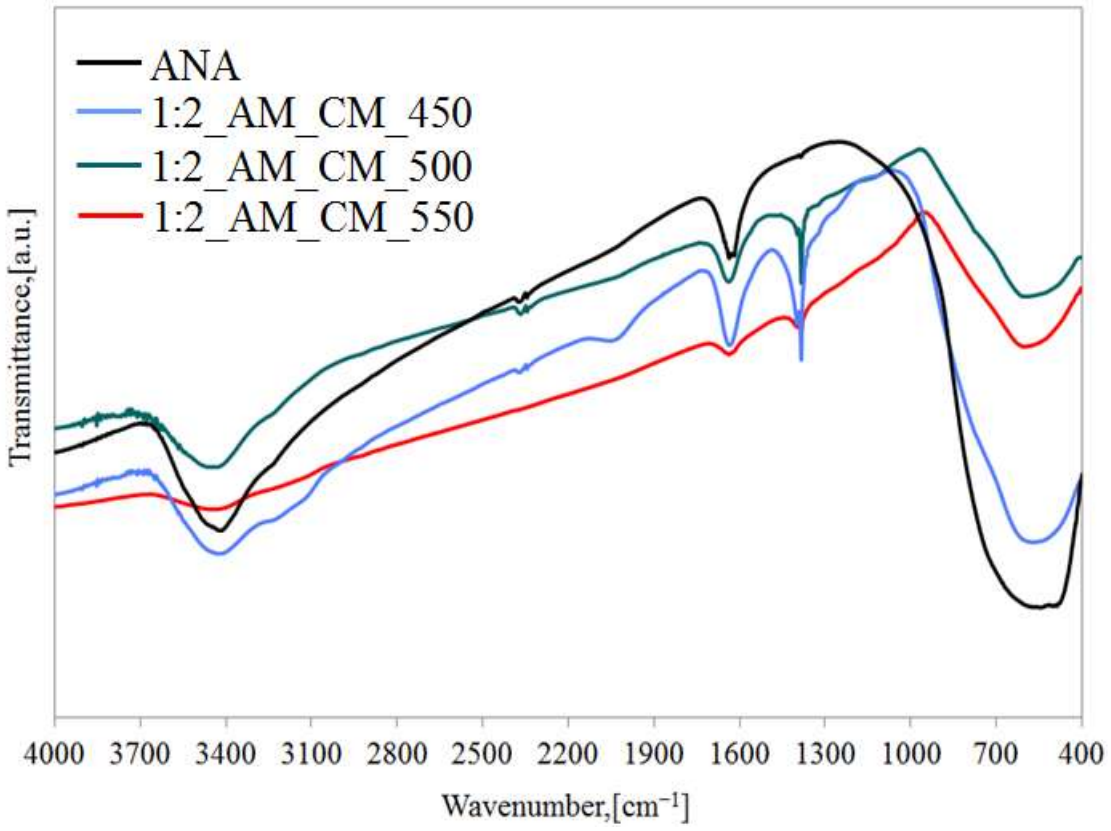

Figure 4- 15: FT-IR spectra of ANA (blank anatase), 1:2_AM_CM (amorphous : cyanamide) at various temperatures 450 ˚C, 500 ˚C and 550 ˚C in N_2.

Table 4- 8: EA of 1:2 AM_CM at 450 ˚C, 500 ˚C and 550 ˚C in N_2.

Sample	Atoms Weight Percentage		
	N	C	H
1:2_ AM_CM_450	8.16	0.83	1.26
1:2_ AM_CM_500	10.32	1.53	0.78
1:2_ AM_CM_550	9.17	2.67	0

4.2.6. Preparation of New Potential Nanoparticles via the Use of Cyanamide

Amorphous (AM) $Ti(OCH(CH_3)_2)_{4-x}(OH)_x$ was used in two different reaction pathways (Figure 4-16). First, it was heated in air for 5 hours at 400 ˚C to form a white anatase titanium dioxide (ANA), which then was used as a blank sample. Second, a light yellow powder of AM $Ti(OCH(CH_3)_2)_{4-x}(OH)_x$ mixed with cyanamide was heated for 5 hours at 400 ˚C in N_2, which produced AM_CM samples in various colours, including light green, green, yellow and dark yellow/orange, for the ratios 1:0.25 AM:CM, 1:0.5 AM:CM, 1:0.75 AM:CM and 1:1 AM:CM, respectively (See Table 4-9). According to Rodgers in 1994, composite are coloured due to absorbing some wavelengths of visible light but reflecting or transmitting others.[15] The white colour of the AM and ANA powder samples, is a result of absorption as well as reflection or transmission of the whole visible light spectrum, and the samples will still absorb ultraviolet light. [11, 15] Therefore, the change in colour of the products obtained was a promising sign that they now absorbed light within the visible light spectrum, thus indicating the possibility of a reduction in band-gap energy by successful N-modification of the TiO_2 structure.

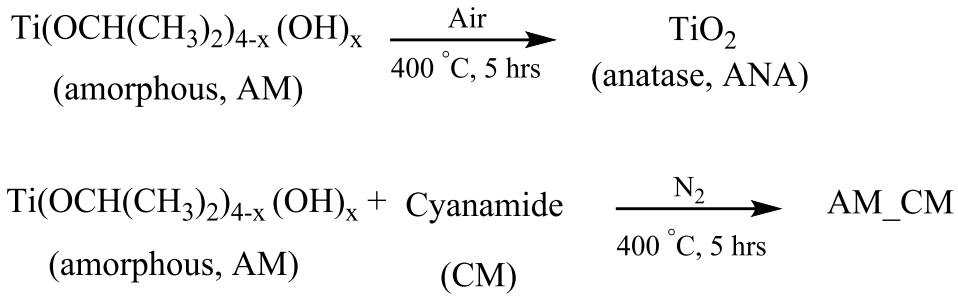

Figure 4- 16: Synthesis of ANA (TiO_2) and of AM_CM (amorphous titanium isopropoxide hydroxide reacted with cyanamide).

The PXRD patterns in Figure 4-17 illustrate how the AM sample converted to crystalline structures (anatase phase) before and after being reacted with cyanamide. Additionally, all patterns of AM_CM samples showed a single pure anatase phase. According to Viswanathan and Krishanmurthy (2012), the formation of an anatase phase could be due to a small amount of nitrogen incorporated into the structure, hence the patterns of doped samples in PXRD are similar to those of pure TiO_2.[85] This means that in general, if the sample before and after doping with nitrogen did not show any changes in PXRD pattern that could be related to the amount of doping.

Table 4-9 shows parameters and volume of unit cell calculated by using the *CHECKCELL* programme and shows crystallite size calculated by using the Scherrer Equation.[11, 12, 128]. Unit cell calculations show that all samples formed tetragonal-body-centred *($\alpha=\beta=\gamma=90°, I4_1/amd$ (141)*). The blank anatase (ANA) has *$a = b = 3.785(10)$* and *$c = 9.514(8)$ Å*, and the AM_CM samples showed fluctuation changes in unit cell volume with increases in the ratios compared to the TiO_2 sample. These changes in the results after heating the amorphous titanium isopropoxide hydroxide with cyanamide indicate that some defect could have occurred in the amorphous $Ti(OCH(CH_3)_2)_{4-x}(OH)_x$. In general, the diffraction peaks in the PXRD patterns of the samples are slightly shifted to lower angles or to higher angles (*2θ)* when compared to the

pattern of TiO_2 (blank). These shifts are perhaps due to changes in unit cell parameters. This could occur because of partial substitution, or doping, of the TiO_2 lattice with an external particle source that has a larger or smaller ionic radius than oxygen.[143] This then leads unit cell parameters to increase (decrease 2θ angles) or decrease (increase 2θ angles) compared to those in pure TiO_2 that leads to decreased or increased 2θ angles for diffraction peaks.[143] For example, the sample 1:0.25_AM_CM showed decrease in unit cell volume and increases in 2θ angles for diffraction peaks compared to those in pure TiO_2. On the other hand, the other patterns of 1:0.5, 1:0.75 and 1:1 (AM:CM) showed increase in unit cell volume and decreases in 2θ angles when the concentration of the cyanamide increases from 0.5 to 1:1. These could be due to the partial substitution, or doping, of the TiO_2 lattice with an external particle source.

Crystallite size was calculated from the highest diffraction peak (101), using the Scherrer Equation.[11, 12, 128] The results of these calculations showed a decrease in size as the AM:CM ratios increased from 1:0.25 to 1:1_AM_CM. In 2000, Dann reported the particle size effect on the width of the reflections (i.e. the growth of peak width with a reduction in particle size).[12] Therefore, the 1:0.25_ANA_CM pattern included bigger particles size and a sharper/narrower peak width compared to the other ratios 1:0.5, 1:0.75, and 1:1, of the ANA_CM patterns. The reason for this decrease and increase in the particle size of these samples compared to pure ANA TiO_2 is still unclear.

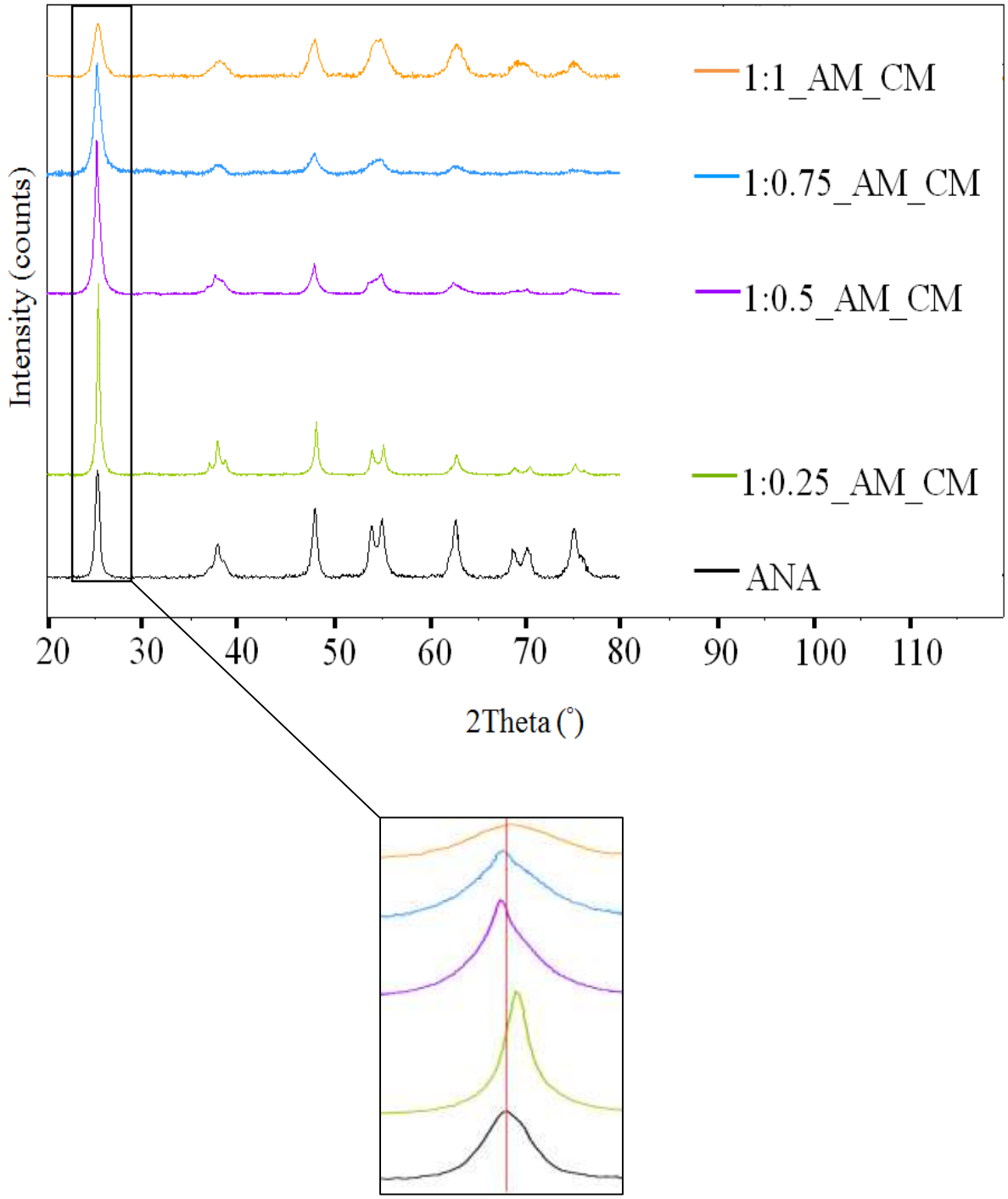

Figure 4- 17: PXRD patterns of ANA (anatase TiO_2, blank) and AM_CM (amorphous, $Ti(OCH(CH_3)_2)_{4-x}(OH)_x$ reacted with cyanamide) at various ratios.

Table 4- 9: Unit cell parameter and crystallite size calculations of ANA (anatase) and AM_CM (amorphous to cyanamide) at various ratios.

Sample	Product Colour	Unit cell parameter (Å)			Volume $(Å)^3$	Crystallite size (nm)
		a	b	C		
ANA	White	3.785(10)	3.785(10)	9.514(8)	136.3(8)	11
1:0.25	Light green	3.7798(8)	3.7798(8)	9.4948(11)	135.65(7)	17
1:0.5	Green	3.799(12)	3.799(12)	9.510(9)	137.28(10)	10
1:0.75	Yellow	3.794(4)	3.794(4)	9.514(13)	137(3)	9
1:1	Dark yellow/orange	3.785(4)	3.785(4)	9.4890(3)	136(3)	4

The FT-IR spectra in Figure 4-20 show that moisture is usually absorbed from the air. For example, a broad band from 3600–3250 cm^{-1} is related to the hydroxide groups (O—H) [83]; a strong, sharp peak at 1636 cm^{-1} is attributed to H—O—H bonds[80, 134]; and weak multi-peaks in the region from 2380 cm^{-1}–2247 cm^{-1} are attributed to O═C═O bonds.[142]

Figure 4-20 also shows the spectrum of anatase (ANA), which is used as a blank, and spectra of amorphous AM and cyanamide CM samples, which are used to compare with the product samples after the reaction of the amorphous sample with cyanamide at ratios 1:0.25, 1:0.5, 1:0.75 and 1:1. Both the anatase and amorphous spectra are interpreted in *Section 3.2.2. in the chapter on Amorphous and Anatase TiO_2*. Because the spectrum of the sample 1:0.25_AM_CM differs from that of the other samples, 1:0.5, 1:0.75 and 1:1 (AM : CM), the interpretation of the IR spectra is divided into two parts as follows.

In the first part, the spectrum of the ratio 1:0.25 AM_CM shows three interesting regions: ≈ 2219 cm^{-1}, 2063–2047 cm^{-1} and 700–400 cm^{-1}. The band at 2219 cm^{-1} shows a broad, weak peak corresponding to the (−C≡N) bond.[144, 145] It is known that nitriles usually absorb in the range from 2260 cm^{-1} to 2200 cm^{-1}.[142] Cyanamide in the IR spectrum shows absorption at ≈2400 cm^{-1} in the (−N−C≡N) fragment.[141]. It was noted that there is no strong peak at the band 2200–2000 cm^{-1} related to the NCO^- group.[142] The band at 2063–2047 cm^{-1} shows a very high-intensity split into two bands due to the conjugation of carbodiimide with substitutes of the hydrogen groups (H−N═C═N−H).[142] So, it could be that the hydrogen groups are substituted with two other groups: one H group replaced with CN and the other with Ti. This is possible because no peak appears in the range of 3500–3300 cm^{-1} related to the (−N−H) bond.[141, 142] Producing carbodiimide in the sample is not surprising, because cyanamide converts to carbodiimide by resonance.[141] In addition, cyanamide has the ability to form dicyandiamide, as described in section *1.6.3., Decomposition of Cyanamide*.[88] The band in the regions ranging from 700–400 cm^{-1} is associated with the typical vibrational mode of the Ti—O bonds.[80, 134] So, from this FT-IR interpretation, it can be seen that two possible formulas could be formed. The first one could be formed as titanium oxy-carbodiimide oxy-nitrile $TiO_{2-x-y}(CN)_x(CN_2)_y$. As studied in section *4.2.3. Preparation of New Potential $TiO_{2-x}(CN_2)_x$ Nanoparticles,* titanium oxy-carbodiimide $TiO_{2-x}(CN_2)_x$ was formed by reacting urea with anatase/amorphous samples. However, due to the nitrile fragment that appeared in the FT-IR spectrum, it was suggested that both oxy-carbodiimide and oxy-nitrile could be formed by using cyanamide as a nitrogen source. The second possible formula that could be formed is $TiO_{2-x}(C_2N_3)_{2x}$ titanium oxy-carbodiimide cyanide. This formula is more favoured because, as mentioned above, cyanamide can dimerize to produce dicyandiamide (see Figure 4-18).[88] However, instead of using polymerization accompanied with produce melamine[88], the dicyandiamide released ammonia

and formed a new decomposition of cyanamide called carbodiimide cyanide (see Figure 4-19). As a result, carbodiimide cyanide could be the chemical used during the reaction.

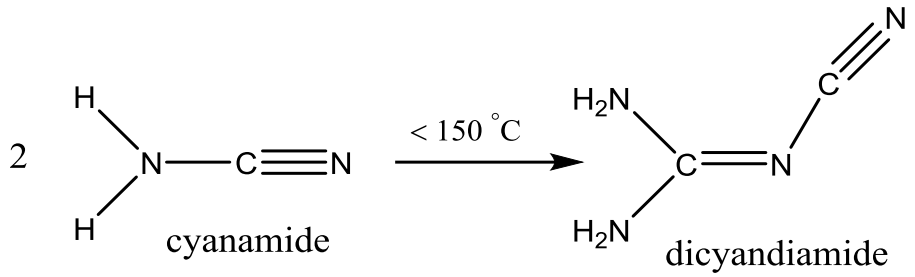

Figure 4- 18 : Cyanamide decomposed to dicyandiamide.[88]

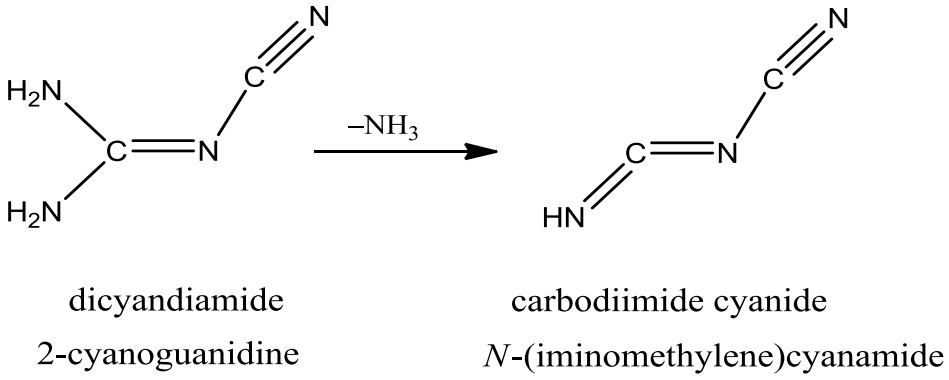

Figure 4- 19: Releasing ammonia from dicyandiamide and forming a new decomposition of cyanamide called carbodiimide cyanide.

In the second part, the spectra of the 1:0.5, 1:0.75 and 1:1 AM_CM samples have similar results (see Figure 4-20). These samples present five interesting regions: 3238–3183 cm^{-1}, 2068 cm^{-1}, 1414 cm^{-1}, 890–773 cm^{-1}, and 590 cm^{-1}. The band at 3238–3183 cm^{-1} and related to the (N−H) bond.[142, 149] This band does not appear in the spectrum of the 1:0.25 AM_CM sample. The band at 2068 cm^{-1} corresponds to carbodiimide (−N═C═N−).[142] This peak was shown in the spectra of the 1:0.25 AM_CM sample; however, the peak in the 1:0.5, 1:0.75, and 1:1 AM_CM samples occurs without splitting. If it compared with the results of the 1:0.25 AM_CM spectrum, this might mean that one of the hydrogen groups is replaced with titanium (Ti) and the other one is still hydrogen. The 1414 cm^{-1} band and the 890–773 cm^{-1} region could be accompanied with two nominated groups, either hydroxide group (OH) or secondary amine group (>NH). The possibility of forming hydroxide group is because the H—O—Ti bending show in-plane at 1414 cm^{-1} and out of plane in the 890–773 cm^{-1} region.[142, 150]. Additionally, because the starting material that used in this reaction was amorphous $Ti(OCH(CH_3)_2)_{4-x}(OH)_x$ and present the (H—O—Ti) bands out-plan at 890–773 cm^{-1} (*see section 3.2.2. for additional explanation*). The 890–773 cm^{-1} band and the 1414 cm^{-1} regions could be also assigned to secondary amine (>NH) group.[136] Accordingly, if the both bands correspond to hydroxide group and presented as a part of the doping compound, the potential formula will be $TiO_{2-x+y}(CN_2H)_x(OH)_y$. Unfortunately, this formula present Ti with oxidation state *+6* which is chemically not possible. However, if these bands corresponded to >NH group, the potential formula will be $TiO_{2-x}(CN_2H)_{2x}$ accompanied with Ti^{4+} which is more likely. Neither of these bands appeared in the 1:0.25 AM_CM sample. The band at 590 cm^{-1} is related to Ti—O bonds, which appear in the spectra of all AM_CM samples and in the spectra of ANA (anatase TiO_2).[80, 134] Therefore, according to FT-IR interpretations, the possible estimation formula could be predicted is $TiO_{2-x}(CN_2H)_{2x}$. This means that after cyanamide is converted by resonance to produce carbodiimide, is then directly involved in the reaction. The Table 4-10 shows

elemental analysis results for these samples; it showed that the nitrogen and carbon present in all the samples. This means that the TiO_2 sample has some N and C could be introduced into its structure after the reaction with cyanamide. The weight percentages of nitrogen (N) increase with increasing the cyanamide concentrations of the samples 1:0.25, 1:0.5 and 1.75 AM_CM. While previous studies showed the presence of carbodiimide $(NCN)^{2-}$ anion in their products, [107, 108, 109] no studies have yet shown the presence of $(C_2N_3)^{2-}$ and $(CN_2H)^{2-}$ anions. Therefore, the presence of these anions are underscores the innovation of this current study.

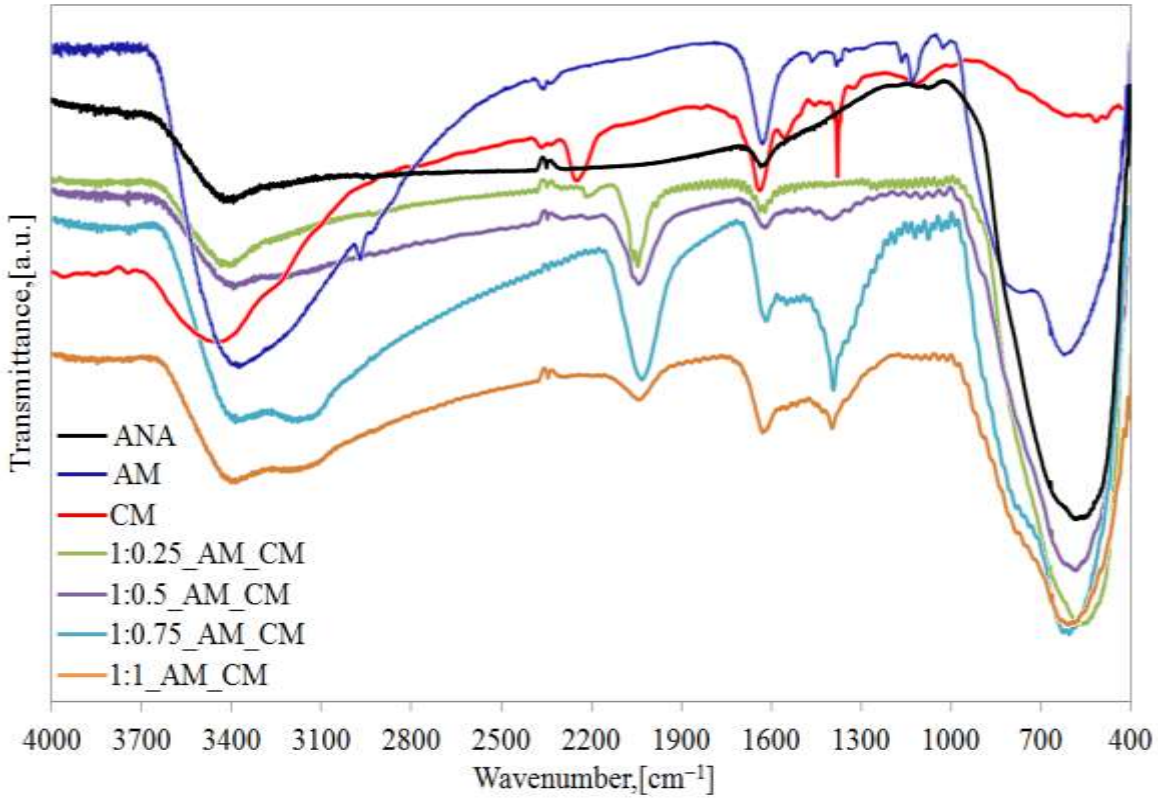

Figure 4- 20: FT-IR spectra of ANA (blank anatase), AM (amorphous), CM (cyanamide) and AM_CM. (amorphous titanium isopropoxide hydroxide reacted with cyanamide).

Table 4- 10: EA of amorphous reacted with cyanamide at 400 °C in N_2.

Sample	Atoms Weight Percentage		
	N	C	H
1:0.25_AM_CM_400	0.26	0.50	0
1:0.5_AM_CM_400	1.75	0.68	0
1:0.75_AM_CM_400	4.70	2.25	0.82
1:1_AM_CM_400	3.24	1.54	0.67

Figure 4-21 shows the UV-Vis spectra of samples 1:0.25, 1:0.5, 1:0.75 and 1:1 AM_CM, which produced two edges, one absorbed in the Vis region and the other in the UV region. Figure 4-22 and Table 4-11 present the results of band-gap calculation. All these samples show decreasing band gap less than 3.22 eV of TiO_2 in the range 2.47–2.24 eV, followed by absorption in the visible region at 502–553 nm. In addition, they show small increases in the band gap of more than 3.22 eV of TiO_2 at 3.37–3.50 eV, and absorption in the ultraviolet region at 368–354 nm. Therefore, these two edges prove that the AM:CM reaction produced doped and undoped TiO_2. These results are in good agreement with the FT-IR results, which indicate the possible formation of $TiO_{2-x}(C_2N_3)_{2x}$ + undoped TiO_2 for the 1:0.25 AM_CM sample and of $TiO_{2-x}(CN_2H)_{2x}$ + undoped TiO_2 for the 1:0.5, 1:0.75 and 1:1 AM_CM samples.

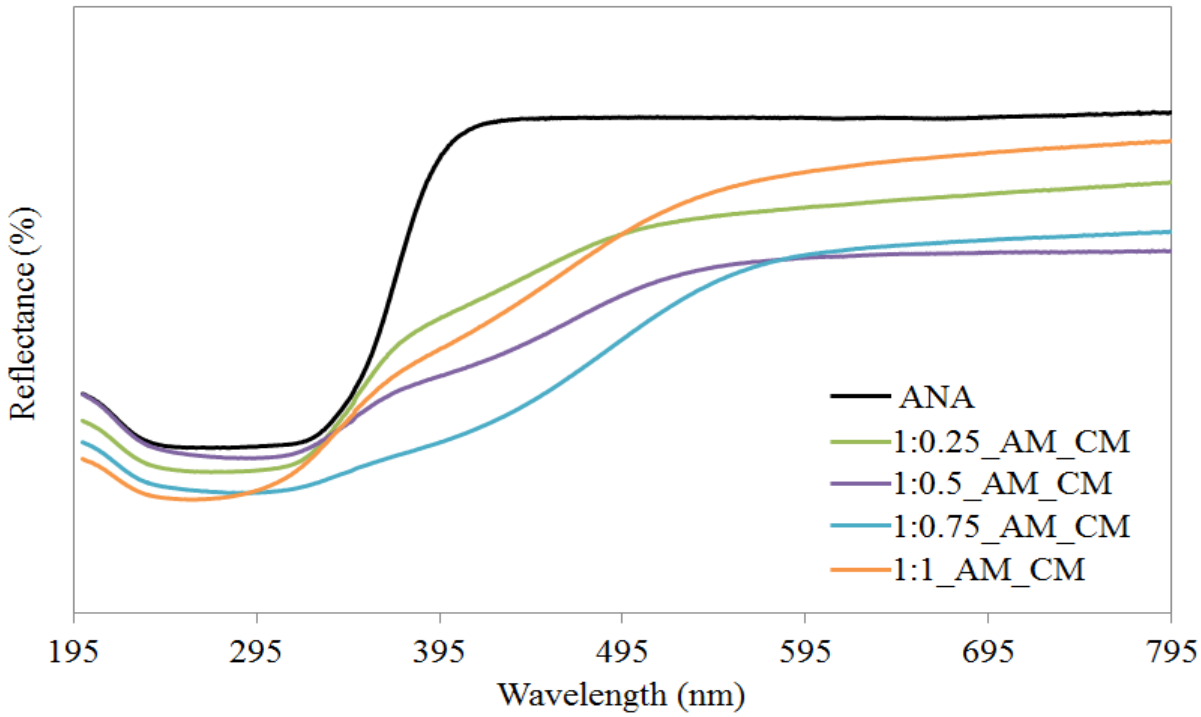

Figure 4- 21: UV-Vis spectra of ANA (blank anatase) and AM_CM (amorphous titanium isopropoxide hydroxide reacted with cyanamide) at various ratios.

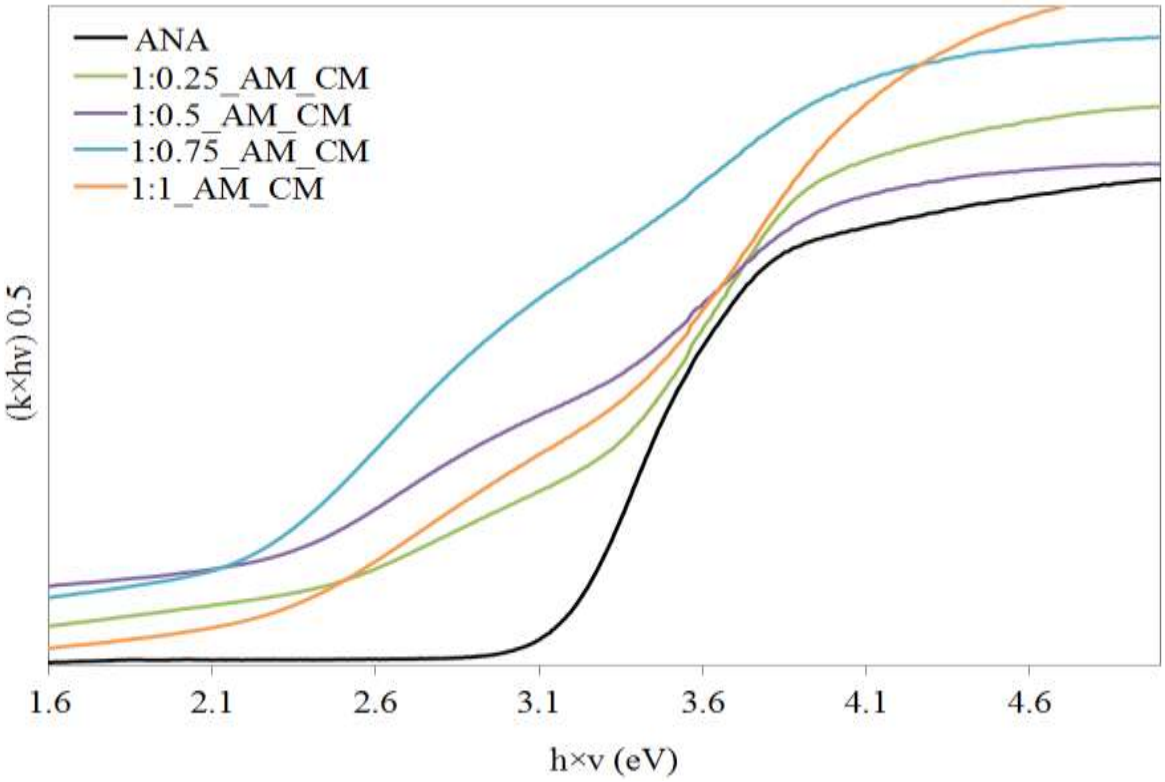

Figure 4- 22: Band-gap calculation using the Kubelka-Munk function of ANA (blank anatase) and AM_CM (amorphous titanium isopropoxide hydroxide reacted with cyanamide) at various ratios.

Table 4- 11: Band-gap energies (E_{bg}) and wavelengths (λ) using Kubelka–Munk function calculation.

Sample	E_{bg} (eV)	λ (nm)
TiO_2	3.22	384
1:0.25_AM_CM	2.47 3.37	502 368
1:0.5_AM_CM	2.34 3.40	529 364
1:0.75_AM_CM	2.24 3.50	553 354
1:1 _AM_CM	2.34 3.44	530 360

4.3. Conclusions

N-modified TiO_2 using urea as a nitrogen source was carried out by heating urea with amorphous titanium isopropoxide hydroxide at temperatures of more than 400 ˚C for 5 hours in air or N_2. Unfortunately, all reactions that used nitrogen gas in the heating process showed amorphous phases. These samples need more study in future. However, when the reaction was applied in air through the heating process, the PXRD patterns showed more crystalline products. The majority of the products showed mixed anatase and rutile phases. Mixed phases were not the focus of this project. Consequently, because samples 1:5_AM_U_400 and 1:10_AM_U_400 changed colour to yellow and formed single phases in PXRD patterns, they

were selected as candidates for the best samples. However, the 1:5_AM_U_400 sample was excluded due to EA results that showed 0% nitrogen. Sample 1:10_AM_U_400 showed 0.24% nitrogen. N-modified TiO_2 samples were prepared by heating urea with anatase TiO_2 at temperatures of more than 400 $^{\circ}C$ for 5 hours in air and N_2. Unfortunately, samples obtained from reactions heated in air showed no changes in colour. However, the reactions carried out under flowing nitrogen gas, produced yellow colours. These samples showed crystalline patterns in PXRD analysis. Because the FT-IR data showed the presence of urea residues with carbodiimide fragments in the 1:10_ANA_U_400 sample and released carbodiimide from the 1:10_ANA_U_500 sample, these samples are not recommended as the best samples. However, the 1:10_ANA_U_450 sample released urea residues and presented an interesting band of carbodiimide fragments at about 2055 cm^{-1}. New potential compounds and photocatalysts with the general formula of $TiO_{2-x}(CN_2)_x$ were successfully prepared in this work. All analysis showed that nitrogen was found inside the TiO_2 lattice by replacing O^{2-} with CN_2^{2-} to form titanium oxy-carbodiimide/oxide carbodiimide. PXRD patterns showed that the anatase structure was maintained, with a slight increase in the unit cell volume. FT-IR spectra showed a band of carbodiimide at about 2060 cm^{-1} and no peaks of urea residues or cyanamide fragments present. EA results showed approximately a 2:1 ratio of N:C, which showed that the $(CN_2)^{2-}$ anion fragments in carbodiimide were present in the 1:10_AM_U_400_Air and 1:10_ANA_U_450_N samples. However, the UV-Vis spectra showed that the AM_U and ANA_U samples both produced two edges, one absorbed in the Vis region and the other in the UV region. The UV-Vis spectra also showed a decrease of the band gap of less than 3.22 eV of pure TiO_2. These two edges indicate that the samples produced a mixture of doped and undoped TiO_2.

Previous interpretations concluded that heating cyanamide with anatase presented a single anatase phase on the PXRD patterns of the ANA_CM _400 samples and the

1:1_ANA_CM_450 sample. Unfortunately, these samples presented a mix of carbodiimide and residues of cyanamide compounds, as shown in the FT-IR spectra. The residues of cyanamide make the estimation of the chemical formula very difficult. Consequently, no further analysis was conducted in this experiment. To sum up the studies of cyanamide with amorphous isopropoxide-hydroxide reactions at temperatures higher than 400 °C under nitrogen gas. The two most interesting results were samples that presented rock-salt structures and samples that presented anatase single phases. Increasing the amount of cyanamide to the ratio (1:2)_AM_CM) at temperatures of 450 °C, 500 °C, and 550 °C, led to the formation of compounds with the NaCl structure (rock-salt structures). Elemental analyses showed a weight percentage of nitrogen greater than that of carbon. The PXRD and EA results suggest the formation of titanium nitride (code 00-031-1403) and/or titanium nitride oxide (code 00-049-1325) and/or new compounds could be formed, such as titanium carbodiimide or titanium oxide carbodiimide. Unfortunately, FT-IR spectra results were not conclusive enough to confirm which compound was presented, thus further work is necessary to clarify this point in the future. The samples that presented anatase single phases showed some changes in unit cell volume with increasing ratios compared to the TiO_2 sample, indicating that some doping occurred during the reaction. For example, the sample 1:0.25_AM_CM showed a decrease in unit cell parameters and an increase in 2θ angles for diffraction peaks compared to those in pure TiO_2. The crystallite size calculations showed a decrease in increasing ratios from 1:0.25 to 1:1 AM:CM. The biggest particle size was shown at the ratio 1:0.25 AM:CM. The UV-Vis spectra of AM_CM samples showed two absorptions, one in the visible region ($E_g < 3.22$ eV) and one in the UV region, meaning that the products are not fully doped, but still have undoped parts. Interpretations of the FT-IR spectrum showed that the 1:0.25 AM_CM sample presents (−C≡N) and (−N═C═N−) fragments. This means that dicyandiamide (the decomposition of cyanamide) was achieved instead of the polymerization to melamine. The dicyandiamide then

released ammonia and formed a new decomposition of cyanamide called carbodiimide cyanide or N-(iminomethylene)cyanamide. However, the other ratios, 1:0.5, 1:0.75 and 1:1 AM:CM, present (−N═C═N−H), (−NH) and (HO—Ti) fragments. So, from these results, two estimation novel formulas were formed: $TiO_{2-x}(C_2N_3)_{2x}$ + TiO_2 by the ratio 1:0.25 AM:CM and $TiO_{2-x}(CN_2H)_{2x}$ + TiO_2 by the ratios 1:0.5, 1:0.75 and 1:1 AM:CM. The next chapter will discuss the final part of this dissertation, S-modified TiO_2.

Chapter 5 – S-modified TiO_2

The N-modifying TiO_2 was carried out in the previous chapter to decrease the band gap of anatase TiO_2 to less than 3.2 eV for shifting its absorption activity from the UV-region to the Vis-region. This chapter will study the second suggestion in this work S-modified TiO_2 for decreasing this band gap. This chapter will be divided into three sections: the S-modification using dodecanethiol, the S-modification using carbon disulphide, and the S-modification using thiourea.

5.1. Experimental

5.1.1. S-modification Using Dodecanethiol

This study starts by using dodecanethiol as a source of sulfur because of dodecanethiol easily releases the sulfur by heating, and it has not been reported as a sulfiding agent.

The yellow powder was produced from grinding amorphous titanium isopropoxide hydroxide, $Ti(OCH(CH_3)_2)_{4-x}(OH)_x$ (*section 3.1.1. of the Amorphous and Anatase TiO_2 chapter*), with the dodecanethiol (*Sigma Aldrich, ≥ 99 %*) in different molar ratios 1:0.3, 1:0.5, and 1:1 (amorphous: dodecanethiol). These samples were then heated under flowing N_2 gas at 400° C for 5 hours to obtain black powder. These samples were analysed using powder x-ray diffraction (PXRD) and energy dispersive x-ray spectroscopy (EDX).

The samples were labelled as ANA (anatase TiO_2, blank), 1:0.3_AM_DT, 1:0.5_AM_DT and 1:1_AM_DT. They were labelled according to the ratios of amorphous titanium isopropoxide hydroxide to dodecanethiol at 400° C for 5 hours.

5.1.2. S-modification Using Carbon Disulfide

Although, the previous section of dodecanethiol (has large carbon content) did not achieve S-modified TiO_2 samples, it opened door of using carbon disulfide (CS_2) that contains less carbon and more sulfur.

Few studies have used CS_2 as a source of sulfur, and some of them employed an autoclave in their reactions. However, the majority used additional materials, such as ethyl acetate, nitric acid, or polyvinylpyrrolidone (PVP), ethanol, and acetic acid in CS_2 reactions.[117, 116, 121] This study will demonstrate a different S-modification method that involves only anatase TiO_2/amorphous $Ti(OCH(CH_3)_2)_{4-x}(OH)_x$ and carbon disulfide and then heats the solution in a *tube furnace (Section 2.1.1. in the Experimental Techniques chapter*). The CS_2 was used in its liquid natural form and also as vapour. Thus, this section will be divided into two subsections: reactions with gaseous CS_2 and reactions with liquid CS_2.

5.1.2.1. Reactions with Gaseous CS_2

Preparation of S-modified titanium dioxide using CS_2 in a gas phase was carried out in two steps. The first step consisted of the reacting of amorphous/anatase with CS_2 at 400 $^{\circ}$C for 5 hours, which produced a black powder. The second step involved the heating of this black powder to 300 $^{\circ}$C for 1 hour and 30 minutes in either N_2 or air. Details of this process follow.

Step 1: In the centre of a long quartz tube, 0.5 g of amorphous $Ti(OCH(CH_3)_2)_{4-x}(OH)_x$ or anatase TiO_2 (Section 3.1.1. of the Amorphous and TiO_2 chapter for synthesis) samples were placed in an alumina boat alone or an alumina boat coated with carbon. Then one side of the long quartz tube was connected with the CS_2 liquid (*Fisher Scientific, 99%*) and N_2 gas, which

allowed the entrance or isolation of CS_2 and N_2 to be adjusted with the controlling keys. The other side was attached to a Dreschel bottle containing paraffin oil, which prevented air from entering the system and acted as a scrubber to remove residual CS_2. After closing the furnace, the nitrogen gas was flushed first for 15 minutes to remove any air from the system. Then, the furnace was programmed to heat up from room temperature to 400 $^{\circ}$C and was kept at that temperature for 5 hours before cooling down to room temperature over a period of 3 hours. When the furnace started heating at a rate of 5 $^{\circ}$C per minute, both the N_2 gas and CS_2 were allowed to pass through the system. Finally, when the system was start to cool down for 3 hours, the CS_2 was isolated and N_2 was allowed to flush until the end to avoid air entering the system. After the reaction, the colour of the amorphous and anatase products changed from white to black, and the products emitted a strong odour resembling that of rotten eggs (i.e. sulfur odour).

Step 2: The black powder with the rotten eggs smell were then calcinated to 300 $^{\circ}$C for 30 minutes and for 1 hour under nitrogen gas or air. Note that 1 gram of black powder was used for each heating.

The black samples that resulted from Step 1 of the reactions of amorphous/anatase with CS_2 gas; were then labelled ANA_CSG_BL and AM_CSG_BL. The samples in Step 2 were labelled as follows: ANA (anatase TiO_2, blank); ANA_CSG_30_Air, ANA_CSG_1_Air, ANA_CSG_30_N, ANA_CSG_1_N, AM_CSG_30_Air, AM_CSG_1_Air, AM_CSG_30_N, and AM_CSG_1_N according to the heating reaction time of the black powder, which resulted from Step 1. (AM= amorphous titanium isopropoxide hydroxide; ANA= anatase titanium dioxide; CSG= carbon disulfide gaseous; N= the reaction carried out under of nitrogen gas; Air= the reaction carried out in air; 1= a reaction time of 1 hour; 30= a reaction time of 30 minutes). The samples were then analysed by powder x-ray diffraction (PXRD), Fourier transform infrared spectra (FT-IR) and ultraviolet visible absorption spectra (UV-vis).

5.1.2.2. Reactions with Liquid CS_2

In this experiment, CS_2 was used in a liquid phase to synthesise S-modified titanium dioxide. The reaction was carried out using two different methods. The differences between these two methods were that Method 1 consisted of cooling down the reaction of amorphous/anatase with liquid CS_2 before the heating process, but Method 2 included of three materials (water, CS_2 (L), and Ti isopropoxide) mixed at room temperature before the heating process. A more detailed description of these two methods is discussed below.

Method 1: In an ice bath, amorphous $Ti(OCH(CH_3)_2)_{4-x}(OH)_x$ or anatase TiO_2 (section 3.1.1. in the Amorphous and Anatase TiO_2 chapter) was mixed with carbon disulfide liquid (CS_2) (*Fisher Scientific, 99%*) at different molar ratios of 1:1, 1:2, and 1:3 (amorphous/anatase : CS_2) and then was sealed with parafilm laboratory film. The Method 1 schematic shown in Figure 5-9. A yellow solution (when the starting material was amorphous) and a white solution (when the starting material was anatase) were formed and then turned to a white powder by releasing the parafilm tape. The reactions were then heated to 400˚C for 5 hours in the presence of both air and nitrogen gas. The samples were then analysed by PXRD.

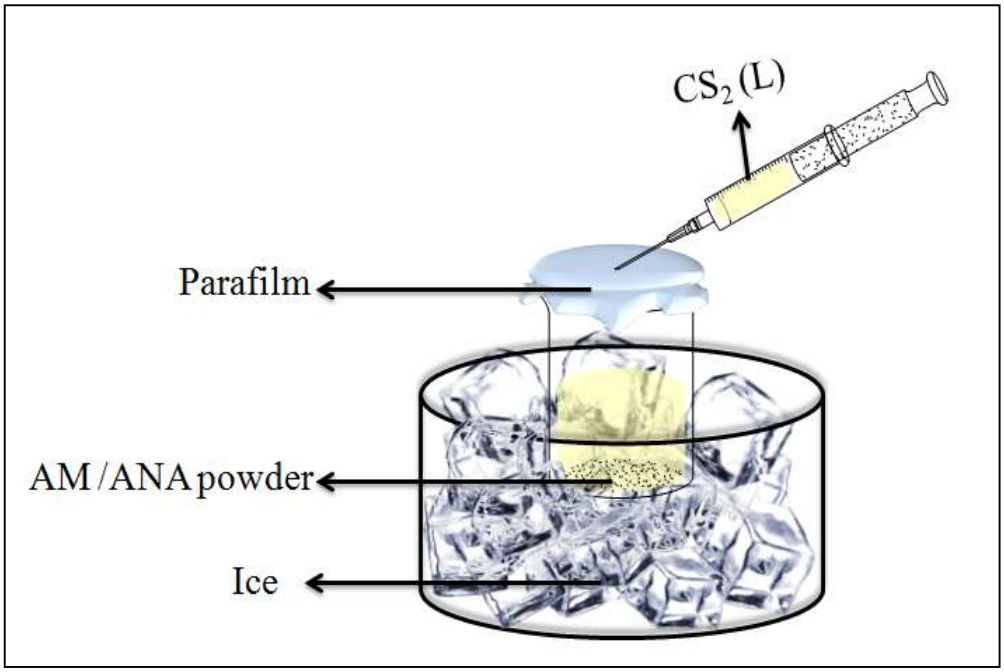

Figure 5- 1: Schematic of Method 1, cooling down the reaction of amorphous/anatase with liquid CS_2 before the heating process. AM= amorphous $Ti(OCH(CH_3)_2)_{4-x}(OH)_x$; ANA= anatase TiO_2.

Method 2: In particular order, 5 mL of Titanium isopropoxide (Sigma-Aldrich, > 97%), 1.25 mL of carbon disulfide in a liquid phase, and 1.25 mL of distilled water were mixed at room temperature to produce a yellowish powder. This yellowish powder was either heated directly (D) to 400 ˚C for 5 hours in N_2 gas or heated indirectly (ID) after first being dried at 100 ˚C for 10 hours and then heated at 400 ˚C for 5 hours in air/N_2. A *tube furnace* was used for the heating process of both methods (section 2.1.1. in the Experimental Techniques chapter). The samples were then analysed by PXRD.

The samples were labelled for Method 1 as follows: ANA (anatase TiO_2, blank); 1:1_ANA_CSL, 1:2_ ANA_CSL, 1:1_AM_CSL, 1:2_AM_CSL and 1:3_AM_CSL. These labels represent the ratios of the anatase / amorphous sample to the carbon disulfide liquid.

For Method 2, the samples were labelled TCSLW_D and TCSLW_ID. These labels represent the mixture of titanium isopropoxide (T), liquid carbon disulfide (CSL), and water (W) was heated directly (D) and indirectly (ID) at 400 °C.

5.1.3. S-modification Using Thiourea

Thiourea is commonly used as a source of sulfide (S^{2-}). Previous studies detailed some preparation techniques and substances for S-modified TiO_2, such as the use of a planetary mill in reactions involving ethanol, acetic acid, water, hydrochloric acid, and titanium butoxide (section *1.7.4. Preparation methods for S-modified TiO_2*). This study will show a different S-modification method, which involves only amorphous $Ti(OCH(CH_3)_2)_{4-x}(OH)_x$ and thiourea, and furnace. This experimental focused on the amorphous titanium isopropoxide hydroxide reactions instead of TiO_2 reactions. This because the reaction of thiourea with TiO_2 produced products have white colour, which still absorb ultraviolet light (section 1.4. Absorption Spectroscopy and Compounds colours).[11, 15]

Amorphous $Ti(OCH(CH_3)_2)_{4-x}(OH)_x$ (*section 3.1.1. Preparation of Anatase TiO_2 Nanoparticles*) was mixed with thiourea (Sigma Aldrich, St Louis, MO; ≥ 99 %) in different molar ratios 1:0.5, 1:1, and 1:1.5 (AM:TU), and then heated in air at 400 °C and 500 °C for 4 hours and 8 hours. All the samples produced yellow powder. These samples were then analysed using powder X-ray diffraction (PXRD), Fourier-Transform Infrared spectroscopy (FT-IR), elemental analysis, and ultraviolet visible spectroscopy (UV-Vis).

The samples heated to 400 °C were labelled as follows according to the amorphous:thiourea ratios for 4 hours and 8 hours: ANA (anatase TiO_2, blank); 1:0.5_AM_TU_400_4, 1:1_AM_TU_400_4, 1:1.5_AM_TU_400_4, 1:0.5_AM_TU_400_8, 1:1_AM_TU_400_8 and

1:1.5_AM_TU_400_8. The samples heated to 500 °C were labelled as follows according to the amorphous:thiourea ratios for 4 hours and 8 hours: 1:0.5_AM_TU_500_4, 1:1_AM_TU_500_4, 1:1.5_AM_TU_500_4, 0.5_AM_TU_500_8, 1:1_AM_TU_500_8 and 1:1.5_AM_TU_500_8.

5.2. Results and Dissection

5.2.1. S-modification Using Dodecanethiol

A yellow, creamy solid of the ratios 1:0.3, 1:0.5 and 1:1 (AM:DT) was converted to black powder and did not have an odour of rotten eggs after heating the samples to 400° C for 5 hours.

The PXRD patterns of 1:0.3_AM_DT, 1:0.5_AM_DT and 1:1_AM_DT compared with a pure anatase TiO_2 (ANA), show in Figure 5-1. A mixture of anatase and amorphous phases produced at the lowest ratio of 1:0.3_AM_DT. However, increasing the concentration of the dodecanethiol to 1:0.5 and 1:1 produced a single anatase phase.

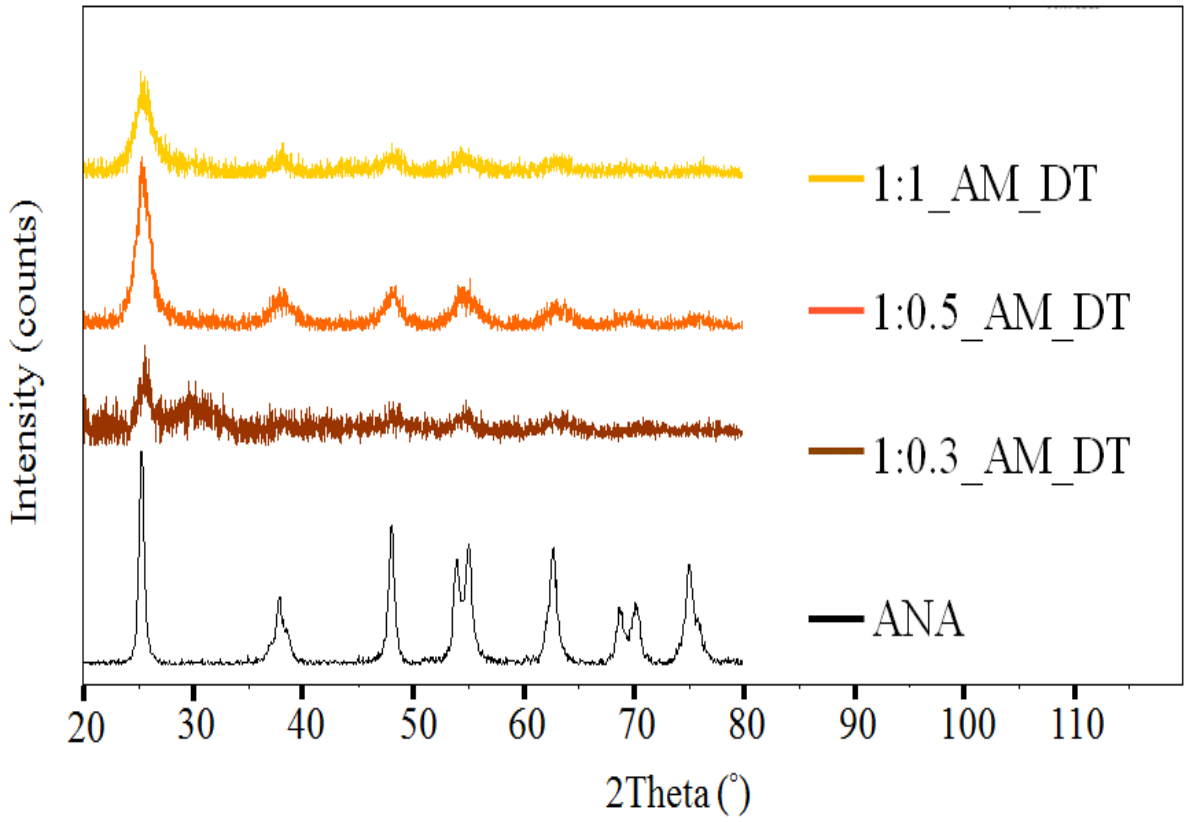

Figure 5- 2: PXRD patterns of ANA for anataseTiO_2, AM_DT for amorphous reacted with dodecanethiol in the ratios 1:0.3, 1:0.5 and 1:1. These samples were heated to 400 °C for 5 hours in N_2.

The EDX analysis was tested on the sample 1:1_AM_DT, and the spectrum is presented in Figure 5-2. The spectrum did not show peaks of energy around 2.1 keV and 2.3 keV, which related to the sulfur positions.[151] This showed that no sulfur doping was achieved, and the black colour could suggest that some carbon elements may be coating the TiO_2 nanoparticles.

Furthermore, the high content of the carbon compared to the sulphur in the dodecanethiol has not favoured the oxygen/sulphur substitution.

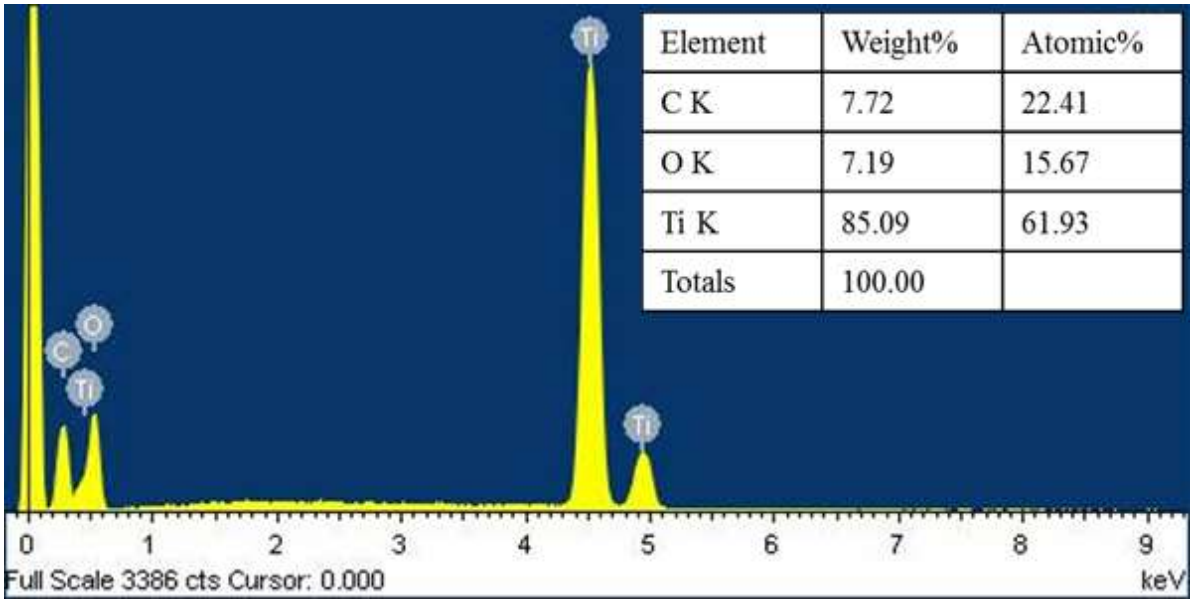

Figure 5- 3**:** EDX spectrum of 1:1_AM_DT sample.

5.2.2. S-modification Using Carbon Disulfide

5.2.2.1. Anionic Doping and Formation of TiS_2

Amorphous titanium isopropoxide hydroxide was used as the starting material; the PXRD patterns in Figure 5-3 show the products from the reaction of the amorphous sample with carbon disulfide gas (CSG), which was carried out in two steps: at 400 ˚C for 5 hours and then re-heated at 300 ˚C. The product AM_CSG_BL from the first step of the reaction (400 ˚C, 5 hours, N_2) produced a black powder, and its pattern presented a mix of three structures: anatase,

rutile, and titanium disulfide. These products were identified through qualitative comparison with reference patterns: JCPDS 21-1272 for anatase, JCPDS 21-1276 for rutile and JCPDS 81-0687 for TiS_2. The same results were shown in the PXRD patterns collected after the second step at 300 °C for both samples of AM_CSG_30_Air and AM_CSG_1_Air, though the colour for these samples changed to grey (Table 5-1). On the other hand, when the second step was performed under nitrogen gas, the PXRD patterns were not clear; they showed only a mix of anatase and TiS_2 or a mix of anatase, rutile and titanium disulfide with no change in the colour (still black). The presence of titanium disulfide in this case indicated that the gaseous carbon disulfide favoured the substitution of O^{2-} with S^{2-} in the TiO_2 lattice.

These results materialized when we used amorphous titanium isopropoxide hydroxide as a starting material, but when anatase was used for the starting material, the results of the PXRD patterns were different (Figure 5-4). The pattern of the black powder ANA_CSG_BL after the first step of the reaction (400 °C, 5 hours, N_2) showed a mix of anatase and TiS_2. These results were also observed in the patterns of ANA_CSG_30_N and ANA_CSG_1_N after the second step of the reaction at 300 °C under nitrogen gas. Surprisingly, the PXRD patterns of the products of ANA_CSG_30_Air and ANA_CSG_1_Air after the second step of the reaction were performed in air presented a single anatase phase that formed and change the colour of the powder from black to beige (Table 5-1). These interesting results open the door for more investigations to determine whether sulfur was doped in the TiO_2 lattice or not, which is explored in next section.

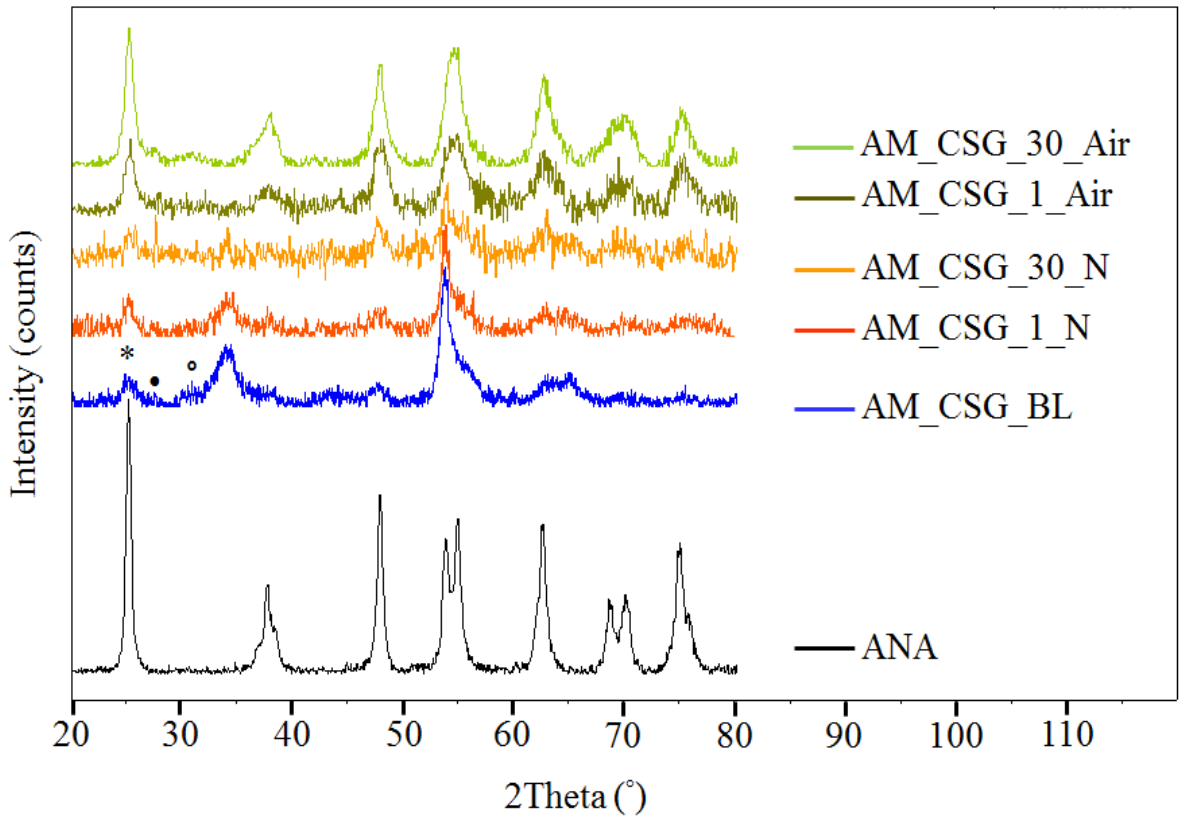

Figure 5- 4: PXRD patterns of ANA (AnataseTiO_2); AM_CSG_BL (a black powder resulting from heating an amorphous sample with CS_2 gas at 400 ˚C for 5 hours in N_2) and AM_CSG (a black product heated at 300 ˚C for 30 minutes and 1 hour in air (Air) or nitrogen gas (N). (*) indicates the peaks for the TiO_2 anatase phase; (•) indicates the peaks for the TiO_2 rutile phase; and (°) indicates the peaks for TiS_2.

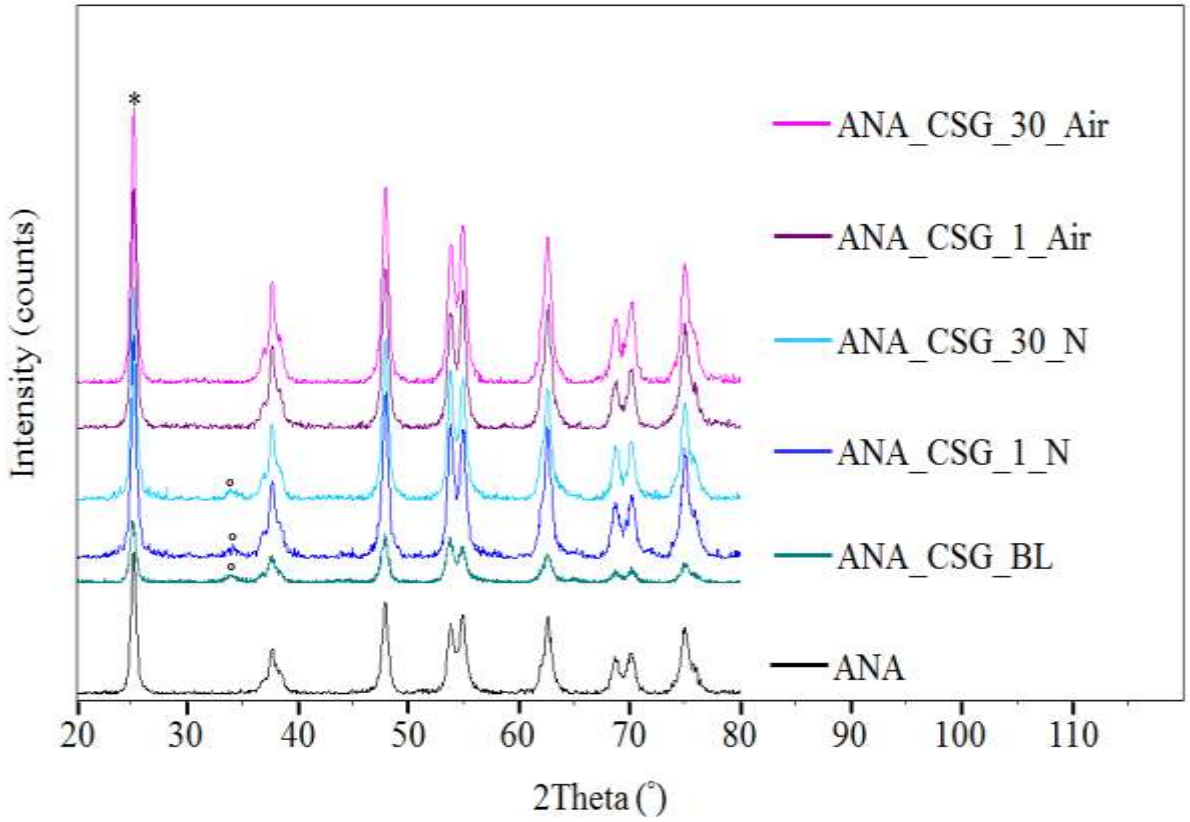

Figure 5- 5: PXRD patterns of ANA (AnataseTiO_2); ANA_CSG_BL (the black powder that resulted from heating the anatase sample with CS_2 gas at 400 °C for 5 hours in N_2), and ANA_CSG (a black product heated at 300 °C for 30 minutes and 1 hour in air (Air) or nitrogen gas (N). (*) indicates the peaks for the TiO_2 anatase phase, and (°) indicates the peaks for TiS_2.

Table 5- 1: Summary of reactions between amorphous/anatase and gaseous carbon disulfide.

Sample	Product Colour	PXRD
ANA (blank)	White	Anatase
AM_CSG_BL	Black	Anatase + rutile + TiS_2
AM_CSG_30_N	Black	Anatase + TiS_2
AM_CSG_1_N	Black	Anatase + TiS_2
AM_CSG_30_Air	Grey	Anatase + rutile + TiS_2
AM_CSG_1_Air	Grey	Anatase + rutile + TiS_2
ANA_CSG_BL	Black	Anatase + TiS_2
ANA_CSG_30_N	Black	Anatase + TiS_2
ANA_CSG_1_N	Black	Anatase + TiS_2
ANA_CSG_30_Air	Beige	Anatase
ANA_CSG_1_Air	Beige	Anatase

5.2.2.2. Forming New Potential Nanoparticles (Cationic-anionic Co-doping)

A black powder was produced after heating anatase TiO_2 (ANA) under flowing carbon disulfide (CS) and N_2 gases at 400 $^{\circ}$C for 5 hours. This black powder changed to a beige colour after the sample was heated for 30 minutes and for 1 hour at 300 $^{\circ}$C in air. According to Rodgers (1994), composite are coloured because they absorb some wavelengths of visible light but reflect or transmit others.[15] The product colour changes that were obtained indicated that, within the visible light spectrum, the products were absorbing light; consequently, this raised

the potential for band gap energy reduction through successful substation that was occurring in the TiO_2 lattice. This finding provided a good omen to proceed to the next analysis, powder x-ray diffraction.

PXRD analysis was used to determine the phase of the product samples, and its results are shown in Figure 5-5 and Table 5-2. Clearly it can be seen that a single anatase phase was formed before and after heating with CS_2. This finding was in agreement with the nano-crystalline anatase structure of the reference pattern (JCPDS 21-1272), and there were no further peak matches with the rutile phase reference pattern (JCPDS 21-1276). Unit cell parameters and crystallite size calculated from the PXRD data are presented in Table 5-2. The results showed that all the samples formed tetragonal-body-centred ($\alpha=\beta=\gamma=90^{\circ}$, $I4_1/amd$ (141)). However, there was no change in the $a=b$ and c axes of unit cell parameters of the ANA_CSG_300_30_Air and ANA_CSG_300_1_Air samples compared with undoped-TiO_2. These results also showed no changing could be noticed in the unit cell volume of the ANA_CSG samples compared to unmodified-TiO_2. In general, the diffraction peaks in the PXRD patterns of the samples slightly shifted to lower angles or to higher diffraction angles (2θ) when compared to the pattern of TiO_2 (blank).[143] These shifts were perhaps due to changes in unit cell parameters. These changes could occur because of partial substitution, or doping, of the TiO_2 lattice with an external particle source that had a larger or smaller ionic radius than oxygen.[143] These shifts then lead unit cell parameters to increase (decrease 2θ angles) or decrease (increase 2θ angles) compared to those in pure TiO_2, which lead to decreased or increased 2θ angles for diffraction peaks. For example, in this study the ANA_CSG_300_30 sample exhibited shifting of the diffraction peak to higher 2θ angles, however its unit cell volume showed no change when compared with the ANA sample. Similar results were reported by Devi and Kavitha in 2014.[143] They observed that the S-TiO_2 sample showed a shifting to higher angles in the PXRD pattern accompanied but with a decrease of unit cell volume when

using sulfur powder as a source of sulfur.[143] On the other hand, increasing the reaction time of ANA_CSG to 1 hour did not show a clear shift of diffraction peak in the PXRD pattern and no change in its unit cell volume.

The crystallite size of these samples was calculated from the most intense diffraction peak (101) using the Scherrer equation.[11, 12, 128] Results of these calculations showed a small increase in the size around 12 nm for both ANA_CSG_300_30 and ANA_CSG_300_1 samples.

These results from the PXRD analysis and the change colour of the ANA_CSG_300_30 and ANA_CSG_300_1 samples were promising signs that the TiO_2 anatase has some modifications in its lattice. Consequently, further analysis will be used on these samples, such as FT-IR and UV-Vis.

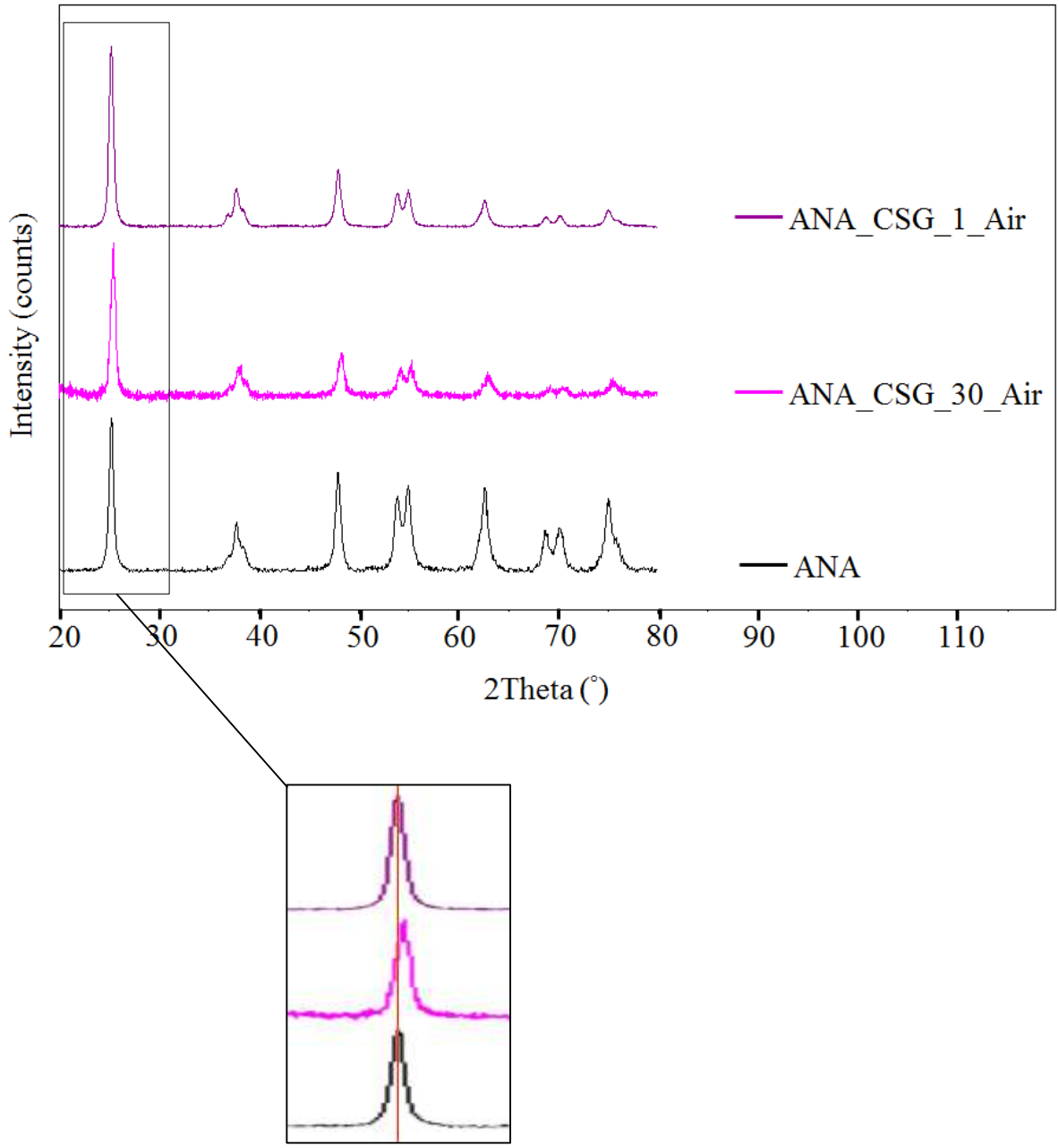

Figure 5- 6: PXRD patterns of ANA (AnataseTiO_2); ANA_CSG_30_Air and ANA_CSG_1_AIR (TiO_2 reacts with gaseous carbon disulfide) heated at 300 °C ion air for 30 minutes and 1 hour respectively.

Table 5- 2: Unit cell parameters, unit cell volume, and crystallite size calculations of ANA (anatase) and ANA_CSG 300 °C in Air (TiO_2 reacts with carbon disulfide gaseous) heated at different periods.

Sample	Product Colour	Unit Cell Parameters (Å)			Volume $(Å)^3$	Crystallite Size (nm)
		a	b	c		
ANA	White	3.785(10)	3.785(10)	9.514(8)	136.3(8)	11
ANA_CSG_30	Beige	3.783(3)	3.783(3)	9.519(4)	136.3(3)	12
ANA_CSG_1	Beige	3.7900(14)	3.7900(14)	9.507(2)	136.55(13)	12

FT-IR spectra of the samples of anatase TiO_2 (ANA) both before and after reacting with carbon disulfide gaseous and being heated at 300 °C in air for 30 minutes (ANA_CSG_30_Air) and for one hour (ANA_CSG_1_Air) are shown in Figure 5-6. The spectra of the ANA_CSG_30_Air and ANA_CSG_1_Air samples showed bands at about 2917 cm^{-1}, 2855 cm^{-1}, 1437 cm^{-1}, 1204 cm^{-1}, 1130 cm^{-1}, 1052 cm^{-1}, and 700-400 cm^{-1}. The two close bands

presenting at 2917 cm^{-1} and 2855 cm^{-1} could be assigned to C═S bonds.[152] This finding was likely due to the symmetric and asymmetric stretching modes of free CS_2 absorbed in the region between 2154 cm^{-1} and 2400 cm^{-1}.[152-154] The FT-IR spectrum of free CS_2 is illustrated in Appendix 10. Because the starting materials in this study were TiO_2 and CS_2, the case of forming C—H was not favoured, which its stretching bond assigned at about 2972 cm^{-1} and 2932 cm^{-1}.[135, 142, 155] Furthermore, the presence of the absorption peak at 1204 cm^{-1} was also assigned to R—CS—R bonds.[156, 142, 157] This may indicate the presence of the CS group within the structure of the ANA_CSG_30_Air and ANA_CSG_1_Air samples. The absorption peak at 1130 cm^{-1} corresponded to the O—S bond. [4, 142, 143, 158, 159] The band at 1052 cm^{-1} was assigned to an S═O bond.[4, 142, 143, 158, 159] Because of the absorption peak of a sulfate group present at the 1437 cm^{-1} band, both bands of O—S and S═O are related to the formation of a SO_4^{2-} group.[157, 116, 118, 135, 141, 142] Due to the absence of the absorption peak at the region's 1047 cm^{-1} and 959 cm^{-1} areas, which were assigned to Ti—S bond, anionic-modification of TiO_2 by replacing O^{2-} with S^{2-} does not occur.[29, 114, 143, 151] This could be because of the size of anionic sulfur S^{2-}, which is bigger than anionic oxygen O^{2-}, therefore, conditions were less favourable for anionic doping than S^{6+}.[4, 5] The region from 700-400 cm^{-1} is present on all three spectra of ANA, ANA_CSG_30_Air and ANA_CSG_1_Air. This region is associated with the typical vibrational mode of the Ti—O bonds.[80, 134] From these primary results, cationic-anionic co-modified of TiO_2 could be resulting in formed of new two possible coordinations: CS—TiO_2, and SO_4—TiO_2. In comparisons to previous studies that used carbon disulfide as a source of sulfur (they used different materials and different techniques), Ma et al. (2014) observed that the formation of the S−Ti−O bond resulted from the substitution of S^{2-} with O^{2-}, and the presence of the SO_4^{2-} group.[121] Moreover, the formation of the S−Ti−O bond was also found by Li et al. (2007).[117] Finally, Dunnill et al. (2009) reported that sulfur was oxidised during the

deposition and changed from S^{2-} to S^{6+}.[116] Due to the size of the sulfate group SO_4, it should reside on the TiO_2 surface.

Not to be forgotten, the three positions that are always absorbed from the air due to mixing the samples with KBr. These regions are 3600-3250 cm^{-1} of hydroxide groups (O—H)[83], 1636 cm^{-1} attributed to H—O—H bonds[80, 134] and the region between 2380 cm^{-1} to 2247 cm^{-1} of O═C═O bonds.[142]

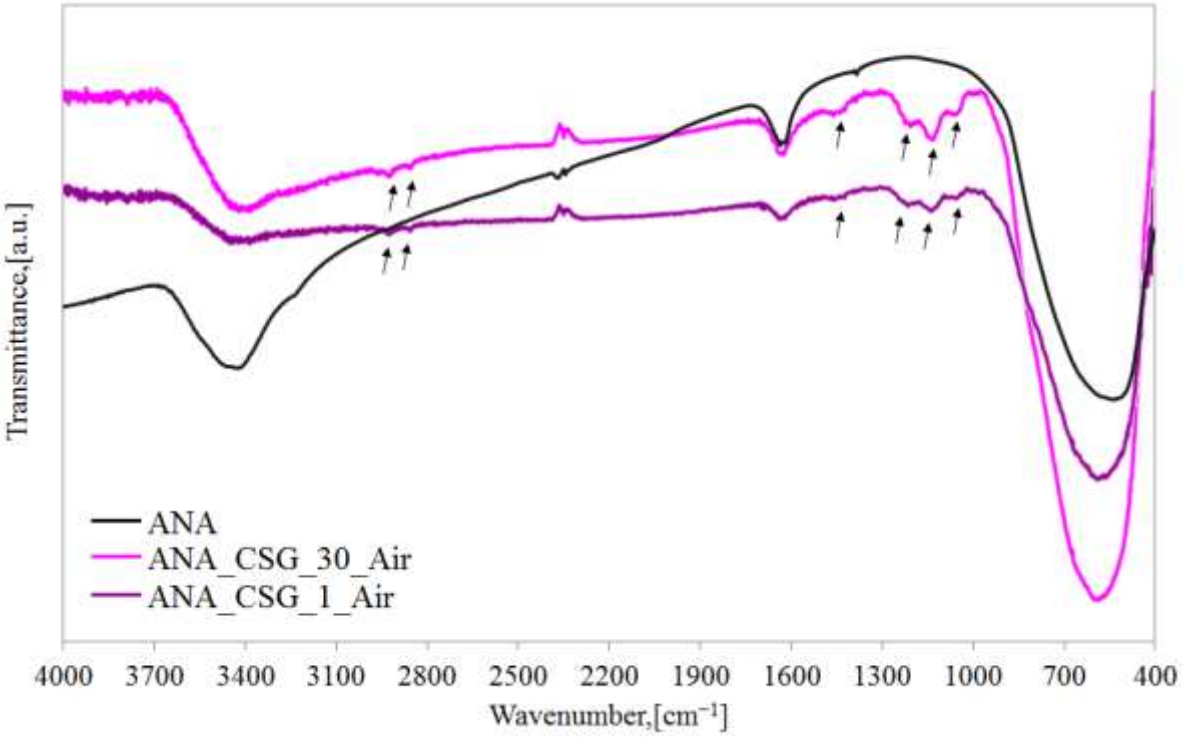

Figure 5- 7: FT-IR spectra of ANA (anatase TiO_2), ANA_CSG_30_Air and ANA_CSG_1_Air are (anatase reacts with carbon disulfide gaseous) heated at 300 ˚C in air for 30 minutes and 1 hour, respectively.

UV-vis absorption spectra of the anatase TiO_2, ANA_CSG_30_Air and ANA_CSG_1_Air are shown in Figure 5-7. In contrast to the unmodified-TiO_2 sample, an additional visible light absorption band was present at wavelengths of 685 nm and 615 nm of the ANA_CSG_30_Air

and ANA_CSG_1_Air samples, respectively. Based upon the plot of the Kubelka–Munk function against the energy of the light absorbed, which is presented in Figure 5-8 and Table 5-3, reacting titanium dioxide with CS_2 decreases the band gap to 1.81 eV and 2.02 eV of the ANA_CSG_30_Air sample and ANA_CSG_1_Air sample, respectively. In other words, there is a possibility that the SO_4—TiO_2 and CS—TiO_2 bonds may contribute to some narrowing of the band gap and enhancing visible light absorption. However, TiO_2 before and after the modification showed an absorption band in the UV region. This finding indicates that TiO_2 was not fully doped and there are still undoped-TiO_2 presents in the samples.

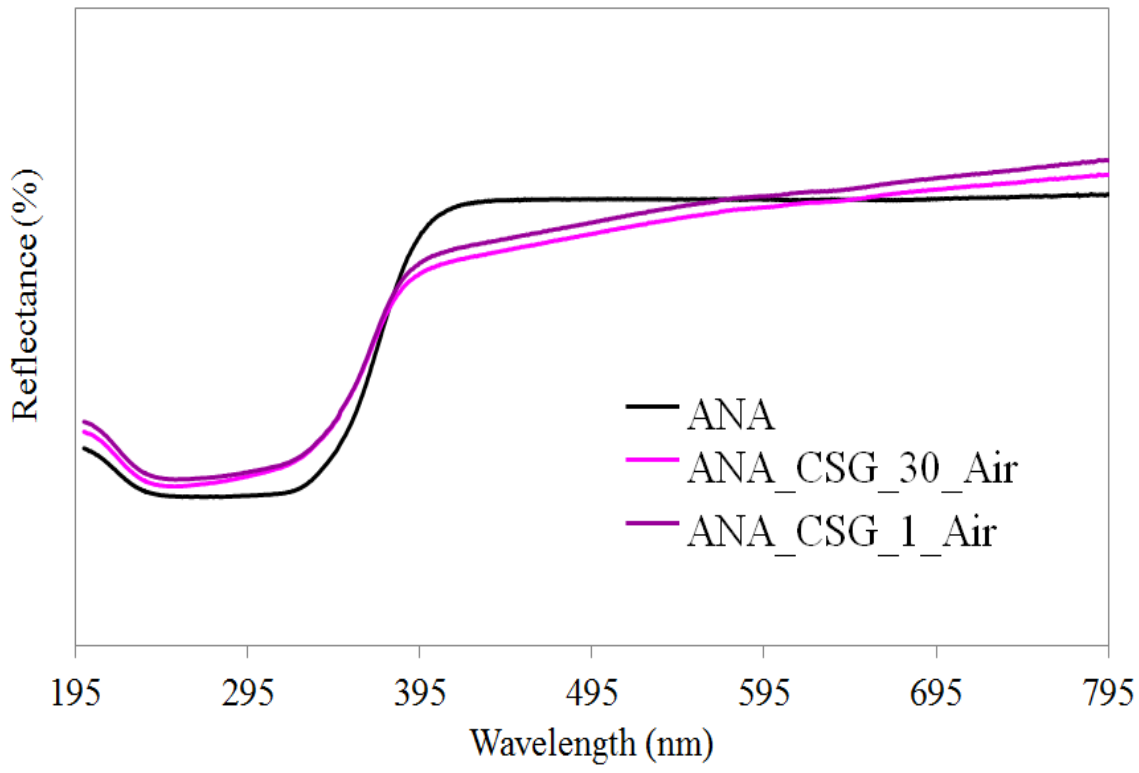

Figure 5- 8: UV-Vis spectra of ANA (TiO_2 anatase) and Anatase heated in carbon disulfide gaseous at 300 ˚C for 30 min and 1 hour (ANA_CSG_30_Air and ANA_CSG_1_Air) respectively.

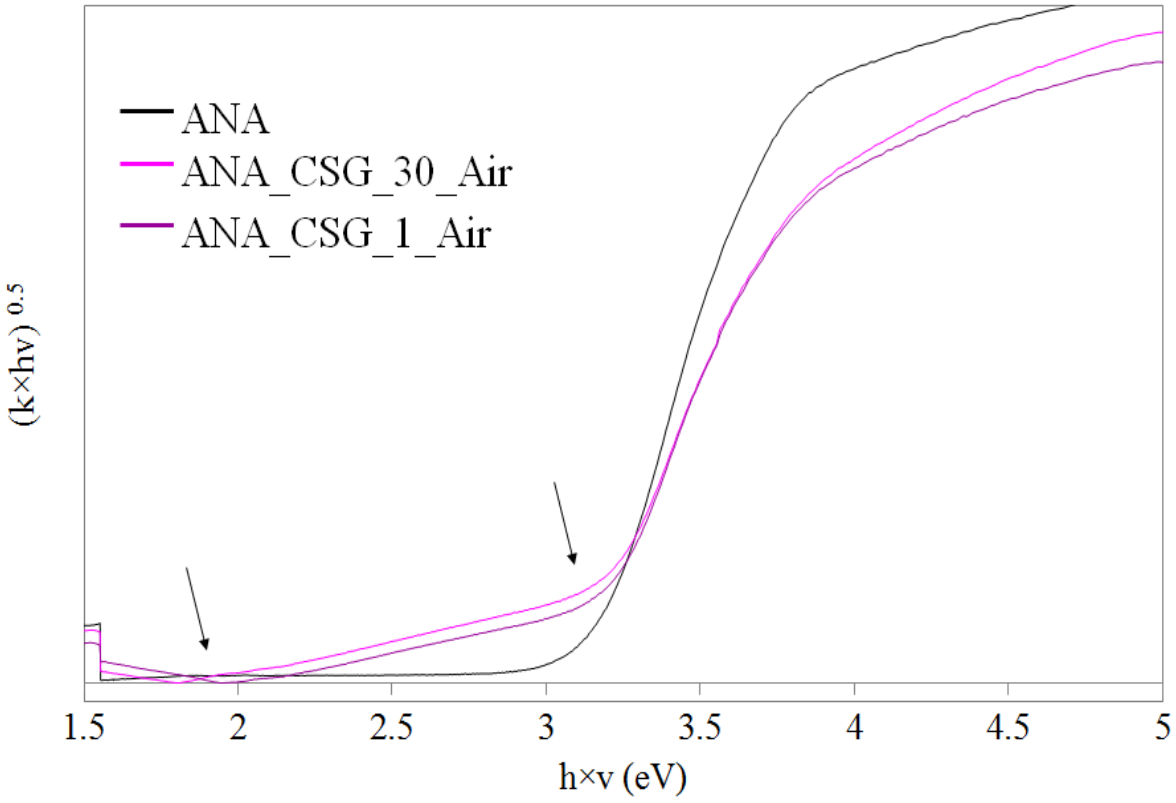

Figure 5- 9: Band gap calculation using the Kubelka–Munk function of ANA (TiO_2 anatase) and anatase heated in carbon disulfide gaseous at 300 °C for 30 min and 1 hour (ANA_CSG_30_Air and ANA_CSG_1_Air), respectively.

Table 5- 3: Band-gap energies (E_{bg}) and wavelengths (λ) obtained using the Kubelka–Munk function calculation.

Sample	E_{bg} (eV)	λ (nm)
TiO_2	3.22	384
ANA_CSG_30_Air	1.81 3.23	685 384
ANA_CSG_1_Air	2.02 3.23	615 384

5.2.2.3. Reactions with Liquid CS_2

In general, PXRD analysis was only carried out on samples showing a change in colour after the reaction with carbon disulfide. Consequently, the PXRD analysis was not conducted on all the liquid CS_2 reactions that were heated in air for both Methods 1 and 2. On the other hand, the PXRD analysis was carried out on all the reactions using nitrogen gas through the heating process for both Methods 1 and 2. These patterns were presented in Figures 5-10, 5-11, and 5-12.

The PXRD patterns of the samples in Method 1, which resulted from the reaction of amorphous/anatase with liquid CS_2 at 400 $^{\circ}$C for 5 hours in N_2, are shown in Figure 5-10 and Figure 5-11. Patterns of the ratios 1:1 and 1:2 of both (AM : CSL) and (ANA : CSL) samples showed in the anatase phase; however, the 1:3 (AM:CSL) sample showed a starting presence of titanium disulfide (TiS_2) with the anatase phase. These patterns were compared with the reference patterns JCPDS 21-1272 for anatase and JCPDS 81-0687 for TiS_2. These products also showed a change in their colour from white to grey after the heating process. The presence of TiS_2 could therefore be indicated sulfur-modified titanium dioxide as anionic doping.

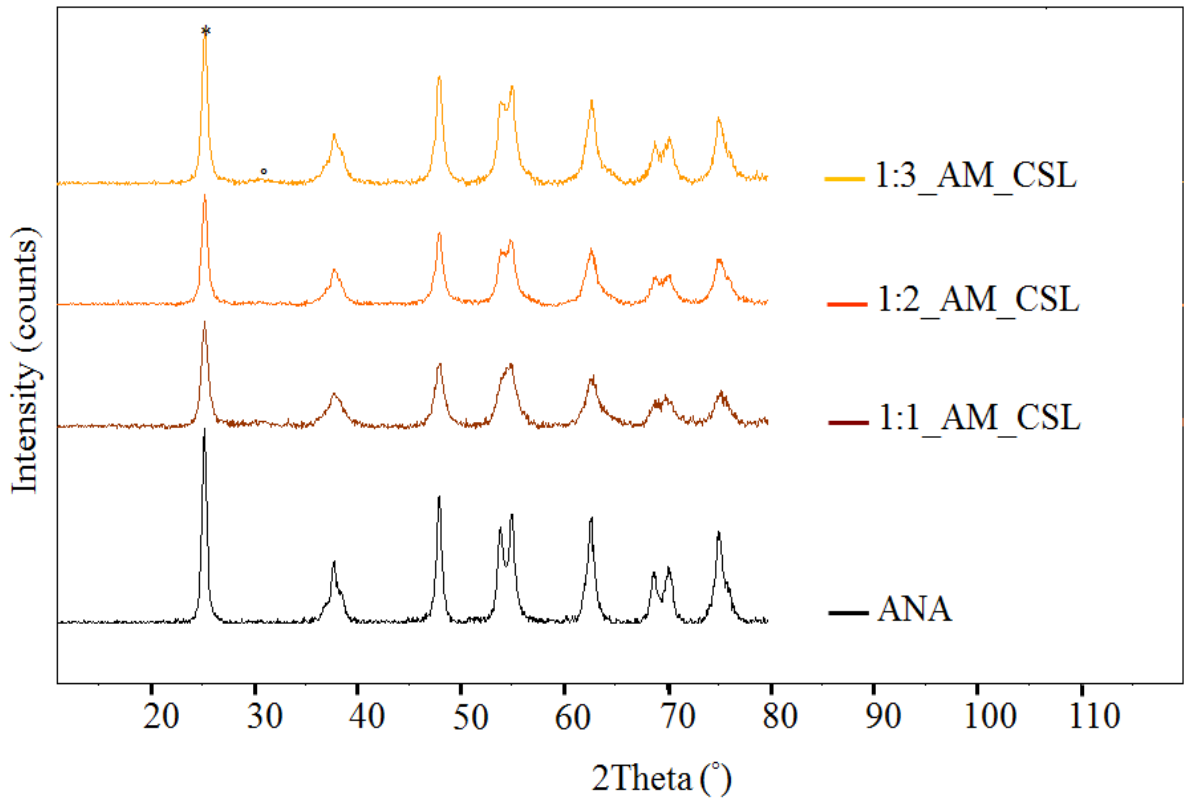

Figure 5- 10: PXRD patterns of ANA (AnataseTiO_2); AM_CSL for amorphous reacted with liquid carbon disulfide at the ratios of 1:1, 1:2, and 1:3. These samples were heated to 400 ˚C for 5 hours in N_2. (*) indicates the peaks for the TiO_2 anatase phase and (°) for TiS_2.

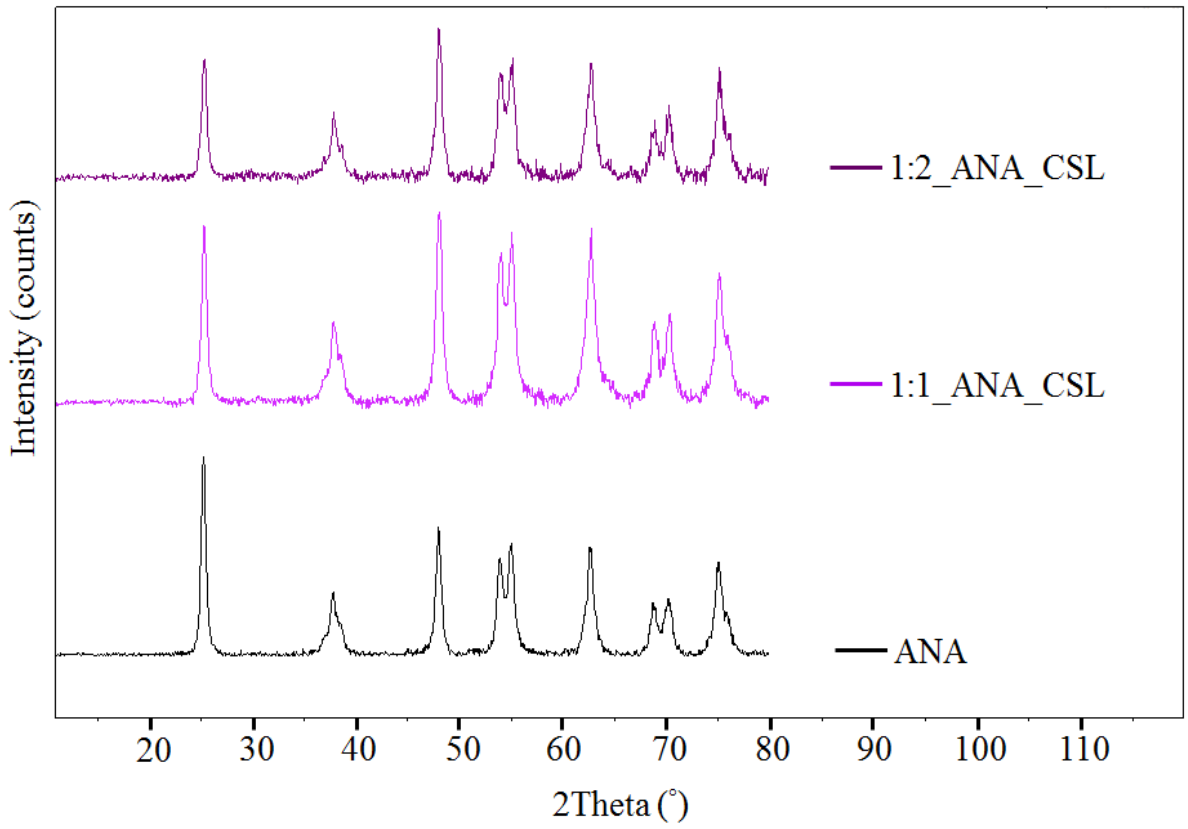

Figure 5- 11: PXRD patterns of ANA (AnataseTiO$_2$) and ANA_CSL for anatase TiO$_2$ reacted with liquid carbon disulfide at the ratios of 1:1 and 1:2. These samples were heated to 400 ˚C for 5 hours in N$_2$.

The PXRD patterns of Method 2, which heated a yellow powder of TCSLW (Ti isopropoxide, liquid CS_2 and water) directly and indirectly to 400 ˚C for 5 hours in N_2 gas, presented some different results (Figure 5-12). The yellow powder was converted to dark grey with an odour of rotten eggs in the TCSLW_D sample and formed a mix of anatase and rutile phases (JCPDS 21-1276). The smelly products could indicate that some sulfur was doped into the TiO_2 lattice. The TiS_2 was partly formed in the TCSLW_ID sample, which produced a light grey powder. This sample also showed the formation of a tiny rutile phase with an anatase phase. A summary of both methods is illustrated in Table 5-4.

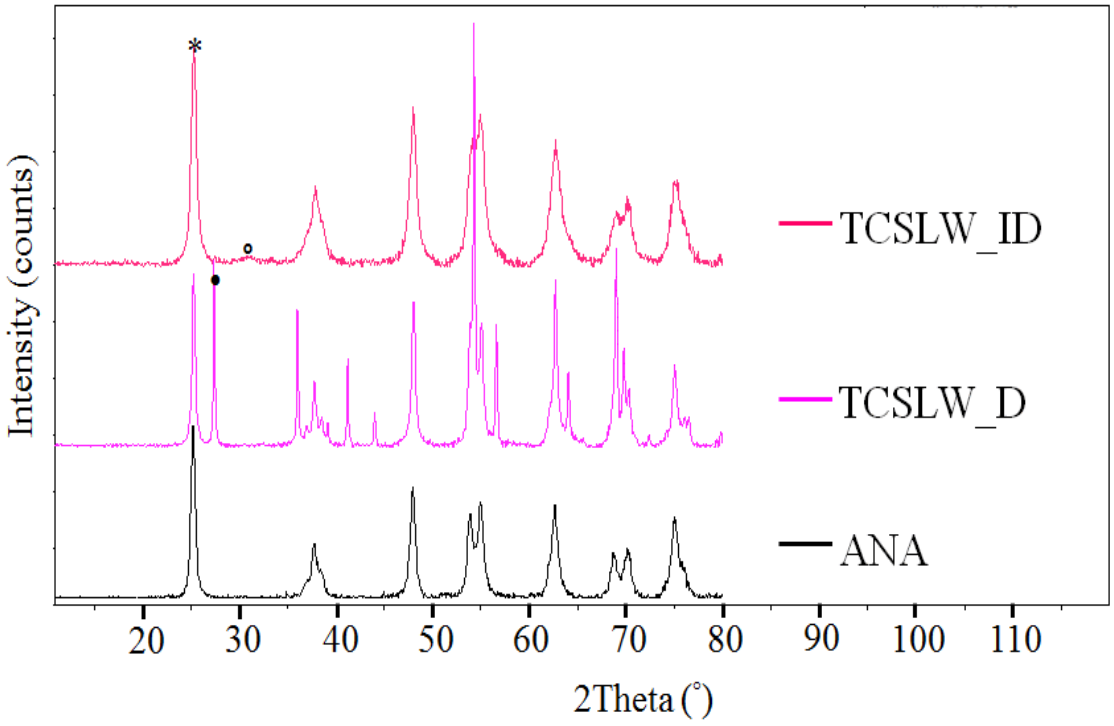

Figure 5- 12: PXRD patterns of ANA (AnataseTiO_2); TCSLW_D, and TCSLW_ID for the reaction of Ti isopropoxide, liquid carbon disulfide and water heated directly (D) at 400 ˚C for 5 hours in N_2 and (ID) indirectly by drying the reaction first at 100 ˚C then heated at 400 ˚C for 5 hours in N_2. (*) indicates the peaks for the TiO_2 anatase phase, (•) for the TiO_2 rutile phase, and (°) for TiS_2.

Table 5- 4: Summary of carbon disulfide liquid reactions

Sample	Product Colour	PXRD
ANA (blank)	White	Anatase
1:1_AM_CSL	Grey	
1:2_AM_CSL		
1:3_AM_CSL		Anatase + TiS_2
1:1_ANA_CSL		Anatase
1:2_ANA_CSL		
TCSLW_D	Dark grey	Anatase + rutile
TCSLW_ID	Light grey	Anatase + rutile + TiS_2

5.2.3. S-modification Using Thiourea

5.2.3.1. Forming of Cationic-cationic-anionic Co-doping TiO_2

All reactions between thiourea and amorphous $Ti(OCH(CH_3)_2)_{4-x}(OH)_x$ in air at 400 °C and 500 °C produced a change in colour from white to yellow and light yellow in the samples (Table 5-5). Colours, in general, result from the portion absorption of the visible spectrum and are then transmitted or reflected off those frequencies that not absorbed through our eyes to produce the sensation called colour.[15] These samples absorb higher frequencies and transmitters or reflects lower frequencies of visible light and then present as yellow in colour.[15] Therefore, the change in colour of the products obtained was a promising sign that they now

absorbed light within the visible light spectrum, thus indicating the possibility of a reduction in band-gap energy by successful S-modification of the TiO_2 structure.

Figures 5-13 and 5-14 show PXRD patterns of the AM : TU samples heated at temperatures of 400 ˚C and 500 ˚C, respectively. The PXRD patterns presented the samples to be anatase-phase after comparison with the reference pattern (JCPDS 21-1272).

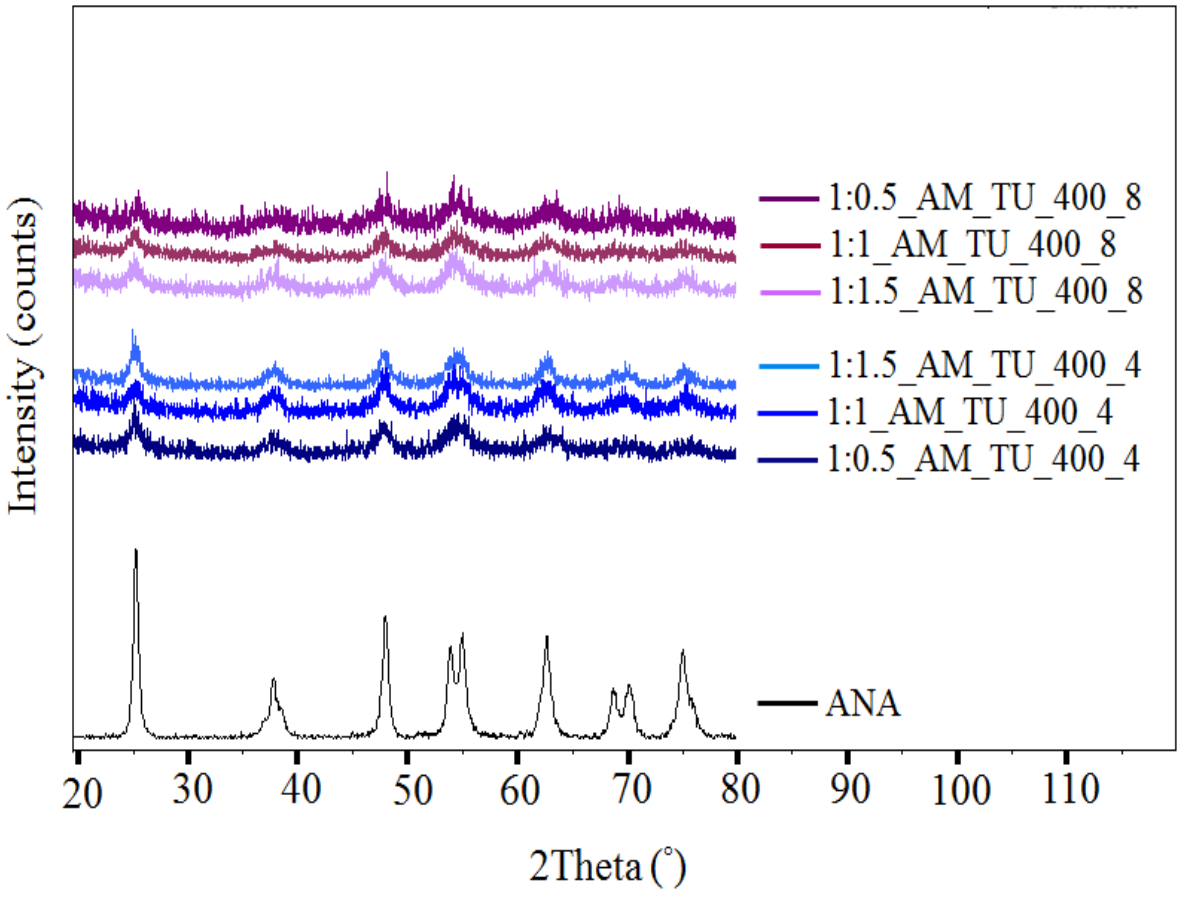

Figure 5- 13: PXRD patterns of ANA (Anatase TiO_2); AM_TU for amorphous $Ti(OCH(CH_3)_2)_{4-x}(OH)_x$ reacted with thiourea in the ratios 1:0.5, 1:1, and 1:1.5. These samples were heated to 400 ˚C for 4 and 8 hours in air.

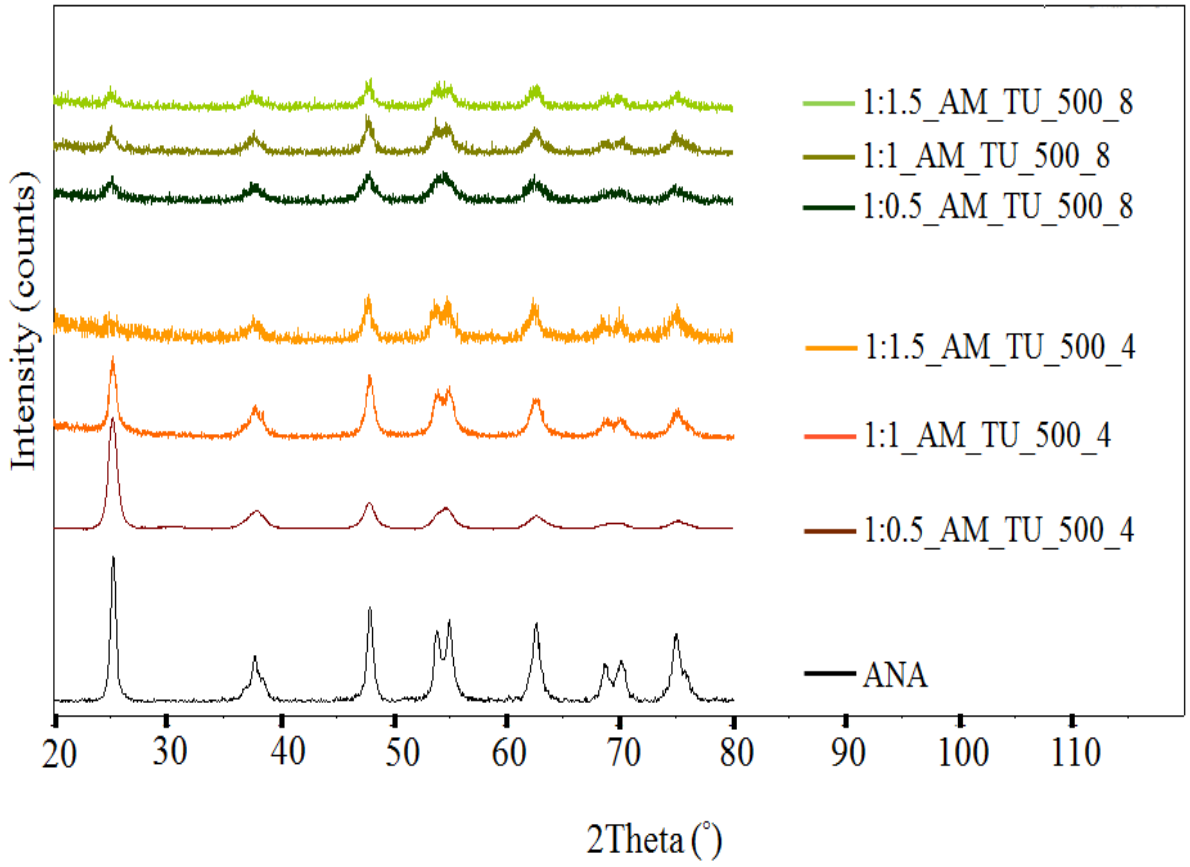

Figure 5- 14: PXRD patterns of ANA (Anatase TiO_2); AM_TU for amorphous $Ti(OCH(CH_3)_2)_{4-x}(OH)_x$ reacted with thiourea in the ratios 1:0.5, 1:1, and 1:1.5. These samples were heated to 500 ˚C for 4 and 8 hours in air.

Table 5- 5: Summary of thiourea with amorphous $Ti(OCH(CH_3)_2)_{4-x}(OH)_x$ reactions; products colour and PXRD results.

Sample	Product Colour	PXRD
ANA (blank)	White	Anatase
1:0.5_AM_TU_400_4	Yellow	
1:1_AM_TU_400_4		
1:1.5_AM_TU_400_4		
1:0.5_AM_TU_400_8		
1:1_AM_TU_400_8		
1:1.5_AM_TU_400_8	Light yellow	
1:0.5_AM_TU_500_4		
1:1_AM_TU_500_4	Yellow	
1:1.5_AM_TU_500_4		
1:0.5_AM_TU_500_8		
1:1_AM_TU_500_8		
1:1.5_AM_TU_500_8		

Because all the production of AM:TU showed a yellow colour, which resulted from the portion absorption of the visible spectrum, as it was previously mentioned, it was decided to apply elemental analysis to these samples.

The elemental analysis (EA) results for samples resulting from reactions carried out at temperatures 400 ˚C and 500 ˚C are shown in Table 5-6. The sample showing the highest percentage of sulfur (3.20 %) was the 1:0.5_AM_TU_400_8 sample, with the lowest percentage of sulfur (0.50 %) appearing in the 1:1.5_AM_TU_500_8 sample. The amount of sulfur decreased when the ratios were increased from 1:0.5 to 1:1.5 (AM:TU) and with increases in the temperature from 400 ˚C to 500 ˚C. The sulfur in all samples indicated that S-doped titanium dioxide could be synthesised. It should not be forgotten that the formula of thiourea (H_2NCSNH_2) has nitrogen; accordingly, the amount of nitrogen in some of the samples should be taken into account. Additionally, thiourea can be decomposed into ammonium thiocyanate, isothiocyanic acid, ammonia, carbon disulfide, cyanamide, and trithiocyanuric acid at temperatures from 149-246 ˚C as described in the section *1.7.2. of Thermal Decomposition of Thiourea*. In general, nitrogen content in the sample increased with increases in the AM : TU ratio and decreased with increase in temperature. The nitrogen percentage was negligible in the AM_TU_500_8 samples. Results for hydrogen percentages fluctuated, and the majority of the samples showed negligible amounts of carbon.

UV-vis spectra of AM_TU_400_4, AM_TU_400_8, AM_TU_500_4, and AM_TU_500_8 for the ratios 1:0.5, 1:1, and 1:1.5 are presented in Figure 5-15. Table 5-6 shows the calculation of the band gap energies with the Kubelka–Munk function. All samples showed two absorption bands except the sample 1:0.5_AM_TU_500_4 which showed one edge. The first absorption band was in the ultra violet regions, while the band shifted to the visible regions for the second absorption. The 1:0.5_AM_TU_500_4 sample that showed one absorption band at wavelength 392 nm with tiny decrease of the band gap energy to 3.16 eV is presented in Figure 5-16. These

decreases in the band gap indicated to the S-doping. Consequently, because the 1:0.5_AM_TU_500_4 sample was the only sample presented one absorption edge in UV-vis spectrum accompanied with a 1.29 % sulfur concentration, FT-IR analysis was applied. Up to date several studies showed two edges in the UV-vis spectra when used thiourea as a source of sulfur.[31, 42, 122]

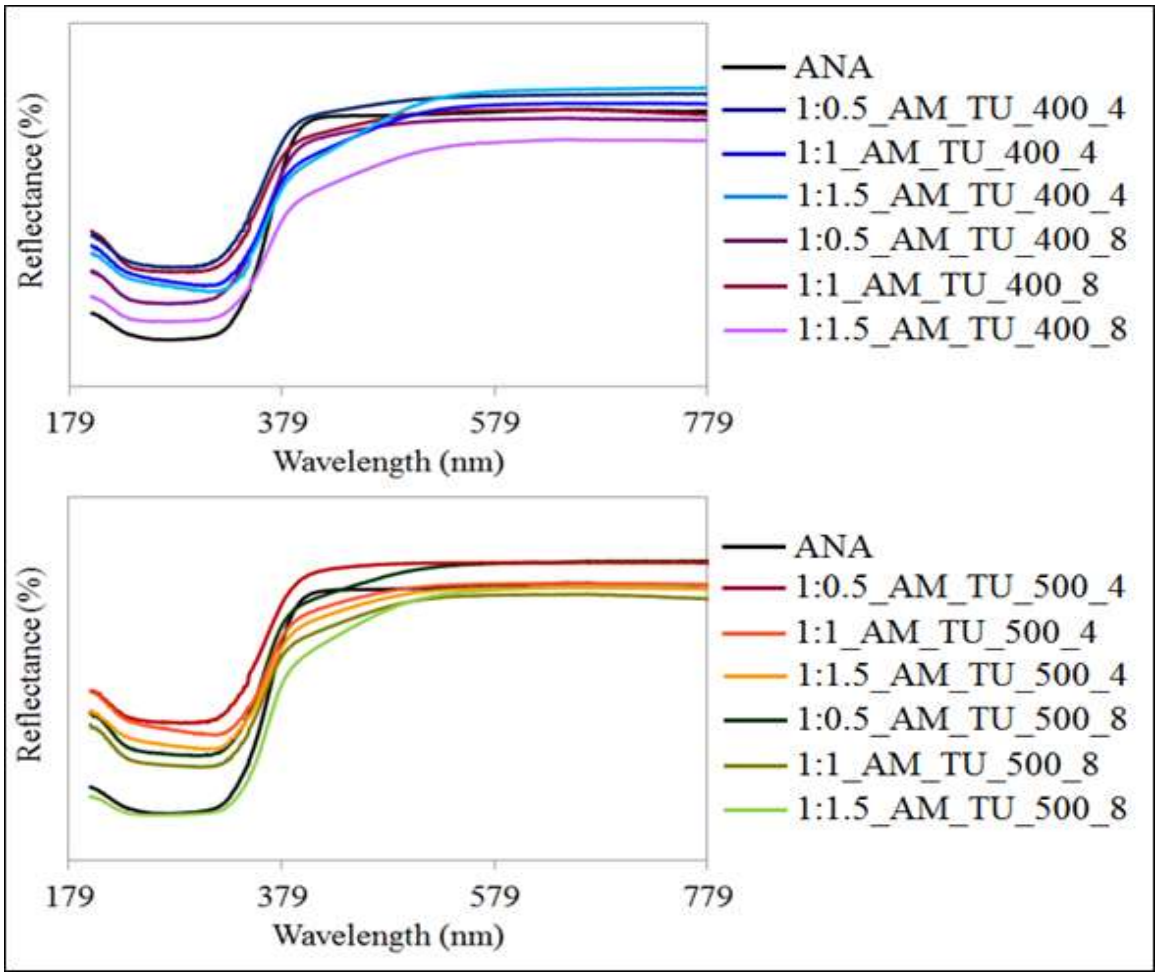

Figure 5- 15: UV-Vis spectra of ANA (TiO_2 anatase) and amorphous (AM) heated with thiourea (TU) at 400 ˚C and 500 ˚C for 4 hours and 8 hours at the ratios 1:0.5, 1:1, and 1:1.5 (AM:TU).

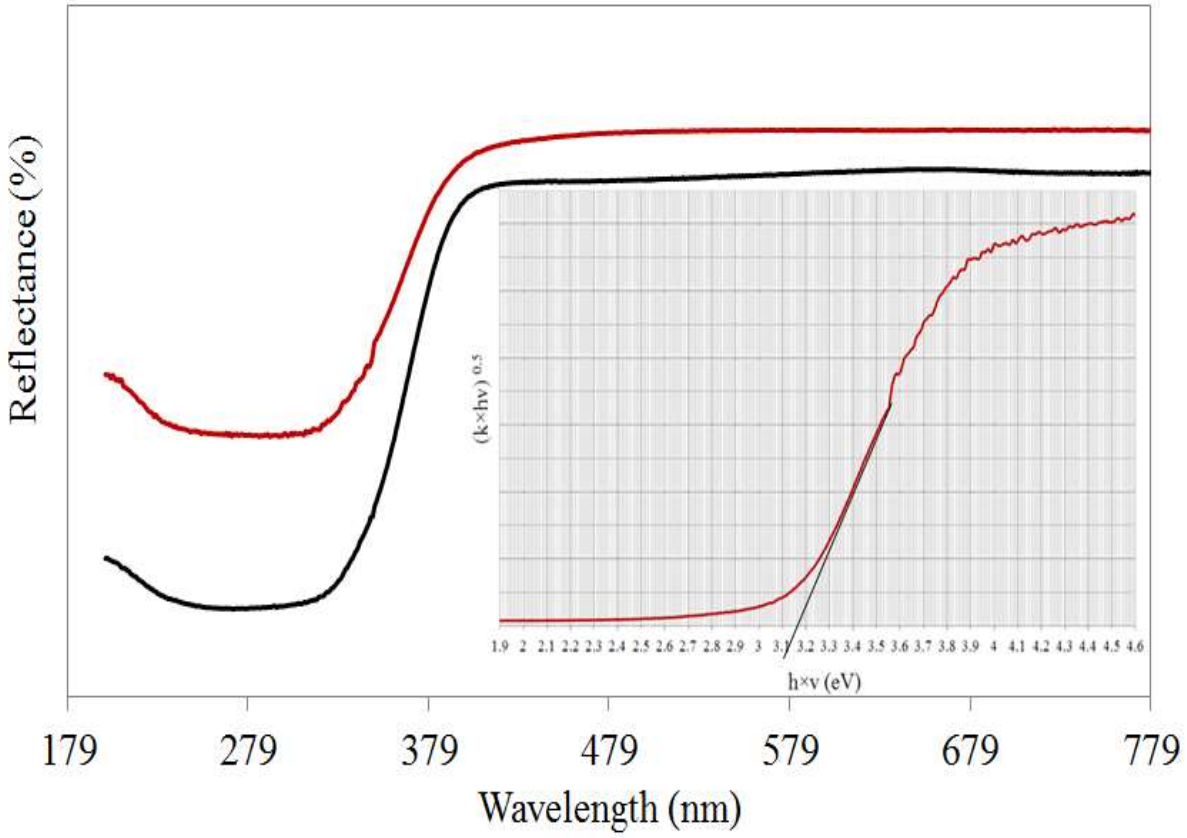

Figure 5- 16: UV-Vis spectra of ANA(TiO_2 anatase)and the sample 1:0.5_AM_TU_500_4. Band gap calculation using the Kubelka–Munk function of 1:0.5_AM_TU_500_4. This sample showed one absorption edge with a small decrease in the band gap to ≈ 3.16 eV.

Table 5- 6: Summary of thiourea reactions; results from the calculation of Band-gap energies (E_{bg}) and elemental analysis.

Sample	E_{bg} (eV)	λ (nm)	EA %			
			S	N	C	H
ANA (blank)	3.22	384	-	0	0.05	0
1:0.5_AM_TU_400_4	3.23 2.42	384 512	2.83	0.15	0	0.96
1:1_AM_TU_400_4	3.26 2.43	380 510	1.55	0.25	0	0.52
1:1.5_AM_TU_400_4	3.25 2.35	381 527	0.83	0.29	0.2	0.2
1:0.5_AM_TU_400_8	3.23 2.26	384 548	3.20	0.14	0	0.83
1:1_AM_TU_400_8	3.25 2.38	382 520	2.78	0.20	0	0.75
1:1.5_AM_TU_400_8	3.26 2.32	380 534	2.08	0.24	0	0.73
1:0.5_AM_TU_500_4	**3.16**	**392**	1.29	0.01	0	0.25

1:1_AM_TU_500_4	3.23 2.46	384 504	0.65	0.12	0	0.07
1:1.5_AM_TU_500_4	3.24 2.54	383 488	0.51	0.13	0	0.12
1:0.5_AM_TU_500_8	3.24 2.98	383 517	1.33	0	0	0.32
1:1_AM_TU_500_8	3.28 2.36	378 525	0.71	0	0.12	0.32
1:1.5_AM_TU_500_8	3.28 2.40	377 516	0.50	0	0.07	0

The FT-IR spectrum of the sample 1:0.5_AM_TU_500_4 and compared with spectra of pure anatase TiO_2, amorphous titanium isopropoxide hydroxide and thiourea samples presented in Figure 5-17. As usual, the three bands absorbed from air as a result of grinding the samples with KBr are present in all samples. These regions are 3600-3250 cm^{-1} of hydroxide groups (O—H)[83], 1636 cm^{-1} attributed to H—O—H bonds[80, 134], and the region between 2380 cm^{-1} to 2247 cm^{-1} of O═C═O bonds.[142]

The spectra of the sample 1:0.5_AM_TU_500_4 showed seven bands: 2926 cm^{-1}, 2851 cm^{-1}, 1204 cm^{-1}, 1131 cm^{-1}, 1047 cm^{-1}, 959 cm^{-1}, and 688-400 cm^{-1}. The bands at both 2926 $cm^{-1}$and 2851 cm^{-1} could be associated with two nominated groups, either the C—H[135, 142, 155]

group or the C═S[152] group. The C—H group was nominated as a possible case for forming into (AM:TU) sample. The first reason for this is because these two bands are presented in the AM spectra as well (full interpretation of AM sample in section 3.2.2.), which corresponds to the C—H stretching bond.[135, 142, 155] The second reason is because amorphous titanium isopropoxide hydroxide Ti (OCH $(CH_3)_2)_{4-x}$ $(OH)_x$, which was used as a starting material of this reaction, has a CH group. However, because these two bands (2926 $cm^{-1}$and 2851 cm^{-1}) also presented in the spectra of the samples ANA_CSG (section *5.2.1.2. Forming New Potential Nanoparticles Cationic-anionic co-doping*) and the starting materials were TiO_2 and CS_2, so the possibility of forming the C—H bond was not favour. As a result, the C═S group could be more favourable than the CH group. First, the symmetric and asymmetric stretching modes of free CS_2 absorbed at the region between 2154 cm^{-1} and 2400 cm^{-1} are shown in the FT-IR spectrum of CS_2 (see appendix 10).[152-154] Thus, the increasing the wavenumbers to 2926 $cm^{-1}$and 2851 cm^{-1} means that C═S could be involved in the structure of the sample 1:0.5_AM_TU_500_4 (the location of CS within the structure not clear yet). Moreover, the presence of the absorption peak at 1204 cm^{-1} is also assigned to R—CS—R bonds.[156, 142, 157] Other proof of forming CS bond, the carbon disulfide is one of the decompositions/residues of thiourea, which is used as a starting material in this experiment (*see section 1.7.2. Thermal Decomposition of Thiourea*). According to these reasons, it could be agreed upon that the sample AM_TU_500_4 has the C═S bond formed into its structure. The band of 1131 cm^{-1} is the absorption peak assigned to O—S bond.[4, 142, 143, 158, 159] The O—S bond that presented in the AM_TU_500_4 spectrum could be for the Ti—O—S bonding not for SO_4^{2-} bonding. This resulted due to the absence of the absorption peak at the region ranging from 1350-1450 cm^{-1} of the sulfate group.[157] This means that the forming of sulfate did not achieve in this reaction. The absorption peak at 1047 cm^{-1} could be assigned for either the S═O[4, 142, 143, 158, 159] bond or assigned to the Ti—S[121, 123, 158] bond. Because sulfate group was not present at the absorption

peak, as previously mentioned, and the O—S group was not present in SO_4^{2-}, so the absorption peak at 1047 cm^{-1} did not correspond to the S═O group in the AM_TU_500_4 spectrum. The 1047 cm^{-1} band could be related to Ti—S bond, which also absorbed at 959 cm^{-1} as reported in many literatures.[33, 123] Accordingly, the band at 1047 cm^{-1} and 959 cm^{-1} were more likely to be associated to the Ti—S bond than to the S═O bond. According to ANA spectrum, the band in the region 688-400 cm^{-1} is present due to the vibrational mode of the Ti—O bonds.[80, 134] From the FT-IR results, the sample 1:0.5_AM_TU_500_4 could be formed cationic-anionic co-doping resulting in formed of new three possible coordination: Ti—O—S, TiO_2—CS, and O—Ti—S. Some previous studies reported that the possibility of presence different oxidation stats of sulfur in the same product such as S^{6+}, S^{4+}, and/or S^{2-}.[121, 143] Crystallite size of the 1:05_AM_TU_500_4_Air sample was calculated to be 7 nm by using Scherrer equation.

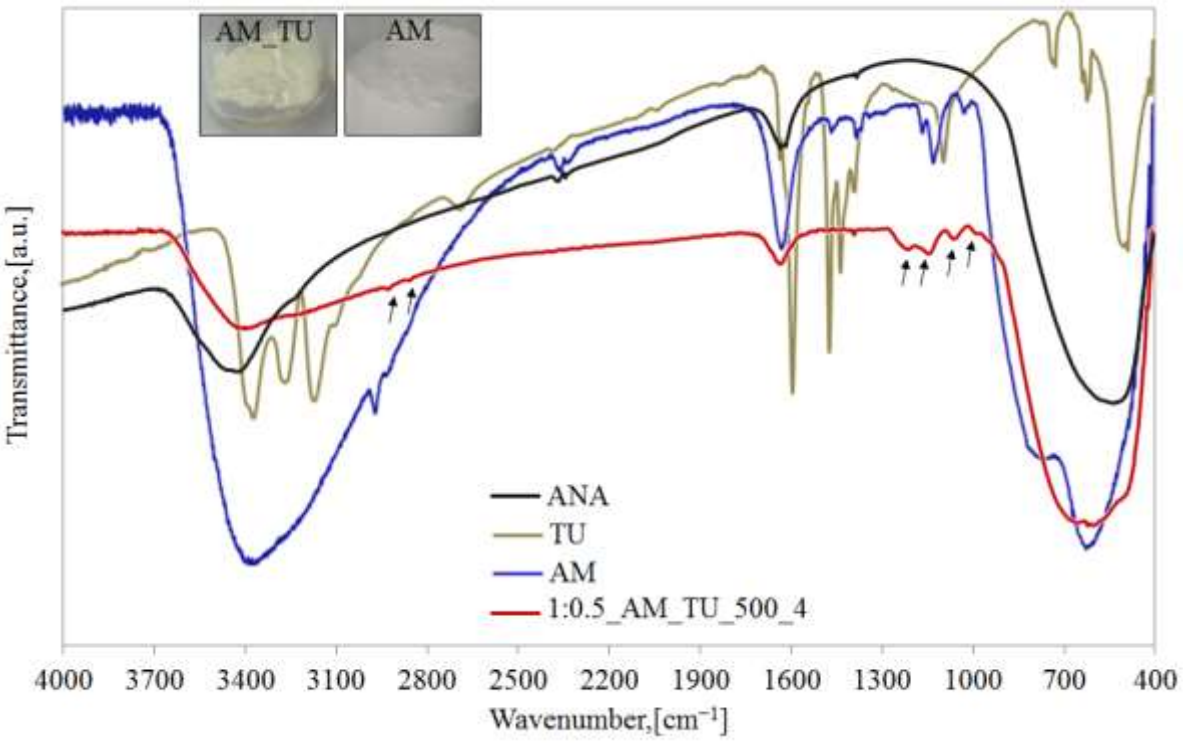

Figure 5- 17: FT-IR spectra of anatase TiO_2 (ANA), thiourea (TU), amorphous titanium isopropoxide hydroxide (AM), and the sample 1:0.5_AM_TU_500_4.

5.3. Conclusions

By using dodecanethiol as a source of sulfur, the S-modified TiO_2 is carried out at a temperature of 400°C for 5 hours. Unfortunately, this reaction did not produce any sulfur. This was proved by the black colour of the sample produced and it did not have an odour of rotten eggs, which could be a sign of the presence of sulfur. The EDX analysis also showed no sulfur percentage was found in the 1:1_AM_DT sample. This experiment did not demonstrate any success. This could be because of the long chain of carbon of the dodecanethiol chemical formula.

In preparation for anionic doping, S-modified TiO_2 was produced using gaseous carbon disulfide as a source of sulfur by heating AM_CSG and ANA_CSG samples to 400 °C and then to 300 °C. All the patterns in PXRD showed either a mix of three phases (anatase, rutile, and TiS_2) or two phases (anatase and TiS_2), with the exception that the ANA_CSG_30_Air and ANA_CSG_1_Air samples showed a single phase (anatase) with the colour changing to beige. The presence of titanium disulfide in this case indicated that the gaseous carbon disulfide favoured to the substitution of S^{2-} with O^{2-} in TiO_2. The primary results of ANA_CSG_30_Air and ANA_CSG_1_Air samples estimated of new potential nanoparticles cationic-anionic co-doping. The crystallite size of TiO_2 both before and after reacting with carbon disulfide gaseous presents on a nanometre scale. Because of the interpretation of FT-IR spectra, showed the presence of absorption peaks related to SO_4^{2-} and SC groups; both cationic doping and anionic doping could be achieved. Thus, by forming two possible coordinations: CS—TiO_2, and SO_4—TiO_2. UV-vis spectra showed two absorptions band; one of these bands was shifted to a visible region and decreased the band gap to 1.81 eV for the sample that heated for 30 minutes and 2.02 eV for the sample that heated for one hour; the other band was still in the UV-region. Because of these two absorption bands, the titanium dioxide was determined not to be fully doped. By using a carbon disulfide liquid as a source of sulfur, S-modified TiO_2 can be carried

out through two methods. Method 1 could produce anionic doping by forming some TiS_2 at a ratio of 1:3_AM_CSL. On the other hand, the ratios 1:1 and 1:2 for ANA_CSL and AM_CSL, respectively showed a single anatase phase. Method 2 observed the starting formation of TiS_2 in the TCSLW_ID sample but not in the TCSLW_D sample. The sample TCSLW_D may have had some sulfur doped in the TiO_2 lattice (mixed anatase and rutile) due to its dark grey colour and its odour of rotten eggs.

S-modification of TiO_2 through use of thiourea as a source of sulfur was performed by reacting the AM sample with the TU sample at two temperatures, 400 ˚C and 500 ˚C. Generally, all the samples showed the anatase phase in PXRD patterns, and the elemental analysis results show the presence of sulfur. These results indicate that it could be S-doped in titanium dioxide lattice, which is proved by the absorption in the Vis-regions and decreased the band gap less than 3.2 eV. The sample 1:0.5_AM_TU_500_4 showed interesting results that included: single-phase (anatase), changes in colour, the presence of sulfur, and the appearance of one absorption band at the 392-nm wavelength with slight decreases in the band gap to 3.16 eV (compared to 3.22 eV in anatase TiO_2 [blank]). As a result of FT-IR data, this sample showed cationic-cationic-anionic co-doping, resulting in formed of new three possible coordination: Ti—O—S, Ti—CS, and Ti—S.

6– Overall Conclusions

This project was divided into three sections: the synthesis of anatase TiO_2, the N-modification of TiO_2 and the S-modification of TiO_2.

In summary of the TiO_2 synthesis chapter, single pure anatase TiO_2 nanoparticles was successfully synthesised with crystallite sized between 6 nm and 20 nm, as it was shown in a PXRD pattern. This was done in two steps. The drying process formed the amorphous titanium isopropoxide hydroxide $Ti(OCH(CH_3)_2)_{4-x}(OH)_x$, and the heating process formed the anatase TiO_2. The FT-IR data proved the formation of the Ti—O—Ti bonds in the regions 700–400 cm^{-1} and the removal of all of the Ti isopropoxide residues at 400 °C. The UV-Vis data showed an absorption at a wavelength of 384 nm with a band gap at 3.22 eV, in agreement with the data reported for TiO_2 in the anatase phase. SAED also proved that defined (*hkl*) planes formed TiO_2. Additionally, EELS clearly showed the splitting of the Ti L-edge present for the Ti^{4+} compounds, particularly TiO_2, and allowed the element atomic percentages to be calculated with 56.8±7 % for Ti and 43.2±5.3 % for O. this was in agreement with the literature values.

In the N-modified TiO_2 chapter, two sources of nitrogen urea and cyanamide were used. Reacting the urea with amorphous $Ti(OCH(CH_3)_2)_{4-x}(OH)_x$ in N_2 did not work. However, when this reaction was carried out in the air, it showed a formation of a new potential of titanium-oxy-carbodiimide in the general formula $TiO_{2-x}(CN_2)_x$. Reacting urea with anatase TiO_2 in the air did not work. However, when this reaction was carried out under the following of N_2, it also formed a new potential of titanium-oxy-carbodiimide. Both the 1:10_AM_U_400_Air and the 1:10_ANA_U_450_N samples showed a single anatase phase in PXRD patterns. The FT-IR spectra showed the band at about 2055 cm^{-1} for the carbodiimide group, and they showed a decrease of the band gap less than 3.22 eV. The elemental analysis data showed approximately a 2:1 ratio of N:C, which showing that the $(CN_2)^{2-}$ anion fragments in the carbodiimide. Some

previous studies showed the presence of $(CN_2)^{2-}$ anion in their products with different metals, such as La, Cu, and Mn, however, this study it was produced with Ti. Using the cyanamide resulted in the cyanamide and the anatase reactions at 400 °C and 450 °C. This presented a single anatase phase in a PXRD pattern and a mix of carbodiimide and cyanamide residues in the FT-IR spectra. The cyanamide and amorphous $Ti(OCH(CH_3)_2)_{4-x}(OH)_x$ reacted at the ratio 1:2 of (AM : CM), and the temperatures between 450 °C and 550 °C achieved a rock-salt structure in the PXRD pattern. However, when this reaction was carried out at 400 °C, it resulted a new decomposition of cyanide, called carbodiimide cyanide or N-(iminomethylene)cyanamide, in a general formula $TiO_{2-x}(C_2N_3)_{2x}$ at the ratio 1:0.25 AM:CM. It also produced a new general formula could be $TiO_{2-x}(CN_2H)_{2x}$ at the ratios 1:0.5, 1:0.75 and 1:1 AM:CM.

In the S-modified TiO_2 chapter, three sources of sulfur dodecanethiol, carbon disulfide (gases and liquid) and thiourea were used. Unfortunately, the dodecanethiol reactions at T = 400° C for t = 5 hours did not work because of its chemicals containing more carbon and less sulfur. The carbon disulfide gaseous/liquid reactions resulted in anionic-doping by partially involved TiS_2 in PXRD patterns of AM_CSG (in N_2 /air) samples and ANA_CSG (in N_2) samples at T = 400 °C and T = 300 °C. However, the ANA_CSG in the air showed a cationic-doping instead of an anionic-doping. The ANA_CSG_Air samples produced an estimated the possible coordinations: SO_4—TiO_2 and CS—TiO_2. For the CS_2 (liquid) reactions, this TiS_2 started presenting in PXRD patterns of the samples ANA_CSL, ANA_CSL and TCSLW_ID. The thiourea reactions resulted in cationic and anionic doping being formed in the sample 1:0.5_AM_TU_500_4, resulting in formed of new three possible coordinations: Ti—O—S, TiO_2—CS, and Ti—S. The sample 1:0.5 (AM:TU) showed a single anatase phase in a PXRD pattern. The absorption bands of Ti—O—S bond, C=S bond and Ti—S presented in the FT-IR

spectra. Its UV-Vis spectra showed one absorption band at the 392 nm wavelength with slight decreases in the band gap to 3.16 eV.

7− References

1. B. Ohtani, *Adv. Inorg. Chem* . 2011, **63**, 395-430.

2. D. S. Bhatkhande, V. G. Pangarkar and A. A. C. M. Beenackers, *J. Chem. Technol. Biotechnol.*, 2002, **77**, 102-116.

3. M. R. Hoffmann, S. T. Martin, W. Y. Choi and D. W. Bahnemann, *Chem. Rev.*, 1995, **95**, 69-96.

4. G. D. Yang, Z. F. Yan and T. C. Xiao, *Appl. Surf. Sci.*, 2012, **258**, 4016-4022.

5. T. P. Ang, J. Y. Law and Y. F. Han, *Catal. Lett.*, 2010, **139**, 77-84.

6. D. R. Myers, *Solar Radiation: Practical Modeling for Renewable Energy Applications*, CRC Press Taylor and Francis, USA, 2013.

7. K. Biernat, A. Malinowski and M. Gnat, *The Possibility of Future Biofuels Production Using Waste Carbon Dioxide and Solar Energy*, InTech, 2013.

8. A. R. Khataee and G. A. Mansoori, *Nanostructured titanium dioxide materials : properties, preparation and applications*, World Scientific, Singapore ; New Jersey, 2012.

9. F. A. Khan, *Biotechnology Fundamentals*, CRC Press, USA, 2011.

10. L. S. Ruzer and N. H. Harley, *Aerosols Handbook: Measurement, Dosimetry, and Health Effects*, CRC Press, 2nd edn., 2012.

11. L. E. Smart and E. A. Moore, *Solid State Chemistry: An Introduction*, Boca Raton, Fla. CRC, London, 3rd edn., 2005.

12. S. E. Dann, *Reactions and characterization of solids*, Royal Society of Chemistry, Cambridge, 2000.

13. A. R. West, *Basic solid state chemistry*, John Wiley and Sons, New York, 2nd edn., 1999.

14. R. Van De Krol, *Sci. Technol.*, 2012, **102**, 13-67.

15. G. E. Rodgers, *Introduction to coordination, solid state, and descriptive inorganic chemistry*, McGraw-Hill, New York, 1994.

16. S. C. Erwin, L. Zu, M. I. Haftel, A. L. Efros, T. A. Kennedy and D. J. Norris, *Nat.*, 2005, **436**, 91-94.

17. D. Mitoraj and H. Kisch, *Chem. Eur. J.*, 2010, **16**, 261-269.

18. T. Kheamrutai, L. Pichet and N. and Boonlaer, *Nat. Sci.*, 2008, **42**, 357-361.

19. K. Yang, Y. Dai and B. Huang, Review of the Structural Stability, Electronic and Magnetic Properties of Nonmetal-Doped TiO_2 from First-Principles Calculations, http://arxiv.org/abs/1202.5651v1, Accessed 08 January 2015.

20. J. F. Banfield, B. L. Bischoff and M. A. Anderson, *Chem. Geol.*, 1993, **110**, 211-231.

21. S. H. Elder, F. M. Cot, Y. Su, S. M. Heald, A. M. Tyryshkin, M. K. Bowman, Y. Gao, A. G. Joly, M. L. Balmer, A. C. Kolwaite, K. A. Magrini and D. M. Blake, *J. Am. Chem. Soc.* , 2000, **122**, 5138-5146.

22. H. Z. Zhang, H. S. Qin and G. R. Chen, *Int. J. Bifurcat. Chaos.*, 1998, **8**, 2041-2046.

23. A. A. Gribb and J. F. Banfield, *Am. Mineral.*, 1997, **82**, 717-728.

24. X. Chen and S. S. Mao, *Chem. Rev.*, 2007, **107**, 2891-2959.

25. L. Castaneda, J. C. Alonso, A. Ortiz, E. Andrade, J. M. Saniger and J. G. Banuelos, *Mater. Chem. Phys.*, 2003, **77**, 938-944.

26. N. Venkatachalam, M. Palanichamy and V. Murugesan, *Mater. Chem. Phys.*, 2007, **104**, 454-459.

27. W. Guo, Z. Lin, X. Wang and G. Song, *Micro. Engn.*, 2003, **66**, 95-101.

28. M. D. Graef and M. E. McHenry, *Structure of Materials: An Introduction to Crystallography, Diffraction and Symmetry*, Cambridge University Press, USA, 2012.

29. M. R. Ranade, *P. Natl. Acad. Sci.*, 2002, **99**, 6476-6481.

30. H. Y. Liu and L. Gao, *J. Am. Ceram. Soc.*, 2004, **87**, 1582-1584.

31. Q. W. Zhang, J. Wang, S. Yin, T. Sato and F. Saito, *J. Am. Ceram. Soc.*, 2004, **87**, 1161-1163.

32. P. C. Maness, S. Smolinski, D. M. Blake, Z. Huang, E. J. Wolfrum and W. A. Jacoby, *Appl. Environ. Microbiol.*, 1999, **65**, 4094-4098.

33. S. T. Hussain, K. Khan and R. Hussain, *J. Nat. Gas. Chem.*, 2009, **18**, 383-391.

34. F. C. Gennari and D. M. Pasquevich, *J. Am. Ceram. Soc.*, 1999, **82**, 1915-1921.

35. H. Zhang and J. F. Banfield, *J. Phys. Chem. B*, 2000, **104**, 3481-3487.

36. G. Rothenberger, J. Moser, M. Gratzel, N. Serpone and D. K. Sharma, *J. Am. Chem. Soc.* , 1985, **107**, 8054-8059.

37. H. Hidaka, Y. Asai, J. C. Zhao, K. Nohara, E. Pelizzetti and N. Serpone, *J. Phys. Chem.*, 1995, **99**, 8244-8248.

38. N. Serpone, D. Lawless and R. Khairutdinov, *J. Phys. Chem-US.*, 1995, **99**, 16646-16654.

39. D. W. Bahnemann, M. Hilgendorff and R. Memming, *J. Phys. Chem. B*, 1997, **101**, 4265-4275.

40. S. Kwon, M. Fan, A. T. Cooper and H. Yang, *Crit. Rev. Env. Sci. Tec.*, 2008, **38**, 197-226.

41. R. Nakamura, T. Tanaka and Y. Nakato, *J. Phys. Chem. B*, 2004, **108**, 10617-10620.

42. T. Tachikawa, S. Tojo, K. Kawai, M. Endo, M. Fujitsuka, T. Ohno, K. Nishijima, Z. Miyamoto and T. Majima, *J. Phys. Chem. B*, 2004, **108**, 19299-19306.

43. K. Hashimoto, H. Irie and A. Fujishima, *Jpn. J. Appl. Phys.* , 2005, **44**, 8269-8285.

44. W. Li, C. Ni, H. Lin, C. P. Huang and S. I. Shah, *J. Appl. Phys.*, 2004, **96**, 6663-6668.

45. A. M. Sackler, *Nanoscience: Underlying Physical Concepts and Phenomena*, National Academies Press, United States of America, 2002.

46. T. Morikawa, R. Asahi, T. Ohwaki, K. Aoki and Y. Taga, *Jpn. J. Appl. Phys. 2*, 2001, **40**, 561-563.

47. T. Lindgren, J. M. Mwabora, E. Avendano, J. Jonsson, A. Hoel, C. G. Granqvist and S. E. Lindquist, *J. Phys. Chem. B*, 2003, **107**, 5709-5716.

48. H. Irie, Y. Watanabe and K. Hashimoto, *Chem. Lett.*, 2003, **32**, 772-773.

49. S. Sakthivel and H. Kisch, *Angew. Chem. Int. Edit.*, 2003, **42**, 4908-4911.

50. T. Umebayashi, T. Yamaki, H. Itoh and K. Asai, *Appl. Phys. Lett.*, 2002, **81**, 454-456.

51. A. Hattori, M. Yamamoto, H. Tada and S. Ito, *Chem. Lett.*, 1998, **27**, 707-708.

52. J. C. Yu, J. G. Yu, W. K. Ho, Z. T. Jiang and L. Z. Zhang, *Chem. Mater.*, 2002, **14**, 3808-3816.

53. S. C. Moon, H. Mametsuka, S. Tabata and E. Suzuki, *Catal. Today*, 2000, **58**, 125-132.

54. L. Lin, W. Lin, J. L. Xie, Y. X. Zhu, B. Y. Zhao and Y. C. Xie, *Appl. Catal. B-Environ.* , 2007, **75**, 52-58.

55. K. S. Yang, Y. Dai and B. B. Huang, *J. Phys. Chem. C*, 2007, **111**, 18985-18994.

56. G. Liu, Z. G. Chen, C. L. Dong, Y. N. Zhao, F. Li, G. Q. Lu and H. M. Cheng, *J. Phys. Chem. B*, 2006, **110**, 20823-20828.

57. M. Hamadanian, A. Reisi-Vanani and A. Majedi, *Mater. Chem. Phys.*, 2009, **116**, 376-382.

58. J. C. Yu, W. Ho, J. Yu, H. Yip, P. K. Wong and J. Zhao, *Environ. Sci. Technol.*, 2005, **39**, 1175-1179.

59. G. Liu, Y. Zhao, C. Sun, F. Li, G. Q. Lu and H. M. Cheng, *Angew. Chem. Int. Edit.*, 2008, **47**, 5277-5277.

60. R. Nagarajan, V. Kumar and S. Ahmad, *Indian. J. Chem. A*, 2012, **51**, 145-154.

61. S. Yin, Y. Aita, M. Komatsu, J. Wang, Q. Tang and T. Sato, *J. Mater. Chem.*, 2005, **15**, 674-682.

62. S. Liu, Q. Ma, F. Gao, S. Song and S. Gao, *J. Alloy. Compd.*, 2012, **543**, 71-78.

63. X. Pan, M.-Q. Yang, X. Fu, N. Zhang and Y. J. Xu, *Nanoscale*, 2013, **5**, 3601-3614.

64. H. R. Chauke, P. Murovhi, P. E. Ngoepe, N. H. de Leeuw and R. Grau-Crespo, *J. Phys. Chem. C*, 2010, **114**, 15403-15409.

65. K. Hashimoto, H. Irie and A. Fujishima, *Jpn. J. Appl. Phys.*, 2005, **44**, 8269-8285.

66. Z. Lin, A. Orlov, R. M. Lambert and M. C. Payne, *J. Phys. Chem. B*, 2005, **109**, 20948-20952.

67. K. S. Rane, R. Mhalsiker, S. Yin, T. Sato, K. Cho, E. Dunbar and P. Biswas, *J. Solid State Chem.*, 2006, **179**, 3033-3044.

68. N. S. Chaudhari, S. S. Warule, S. A. Dhanmane, M. V. Kulkarni, M. Valant and B. B. Kale, *Nanoscale*, 2013, **5**, 9383-9390.

69. X. Xi, P. Dong, H. Pei, G. Hou, Q. Zhang, R. Guan, N. Xu and Y. Wang, *Comp. Mater. Sci.*, 2014, **93**, 1-5.

70. S. Carrettin, Y. Hao, V. Aguilar‐Guerrero, B. C. Gates, S. Trasobares, J. J. Calvino and A. Corma, *Chem-Eur. J.*, 2007, **13**, 7771-7779.

71. A. Fujishima and K. Honda, *Nat. Sci.* , 1972, **238**, 37-38.

72. Z. Ye, H. H. Zhang and H. B. Pan, *Guang Pu Xue Yu Guang Pu Fen Xi*, 2004, **24**, 261-265.

73. J. Beusen, M. K. Van Bael, H. Van den Rul, J. D'Haen and J. Mullens, *J. Eur. Ceram. Soc.*, 2007, **27**, 4529-4535.

74. S. Y. Chae, M. K. Park, S. K. Lee, T. Y. Kim, S. K. Kim and W. I. Lee, *Chem. Mater.* , 2003, **15**, 3326-3331.

75. S. Qourzal, A. Assabbane and Y. Ait-Ichou, *J. Photoch. Photobio. A*, 2004, **163**, 317-321.

76. H. Jensen, A. Soloviev, Z. Li and E. G. Søgaard, *Appl. Surf. Sci.*, 2005, **246**, 239-249.

77. H. Jensen, K. D. Joensen, S. B. Iversen and E. G. Sogaard, *Ind. Eng. Chem. Res.*, 2006, **45**, 3348-3353.

78. S. Mahshid, M. Askari and M. S. Ghamsari, *J. Mater. Process. Tech.*, 2007, **189**, 296-300.

79. Z. R. Ismagilov, L. T. Tsikoza, N. V. Shikina, V. F. Zarytova, V. V. Zinoviev and S. N. Zagrebelnyi, *Russ. Chem. Rev.*, 2009, **78**, 873-885.

80. G. C. Collazzo, S. L. Jahn, N. L. V. Carreno and E. L. Foletto, *Braz. J. Chem. Eng.*, 2011, **28**, 265-272.

81. J. Wang, J. Polleux, J. Lim and B. Dunn, *J. Phys. Chem. C*, 2007, **111**, 14925-14931.

82. H. Yin, Y. Wada, T. Kitamura, T. Sumida, Y. Hasegawa and S. Yanagida, *J. Mater. Chem.*, 2002, **12**, 378-383.

83. M. Factorovich, L. Guz and R. Candal, *Adv. Phys. Chem.*, 2011, **2011**, 1-8.

84. M. Fittipaldi, D. Gatteschi and P. Fornasiero, *Catal. Today*, 2013, **206**, 2-11.

85. B. Viswanathan and K. Krishanmurthy, *Int. J. Photoenergy*, 2012, **2012**, 10.

86. P. A. Schaber, J. Colson, S. Higgins, D. Thielen, B. Anspach and J. Brauer, *Thermochim. Acta*, 2004, **424**, 131-142.

87. Y. Y. Gao, N. Zhao, W. Wei and Y. H. Sun, *Comput. Theor. Chem.*, 2012, **992**, 1-8.

88. K. D. Wehrstedt, W. Wildner, T. Guthner, K. Holzrichter, B. Mertschenk and A. Ulrich, *J. Hazard. Mater.*, 2009, **170**, 829-835.

89. Y. Hashimoto, M. Takahashi, S. Kikkawa and F. Kanamaru, *Chem. Lett.*, 1994, **23**, 1963-1966.

90. F. Duvernay, T. Chiavassa, F. Borget and J. P. Aycard, *J. Phys. Chem. A*,, 2005, **109**, 603-608.

91. Y. Liu, J. Li, X. F. Qiu and C. Burda, *J. Photoch. Photobio. A*, 2007, **190**, 94-100.

92. S. Rtimi, O. Baghriche, C. Pulgarin, R. Sanjines and J. Kiwi, *Rsc. Adv.*, 2012, **2**, 8591-8595.

93. H. Irie, Y. Watanabe and K. Hashimoto, *J. Phys. Chem. B*, 2003, **107**, 5483-5486.

94. R. Asahi, T. Morikawa, T. Ohwaki, K. Aoki and Y. Taga, *Science*, 2001, **293**, 269-271.

95. I. S. Kim and P. N. Kumta, *Mat. Sci. Eng. B-Solid*, 2003, **98**, 123-134.

96. Y. Aita, M. Komatsu, S. Yin and T. Sato, *J. Solid. State. Chem.*, 2004, **177**, 3235-3238.

97. Y. Cong, L. Xiao, J. L. Zhang, F. Chen and M. Anpo, *Res. Chem. Intermediat.*, 2006, **32**, 717-724.

98. E. Martinez-Ferrero, Y. Sakatani, C. Boissiere, D. Grosso, A. Fuertes, J. Fraxedas and C. Sanchez, *Adv. Funct. Mater.*, 2007, **17**, 3348-3354.

99. J. Graciani, S. Hamad and J. F. Sanz, *Phys. Rev. B*, 2009, **80**, 184112.

100. J. H. Ma, M. N. Wu, Y. H. Du, S. Q. Chen, G. X. Li and J. B. Hu, *J. Alloy. Compd.*, 2009, **476**, 603-605.

101. V. Legrand, O. Merdrignac-Conanec, W. Paulus and T. Hansen, *J. Phys. Chem. A*,, 2012, **116**, 9561-9567.

102. S. G. Seo, C. H. Park, H. Y. Kim, W. H. Nam, M. Jeong, Y. N. Choi, Y. S. Lim, W. S. Seo, S. J. Kim, J. Y. Lee and Y. S. Cho, *J. Mater. Chem. A*, 2013, **1**, 3639-3644.

103. K. Kobayakawa, Y. Murakami and Y. Sato, *J. Photoch. Photobio. A*, 2005, **170**, 177-179.

104. J. Buha, I. Djerdj, M. Antonietti and M. Niederberger, *Chem. Mater.*, 2007, **19**, 3499-3505.

105. S. Livraghi, M. Pelaez, J. Biedrzycki, I. Corazzari, E. Giamello and D. D. Dionysiou, *Catal. Today*, 2013, **209**, 54-59.

106. R. Amadelli, L. Samiolo, M. Borsa, M. Bellardita and L. Palmisano, *Catal. Today*, 2013, **206**, 19-25.

107. Y. Hashimoto, M. Takahashi, S. Kikkawa and F. Kanamaru, *J. Solid State Chem.*, 1995, **114**, 592-594.

108. X. H. Liu, M. Krott, P. Muller, C. H. Hu, H. Lueken and R. Dronskowski, *Inorg. Chem.*, 2005, **44**, 3001-3003.

109. G. Xin, H. F. Pan, D. Chen, Z. H. Zhang and B. Wen, *J. Phys. Chem. Solids*, 2013, **74**, 286-290.

110. A. M. Bernhard, D. Peitz, M. Elsener, A. Wokaun and O. Krocher, *Appl. Catal. B-Environ.*, 2012, **115**, 129-137.

111. H. Y. He, *Res. Chem. Intermediat.*, 2010, **36**, 155-161.

112. Z. Q. Zhou, X. Y. Zhang, Z. Wu and L. M. Dong, *Chin. Sci. Bull.* , 2005, **50**, 2691-2695.

113. T. Ohno, M. Akiyoshi, T. Umebayashi, K. Asai, T. Mitsui and M. Matsumura, *Appl. Catal. a-Gen.*, 2004, **265**, 115-121.

114. S. Wang, Q. Y. Gao and J. C. Wang, *J. Phys. Chem. B*, 2005, **109**, 17281-17289.

115. Z. D. Wang, M. Yoshida and B. George, *Comput. Theor. Chem.*, 2013, **1017**, 91-98.

116. C. W. Dunnill, Z. A. Aiken, A. Kafizas, J. Pratten, M. Wilson, D. J. Morgan and I. P. Parkin, *J. Mater. Chem.*, 2009, **19**, 8747-8754.

117. H. X. Li, X. Y. Zhang, Y. N. Huo and J. Zhu, *Environ. Sci. Technol.*, 2007, **41**, 4410-4414.

118. P. P. Bidaye, D. Khushalani and J. B. Fernandes, *Catal. Lett.*, 2010, **134**, 169-174.

119. G. Liu, C. Sun, S. C. Smith, L. Wang, G. Q. Lu and H. M. Cheng, *J. Colloid Interf. Sci.*, 2010, **349**, 477-483.

120. L. K. Randeniya, A. B. Murphy and I. C. Plumb, *J. Mater. Sci.*, 2008, **43**, 1389-1399.

121. D. Ma, Y. J. Xin, M. C. Gao and J. Wu, *Appl. Catal. B-Environ.*, 2014, **147**, 49-57.

122. L. Szatmary, S. Bakardjieva, J. Subrt, P. Bezdicka, J. Jirkovsky, Z. Bastl, V. Brezova and M. Korenko, *Catal.Today*, 2011, **161**, 23-28.

123. S. W. Kim, R. Khan, T. J. Kim and W. J. Kim, *Bull. Korean Chem. Soc.*, 2008, **29**, 1217-1223.

124. H. Tian, J. Ma, K. Li and J. Li, *Ceram. Int.*, 2009, **35**, 1289-1292.

125. Y. Liu, J. Liu, Y. Lin, Y. Zhang and Y. Wei, *Ceram. Int.*, 2009, **35**, 3061-3065.

126. K. Takeshita, A. Yamakata, T. Ishibashi, H. Onishi, K. Nishijima and T. Ohno, *J. Photoch. Photobio. A*, 2006, **177**, 269-275.

127. J. W. Robinson, *Undergraduate Instrumental Analysis*, M. Dekker, New York, 4th edn., 1987.

128. P. K. Harold and E. A. Leroy, *X-Ray diffraction procedures : for polycrystalline and amorphous materials*, Wiley, New York, 1976.

129. P. R. Griffiths and J. A. DeHaseth, *Fourier transform infrared spectrometry*, Wiley, New York, 1986.

130. S. Valencia, J. M. Marín and G. Restrepo, *Open. Mater. Sci. J.*, 2010, **4**, 9-14.

131. K. Madhusudan Reddy, S. V. Manorama and A. Ramachandra Reddy, *Mater. Chem. Phys.*, 2003, **78**, 239-245.

132. R. J. Ross, *Microelectronics failure analysis : desk reference*, ASM International USA, 6th edn., 2011.

133. T. Sugimoto, X. P. Zhou and A. Muramatsu, *J. Colloid Interface Sci.*, 2003, **259**, 43-52.

134. M. M. Viana, V. F. Soares and N. D. S. Mohallem, *Ceram. Int.*, 2010, **36**, 2047-2053.

135. D. H. Williams and I. Fleming, *Spectroscopic methods in organic chemistry*, McGraw-Hill, London ; New York, 3d edn., 1980.

136. I. S. Kim and P. N. Kumta, *J. Mater. Chem.*, 2003, **13**, 2028-2035.

137. C. Di Valentin, G. Pacchioni, A. Selloni, S. Livraghi and E. Giamello, *J. Phys. Chem. B*, 2005, **109**, 11414-11419.

138. J. Yuan, M. X. Chen, J. W. Shi and W. F. Shangguan, *Int. J. Hydrogen Energ.*, 2006, **31**, 1326-1331.

139. M. Pelaez, N. T. Nolan, S. C. Pillai, M. K. Seery, P. Falaras, A. G. Kontos, P. S. M. Dunlop, J. W. J. Hamilton, J. A. Byrne, K. O'Shea, M. H. Entezari and D. D. Dionysiou, *Appl. Catal. B-Environ.*, 2012, **125**, 331-349.

140. C. N. Huang, J. S. Bow, Y. Zheng, S. Y. Chen, N. Ho and P. Shen, *Nanoscale Res. Lett.*, 2010, **5**, 972-985.

141. N. Hering, K. Schreiber, R. Riedel, O. Lichtenberger and J. Woltersdorf, *Appl. Organomet. Chem.*, 2001, **15**, 879-886.

142. H. W. Dudley and F. Ian, *Spectroscopic methods in organic chemistry*, McGraw-Hill, London, 6th edn., 2008.

143. L. G. Devi and R. Kavitha, *Mater. Chem. Phys.*, 2014, **143**, 1300-1308.

144. B. V. Lotsch and W. Schnick, *Chem. Mater.*, 2005, **17**, 3976-3982.

145. E. R. Kotb, M. M. Anwar, H. A. S. Abbas and S. I. Abd El-Moez, *Acta Pol. Pharm.*, 2013, **70**, 667-679.

146. X. Liu, M. A. Wankeu, H. Lueken and R. Dronskowski, *Cell*, 2005, **173**, 593-596.

147. P. Jacobs, A. Houben, A. L. Tchougréeff and R. Dronskowski, *J. Chem. Phys.*, 2013, **139**, 224707.

148. Y. Cong, J. Zhang, F. Chen and M. Anpo, *J. Phys. Chem. C*, 2007, **111**, 6976-6982.

149. J. Shen, H. Yang, Q. Shen, Y. Feng and Q. Cai, *Cryst. Eng. Comm.*, 2014, **16**, 1868-1872.

150. B. C. Smith, *Infrared spectral interpretation: a systematic approach*, Boca Raton CRC Press, USA, 1999.

151. S. H. Nam, T. K. Kim and J. H. Boo, *Catal. Today*, 2012, **185**, 259-262.

152. J. W. Robinson, E. M. S. Frame and G. M. Frame, *Undergraduate Instrumental Analysis, Sixth Edition*, Taylor and Francis, New York, 2004.

153. E. K. Plyler and C. J. Humphreys, *J. Res. Natl. Bur. Stand.* , 1947, **39**, 59-65.

154. S. Maity, Y. S. Kim, R. I. Kaiser, H. M. Lin, B. J. Sun and A. H. H. Chang, *Chem. Phys. Lett.*, 2013, **577**, 42-47.

155. F. Zhang, X. Wu, C. Liang, X. Li, Z. Wang and H. Li, *Green Chem.*, 2014, **16**, 3768-3777.

156. W. J. Lo, H. F. Chen, P. H. Chou and Y. P. Lee, *J. Chem. Phys.*, 2004, **121**, 12371-12378.

157. R. D. Vasquez and J. D. A. Ramos, *J. Res. Phytochem. Pharmacol.*, 2012, **2**, 55-63.

158. H. Changseok, A. Joel, L. Vlassis, F. Polycarpos, L. Jacob and D. D. Dionysios, *Catal. Today*, 2014, **224**, 132-139.

159. F. L. Pua, C. H. Chia, S. Zakaria, T. K. Liew, M. A. Yarmo and N. M. Huang, *Sains Malays.*, 2010, **39**, 243-248.

8– Appendixes

Appendix 1: PXRD pattern showing an amorphous /unstructured phase of $Ti(OCH(CH_3)_2)_{4-x}(OH)_x$

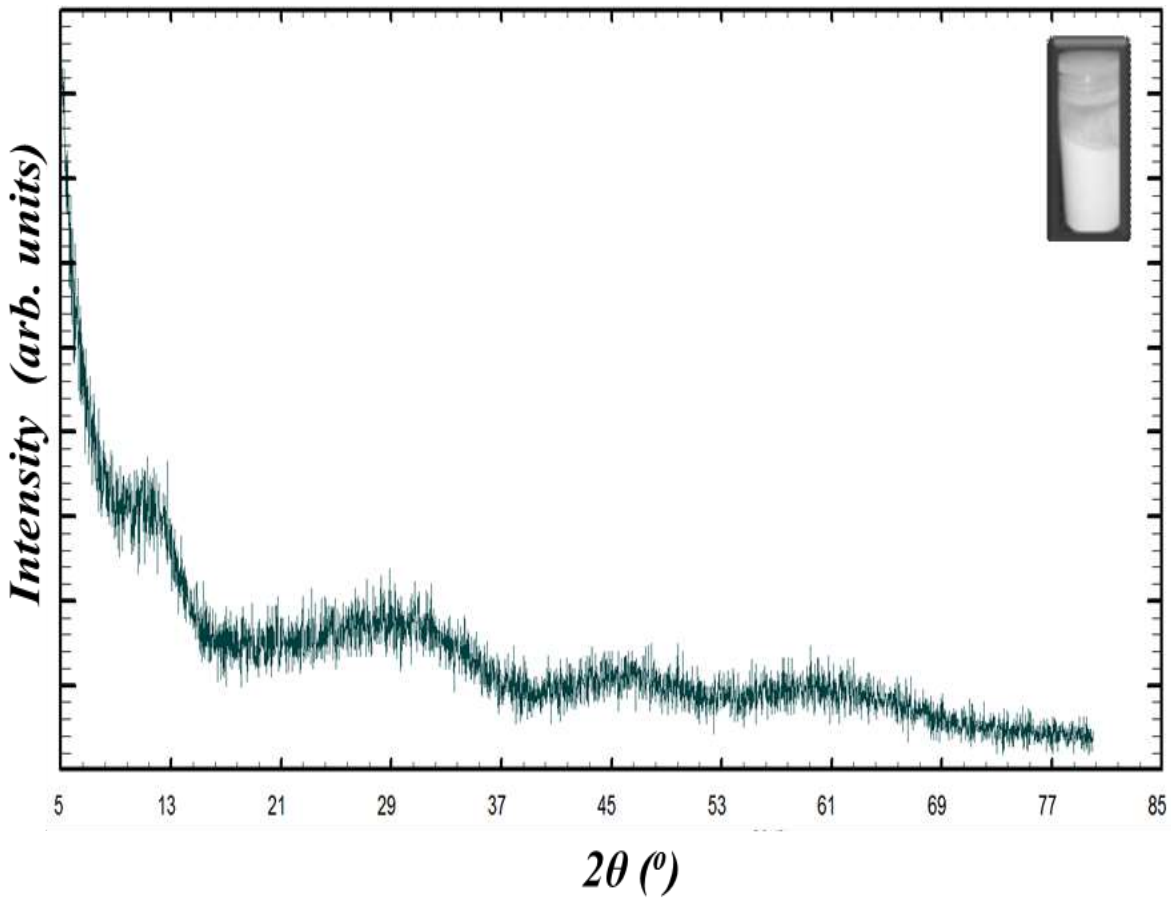

Appendix 2: FT-IR spectra of Ti isopropoxide (http://www.sigmaaldrich.com/spectra/ftir/FTIR002655.PDF

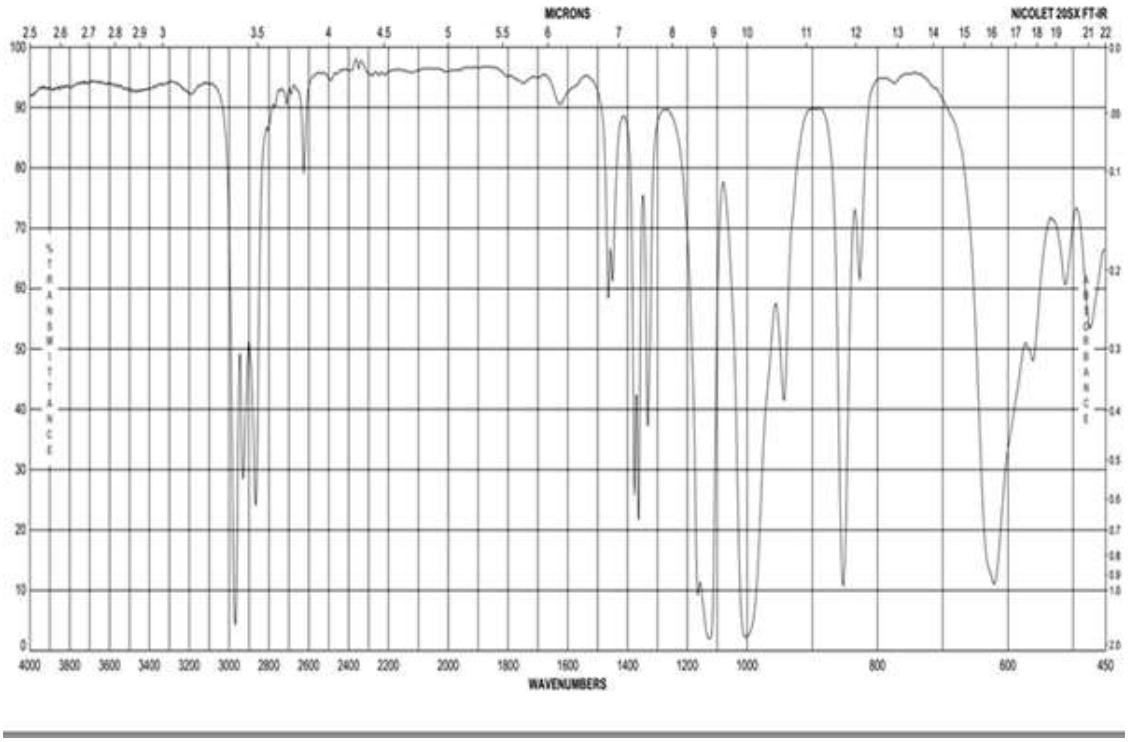

Appendix 3: EEL spectra of Ti^{4+} and Ti^{3+}
(http://muller.research.engineering.cornell.edu/sites/WEELS/)

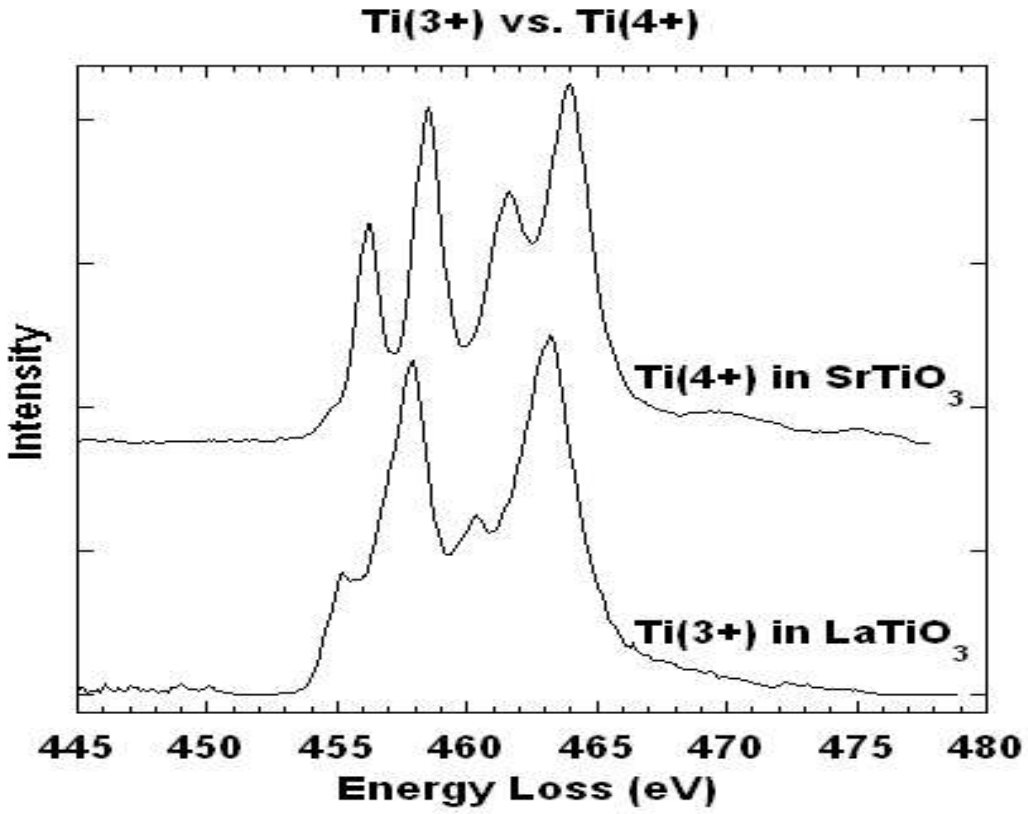

Appendix 4: FT-IR spectra of impure KBr and cyanamide

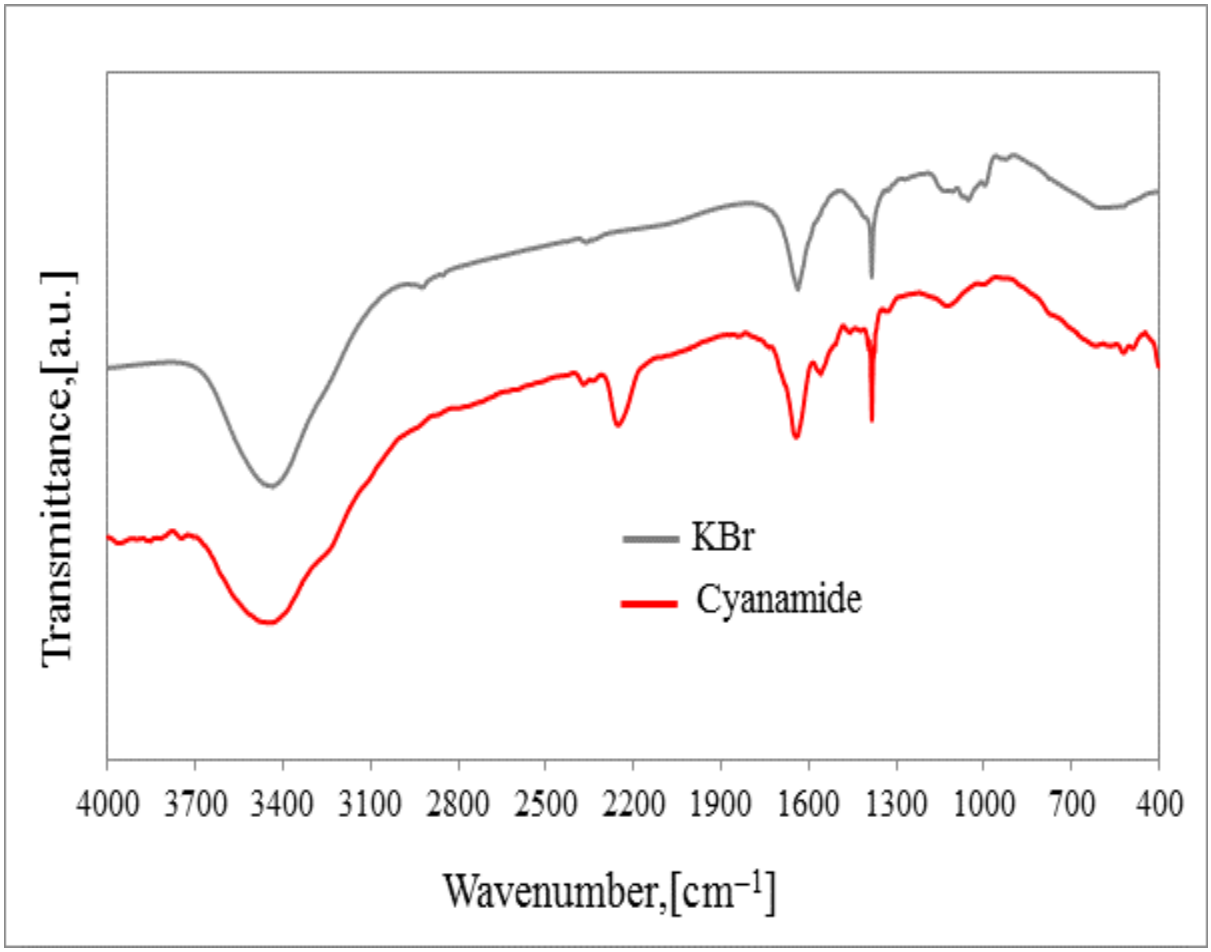

Appendix 5: FT-IR spectra of KBr and urea

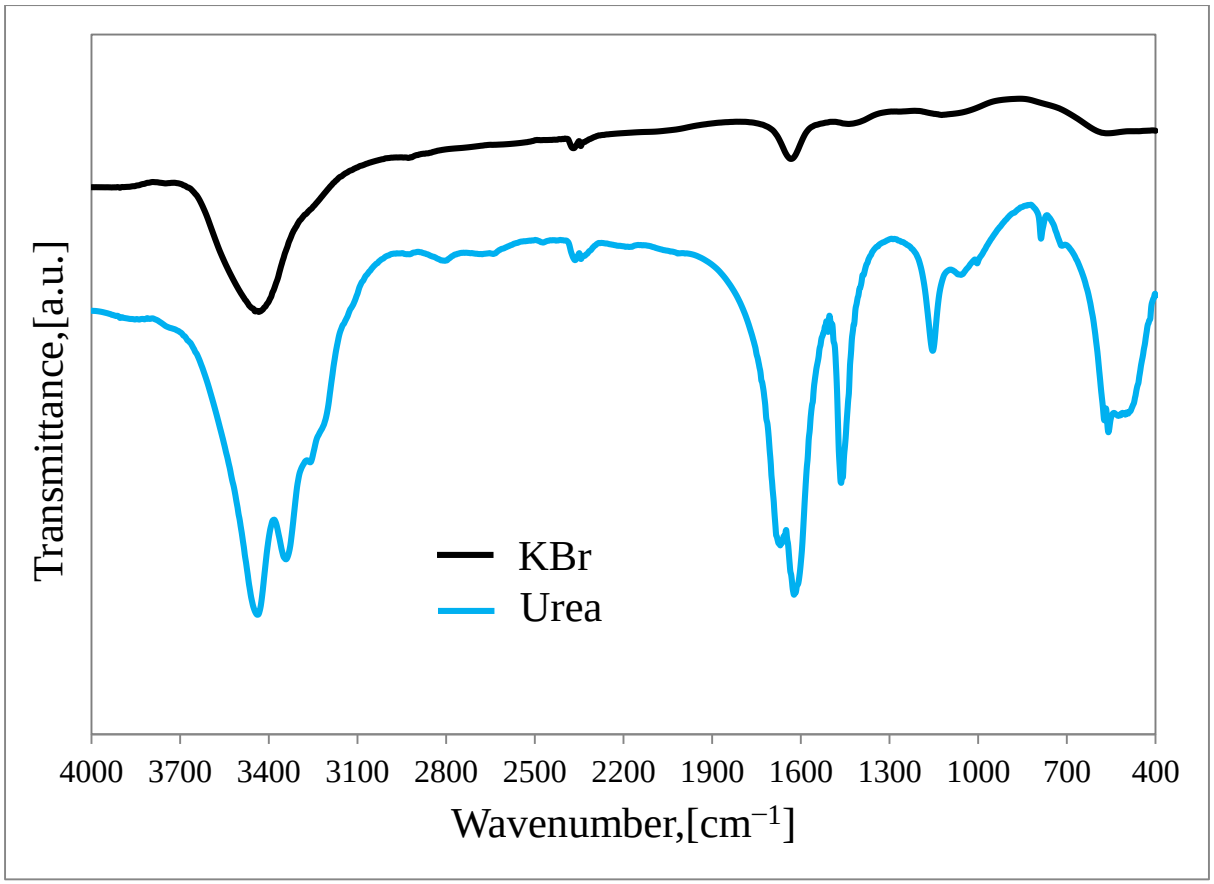

Appendix 6: Calculation of Crystallite size by using Scherrer Formula

sample name	X-ray wavelength λ nm	K constance dependent on crystallite shape	2θ	θ_B= Bragg angle= 2θ/2 (Radians)	COS(θ_B)	$2\theta_2$	$2\theta_1$	FWHM B=$2\theta_2$-$2\theta_1$ in Radians	Thickness of crystallite D nm (101)
ANA	0.154	0.9	25.249	0.220339	0.975823	25.612	24.89	0.012601	11.27139

1:0.25_AM_CM_400_5_N	0.154	0.9	25.344	0.221168	0.975642	25.58	25.11	0.008203	17.31799
1:0.5_AM_CM_400_5_N	0.154	0.9	25.219	0.220077	0.975881	25.632	24.823	0.01412	10.05867
1:0.75_AM_CM_400_5_N	0.154	0.9	25.253	0.220374	0.975816	25.725	24.772	0.016633	8.539356

1:1_AM_CM_400_5_N	0.154	0.9	25.318	0.220941	0.975692	26.672	24.622	0.035779	3.970264
1:10_AM_U_400_5_Air	0.154	0.9	25.2424	0.220281	0.975836	25.626	24.876	0.01309	10.85045
1:10_ANA_U_450_5_N	0.154	0.9	25.2486	0.220336	0.975824	25.729	24.753	0.017034	8.33805

ANA_CS2_300_30_air	0.154	0.9	25.425	0.221875	0.975487	25.786	25.091	0.01213	11.71331
ANA_CS2_300_1_air	0.154	0.9	25.243	0.220287	0.975835	25.577	24.902	0.011781	12.05607
1:05_AM_TU_500_4_Air	0.154	0.9	25.216	0.220051	0.975886	25.779	24.646	0.019775	7.182187

Appendix 7: FT-IR spectra of; ANA (AnataseTiO_2); ANA_U for anatase TiO_2 reacted with urea in the ratios 1:10 and 1:15. The reaction temperature T= 400 ˚C, 5 hours under following of nitrogen gas.

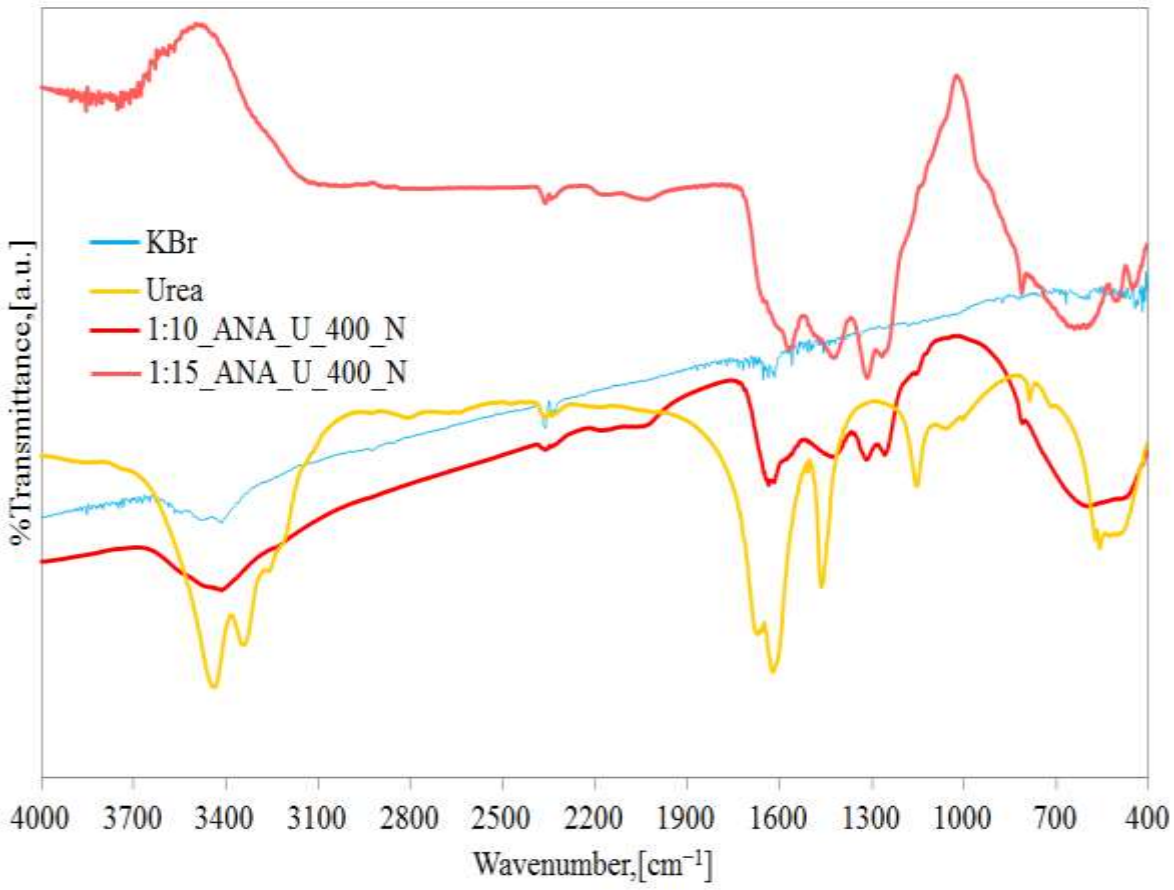

Appendix 8: FT-IR spectra of; ANA (AnataseTiO_2); ANA_U for anatase TiO_2 reacted with urea in the ratios 1:5, 1:10 and 1:15. The reactions were heated to 500 ˚C for 5 hours under following of nitrogen gas.

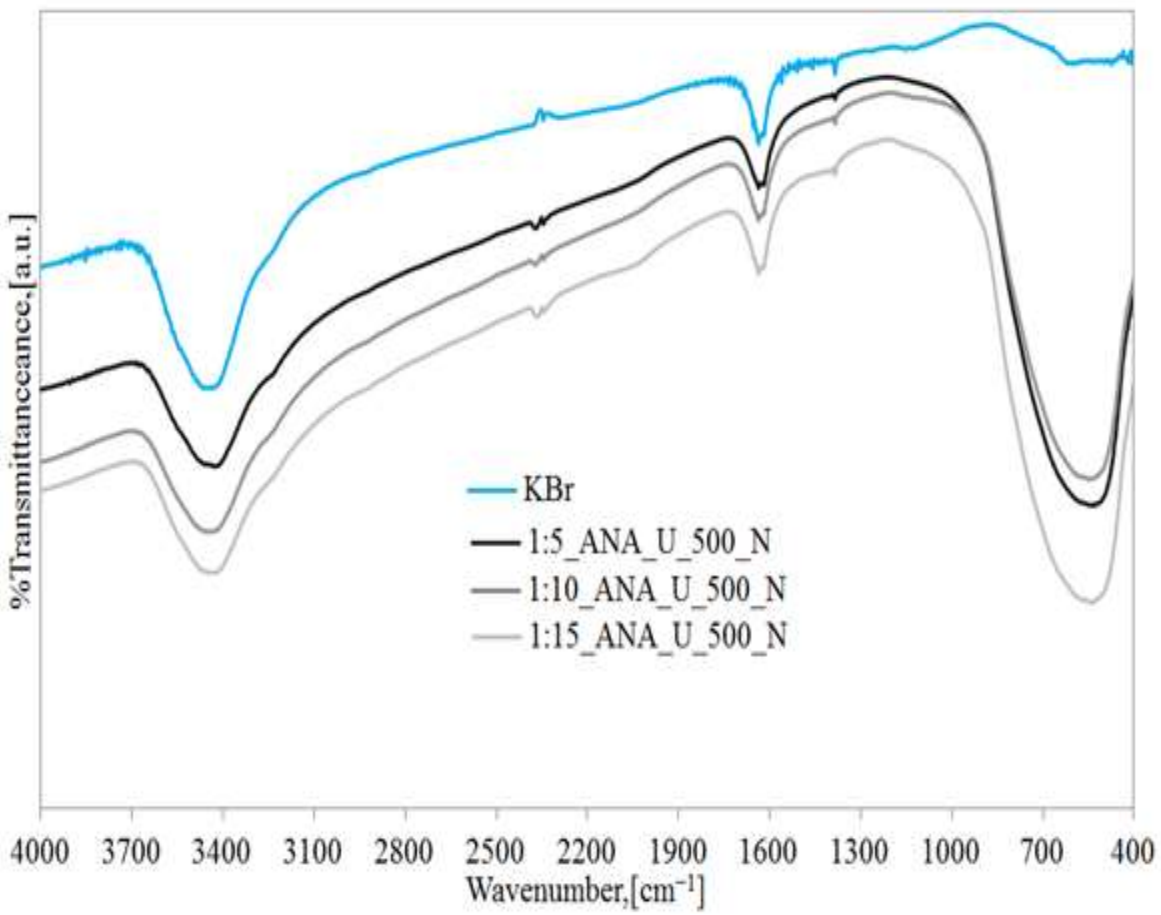

Appendix 9: FT-IR spectrum of melamine

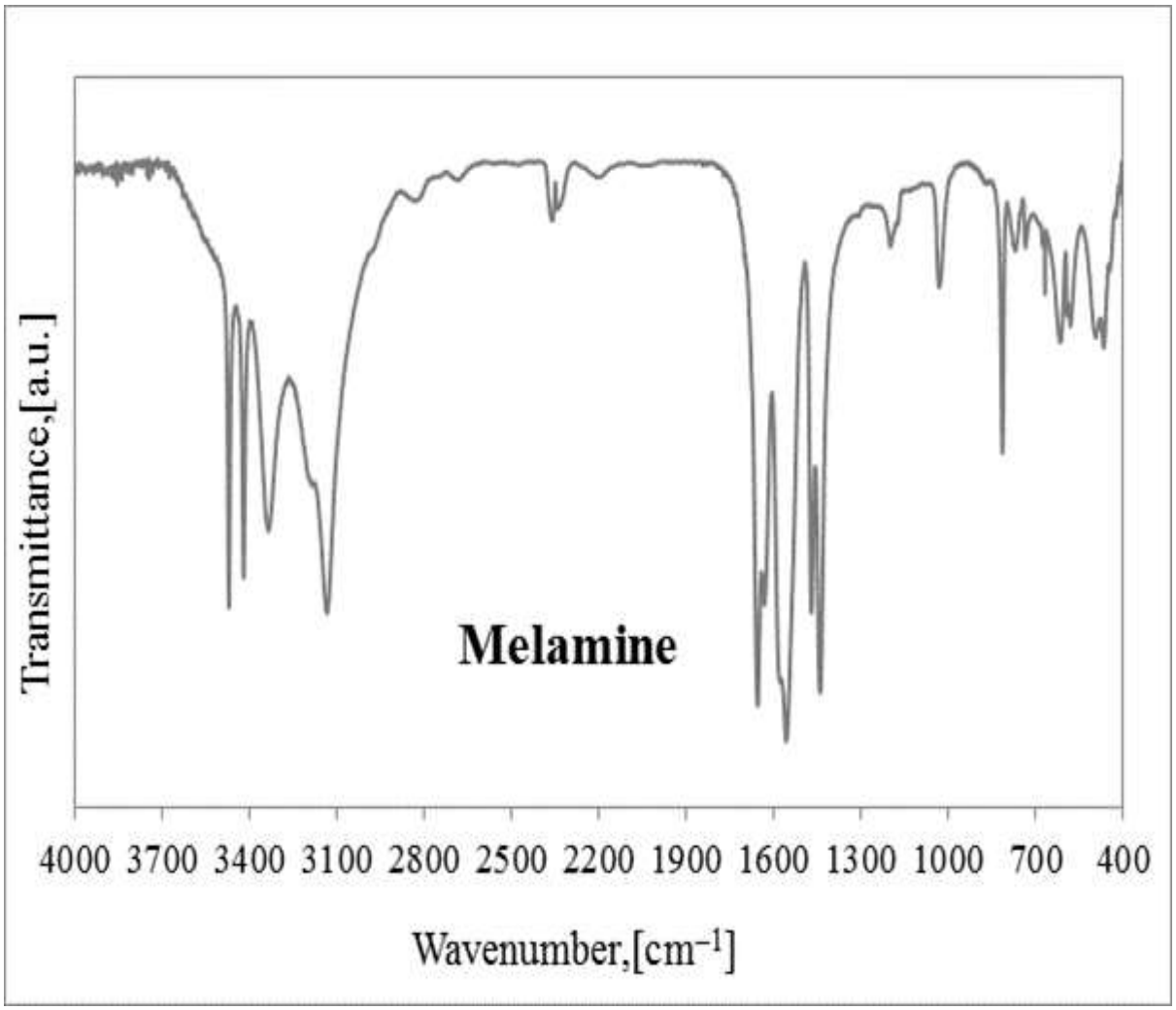

Appendix 10: IR-spectrum of free carbon disulfide CS_2 (S. Maity, Y. S. Kim, R. I. Kaiser, H. M. Lin, B. J. Sun and A. H. H. Chang, *Chem. Phys. Lett.*, 2013, 577, 42-47)

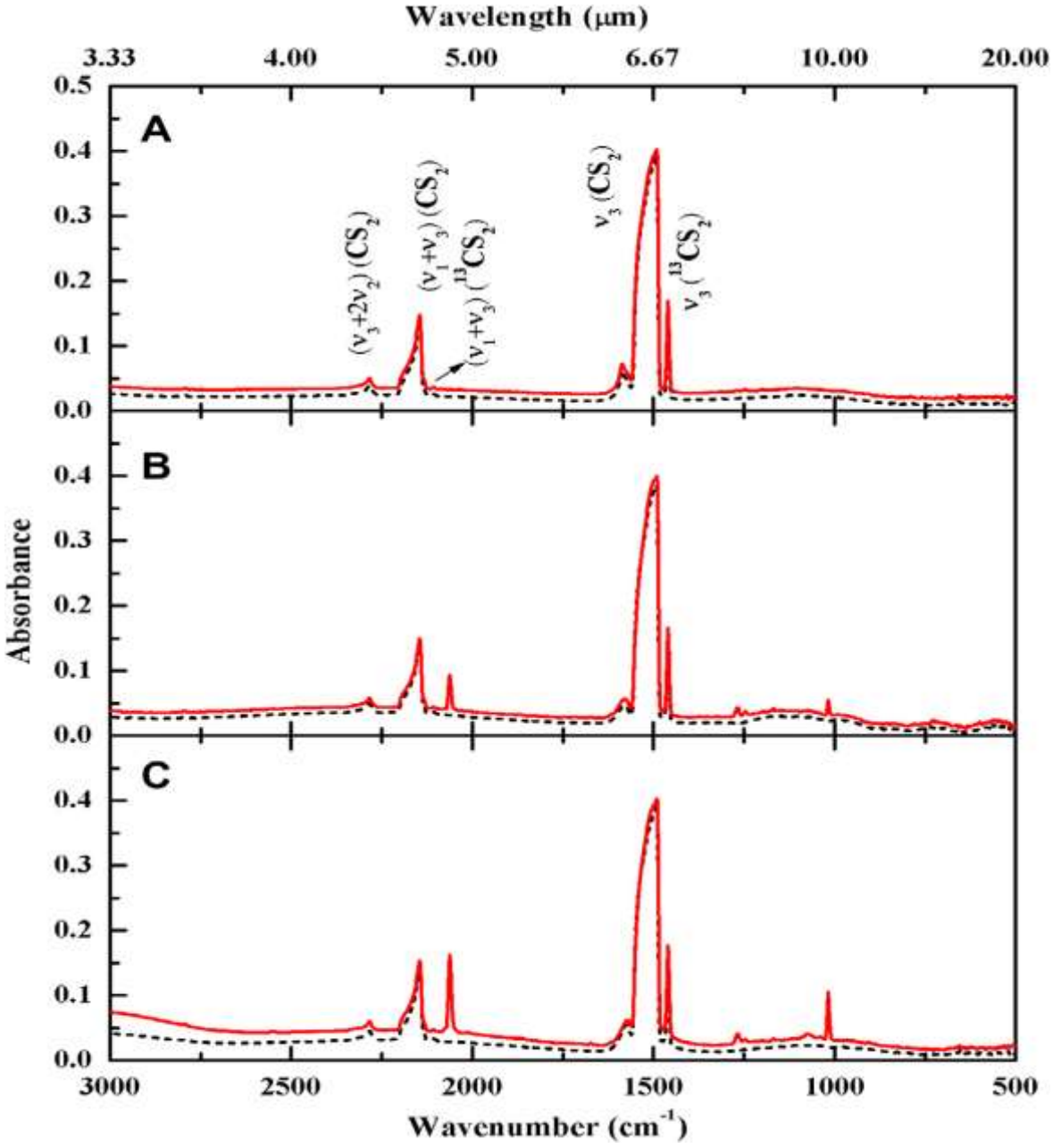

http://ed.augie.edu/~mahelber/ChemistryResearch/Spectra/Carbon_disulfide.html

http://www.sigmaaldrich.com/catalog/product/riedel/34933?lang=en&region=GB

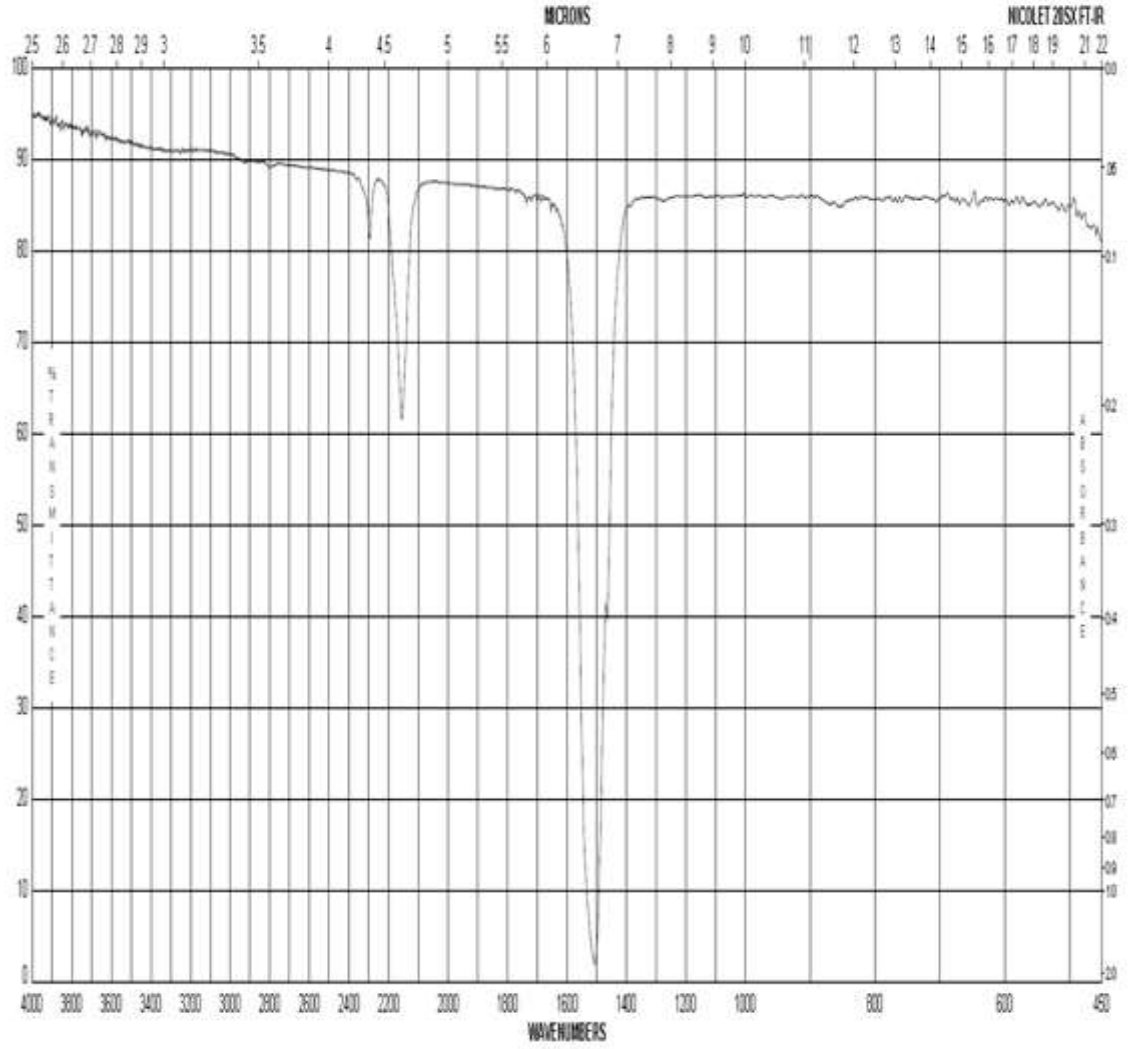

http://ed.augie.edu/~kllunder/e4.html

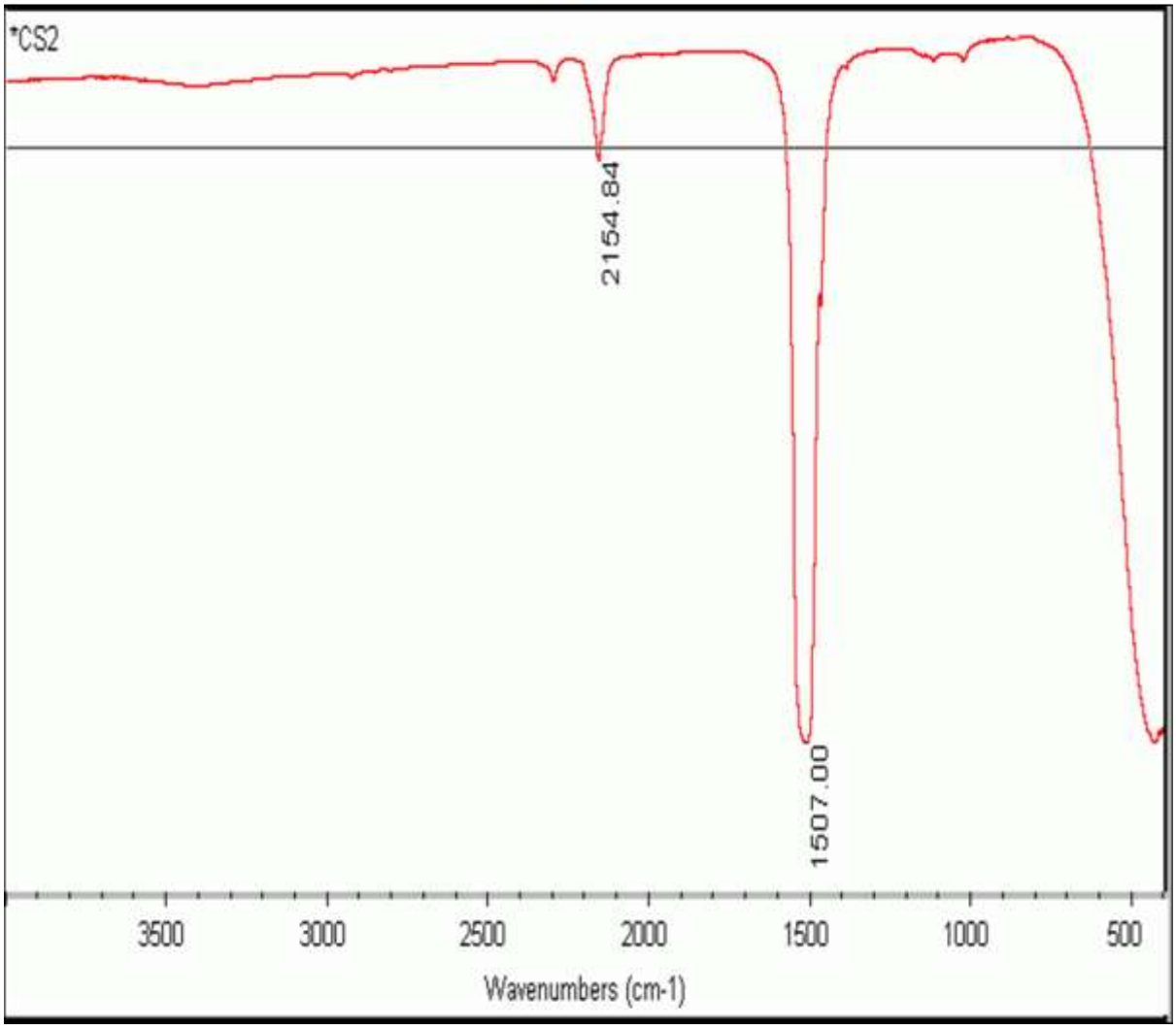

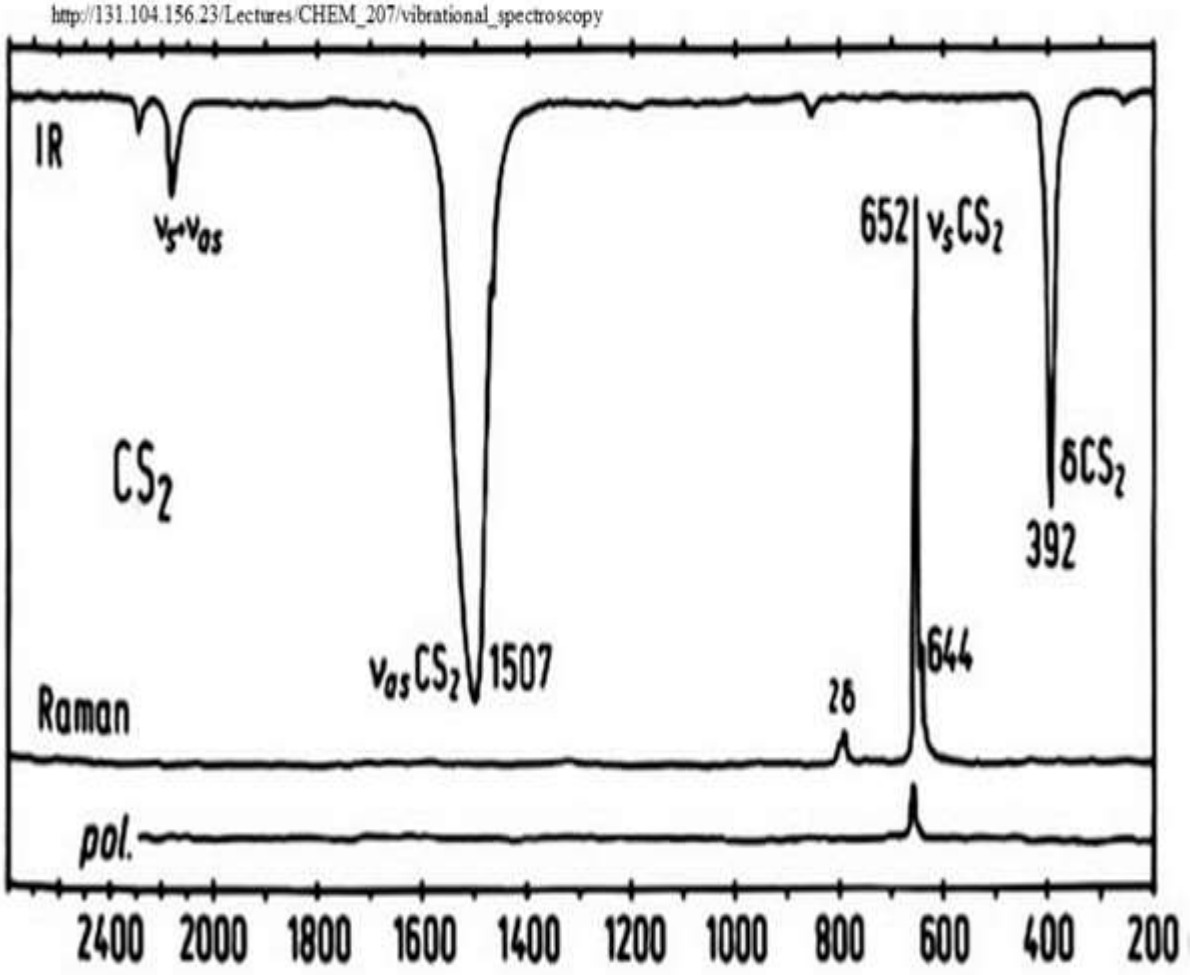
http://131.104.156.23/Lectures/CHEM_207/vibrational_spectroscopy
IR
$\nu_s+\nu_{as}$
652 $\nu_s CS_2$
CS_2
δCS_2
392
$\nu_{as} CS_2$ 1507
644
Raman
28
pol.
2400 2000 1800 1600 1400 1200 1000 800 600 400 200

Appendix 11: Two coordinations of cationic-doping SO_4-TiO_2 (L. G. Devi and R. Kavitha, Mater. *Chem. Phys*., 2014, 143, 1300-1308)

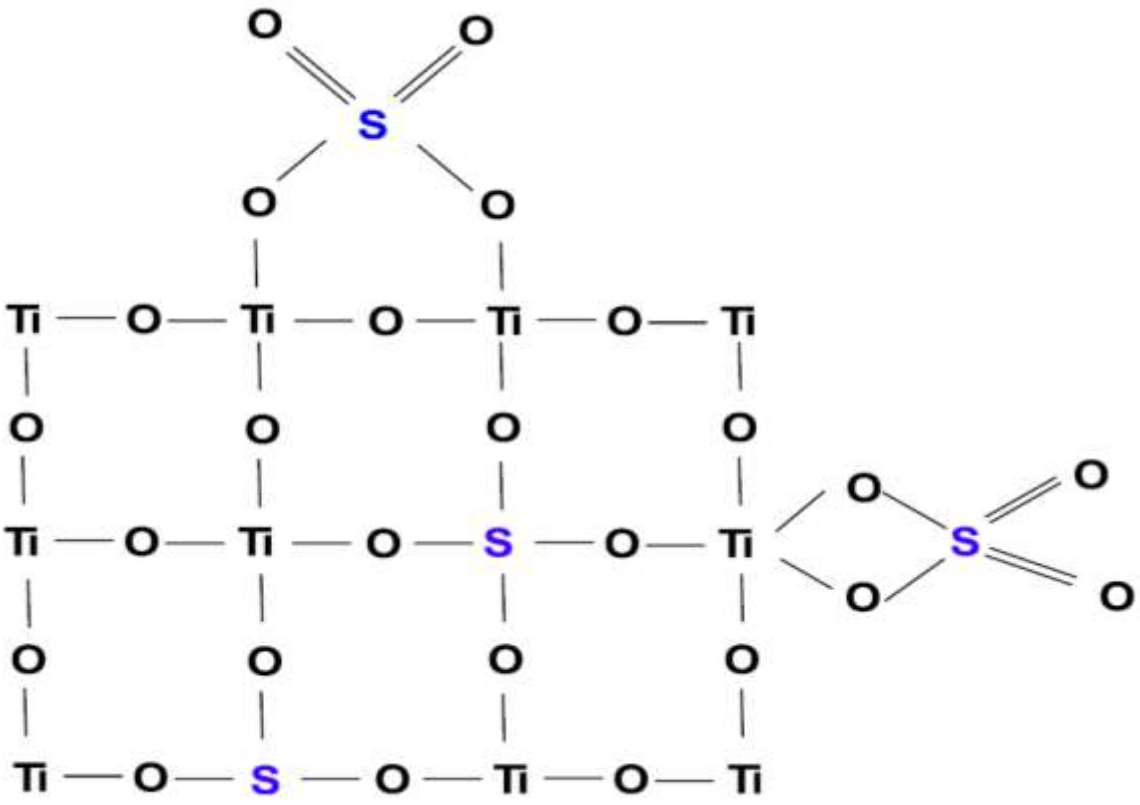

Appendix 12: COSHH Form

Amount to be used	**Substances (also list reaction products)**	**Hazards**	**Source of information (should be MSDS)**
<1mL	Ti $(OCH(CH_3)_2)_4$ titanium isopropoxide	Flammable liquid and vapour, Causes serious eye irritation, Toxic if inhaled.	MSDS
<10mL	1-Dodecanethiol, $HSC_{12}H_{25}$	Flammable liquids, oxidizing liquids, pyrophoric, toxicity, irritation and corrosive.	MSDS

<100 mL	Acetone	Highly flammable. Irritating to eyes. Repeated exposure may cause skin dryness or cracking. Vapours may cause drowsiness and dizziness	MSDS
Cylinder	Nitrogen, N_2	Not hazardous according to directive 67/548/EEC. Stored under high pressure.	MSDS

<100 mL	Hexane, C_6H_{14}	Highly flammable. Irritating to the skin. Danger of serious damage to health by prolonged exposure inhalation. Possible risk of impaired fertility. Harmful: may cause lung damage if swallowed. Vapours may cause drowsiness and dizziness. Toxic to aquatic organisms, may cause long-term adverse effects in the aquatic environment.	MSDS

<1g	Thiourea, $(NH_2)_2CS$	Flammable at high temperature, inhalation, ingestion, irritation	MSDS
<10g	Titanium dioxide, TiO_2	irritation	MSDS
<1g	Urea, $(NH_2)_2CO$	Non-flammable, irritation, explosive salt with nitric acid	MSDS
<10mL	Paraffin oil	Irritation	MSDS

<10mL	Carbon disulfide CS_2	Highly Flammable liquids and vapour, toxicity and irritation	MSDS
< 1 g	potassium bromide, KBr	Irritation	MSDS
< 1 g	Hydrogen Cyanamide/ Carbimide, CN_2H_2	Harmful, toxic if swallowed, irritation, need to be in cool place	MSDS

Appendix 13: PXRD patterns of AM_CM samples using *Highscore Plus* programme

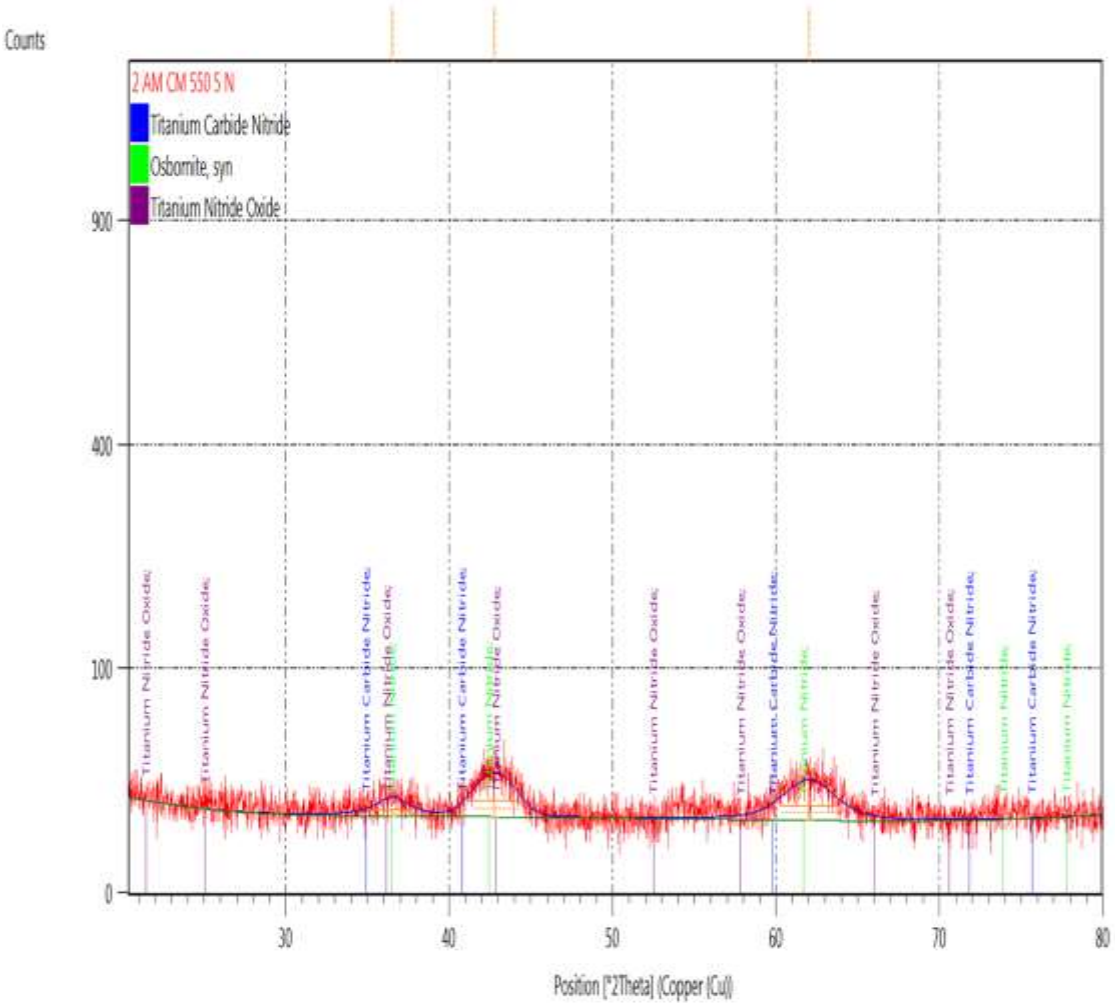

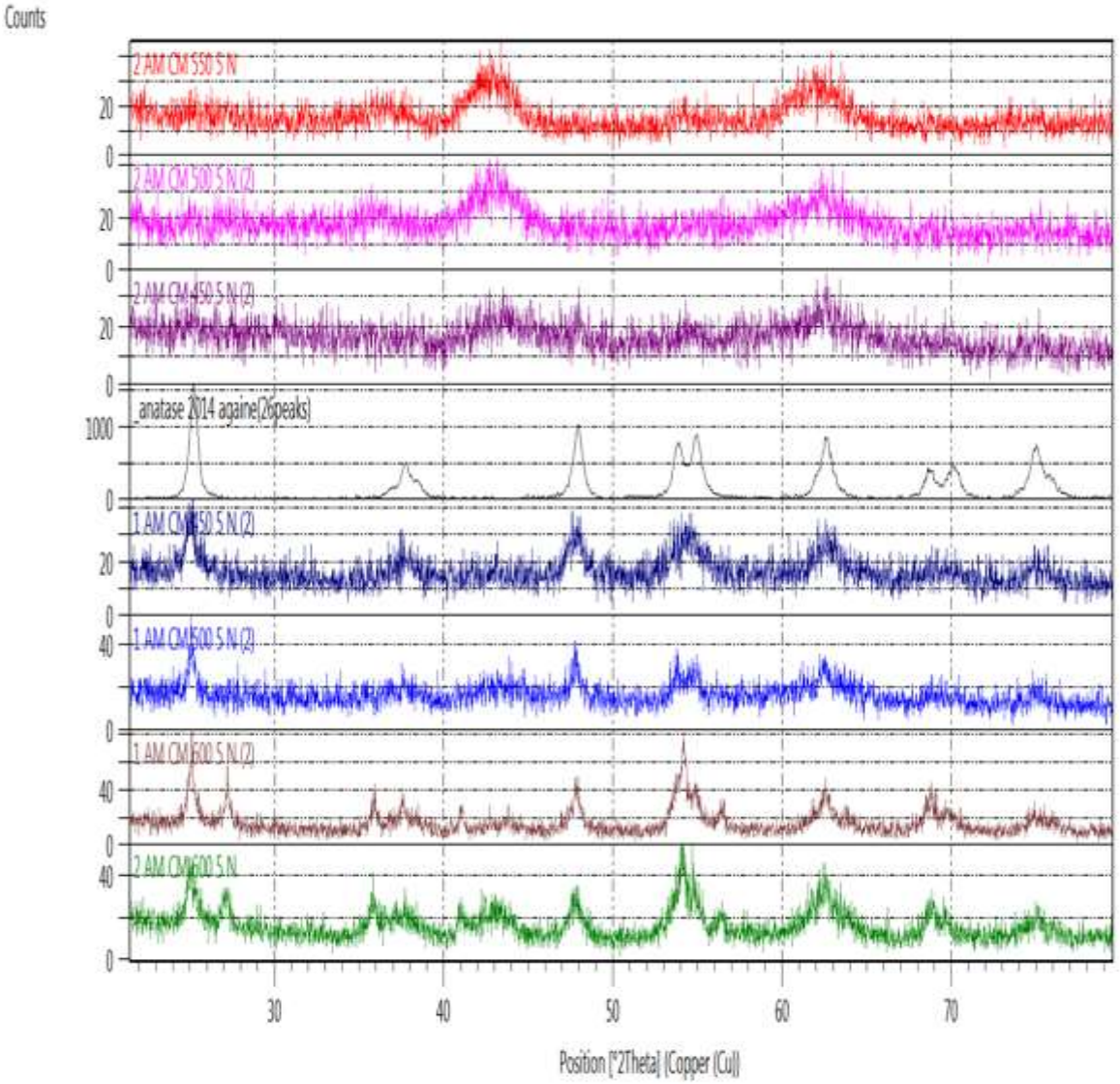
Counts
2 AM CM 550 5 N
2 AM CM 500 5 N (2)
2 AM CM 450 5 N (2)
_anatase 2014 againe(26peaks)
1 AM CM 450 5 N (2)
1 AM CM 500 5 N (2)
1 AM CM 600 5 N (2)
2 AM CM 600 5 N
30
40
50
60
70
Position [°2Theta] (Copper (Cu))

Appendix 14: Joint Committee on Powder Diffraction Standards

Name	Formula	Reference Code	References
Anatase Titanium Oxide	**TiO_2**	**00-021-1272**	**Primary reference**: *Natl. Bur. Stand. (U.S.) Monogr*. 25,**7,**82, (1969)
Rutile Titanium Oxide/ Titania	**TiO_2**	**00-021-1276**	**Primary reference**: Natl. Bur. Stand. (U. S.) Monogr. 25, **7**, 83, (1969) **Optical data:** Dana's System of Mineralogy, 7th Ed., **I**, 575
Brookite Titanium Oxide	**TiO_2**	**00-029-1360**	**Primary reference:** *Natl. Bur. Stand. (U. S.) Monogr. 25*, 3, 57, (1964) **Optical data:** *Dana's System of Mineralogy, 7th Ed.*, **I**, 588, (1944)

Osbornite / Titanium Nitrate	**$TiN_{0.90}$**	**00-031-1403**	**Primary reference:** Christensen, A., *Acta Chem. Scand., Ser. A*, **29**, 563, (1975) **Unit Cell:** Christensen, A., *J. Cryst. Growth*, **33**, 99, (1976)
Titanium Nitrate Oxide	**$TiN_{0.6}O_{0.4}$**	**00-049-1325**	**Primary reference:** Hunt, J., Solleta, I., Battezzati, L., Cowlam, N., Cocco, G., *J. Alloys Compds.*, **194**, 311, (1993)
Titanium Carbide Nitride	**Ti_2CN**	**01-071-6059**	**Primary reference:** *Calculated from ICSD using POWD-12++* **Structure:** Duwez, P., Odell, F., *Metal (Berline)*, **26**, 701, (1972)

Titanium Sulfide	**TiS_2**	**01-081-0687**	**Primary reference:** *Calculated from ICSD using POWD-12++, (1992)* **Structure:** Lightfoot, P., Krok, F., Nowinski, J. L., Bruce, P. G., *J. Mater. Chem.*, **2**, 139, (1992)

Appendix 15: PXRD patterns of ANA (anataseTiO_2, blank) and AM_CM (amorphous: cyanamide) at various ratios and temperatures in N_2.